An Observational Overview of Active Galactic Nuclei

Niel Brandt (Penn State University)

Summary of Lectures

Introduction, AGN Basics, Finding AGNs, and Terminology

Observations on Small Scales: Black Hole Region, Broad Line Region, Outflowing Winds

Observations on Large Scales: Narrow Line Region, Torus, Jets

Summary of Lectures

Focused Lecture – AGN Demography, Physics, and Ecology from X-ray Surveys

Some Warnings

Even with 5 lectures, we can only scratch the surface of this truly massive field.

Literally thousands of papers in the literature.

I will aim to give the main ideas, without noting every special case or technical exception.

My lectures will be *observationally* focused.

A tremendous amount to learn and explore!

Some Useful Books

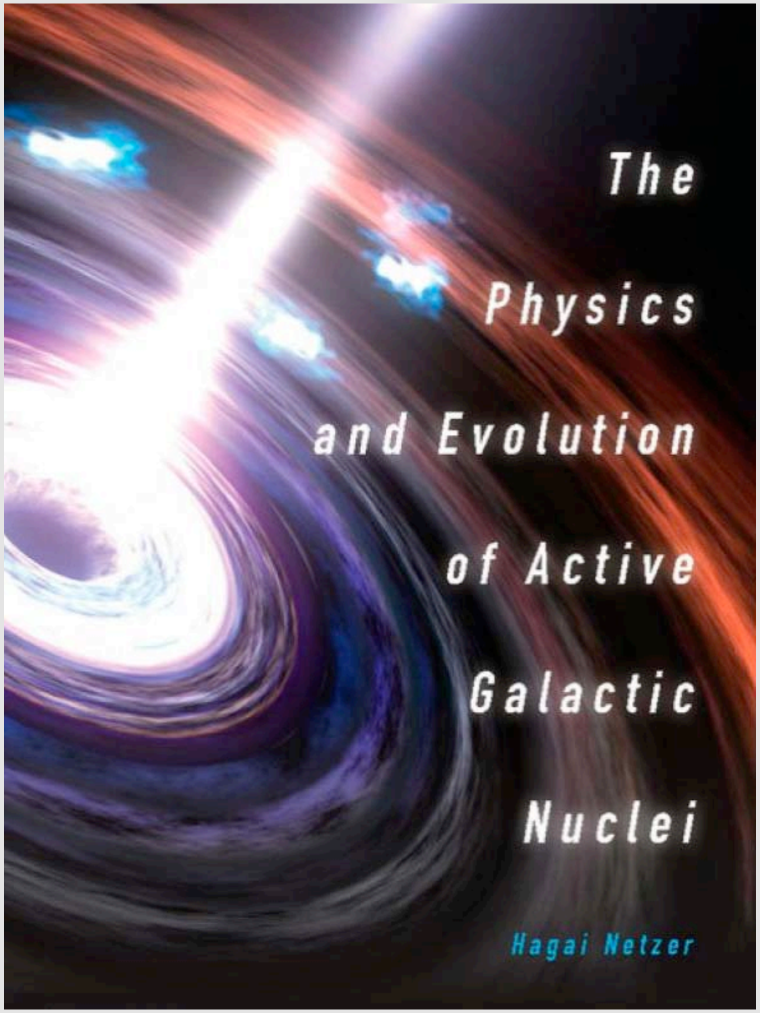

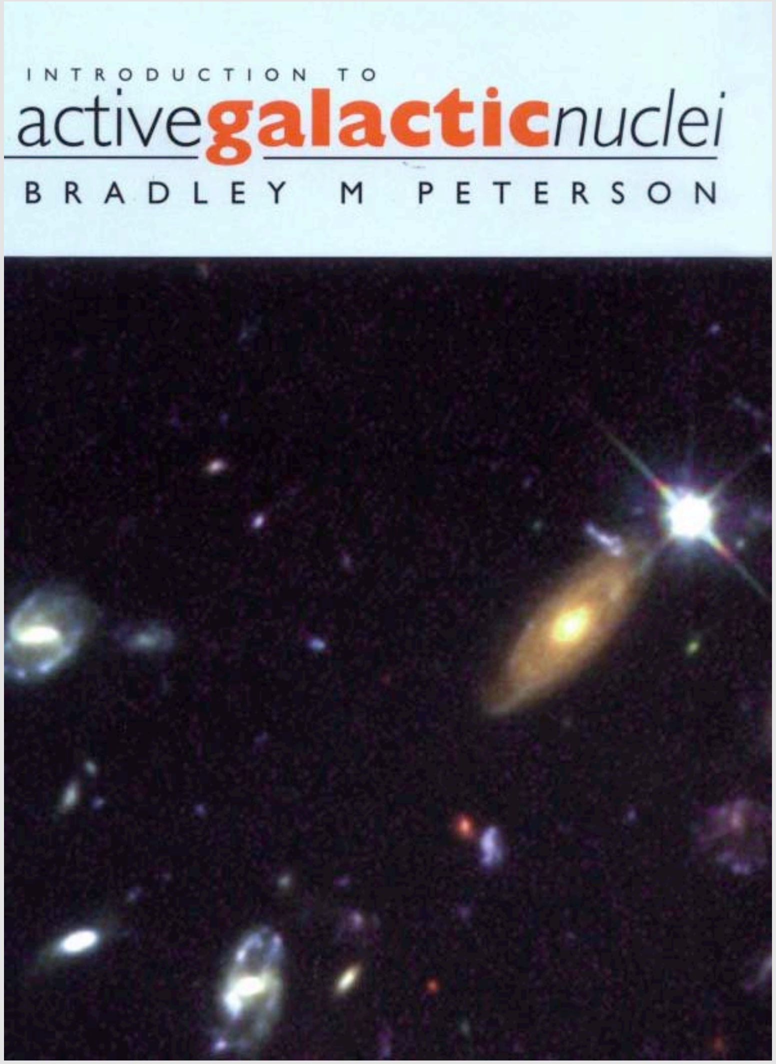

Some Useful Books

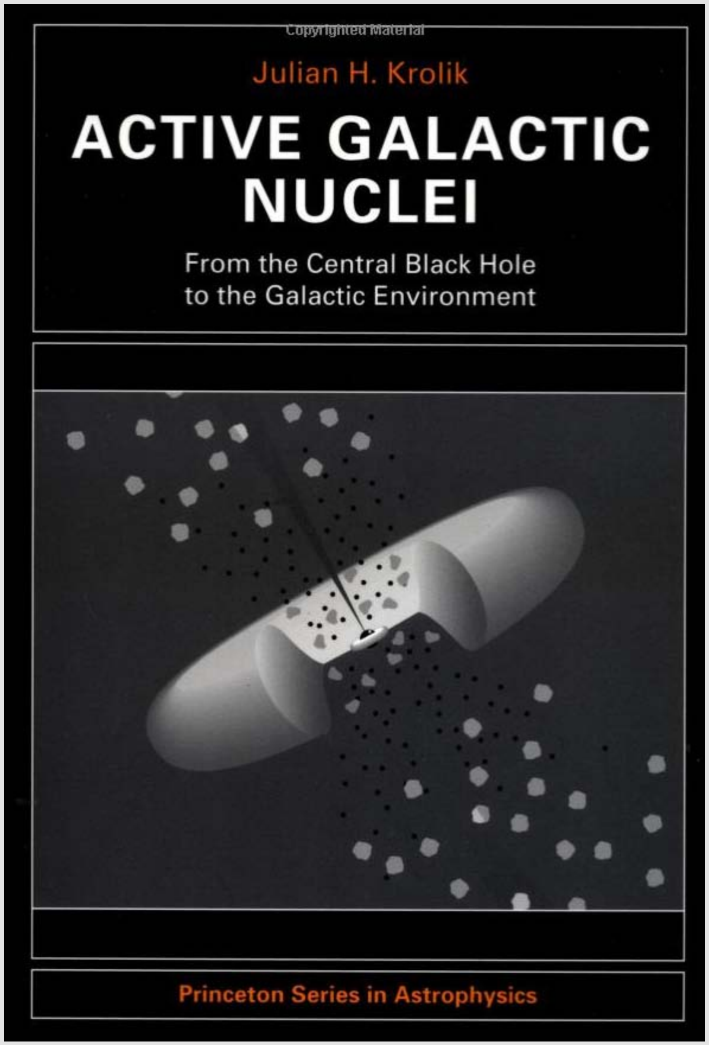

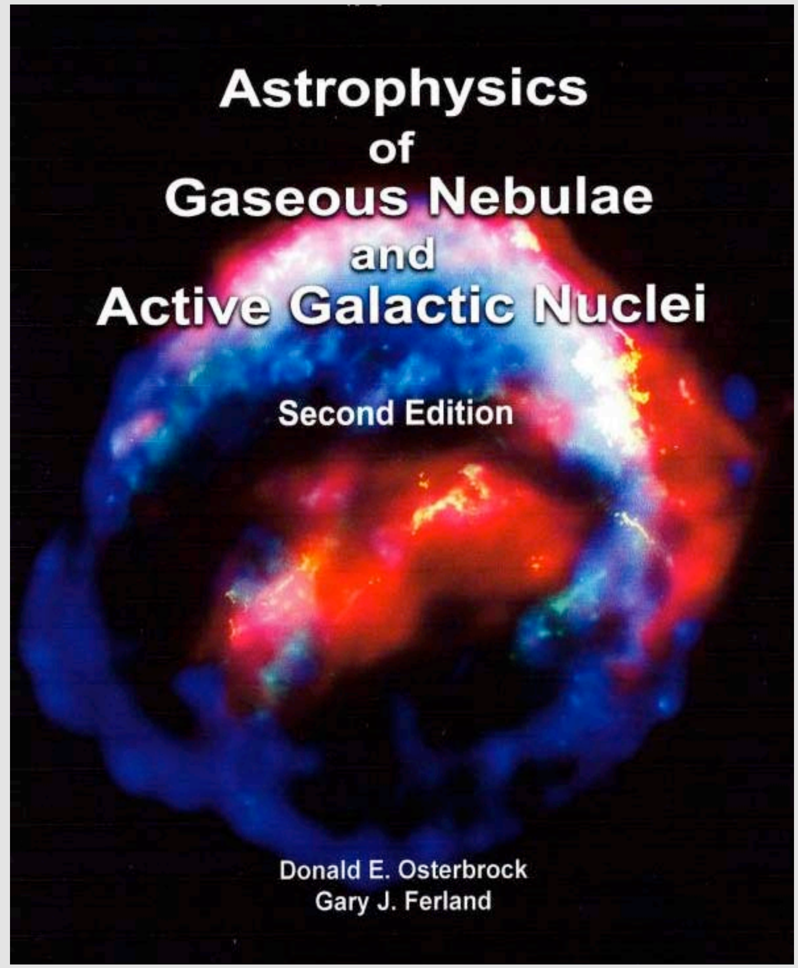

Questions

Questions are strongly encouraged at any time!

I may defer some questions until I have had time to develop the relevant underlying context to address them well (remind me if I forget a deferred question).

Certainly happy to talk outside the lectures as well.

Introduction, AGN Basics, Finding AGNs, and Terminology

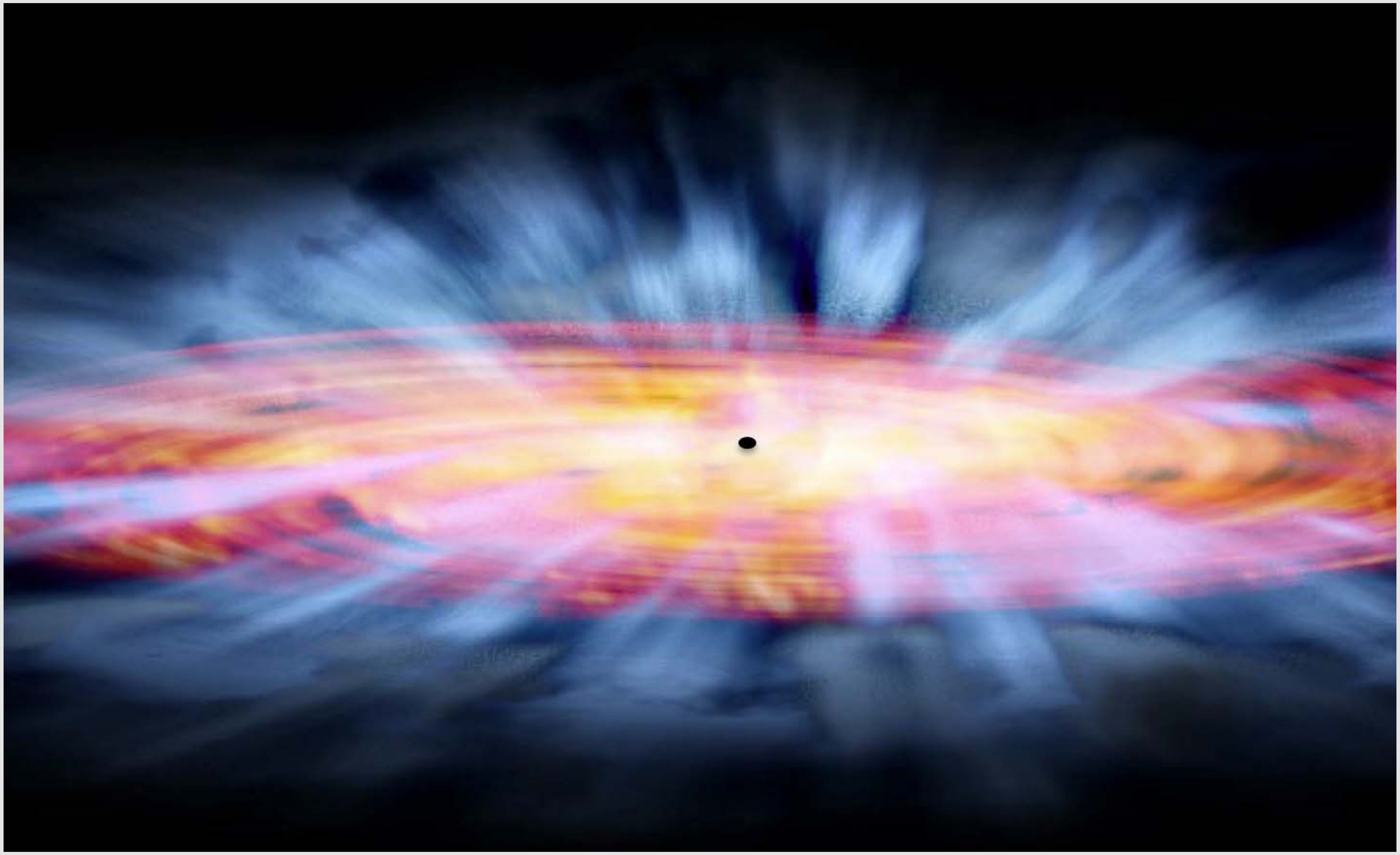

Some Early History of AGN Studies

Some Early History

1908 – Edward Fath notices strong emission lines from H, O, Ne in the nuclear spectrum of NGC 1068

1915 – General Relativity

1916 – Schwarzschild solution found, but not fully understood

1917 – Vesto Slipher obtains a higher quality spectrum of NGC 1068 and notes its emission lines are unusually broad

1918 – Herber Curtis notes in M87 a "curious straight ray … connected with the nucleus by a thin line of matter"

1924-1929 – General realization that galaxies are extragalactic – led by Edwin Hubble

1926 – Edwin Hubble notices the nuclear emission-line spectra of NGC 1068, NGC 4051, NGC 4151

Some Early History

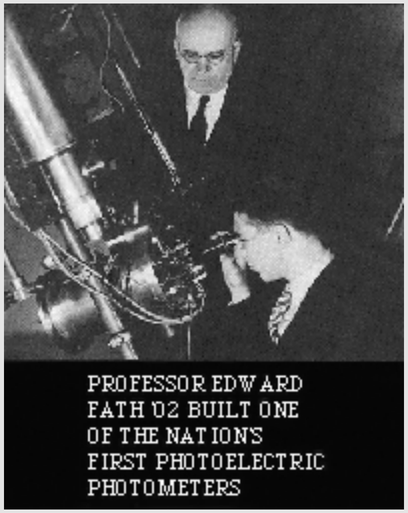

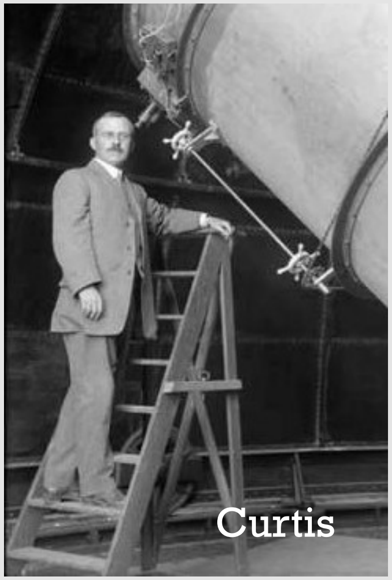

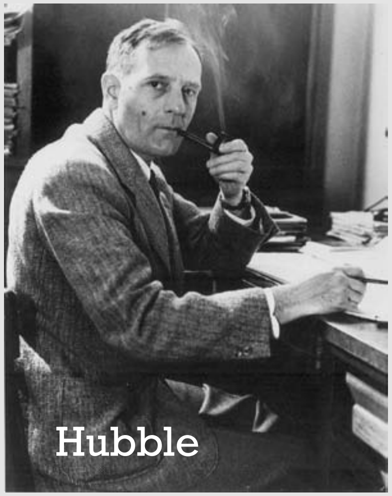

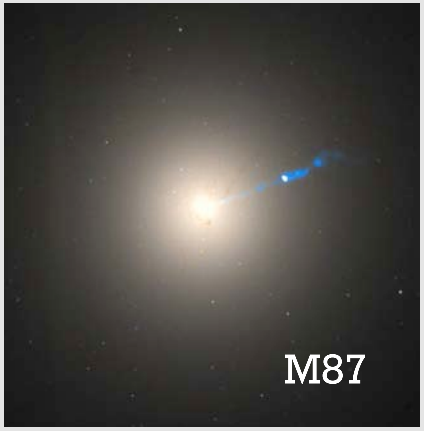

Some Early History

1939 – Grote Reber discovers the radio source Cygnus A

1943 – Carl Seyfert shows that a fraction of galaxies have strong, broad emission lines and that these galaxies are especially luminous – now known as "Seyfert galaxies"

1954 – Walter Baade and Rudolph Minkowski find the counterpart to Cygnus A at $z = 0.057$

1963 – Maarten Schmidt discovers 3C273 to have $z = 0.158$

1964 – Zeldovich & Novikov and Salpeter speculate about black holes powering quasars

1967 – The term "black hole" comes into general use

1968 – Donald Lynden Bell notes that many galactic nuclei may contain "collapsed old quasars"

After – AGNs become a topic of widespread study

Some Early History

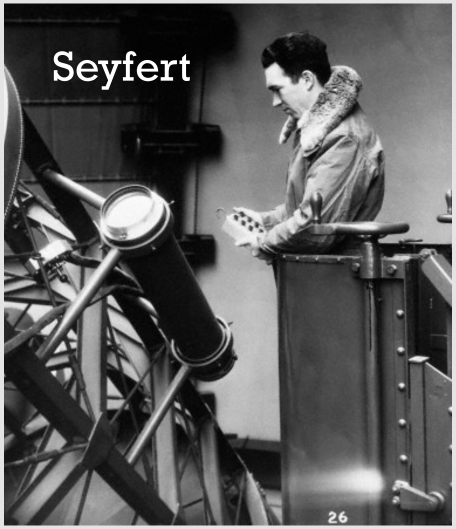

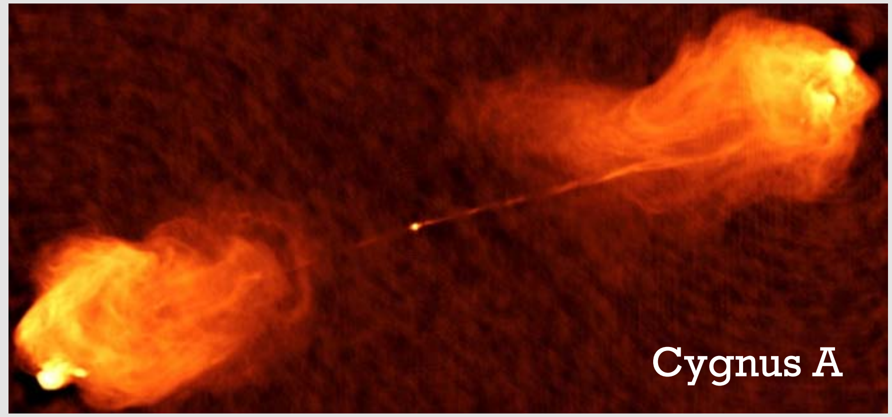

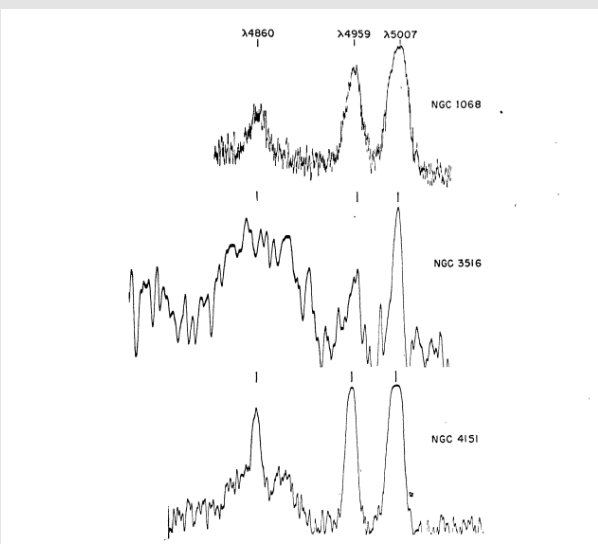

FIG. 1.—Microphotometer tracings of the emission lines λλ 4860 ($H\beta$), 4959 and 5007 [O III] in the nebulae NGC 1068, 3516, and 4151.

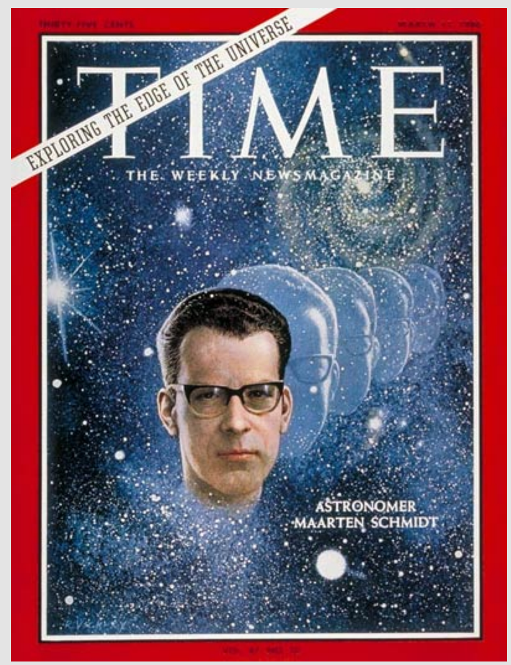

Basic Observed Properties

Normal Versus Active Galaxies

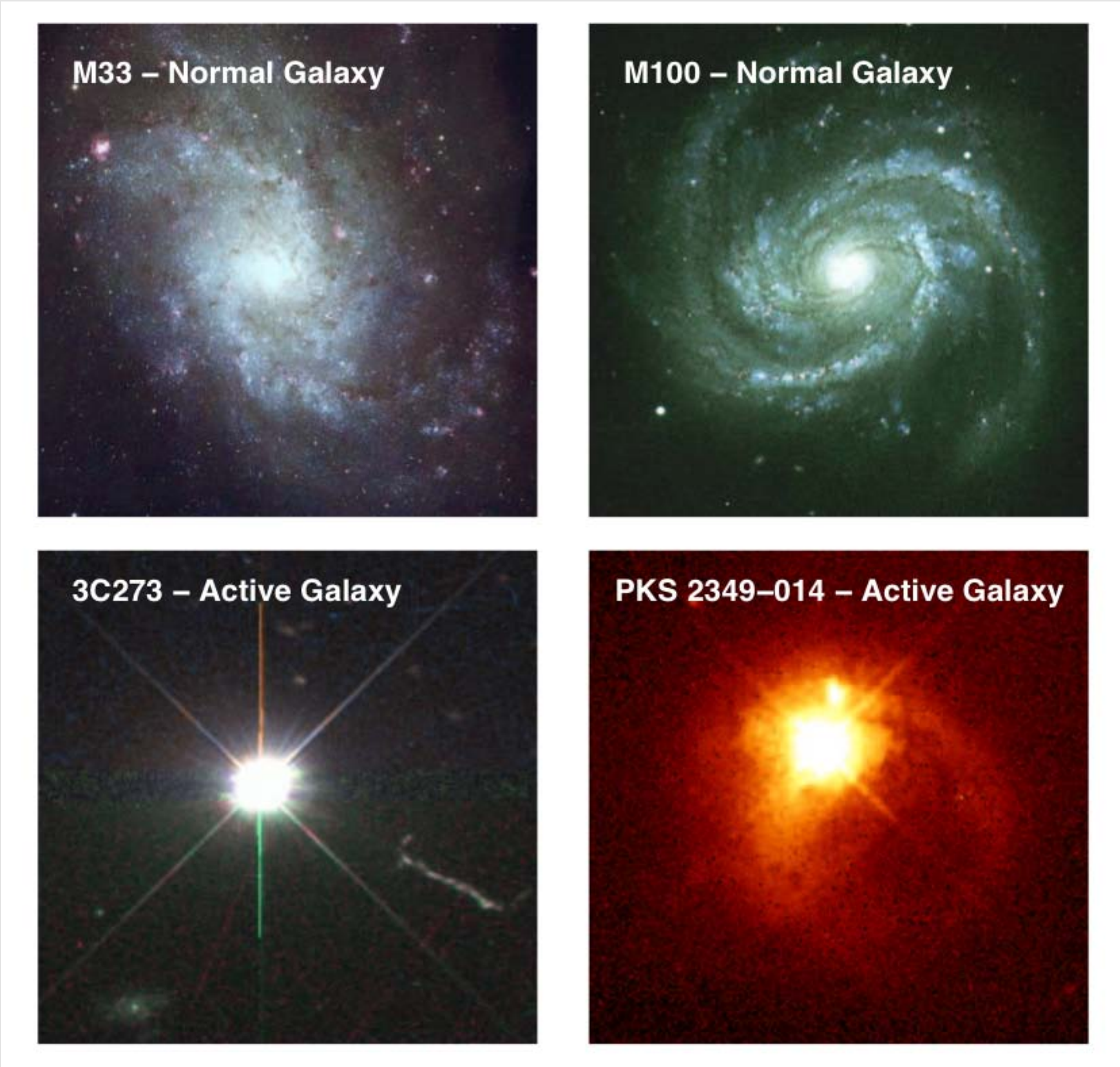

In the local universe…

~ 10^{-6} of massive galaxies contain luminous quasars

~ 5% are moderately luminous (Seyfert galaxies)

~ 30% show signs of low-level nuclear activity

Basic Observed Properties of AGNs

Broad range of luminosities, reaching very large values.

Strong and broad optical/UV emission lines.

Emission over a very broad band.

Variability.

Particle jets.

Broad Range of Luminosities, Reaching Very Large Values

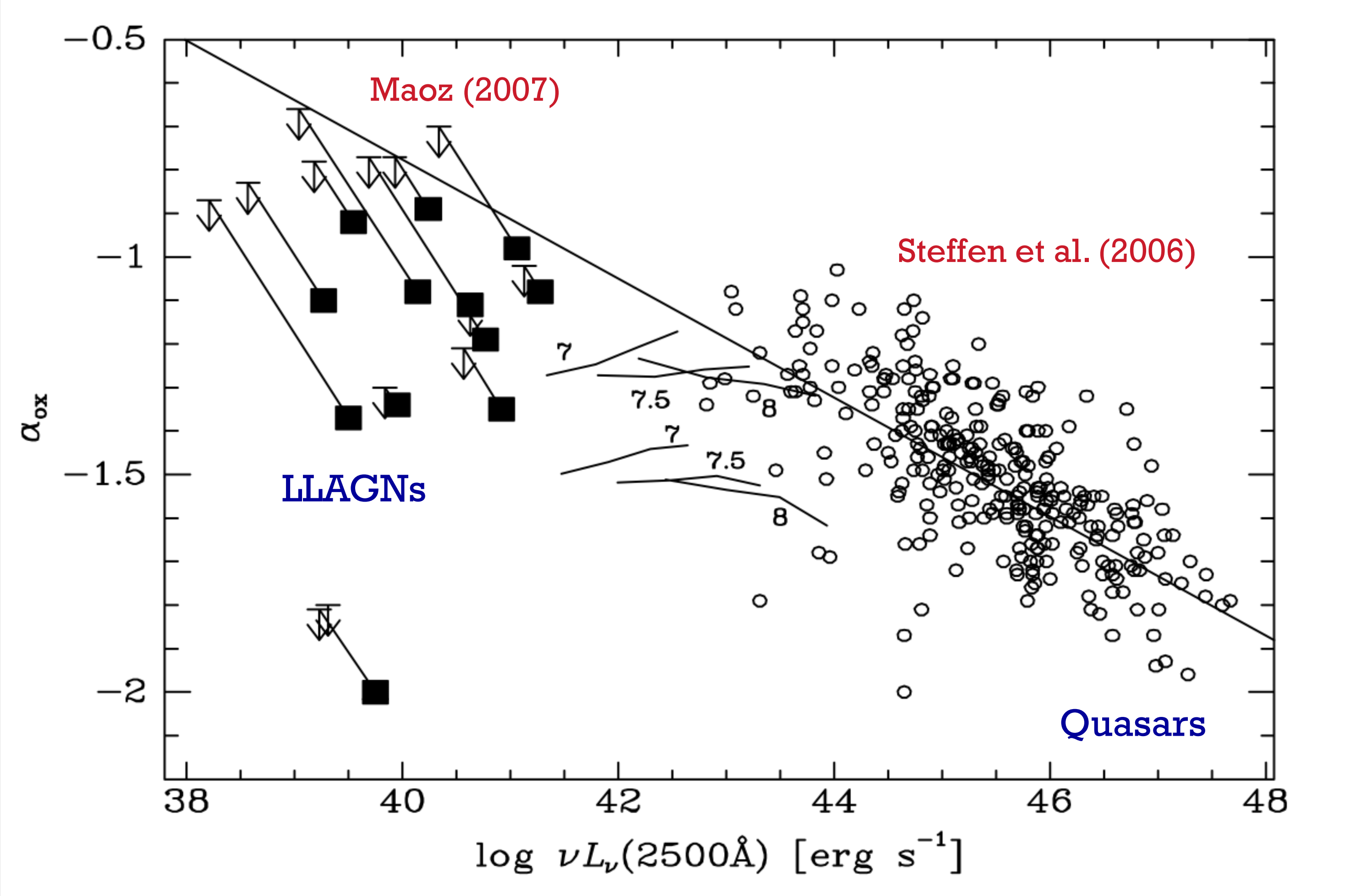

Broad Range of Luminosities, Reaching Very Large Values

Span 9+ orders of magnitude in luminosity.

There is no strict lower limit on luminosity; e.g., even the black hole at the center of our Galaxy shows some intermittent activity at very low levels.

At very low luminosities, the distinction between active and normal galaxies is largely semantic. There is no clear bimodal separation of properties, for example.

There is a maximum observed luminosity, and we believe that we have found examples of the most luminous AGNs that exist (i.e., the most luminous quasars).

Strong and Broad Optical/UV Emission Lines

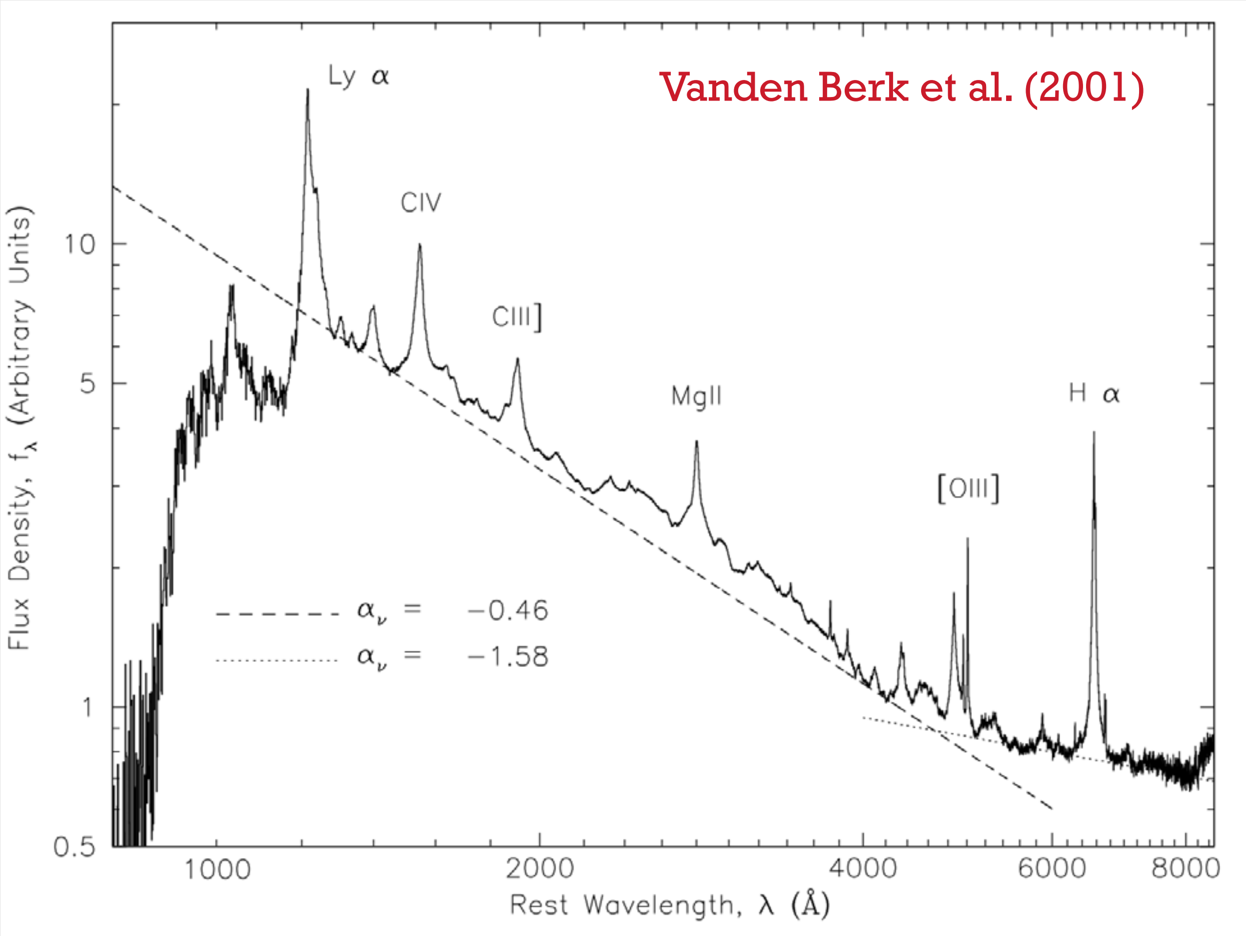

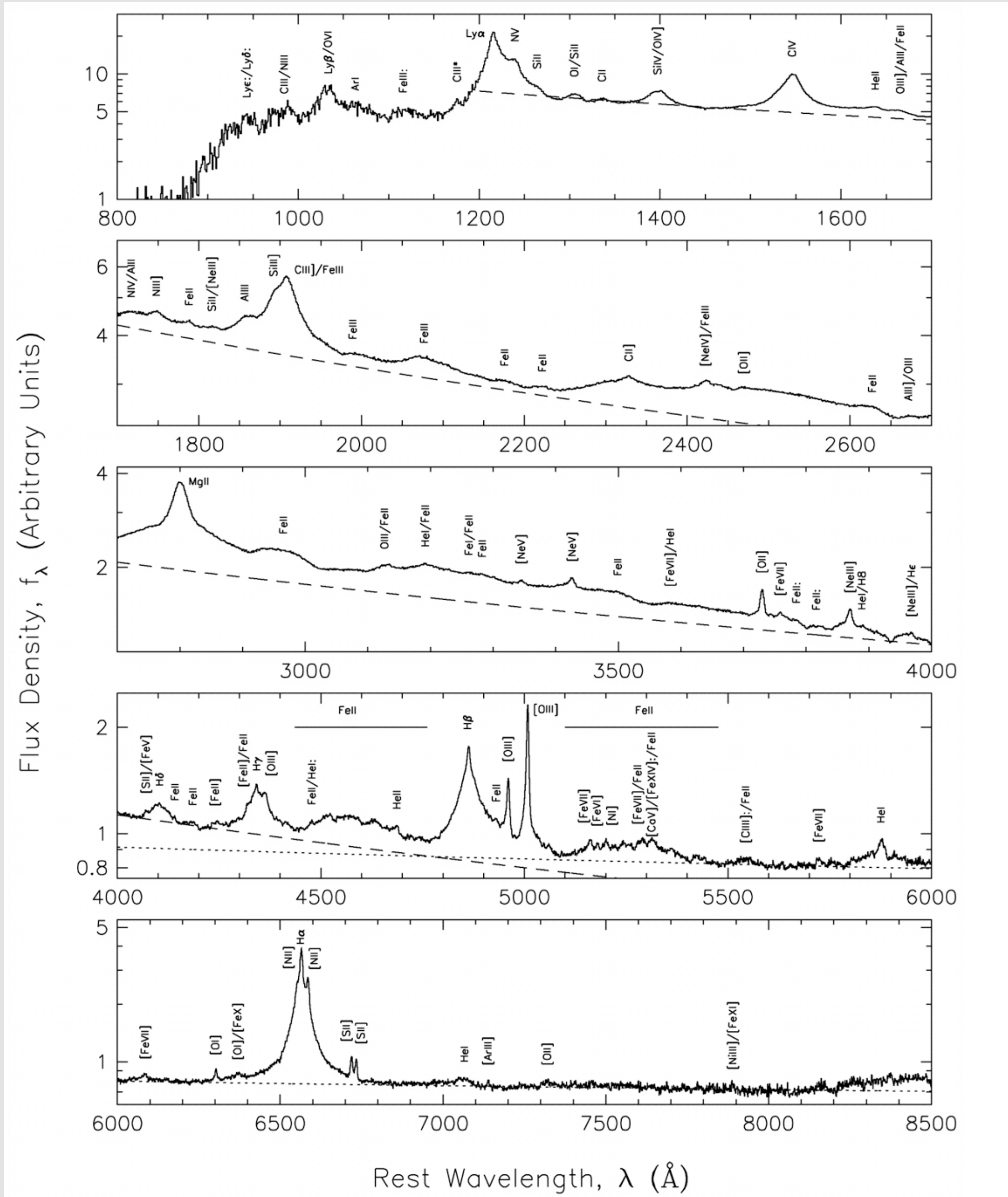

Vanden Berk et al. (2001)

Strong and Broad Optical/UV Emission Lines

Indicate the presence of ionized nebular gas.

Gas is photoionized by the brilliant central source.

Line widths indicate high-speed motions with a wide range of velocities, up to ~ 25000 km s^{-1}.

Abundances about solar or slightly supersolar.

Also Often See Blueshifted Absorption Lines

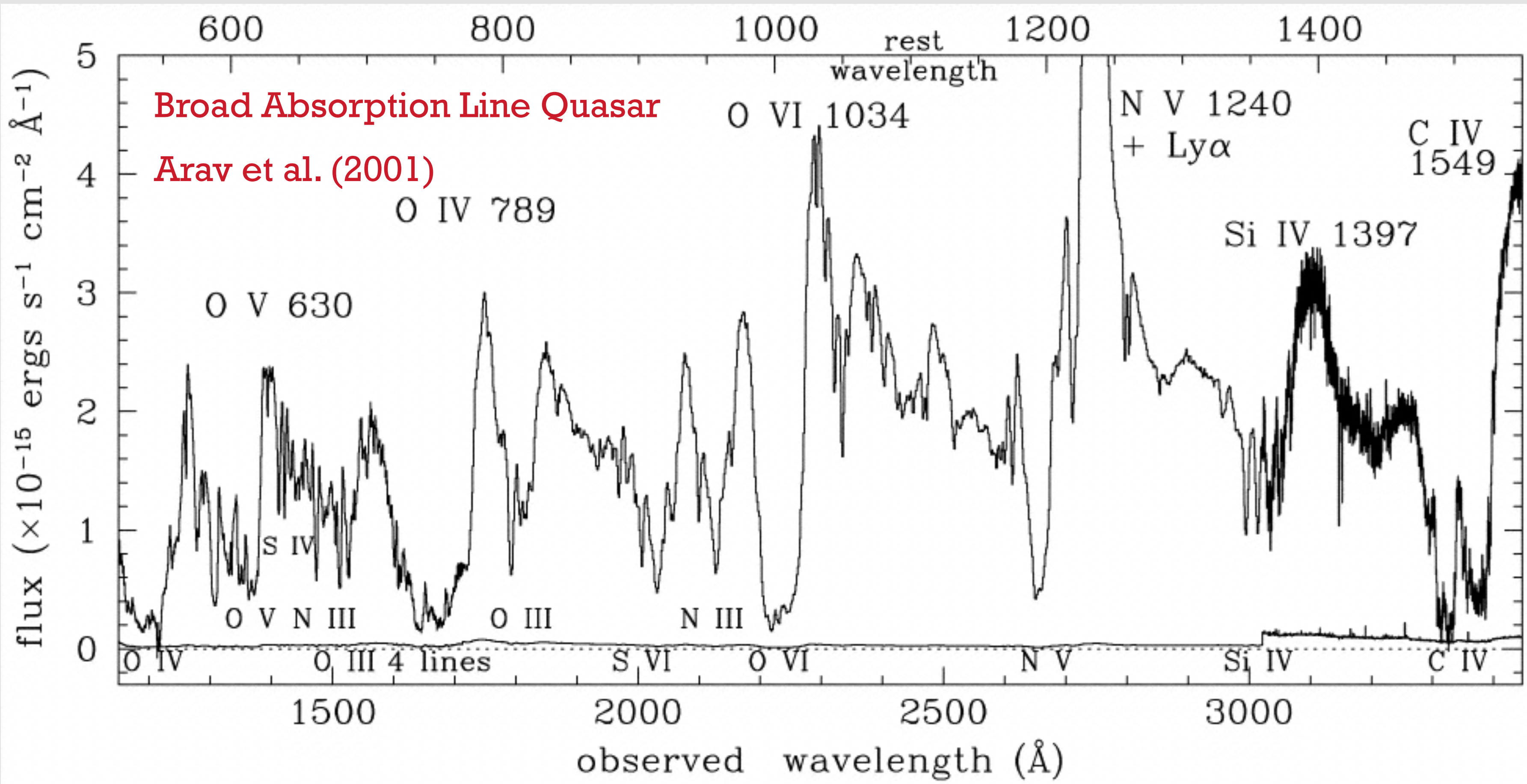

Emission Over a Very Broad Band

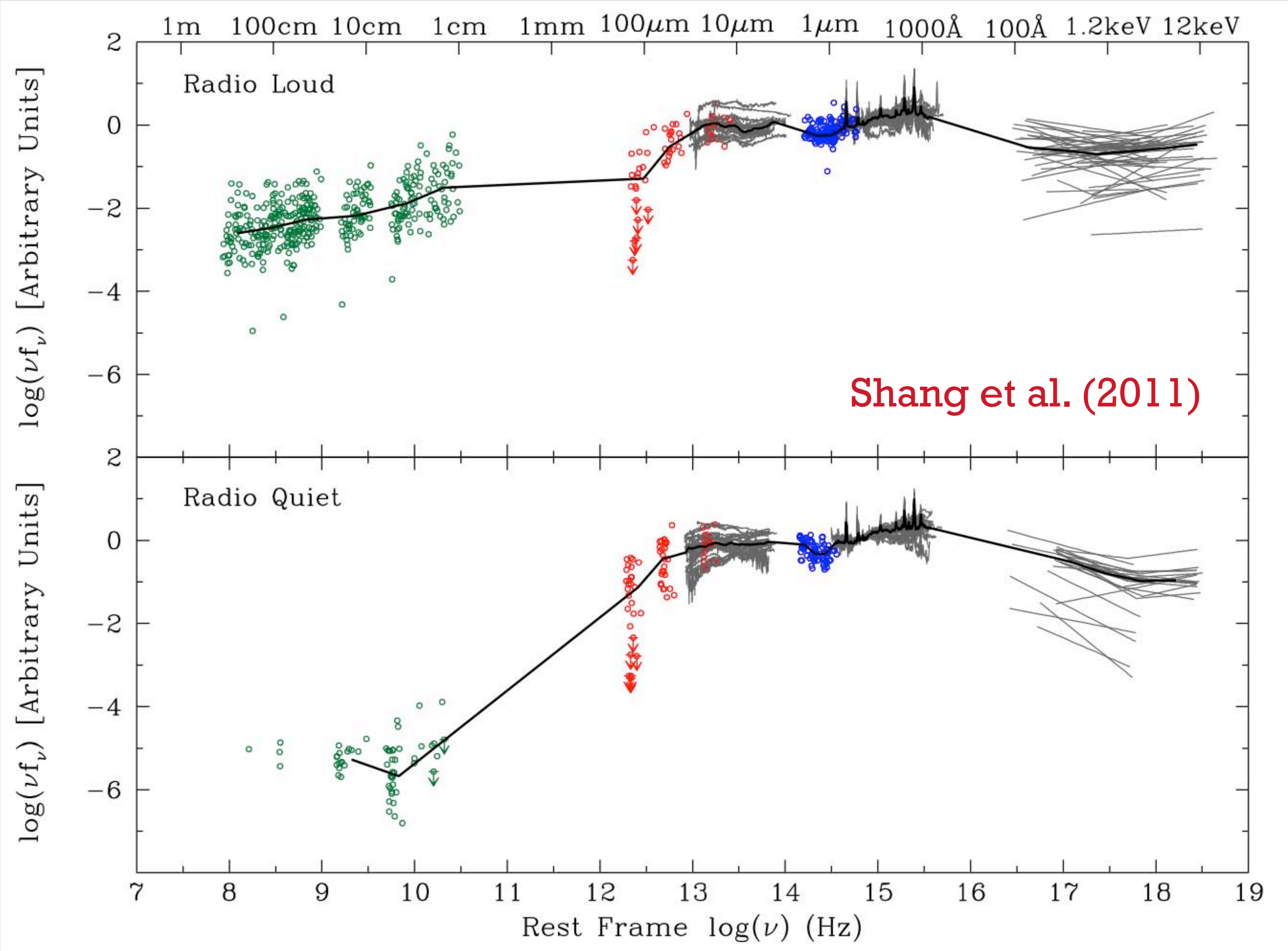

Emission Over a Very Broad Band

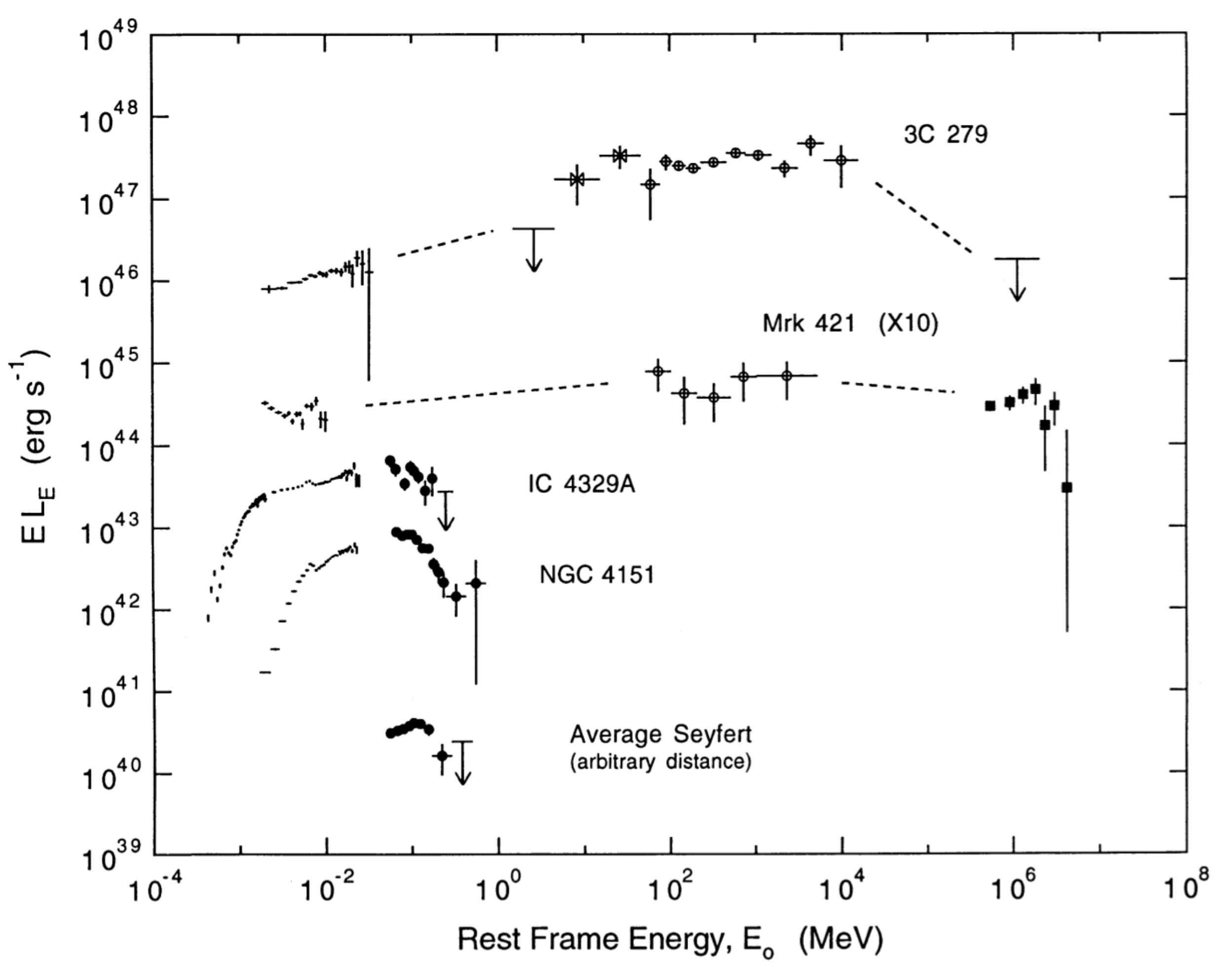

Dermer & Gehrels (1995)

Variability of AGNs

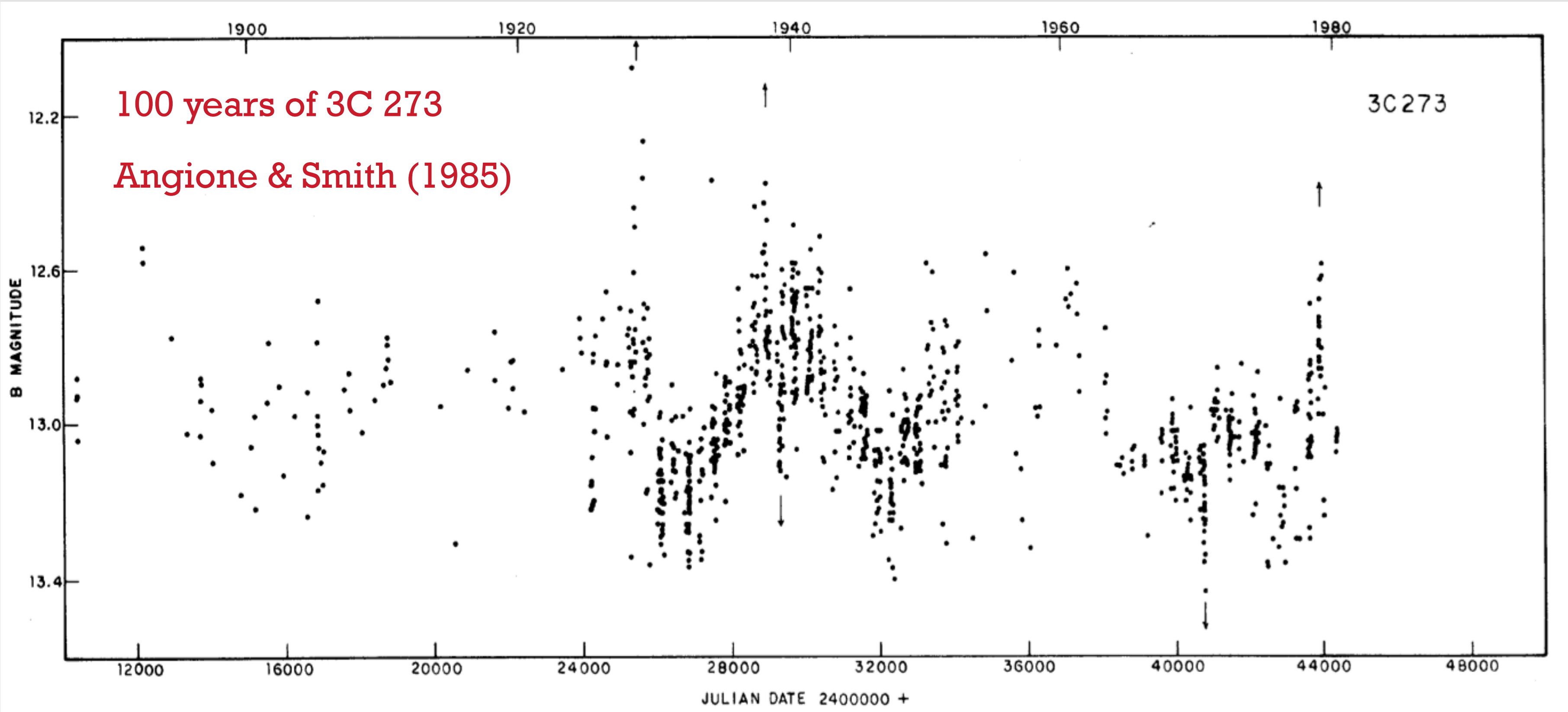

Noted as variable sources even in the 19th century, but misclassified as variable stars.

Variability could have allowed their discovery even earlier.

The variability is generally chaotic without a clear period or quasi-period.

Multiwavelength Variability of AGNs

Long-Term Variability of 3C 273 at Many Wavelengths

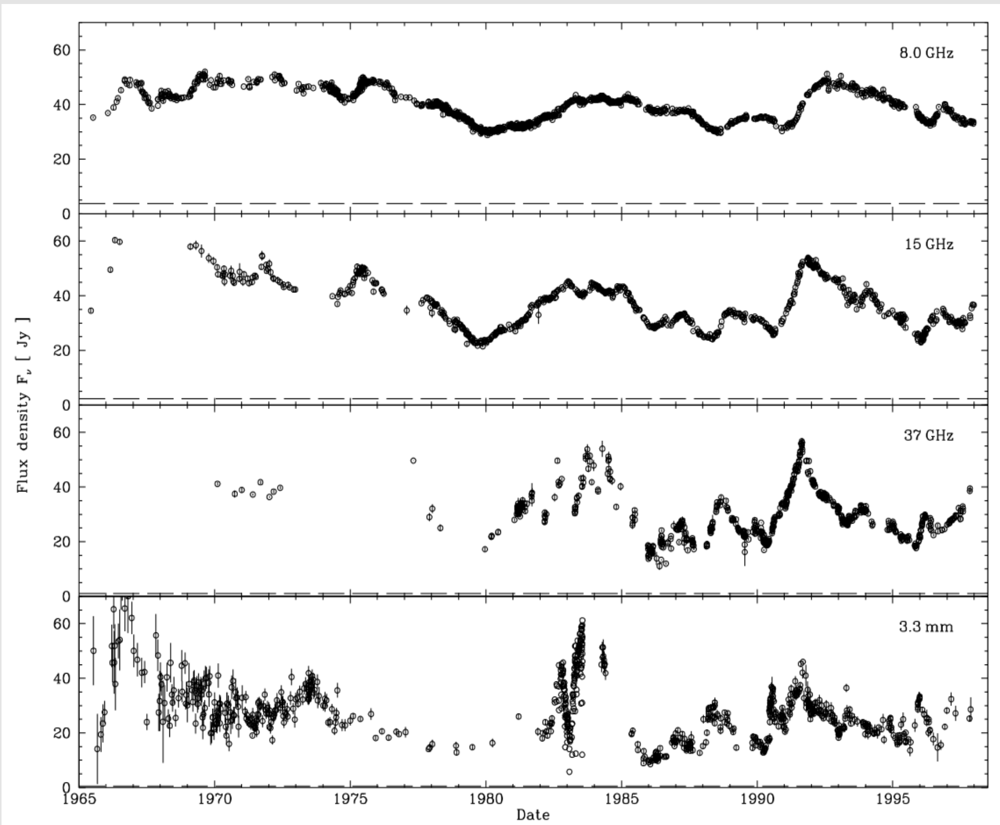

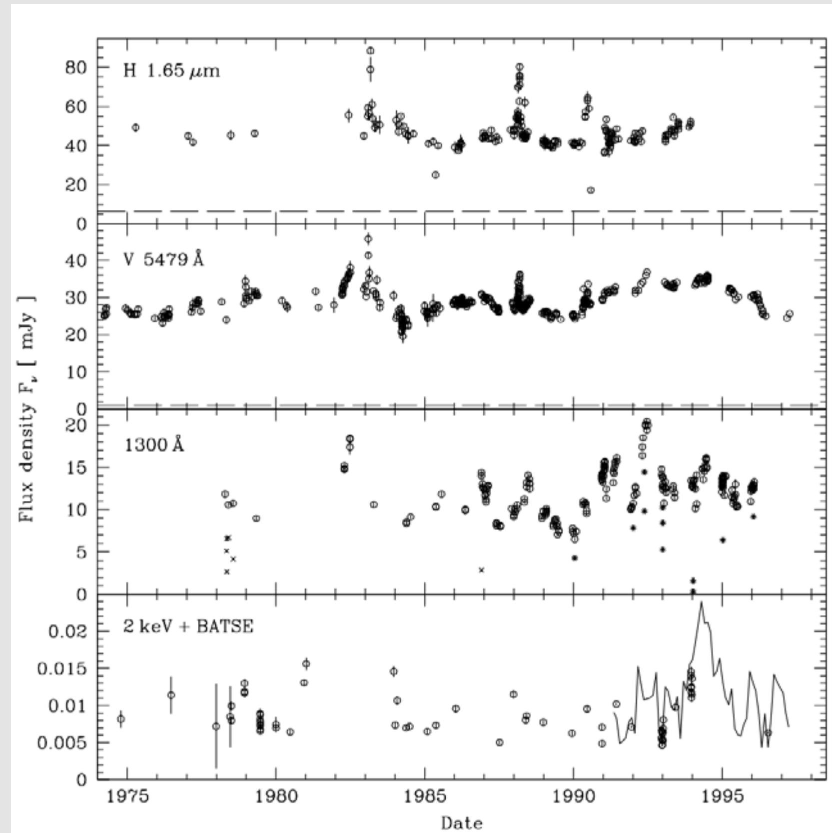

Variability in different bands is often correlated.

Turler et al. (1999)

X-ray Variability of AGNs

Example of Rapid X-ray Variability on Timescales Down to Minutes

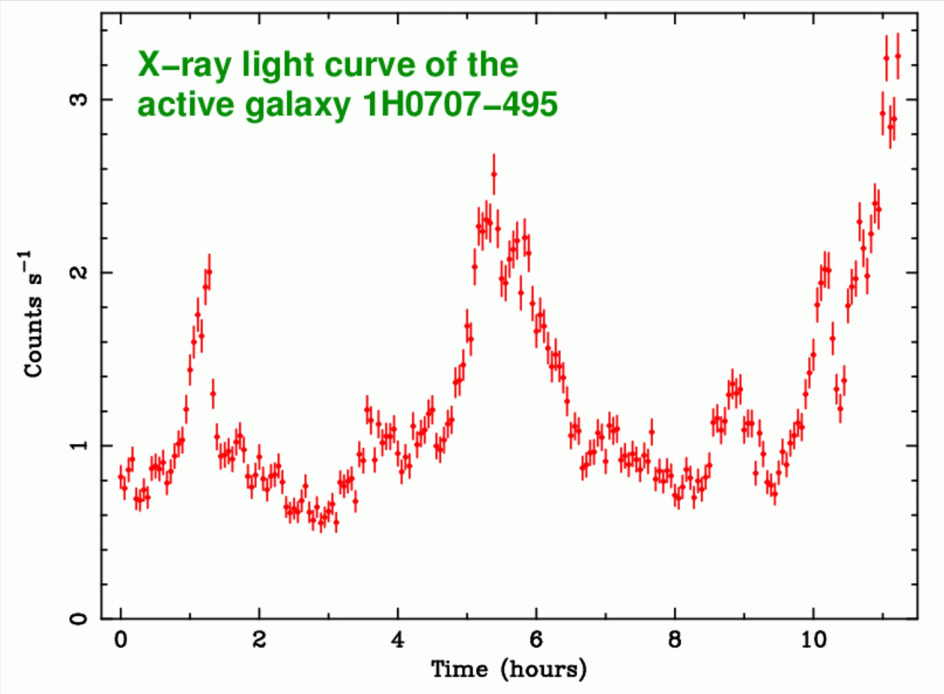

Long-Term 2-10 keV Monitoring of Five Seyfert Galaxies

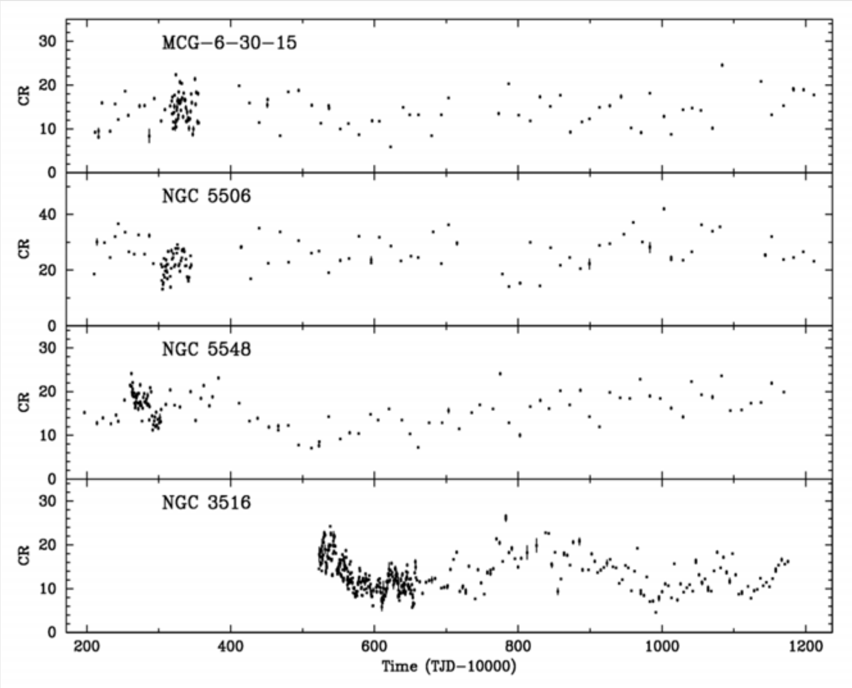

Broadly speaking, variability becomes larger amplitude and more rapid as one moves to higher frequencies.

X-ray variability often implies an emission-region size of light hours or less.

Emission-Line Variability

C IV Variability in NGC 5548

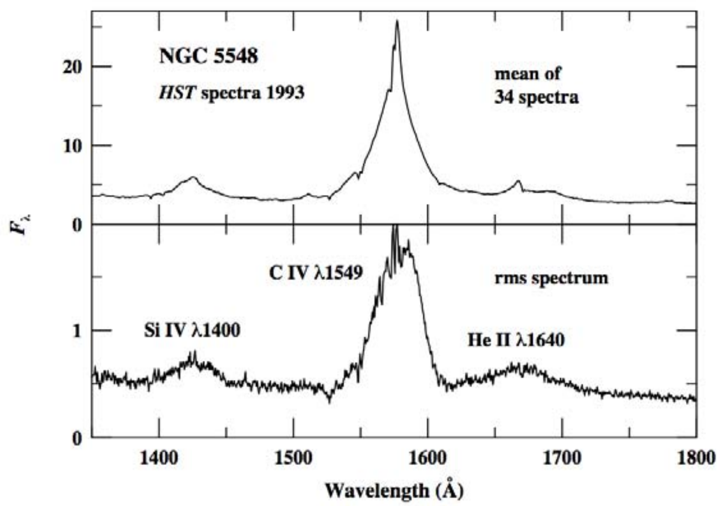

Figure 4. The top panel shows the mean spectrum computed from 34 HST spectra of the variable Seyfert 1 galaxy NGC 5548[40]. The lower panel shows the rms spectrum based on variations around this mean. The rms spectrum thus isolates the variable components of the spectrum. Fluxes are in units of 10^{-15} ergs s^{-1} cm^{-2} $Å^{-1}$.

Hβ Variability of Markarian 335

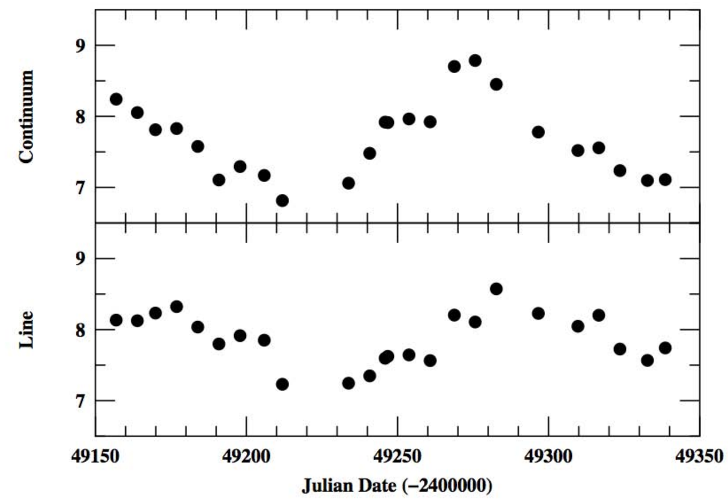

Figure 23. The Hβ emission-line and optical continuum fluxes for Mrk 335, as shown in Fig. 22, are plotted as a function of time. It is clear from the figure that the continuum and emission-line fluxes are well-correlated, and that the correlation can be improved by a linear shift in time of one time series relative to the other. The optimum linear correlation occurs by shifting the emission-line light curve backwards by 15.6 days.

Peterson (2001)

The broad emission lines also vary, generally following the continuum with a lag.

Leads to the idea of "reverberation mapping", as will be discussed later.

Cannot Image the Main Emission Regions

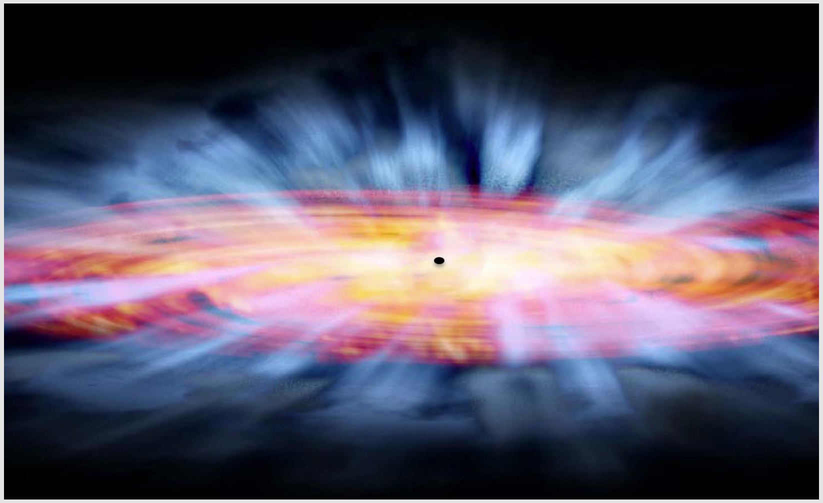

The observed variability implies that the main emission regions have sizes of light hours to light days (or less).

Even for close AGNs, this implies angular sizes of ~ 10^{-6} to 10^{-5} arcsec.

This is too small to image directly.

For comparison, VLBA interferometry gives typical resolutions of ~ 0.0002 arcsec.

Images like those shown are only artist's impressions.

Particle Jets

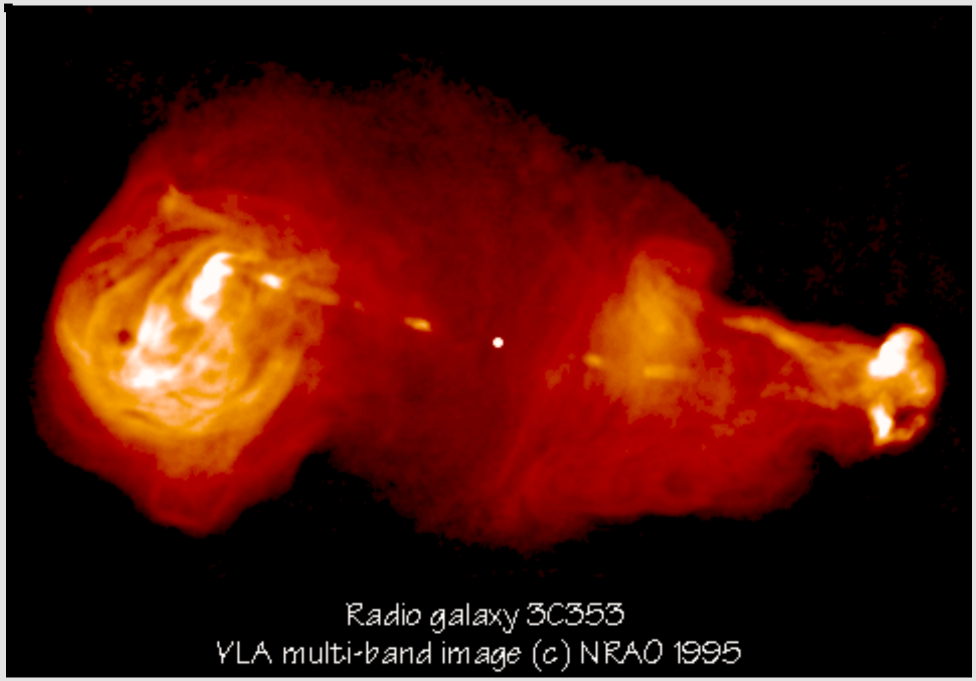

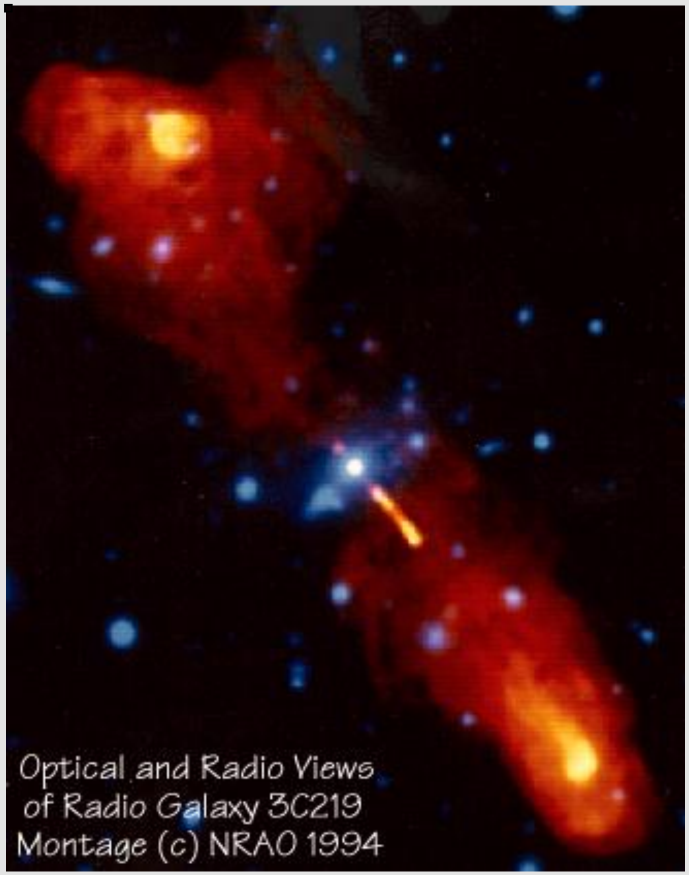

A significant minority of AGNs (about 10%) emit powerful particle jets.

These produce strong radio emission via synchrotron – such AGNs are "radio loud".

Particle Jets

Zooming in on the jet of M87.

Note the pointing stability over a very long timescale.

Implies some "gyroscope" keeping the pointing fixed.

Can trace the jet down to the vicinity of the SMBH.

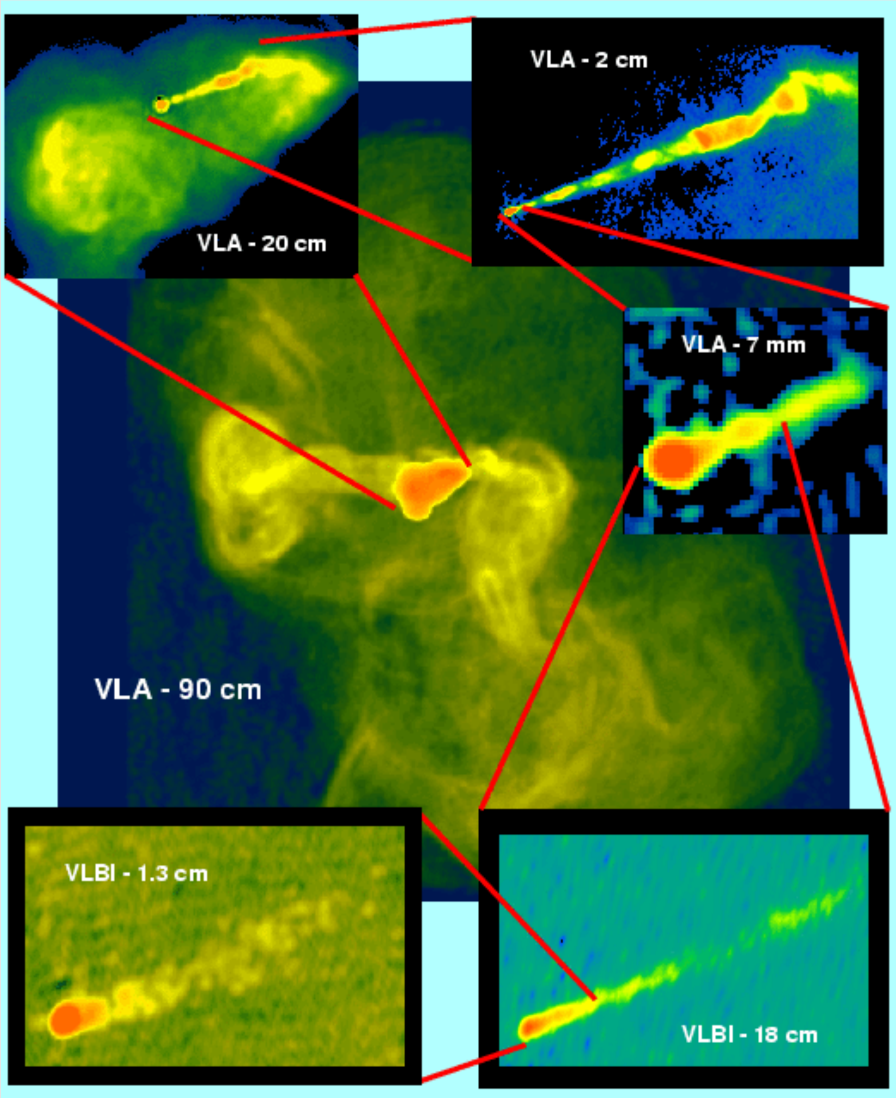

Basics of the Black Hole Plus Accretion Disk Model

Observed Phenomena Needing Explanation

Broad range of luminosities, reaching very large values.

Strong and broad optical/UV emission lines.

Emission over a very broad band.

Variability.

Particle jets.

Black Hole + Accretion Disk Model

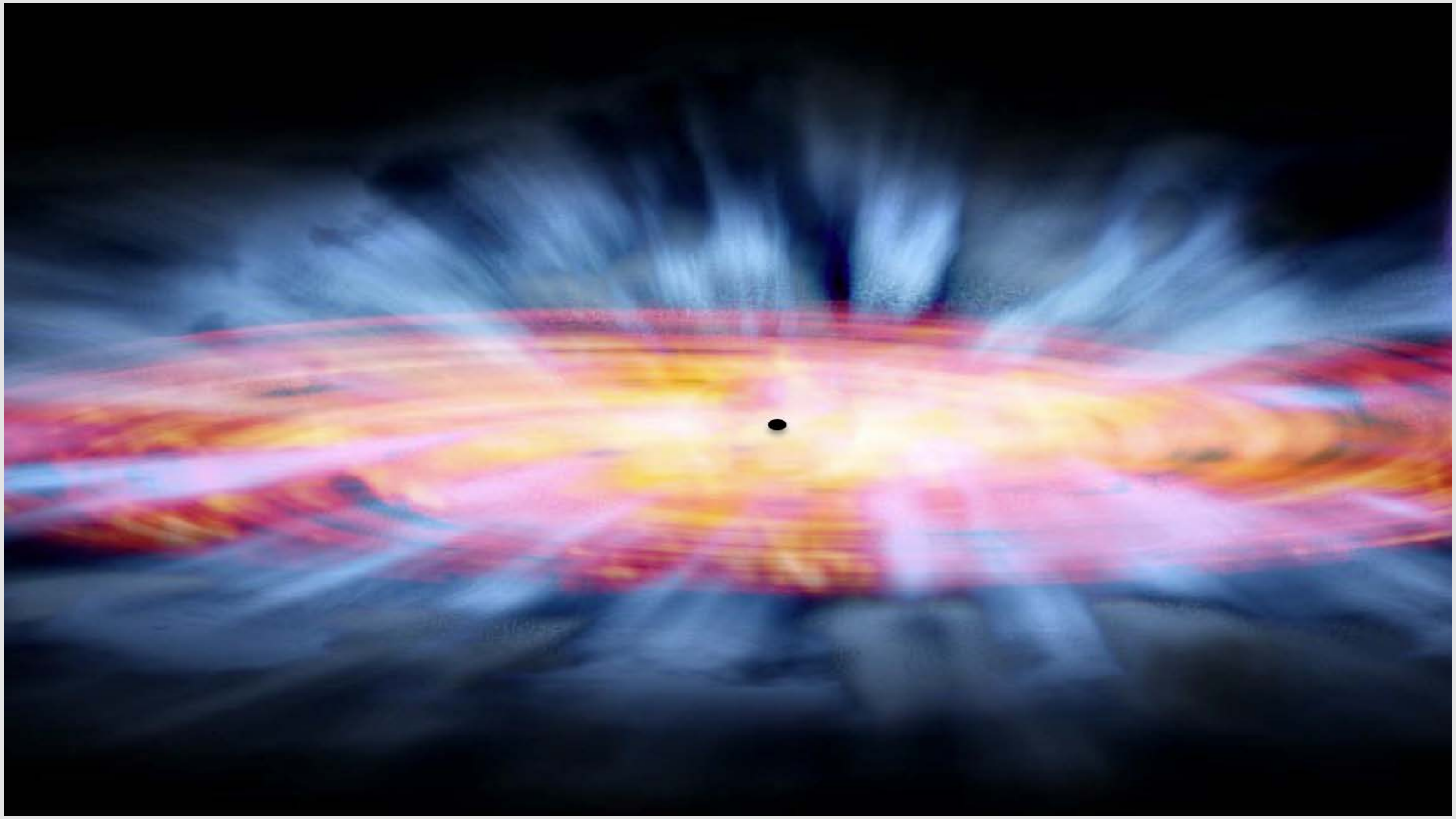

AGNs are accreting supermassive black holes (10^5-10^{10} $M_\odot$) radiating ~ 10^6-10^{15} $L_\odot$.

Accretion disk is multi-temperature, partly accounting for broad-band emission.

Optical/UV emission lines come from high-speed photoionized gas – disk, winds, clouds.

Black-Hole Accretion is Very Efficient

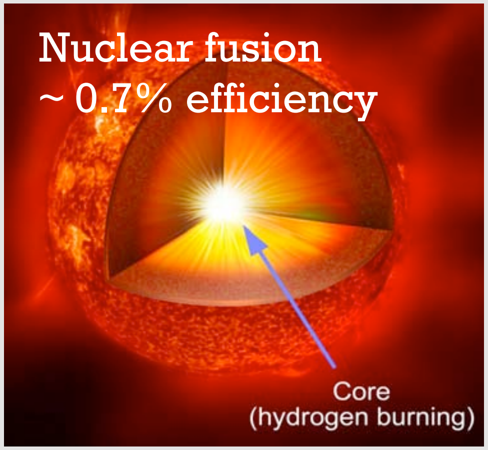

Origin of the X-ray Emission

~ Light-minutes scale

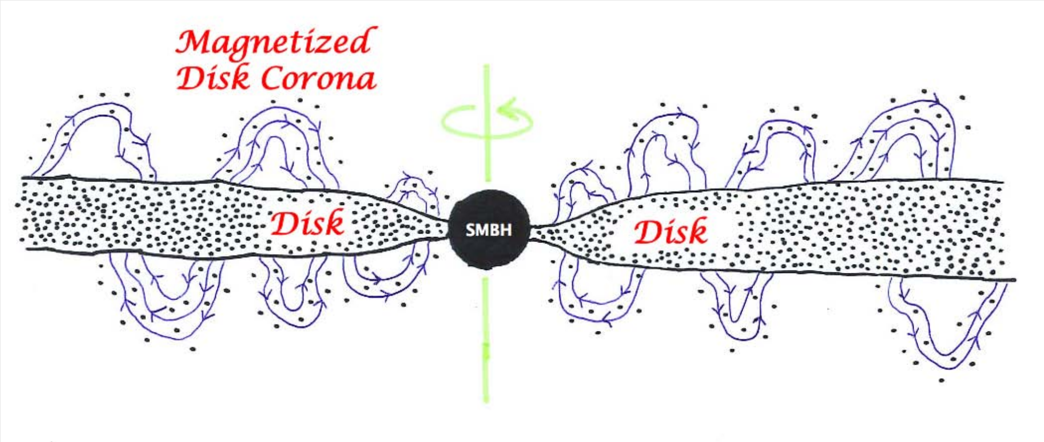

X-rays are not naturally produced by AGN disks; the disk is too cool.

Need to add an accretion disk "corona" with a temperature of ~ 150 keV.

This makes X-rays by Compton scattering.

Perhaps low-energy X-rays from disk component.

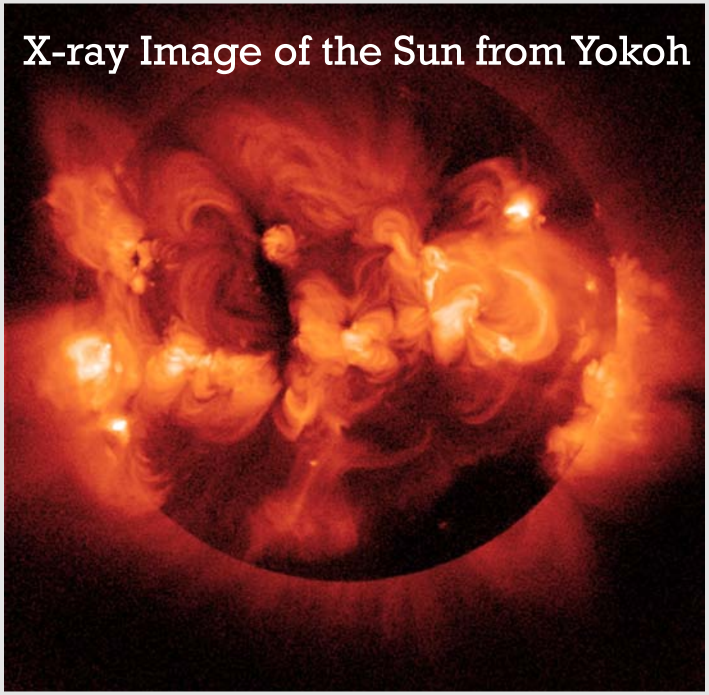

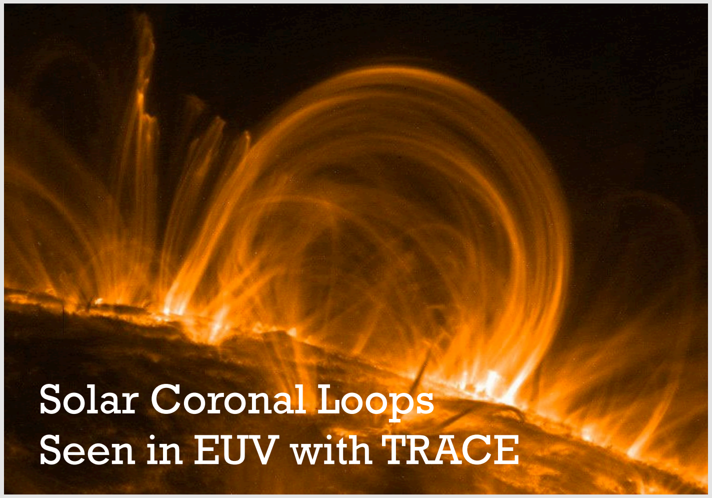

Schematic Spectrum from Disk + Corona

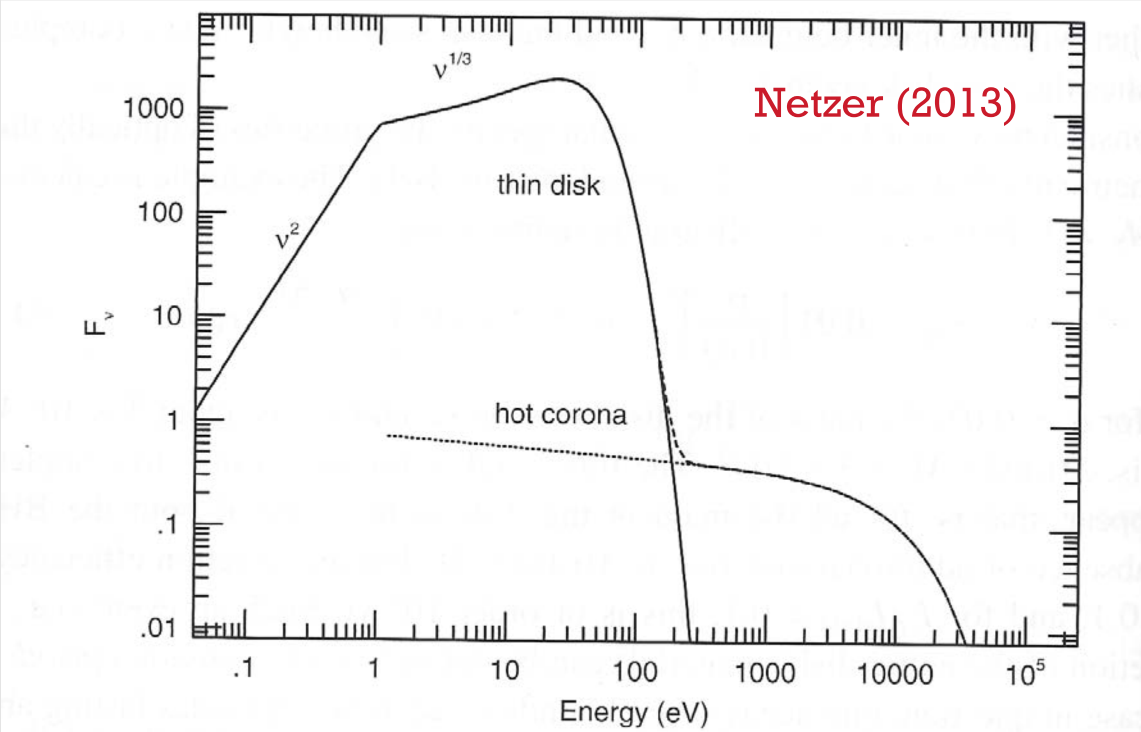

Figure 4.3. A schematic of a combined disk–corona spectrum. The maximum temperature of the geometrically thin, optically thick accretion disk is $T_{max} = 10^5$ K, and its outer boundary temperature is determined by the conditions at the self-gravity radius. The disk is surrounded by an optically thin corona with $T_{cor} = 10^8$ K.

Obscuration and Radiation Reprocessing

~ 0.1-100 light-years scale

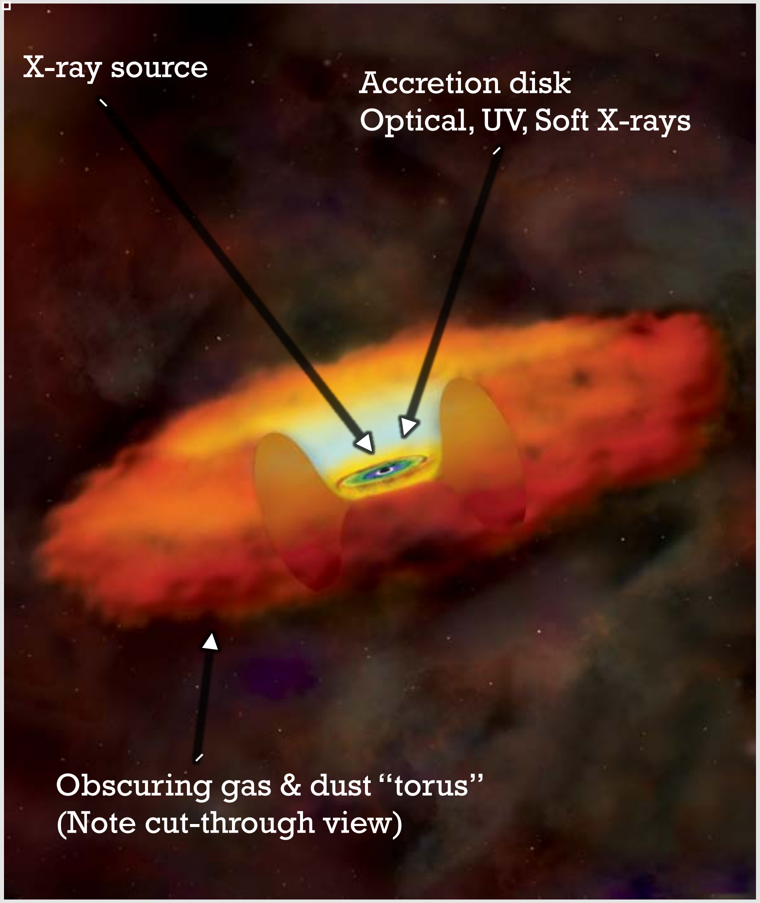

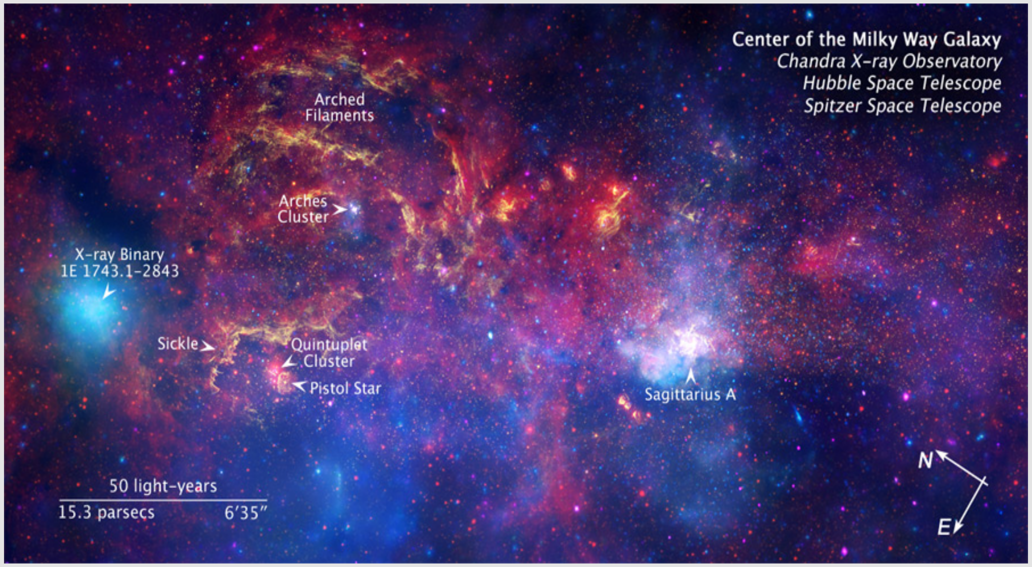

Many active galaxies have obscuring/reprocessing material, often envisioned to be in the form of a "torus".

This material likely produces much of the infrared emission as reprocessed "waste heat" from dust.

Explaining Emission Over a Very Broad Band

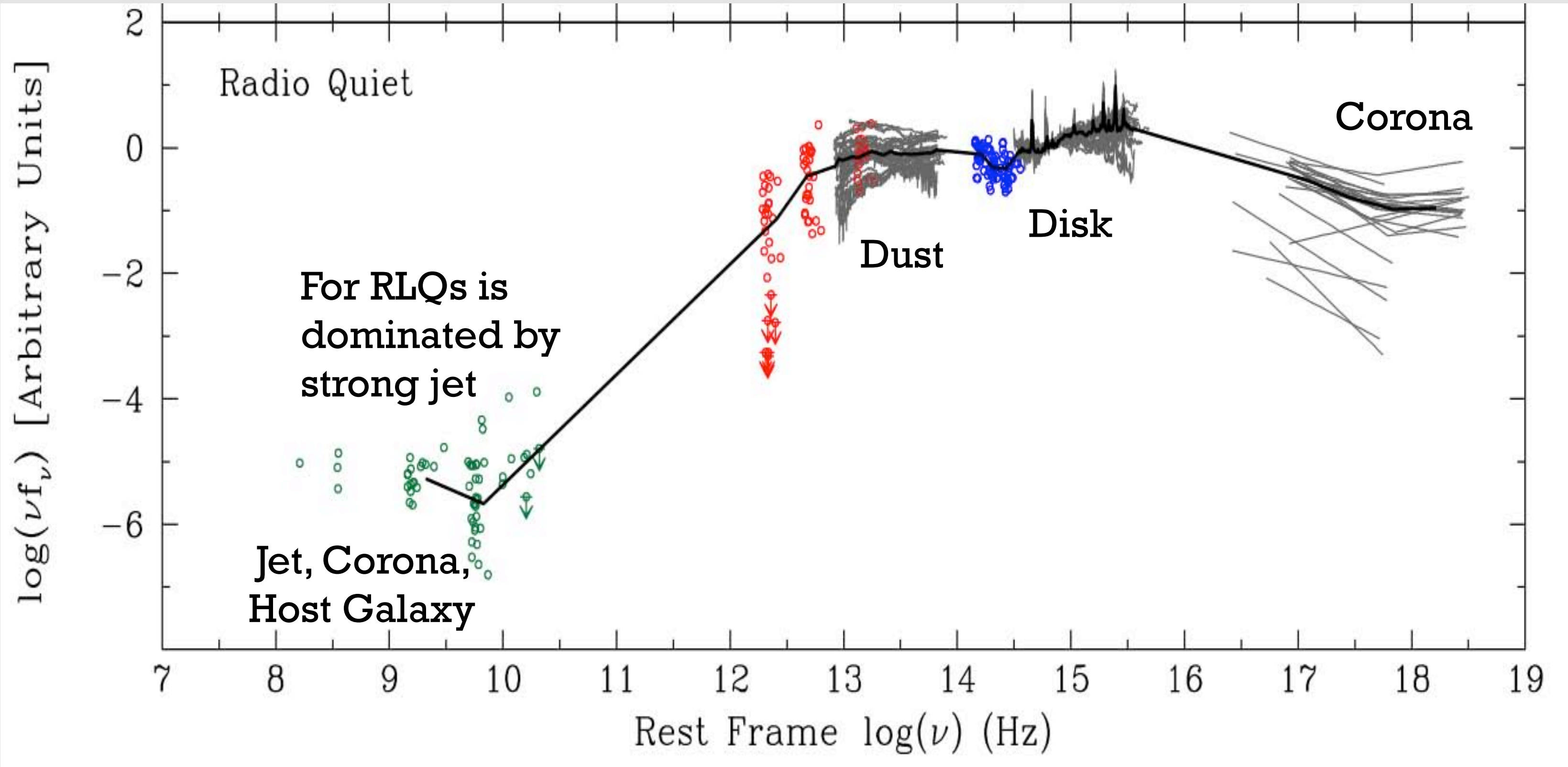

Shang et al. (2011)

Explaining Variability

The accretion disk is expected to have about the correct size to explain the observed variability timescales.

But, at a fundamental level, the physical origin of the variations remains poorly understood.

MHD simulations of accretion disks indicate several possible causes of variability: local random variations in dissipation, nonaxisymmetric structures, global precession of tilted flows, etc.

A deeper understanding will require proper simulation of both dynamics (good progress) and thermodynamics (slow progress).

Also can have variable accretion rates, variable obscuration, microlensing.

Explaining Particle Jets

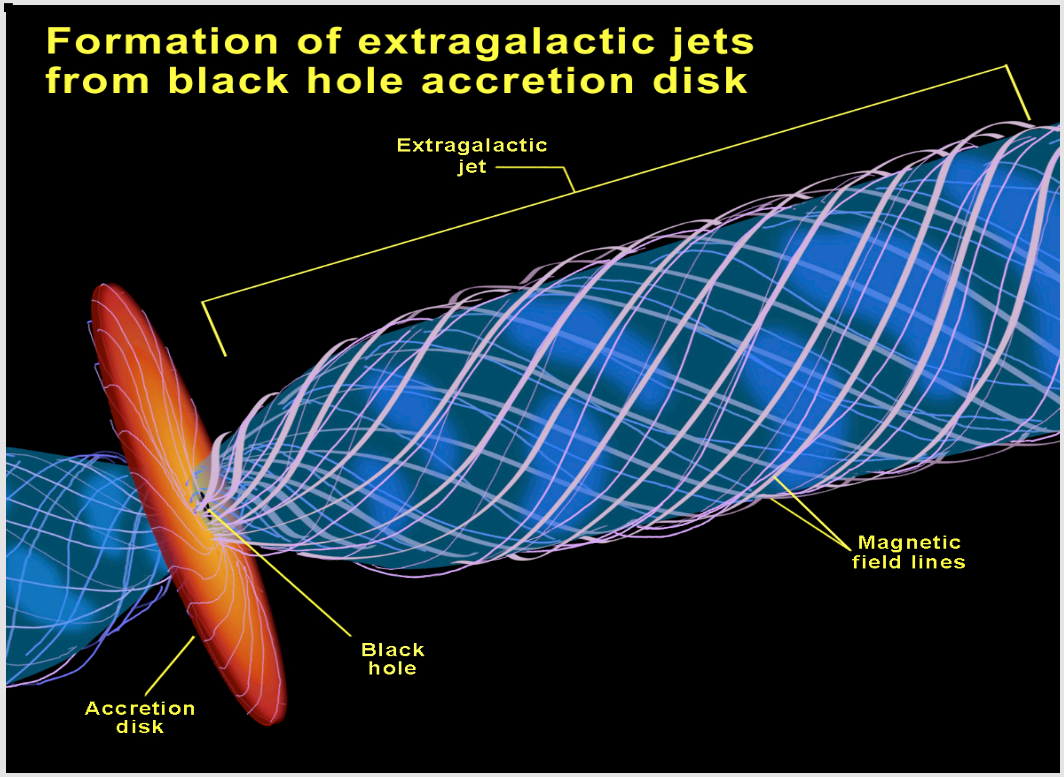

Have relativistic motions, magnetic fields, stable "gyroscope".

Finding AGNs

Need for Multiple Methods

There are many methods for finding AGNs, some as old as the subject itself.

All methods devised for finding AGNs have limitations and selection effects.

Though some are more effective and give purer samples than others.

For a complete census, want to apply as many methods as possible enabling cross-checks.

Our current census appears sufficient to answer many of the key questions about AGN populations.

Optical/UV Colors

Look for Point Sources Brighter in UV Than Normal Stars – Works to $z \sim$ 2-2.5

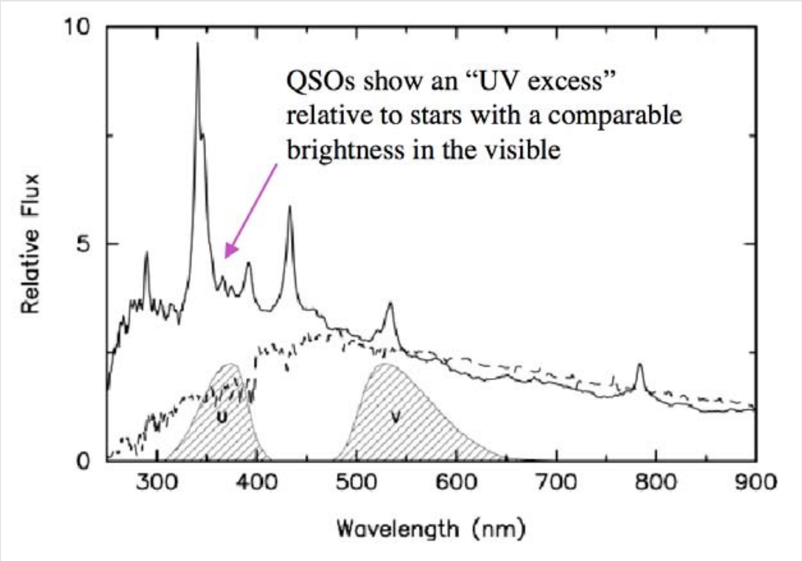

At Higher Redshifts, Absorption by the IGM Makes Quasars Very Red in Blue Part of Spectrum

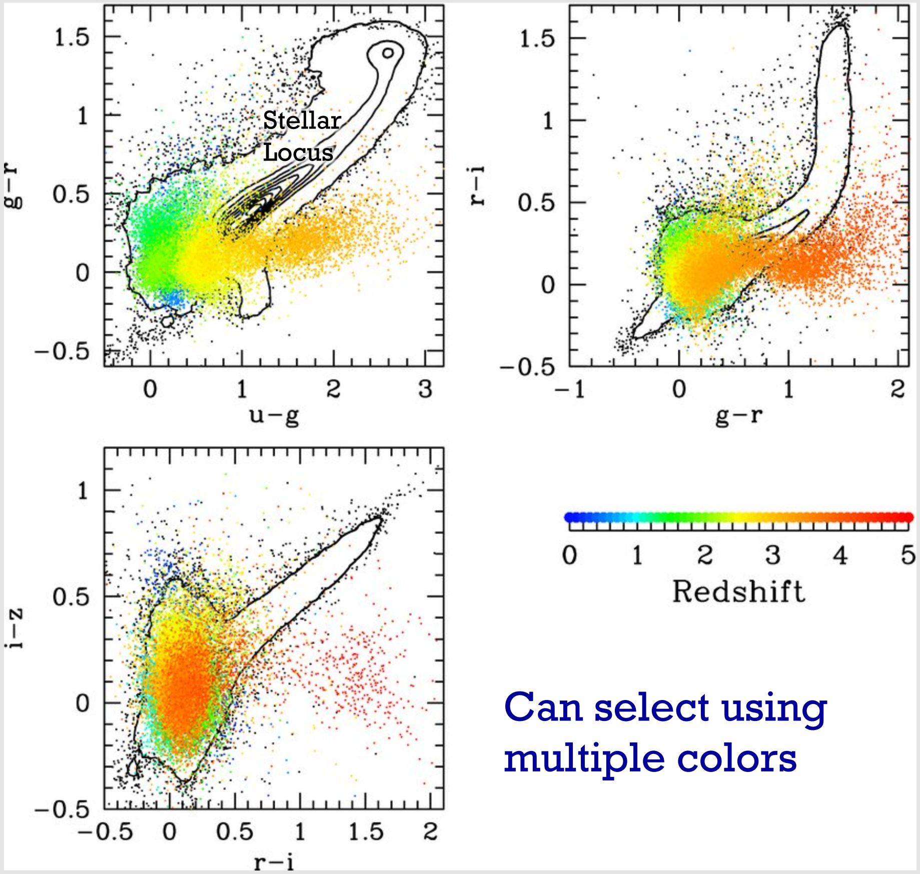

These methods work best for unobscured quasars; e.g., reddening causes trouble.

Furthermore, at lower AGN luminosities, host-galaxy light becomes problematic.

Can also use objective prism surveys.

Can select using multiple colors

Schneider et al. (2010)

Luminosity-Redshift Coverage from Optical/UV Surveys

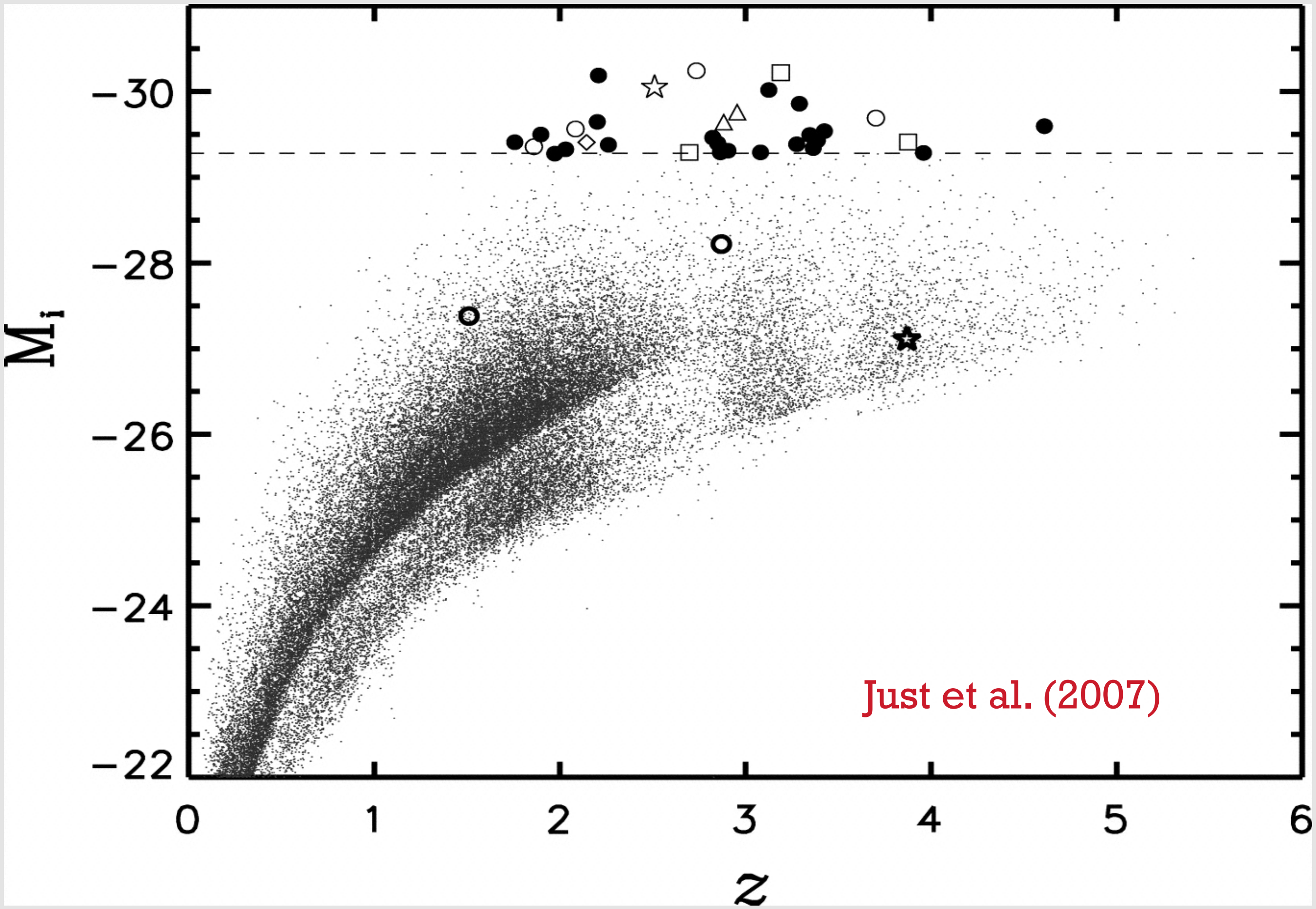

The SDSS has now identified more than 200,000 AGNs.

These span a broad range of luminosity and redshift.

Note the inevitable luminosity-redshift correlation, common to surveys of all types.

X-ray Surveys for AGNs

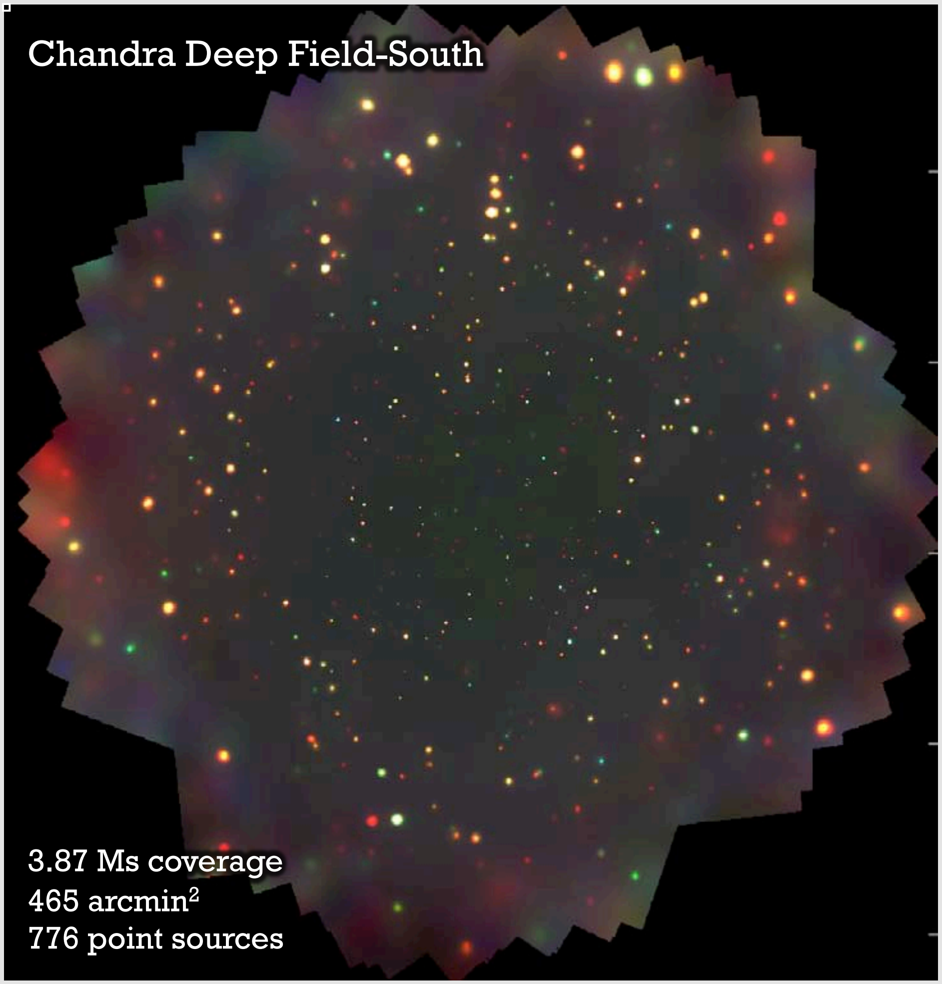

Xue et al. (2011)

X-ray emission nearly universal from AGNs.

X-rays have reduced absorption bias compared to optical/UV, especially for high-energy X-rays.

X-rays maximize contrast between black-hole vs. host-galaxy light.

Can find obscured AGNs and lower luminosity AGNs than in optical/UV.

Now are a wide variety of X-ray surveys, ranging from shallow all-sky to deep pencil-beam.

Gamma-Ray Surveys for AGNs

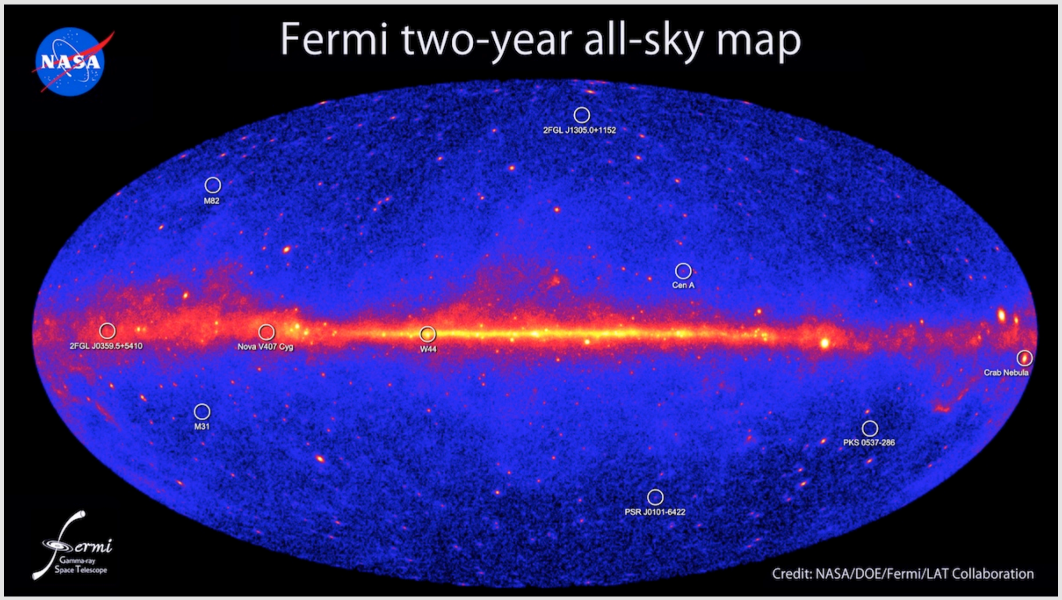

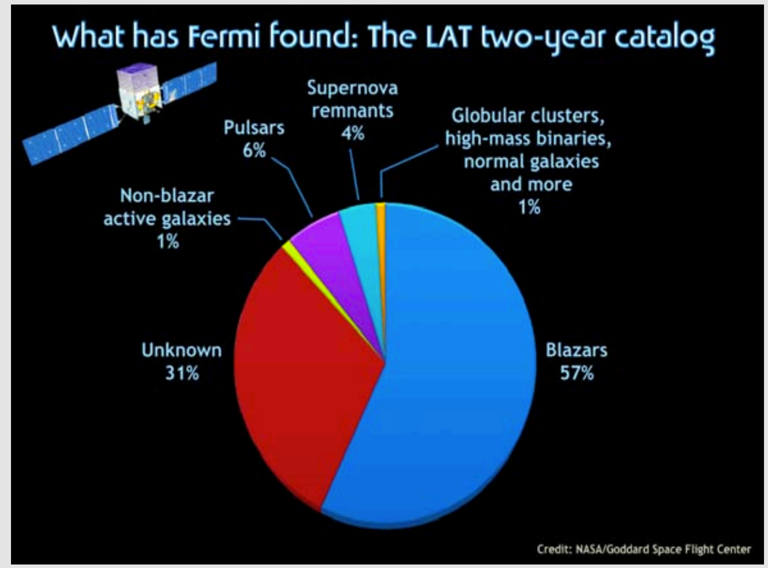

Gamma-ray surveys mostly find AGNs with radio jets pointed right at us, commonly called "blazars".

Infrared Selection of AGNs

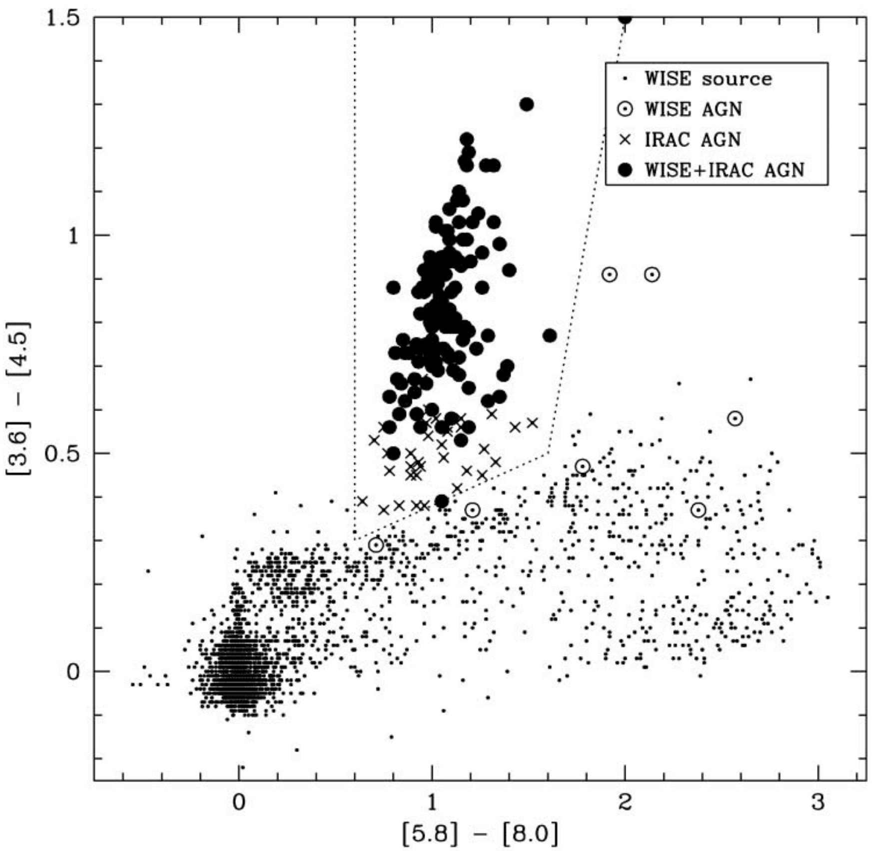

Figure 4. IRAC color–color diagram of *WISE*-selected sources in the COSMOS field. We only plot sources with $S/N \geqslant 10$ in $W1$ and $W2$, and we require $[3.6] > 11$ to avoid saturated stars. Sources with $W1 - W2 \geqslant 0.8$ are indicated with larger circles; filled circles indicate sources that were also identified as AGNs using the Stern et al. (2005) mid-infrared color criteria. Sources identified as AGNs using *Spitzer* criteria but not using the *WISE* criterion are indicated with ×'s.

Stern et al. (2012)

Several methods have been developed for the effective selection of AGNs in sensitive infrared data.

Often are seeing infrared power-law emission or "waste heat" from the AGN re-emitted by warm dust.

These are also relatively resistant against obscuration effects. They sometimes even find AGNs missed in X-ray surveys.

At lower AGN luminosities, such surveys suffer substantial contamination from star-forming galaxies.

Radio Surveys for AGNs

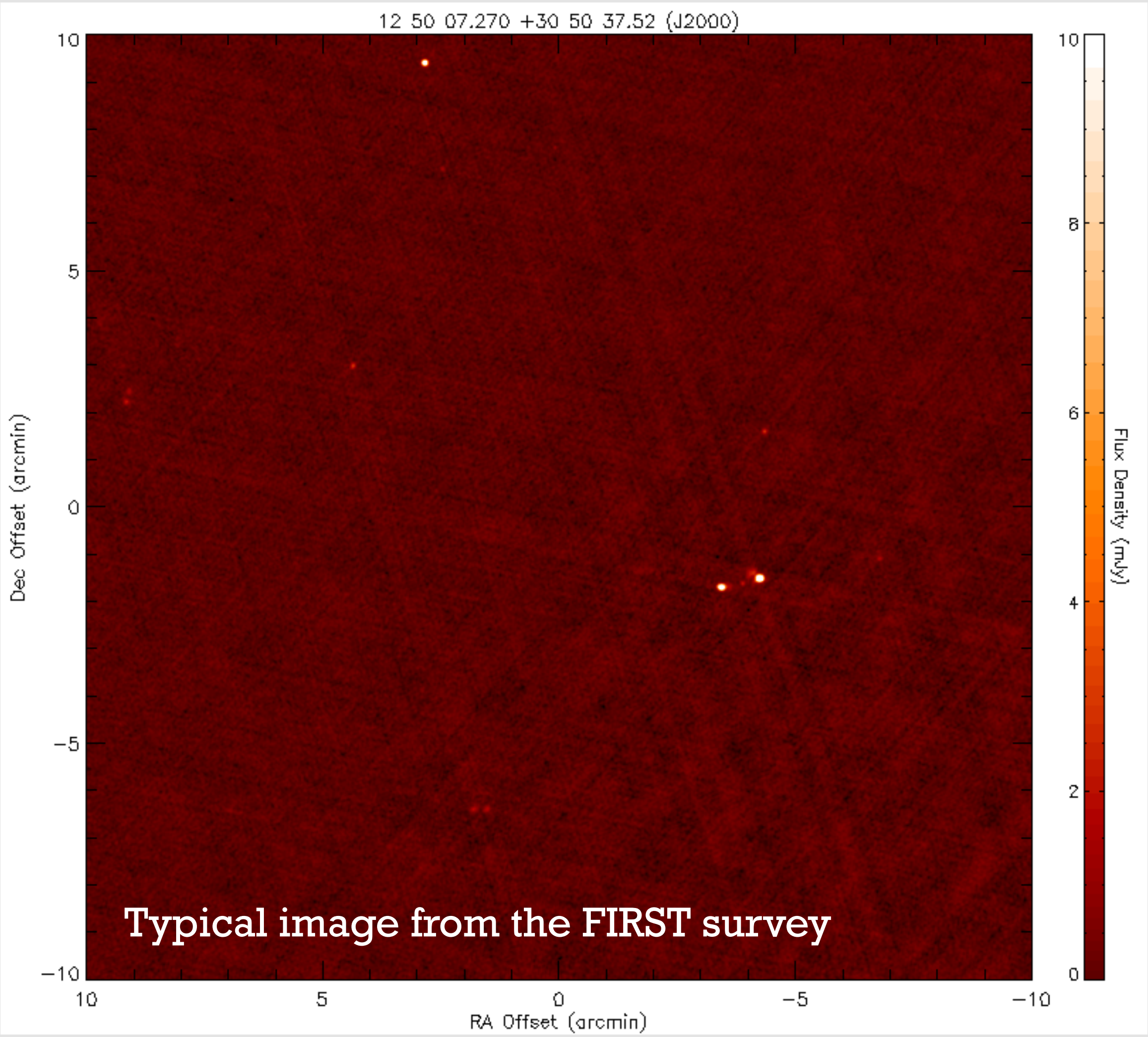

Many of the first quasars were found via radio selection (3C).

About 10% of AGNs are radio-loud sources.

Sensitive radio surveys can detect many radio-quiet AGNs too.

Stars are usually very weak radio sources, so little stellar contamination.

Generally good radio positions allow efficient follow-up studies.

Often quite incomplete, owing to radio-quietness of many AGNs.

Terminology

AGN Names in Popular Culture

Examples of AGN Names (No Ordering Implied)

BAL Quasar

Seyfert 1 galaxy

Radio Loud Quasar

FR I

Radio-Quiet Quasar

Blazar

Broad Line Radio galaxy

OVVs

Seyfert 2 galaxy

Narrow-Line Radio Galaxy

LLAGN

FR II

Narrow-Line Seyfert 1

LINER

Type 2 Quasar

BL Lac Object

Weak Line Quasars

AGN Terminology Is Somewhat of a Mess

Much of AGN terminology was developed as people were coming to understand AGNs for the first time. They did not have a complete understanding when the terminology was being set.

Via subsequent unifications of ideas, some of this terminology has been seen not to reflect real, internal, physical differences.

As a result, AGN terminology can be confusing, and there is a lot of historical "baggage" that doesn't have much physical importance.

There is also, even today, fairly sloppy usage of AGN type names in some of the literature; e.g., "Type 2" and "blazar".

Too late to redo the terminology more logically, so need to learn it.

Key Classification Variables

Strength of Radio Emission

- Radio-Loud Quasar vs. Radio-Quiet Quasar

Optical/UV Emission-Line Properties

- Seyfert 1 galaxy vs. Seyfert 2 galaxy
- Type 1 Quasar vs. Type 2 Quasar
- Broad Line vs. Narrow Line Radio Galaxy
- Also intermediate Seyfert types, Narrow-Line Seyfert 1, BL Lac, Weak-Line Quasar

Also Variability and UV Absorption-Line Properties

Luminosity is also often used in classifications for largely historical reasons; usually not so fundamental (e.g., Seyferts are just low-luminosity quasars).

The AGN Bestiary

Table 1.2: The AGN Bestiary

Beast	Pointlike	Broad-band	Broad Lines	Narrow Lines	Radio	Variable	Polarized
Radio-loud quasars	Yes	Yes	Yes	Yes	Yes	Some	Some
Radio-quiet quasars	Yes	Yes	Yes	Yes	Weak	Weak	Weak
Broad line radio galaxies (FR2 only)	Yes	Yes	Yes	Yes	Yes	Weak	Weak
Narrow line radio galaxies (FR1 and FR2)	No	No	No	Yes	Yes	No	No
OVV quasars	Yes	Yes	Yes	Yes	Yes	Yes	Yes
BL Lac objects	Yes	Yes	No	No	Yes	Yes	Yes
Seyferts type 1	Yes	Yes	Yes	Yes	Weak	Some	Weak
Seyferts type 2	No	Yes	No	Yes	Weak	No	Some
LINERs	No	No	No	Yes	No	No	No

Krolik (1999)

Example Classification Scheme

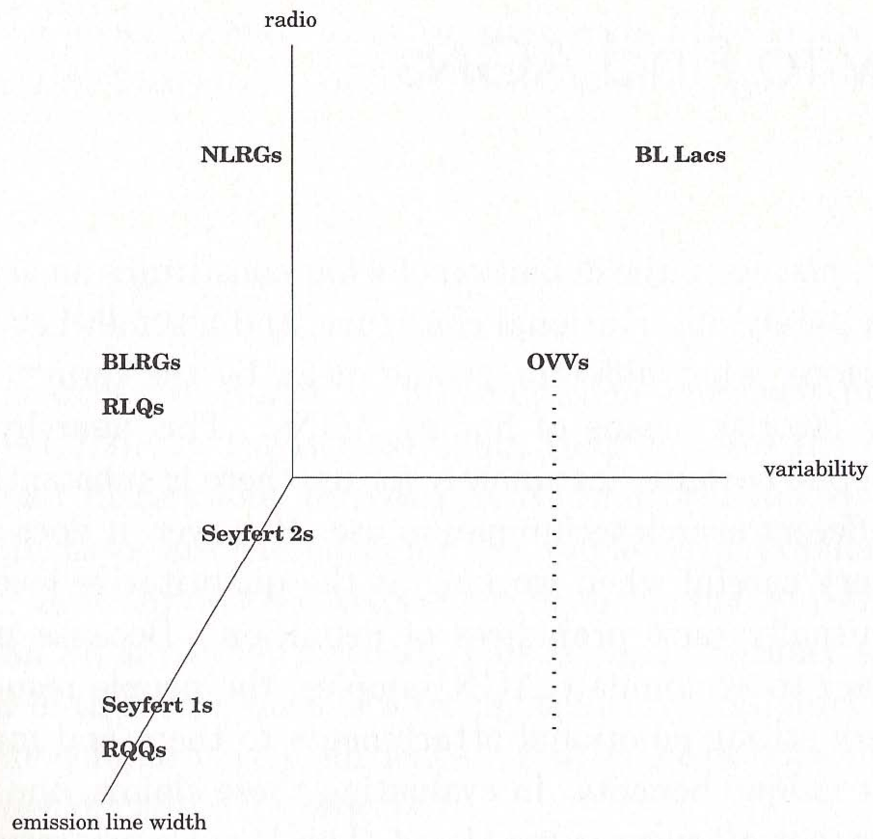

Fig. 1.9 The principal subvarieties of AGNs schematically arranged according to relative power in the radio band, emission line width, and variability. All combinations are possible except that there are no highly variable radio-quiet objects.

Krolik (1999)

Example of Orientation-Based Unification

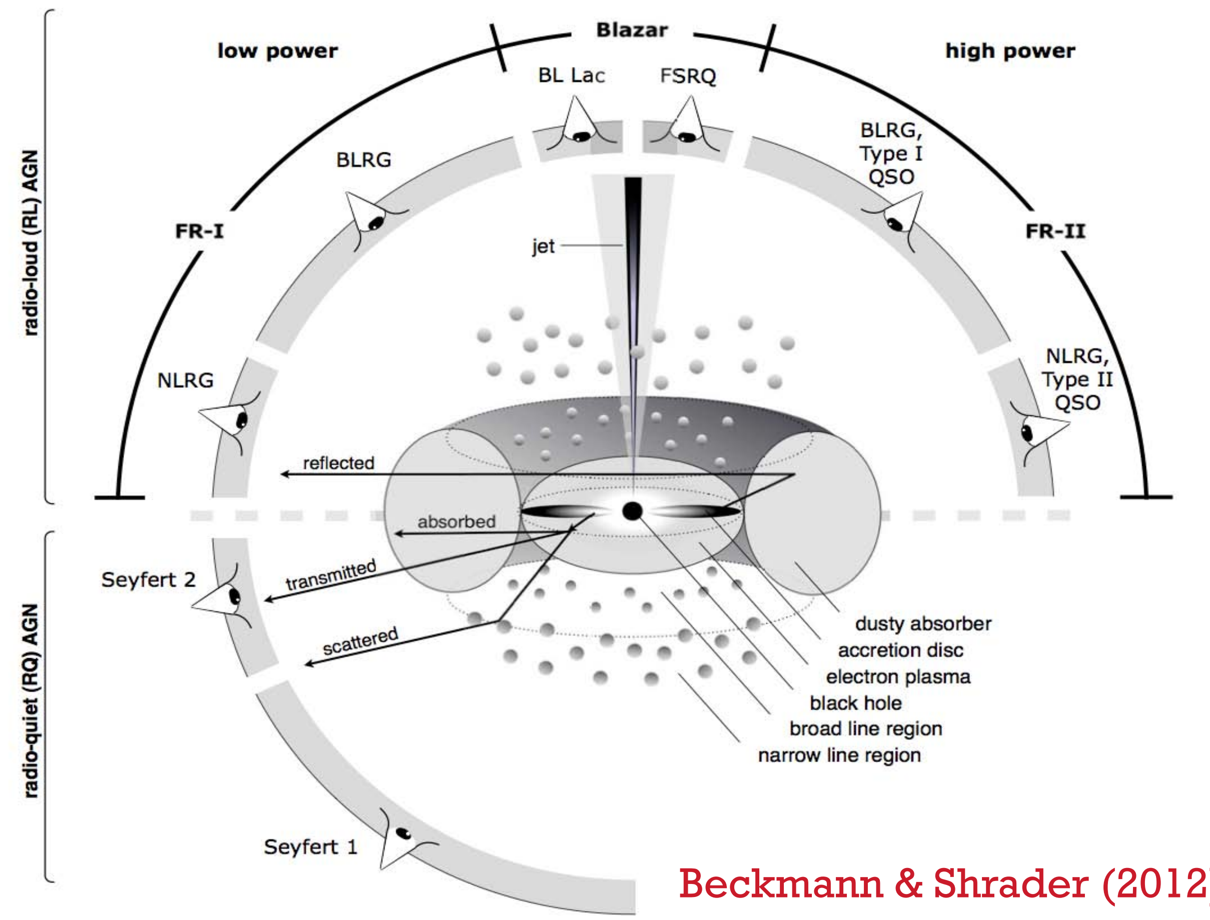

Beckmann & Shrader (2012)

AGN
“Powers of 10”

Powers of 10

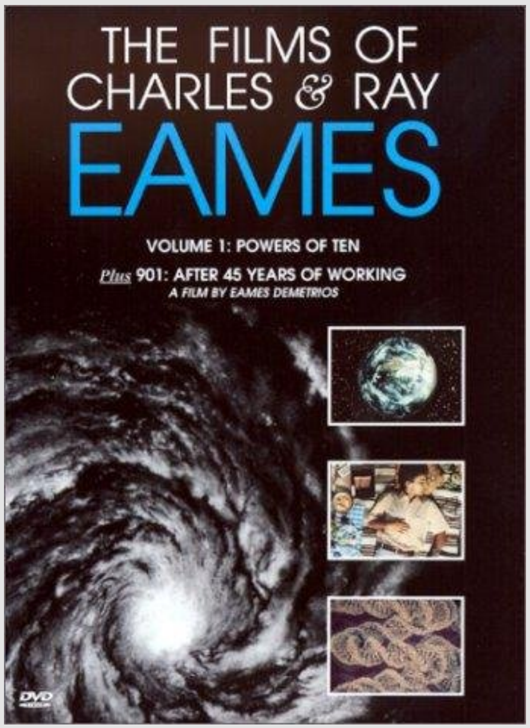
THE FILMS OF
CHARLES & RAY
EAMES
VOLUME 1: POWERS OF TEN
Plus 901: AFTER 45 YEARS OF WORKING
A FILM BY EAMES DEMETRIOS
DVD

AGN "Powers of Ten"

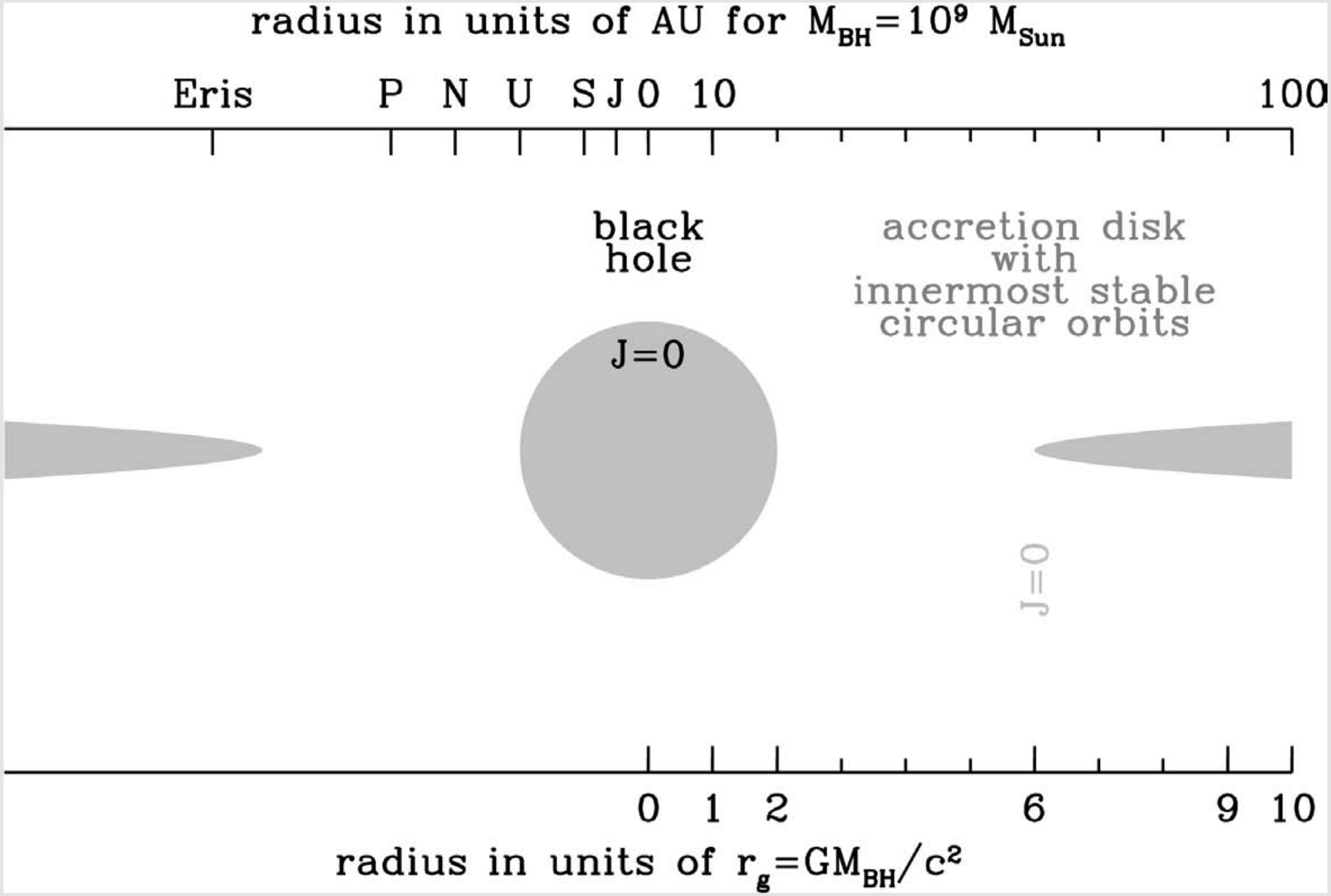

Courtesy of Pat Hall

AGN "Powers of Ten"

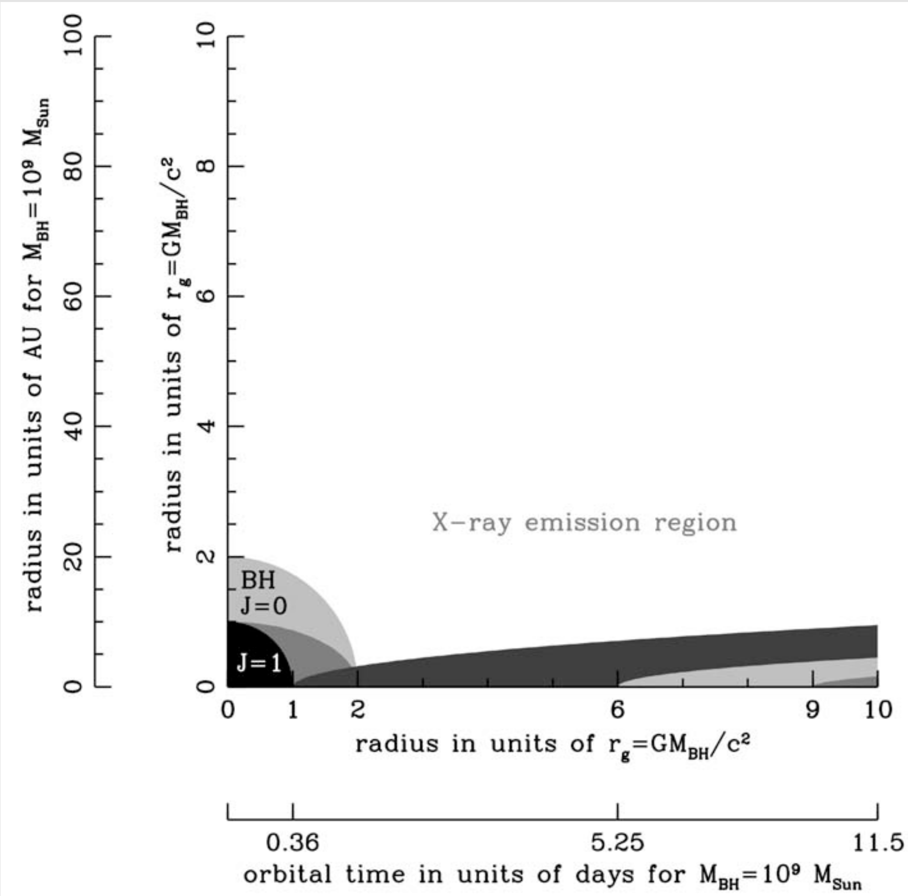

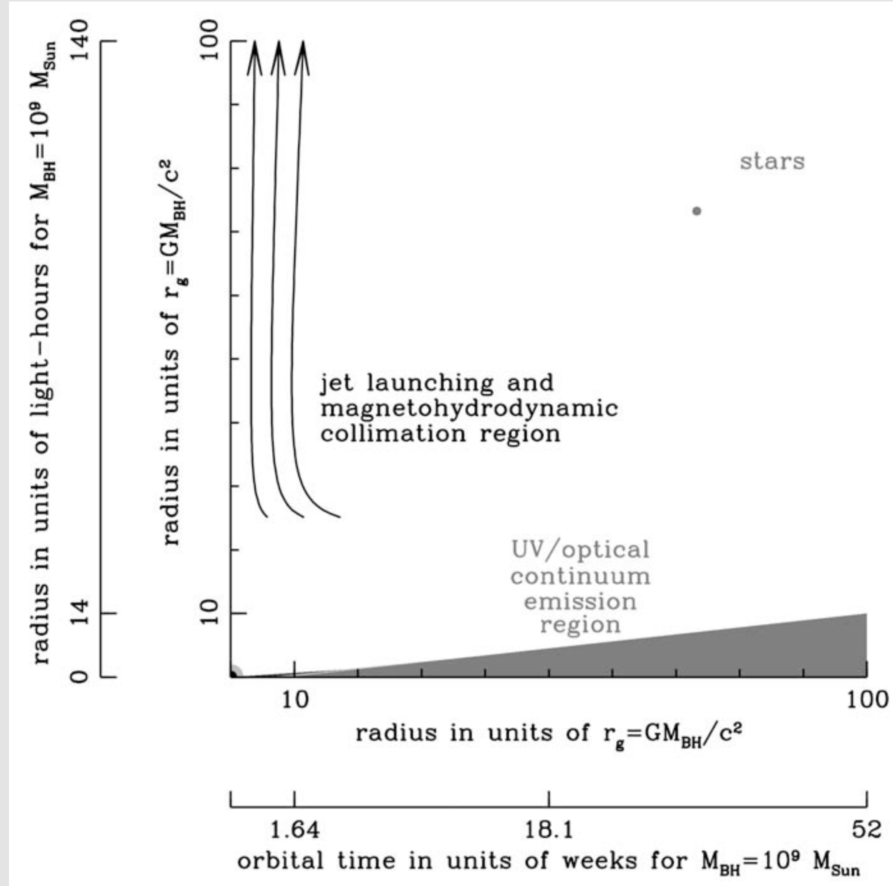

Courtesy of Pat Hall

AGN "Powers of Ten"

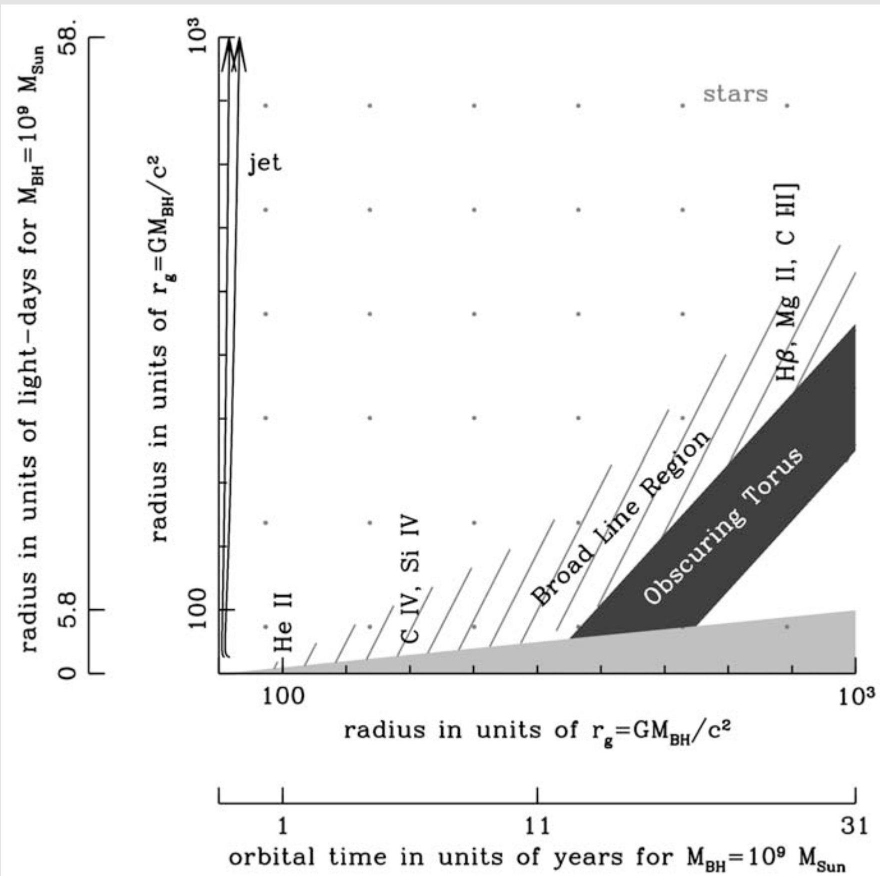

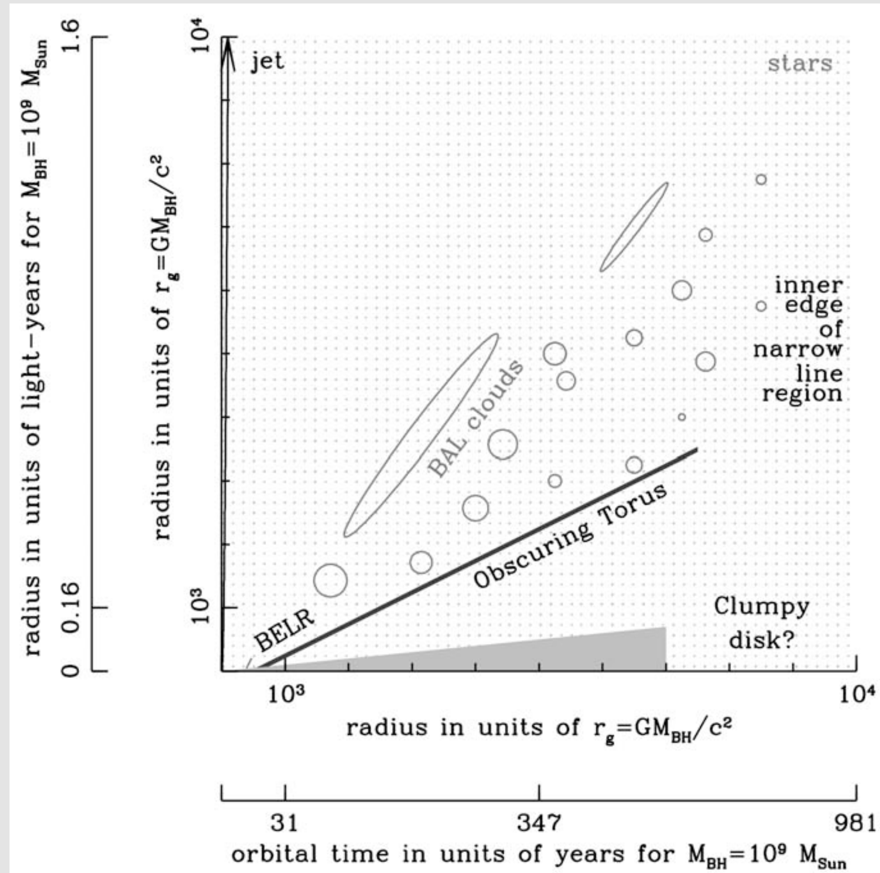

Courtesy of Pat Hall

A Historical Analogy?

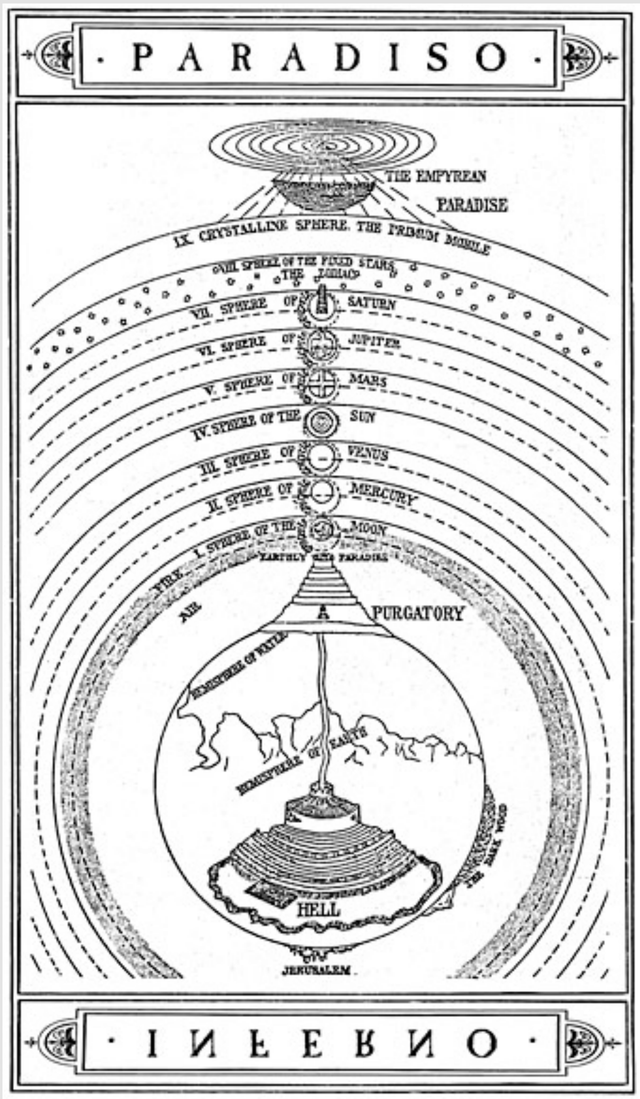

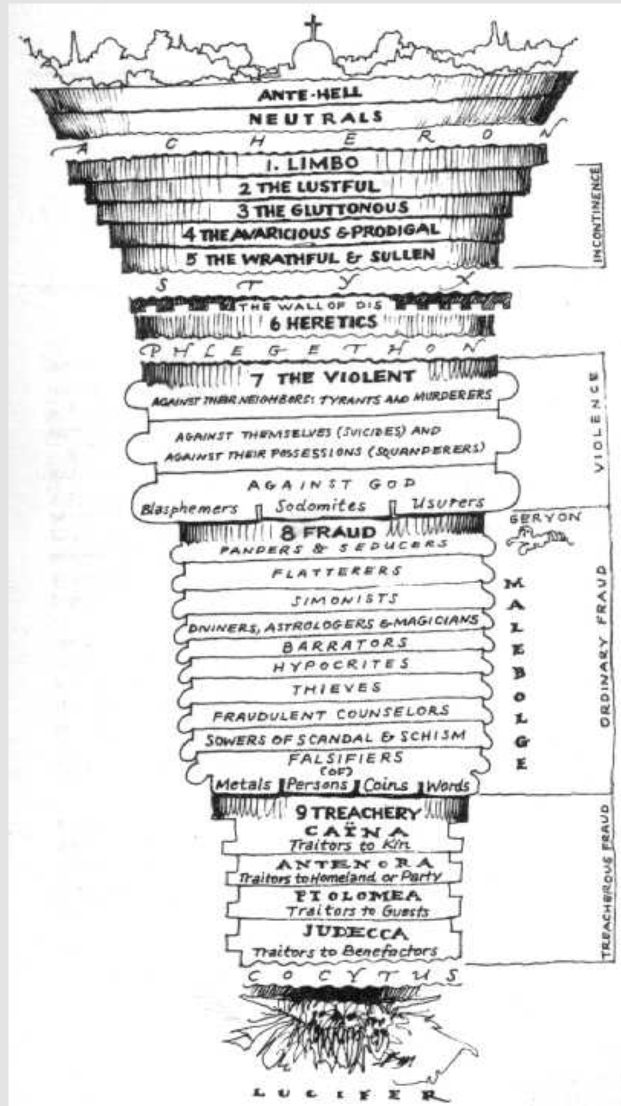

Dante (1320)

The End

An Observational Overview of Active Galactic Nuclei

Niel Brandt (Penn State University)

Summary of Lectures

Introduction, AGN Basics, Finding AGNs, and Terminology

Observations on Small Scales: Black Hole Region, Broad Line Region, Outflowing Winds

Observations on Large Scales: Narrow Line Region, Torus, Jets

Summary of Lectures

Focused Lecture – AGN Demography, Physics, and Ecology from X-ray Surveys

Observations on Small Scales: Black Hole Region, Broad Line Region, and Outflowing Winds

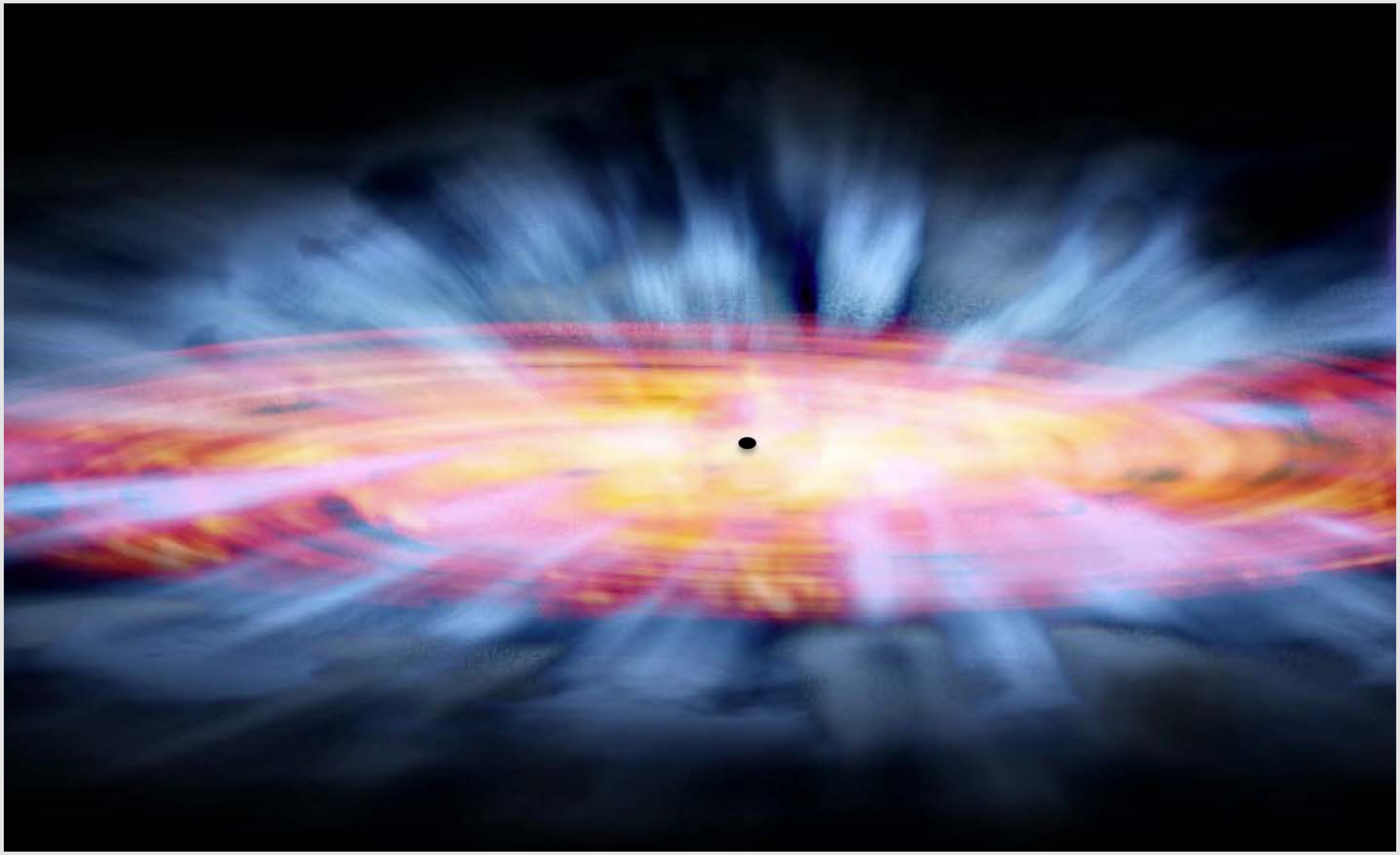

A Few General Points

Focus today will be on the innermost regions.

Will generally be considering objects where we have a clear view of the innermost regions.

Unification models indicate that the same physical processes should be happening in obscured objects as well (just can't see them as clearly).

For simplicity, will focus on majority population of radio-quiet AGNs, where jet does not add major complications.

More on jets later!

Example of Orientation-Based Unification

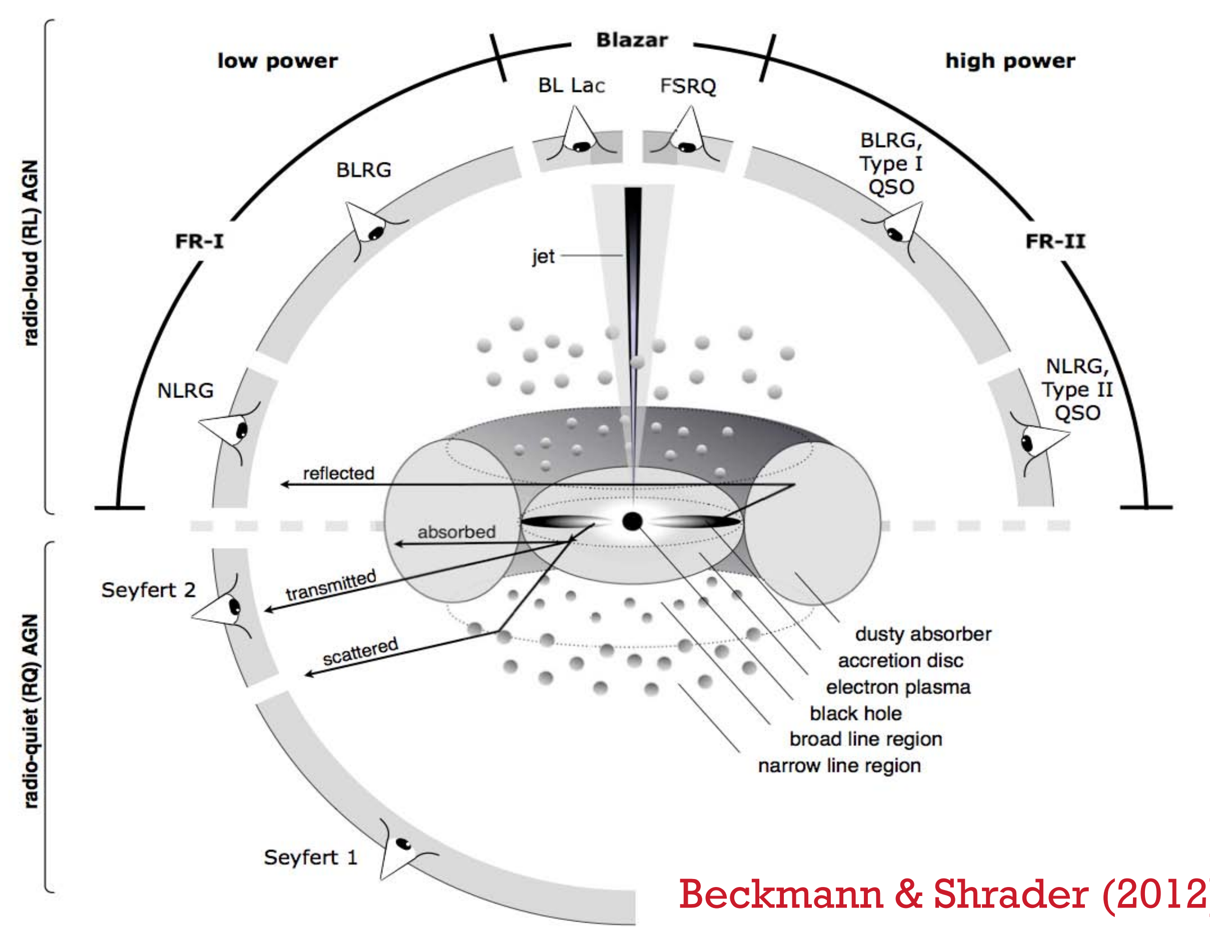

Beckmann & Shrader (2012)

AGN "Powers of Ten"

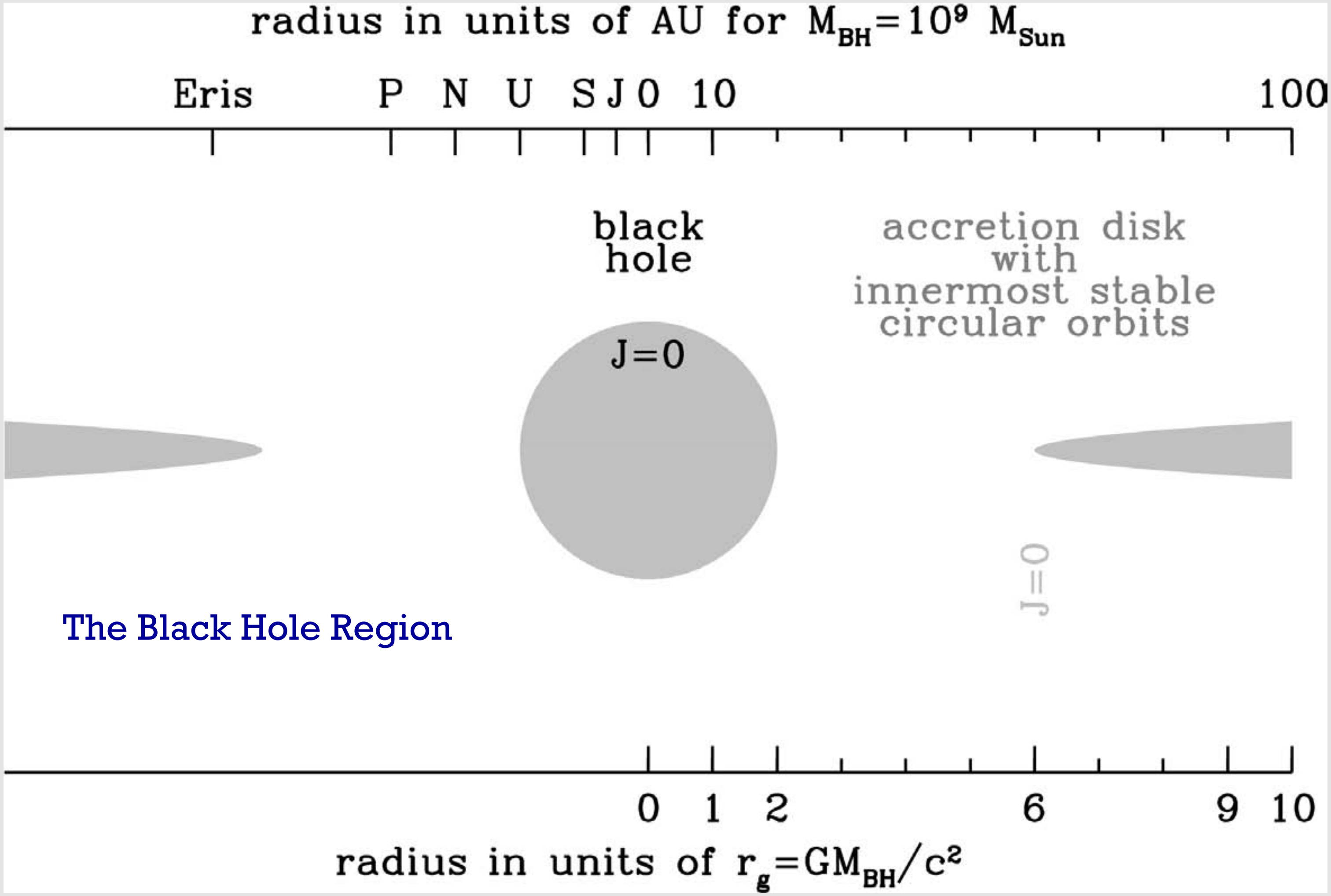

The Black Hole Region

Courtesy of Pat Hall

AGN "Powers of Ten"

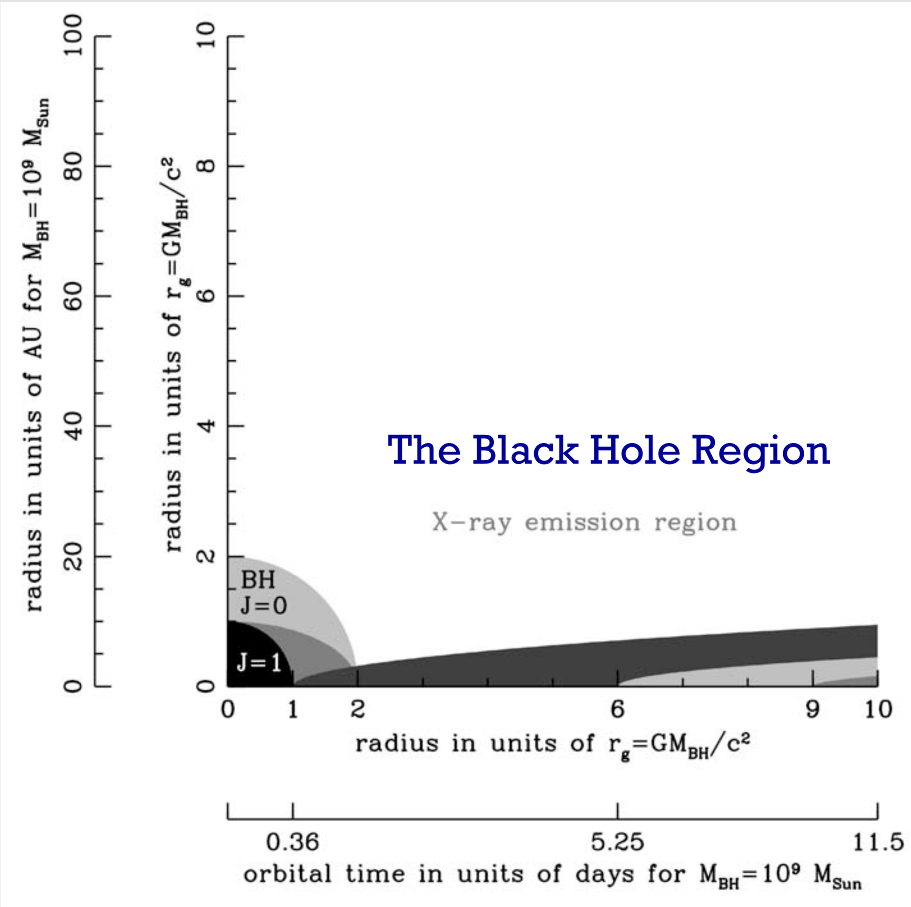

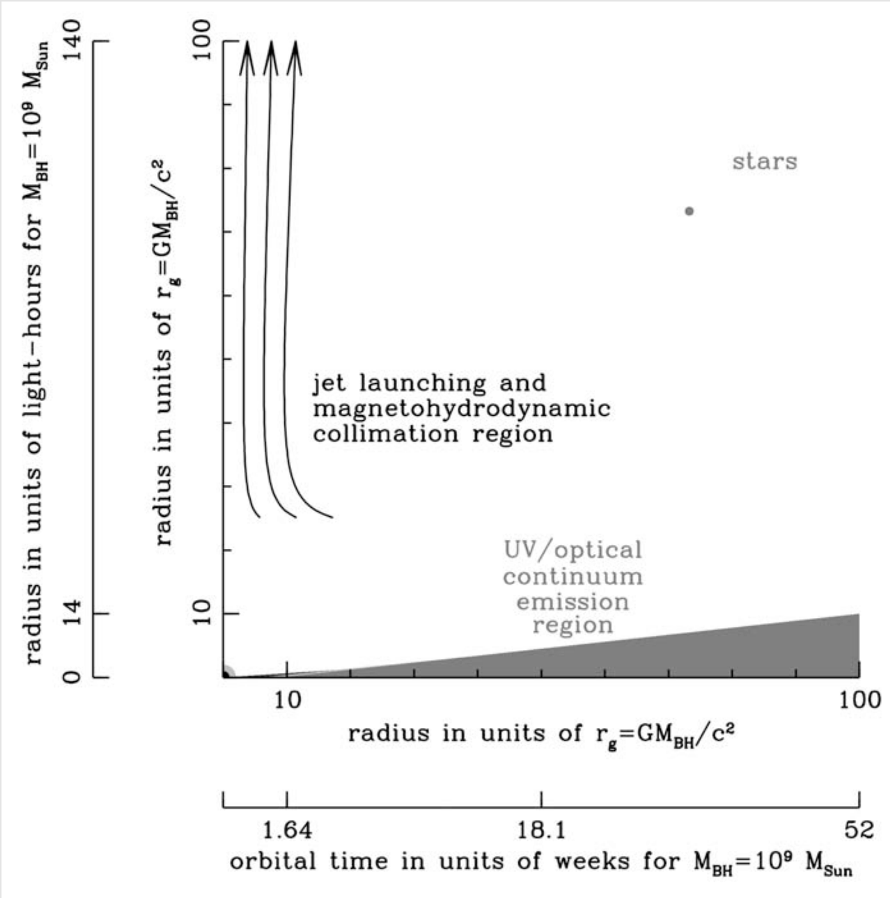

Courtesy of Pat Hall

AGN "Powers of Ten"

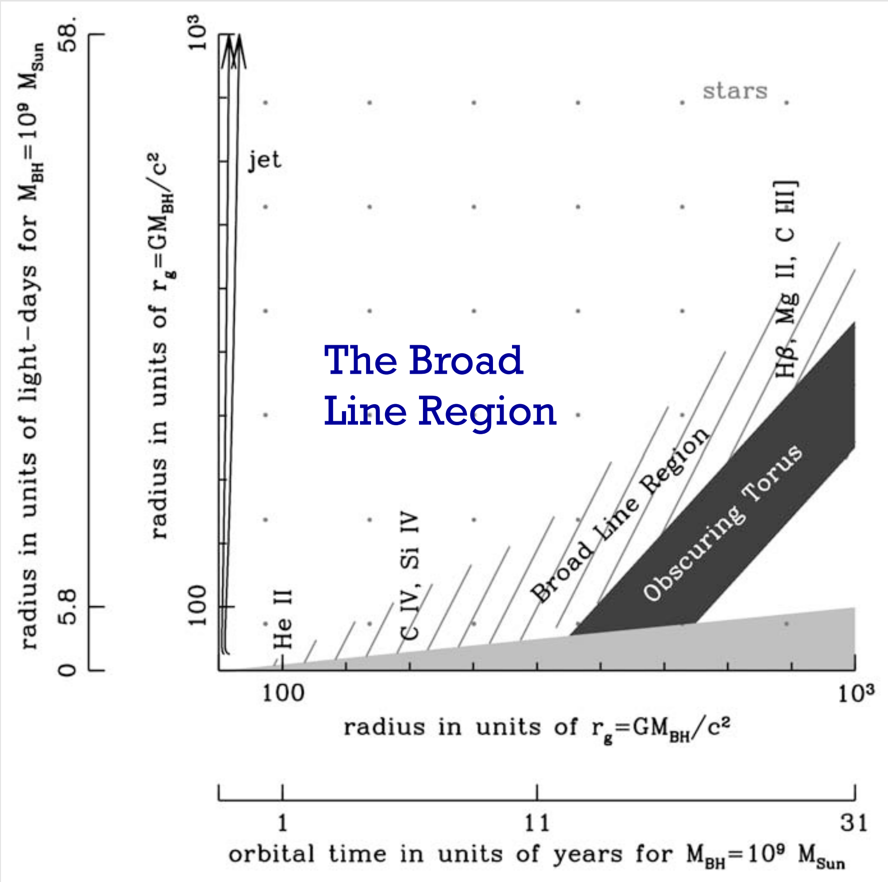

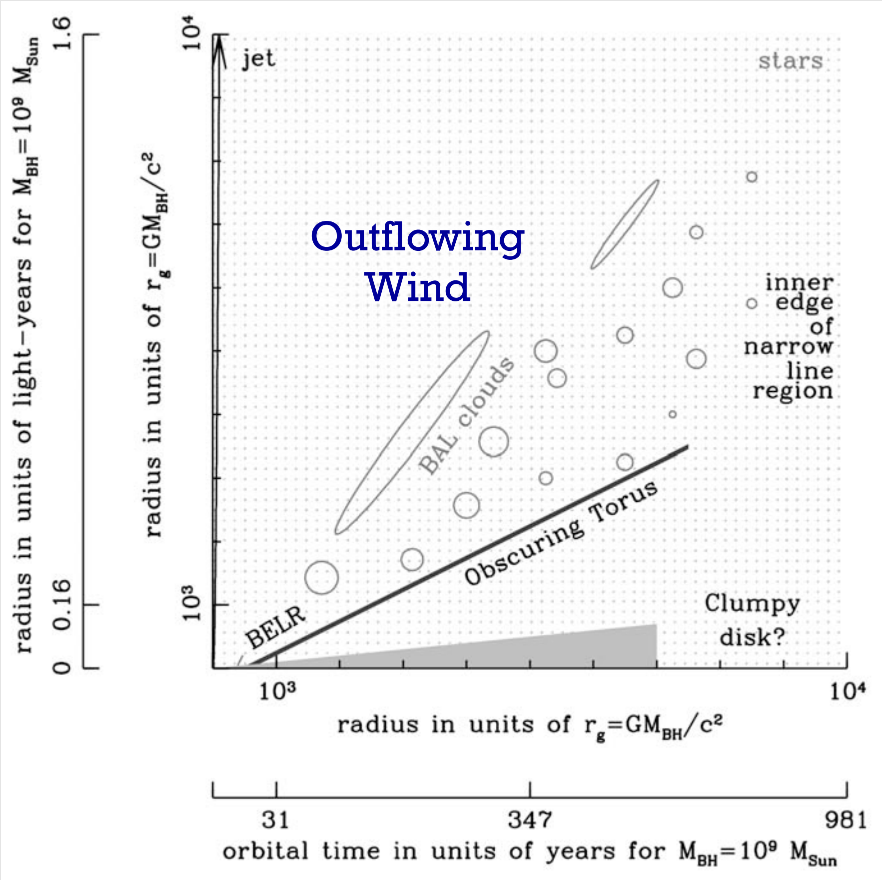

Courtesy of Pat Hall

The Black Hole Region (within ~ 50 R_S)

A Region of Strong Gravity and Relativistic Motions

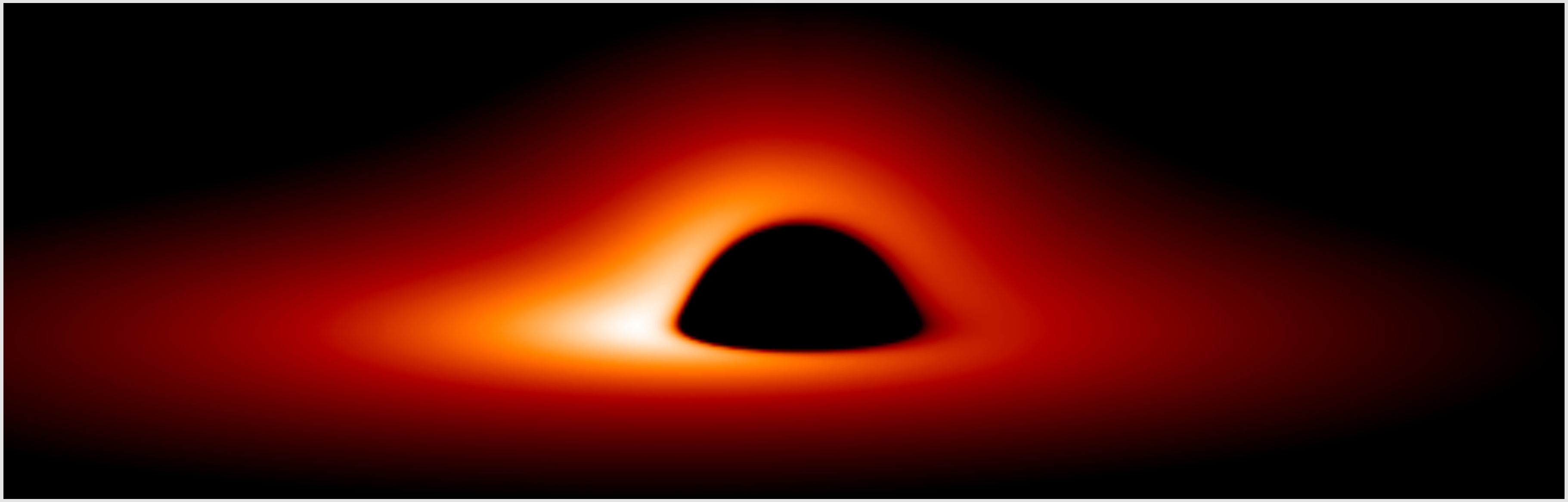

Prediction for smooth disk emissivity.

A Region of Strong Gravity and Relativistic Motions

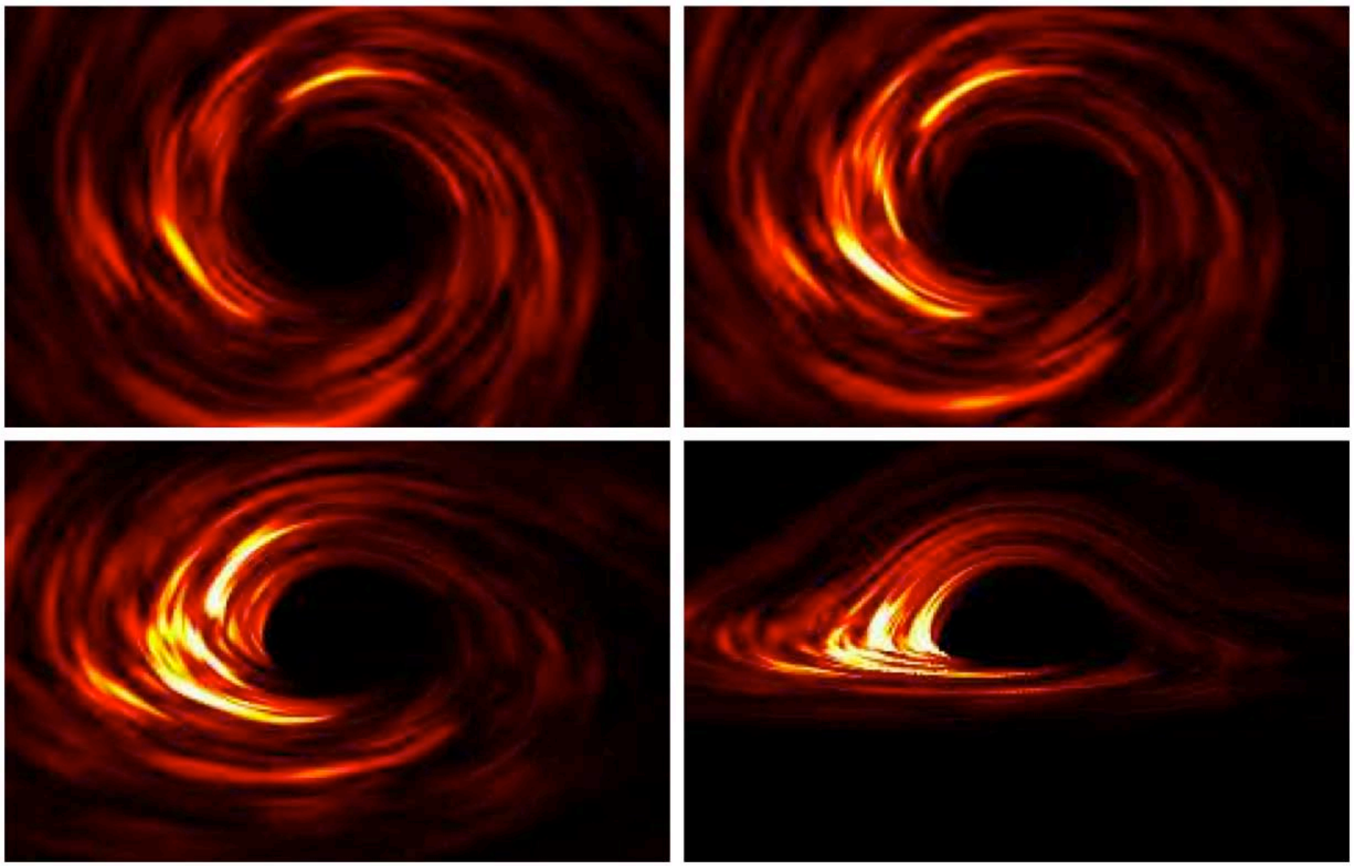

Figure 4. View of the disc as seen by a distant observer at an inclination angle of 5° (upper left), 30° (upper right), 55° (lower left) and 80° (lower right). In these raw images, note the presence of stress extending to the inner boundary of the computational domain, within the marginally stable circular orbit. Movies showing the evolution of the simulated disc are available at `http://jilawww.colorado.edu/~pja/black_hole.html`.

Armitage & Reynolds (2003)

Schematic AGN X-ray Spectral Energy Distribution

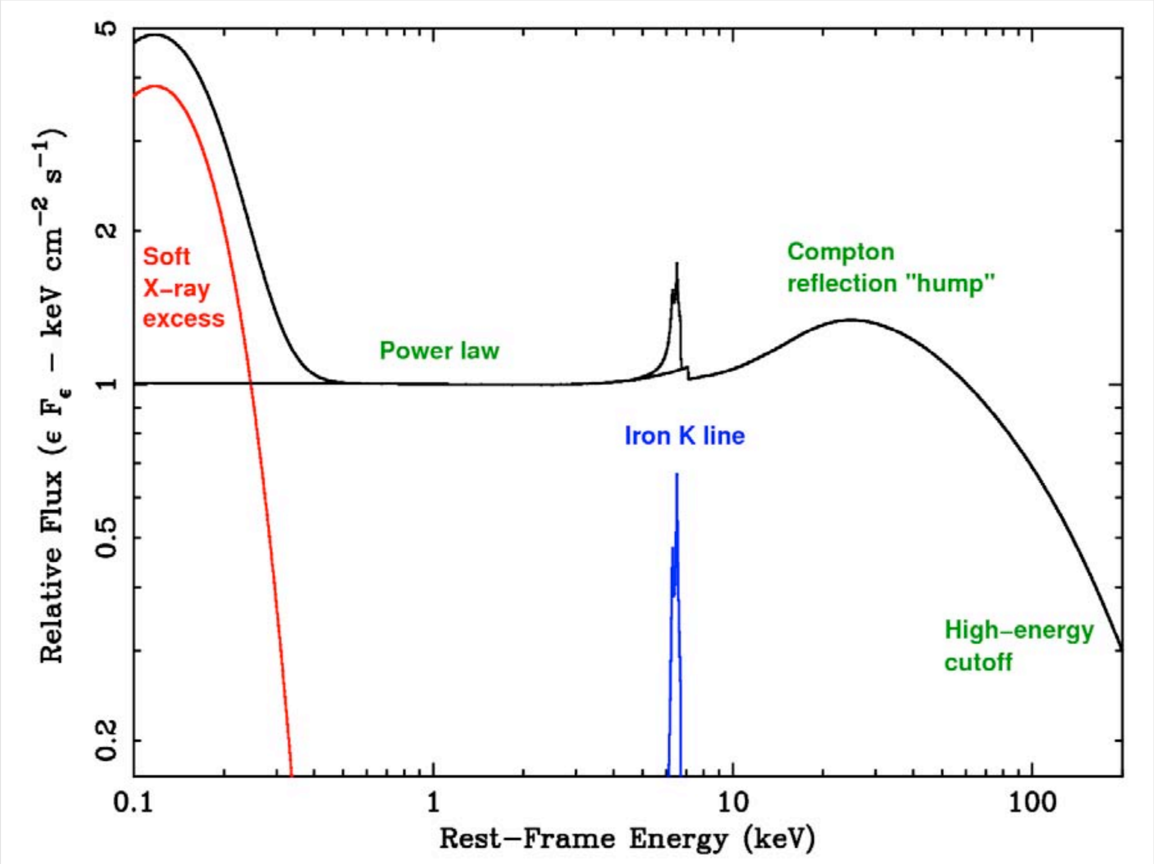

Medical X-rays from a Tungsten (Z = 74) Target

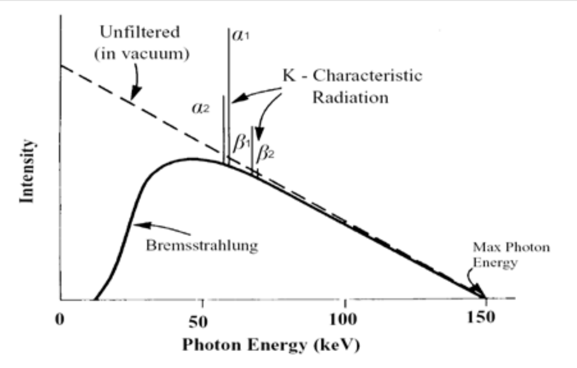

The black hole region is usually studied in the X-ray band.

Schematic Spectrum from Disk + Corona

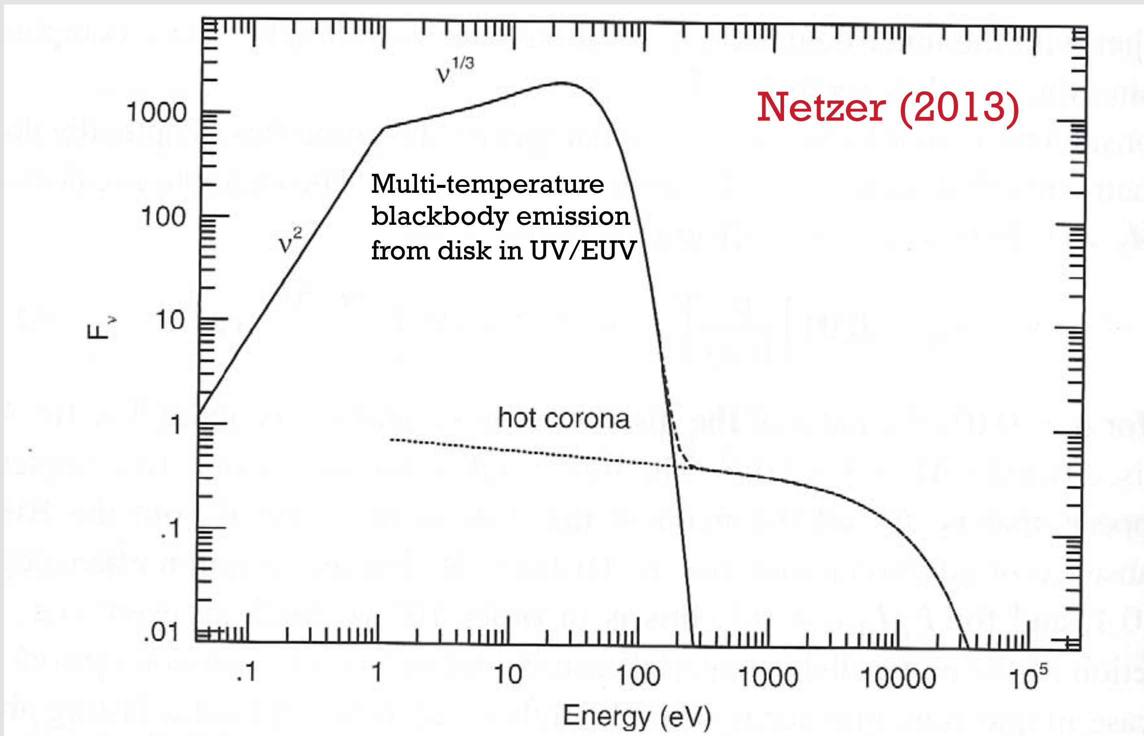

Figure 4.3. A schematic of a combined disk–corona spectrum. The maximum temperature of the geometrically thin, optically thick accretion disk is $T_{max} = 10^5$ K, and its outer boundary temperature is determined by the conditions at the self-gravity radius. The disk is surrounded by an optically thin corona with $T_{cor} = 10^8$ K.

Rapid X-ray Variability

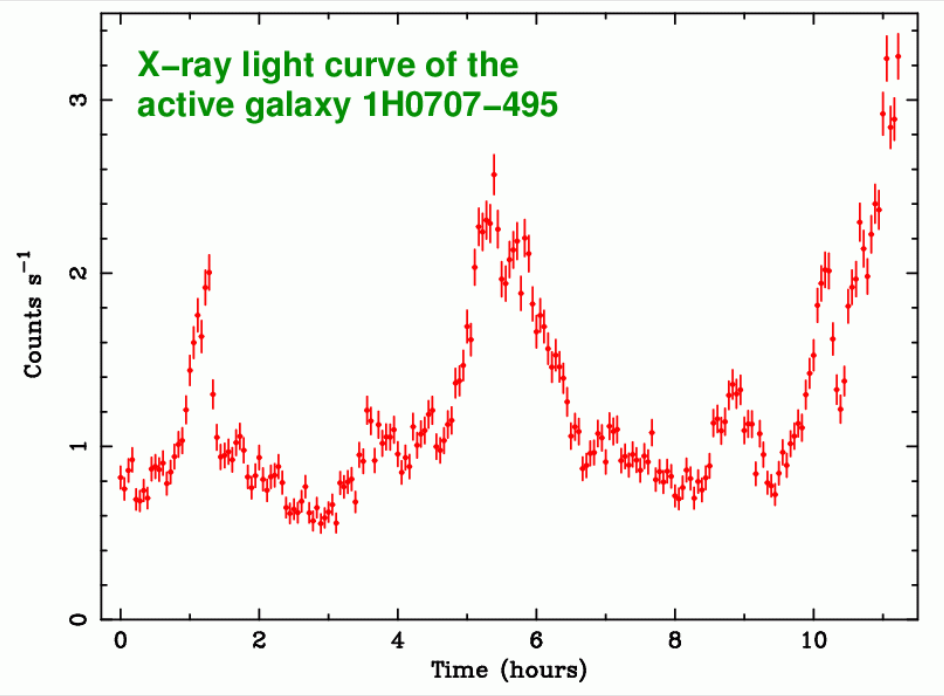

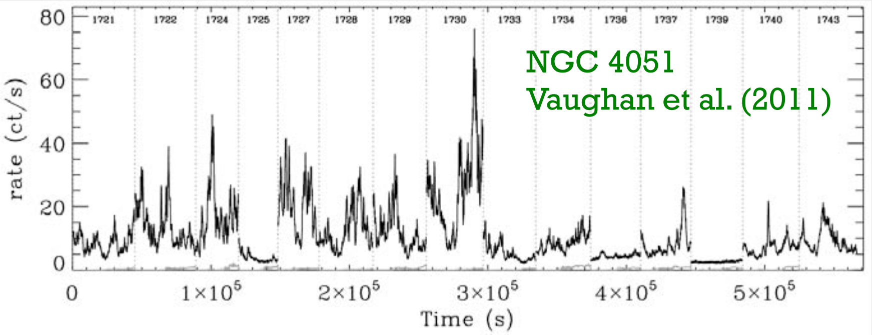

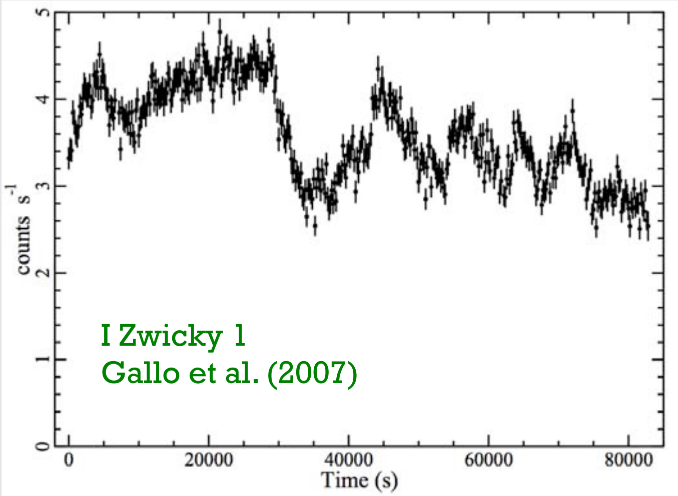

Such rapid variability is common, being seen in hundreds of cases.

X-ray variability often implies an emission-region size of light hours or less.

Stronger variability is generally seen for objects with smaller mass/luminosity.

X-ray Spectral Components from the Black Hole Region

Continuum components

- Power law
- Soft X-ray excess
- Compton reflection hump

Discrete atomic features

- Iron Kα line
- Other line emission

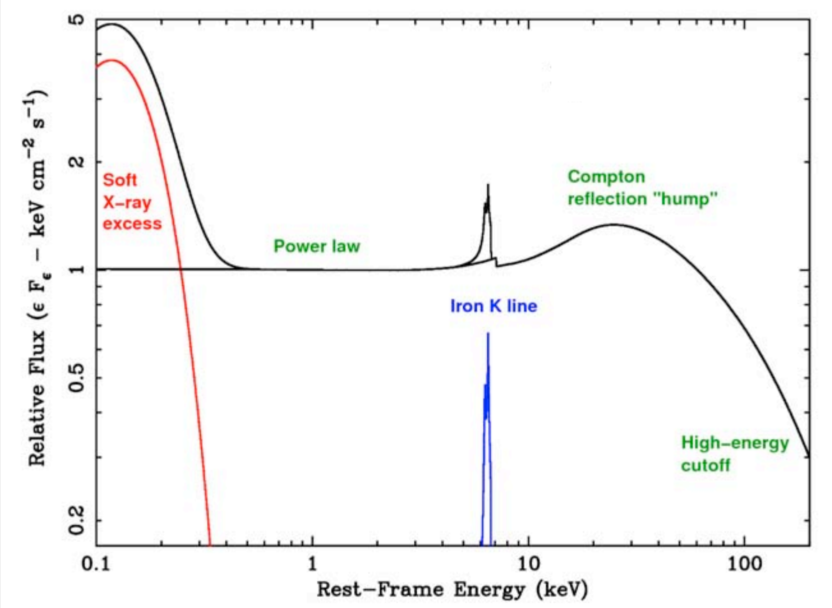

X-ray Spectral Components in Actual Data

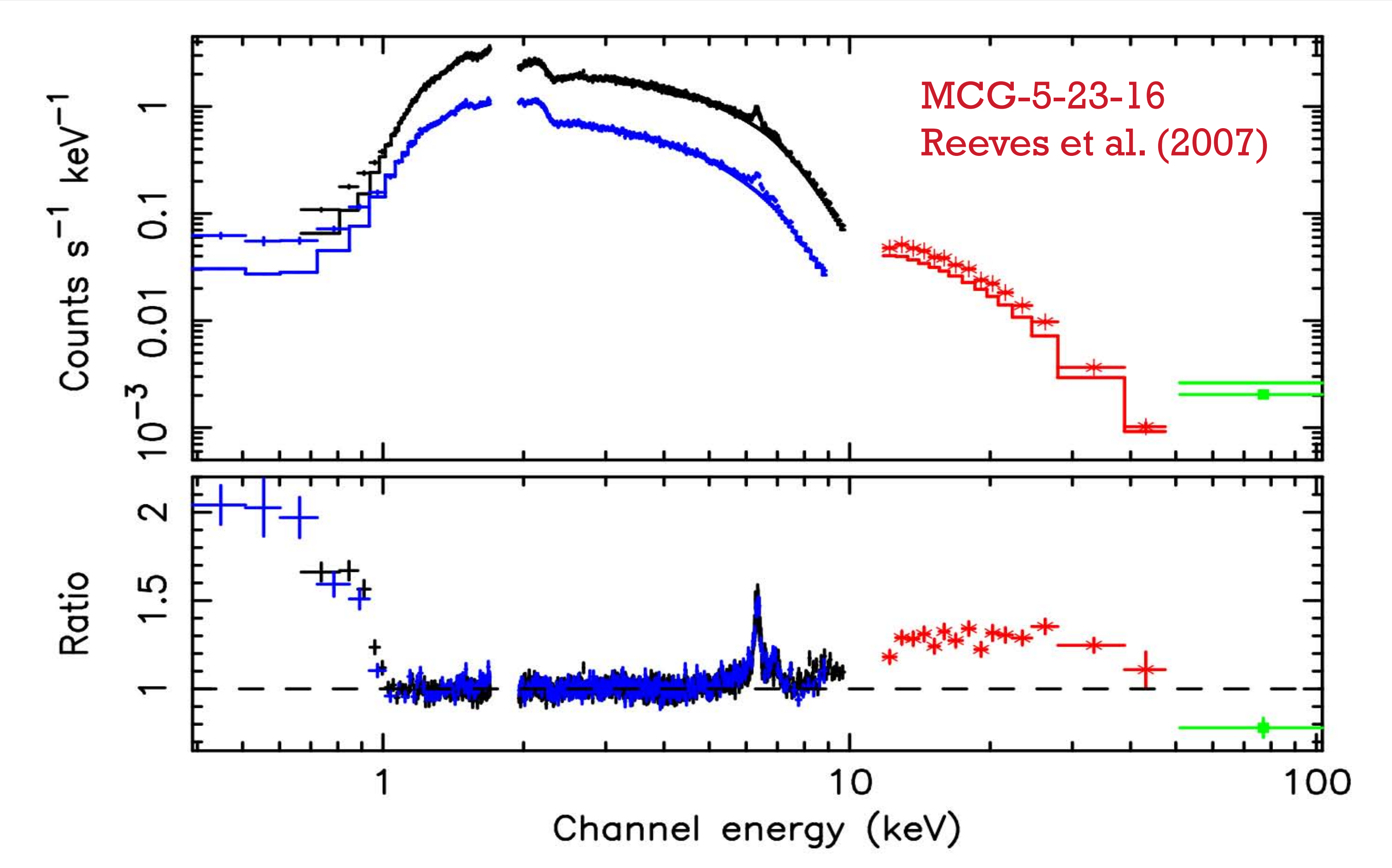

X-ray Power Law

Power law has a photon index of Γ = 1.7-2.2.

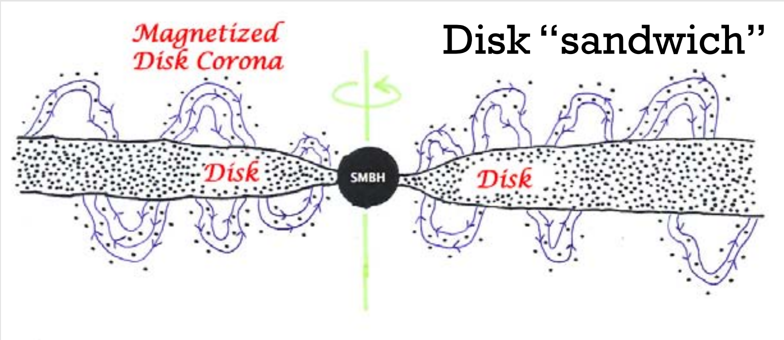

The "corona" Compton up-scatters EUV/UV/optical photons from the disk to create the power law.

Corona likely heated by magnetic flares.

Corona has a temperature of ~ 150 keV, beyond which an ~ exponential cutoff is observed.

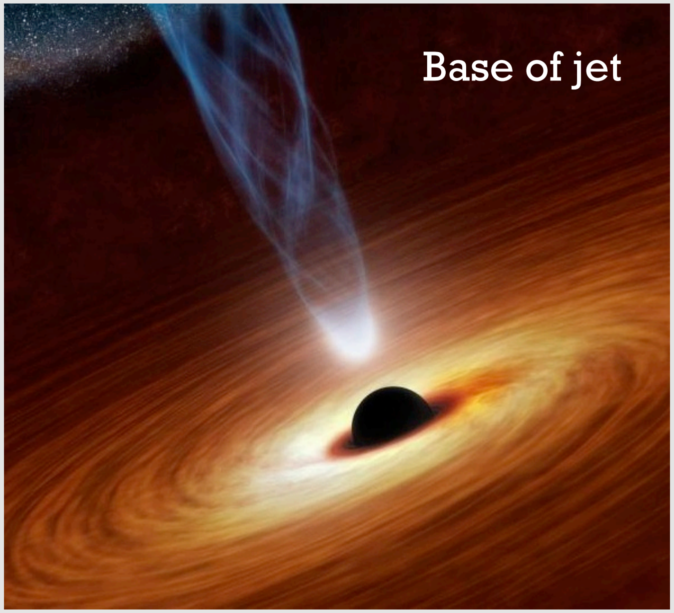

The corona's properties cannot yet be computed from first principles, but progress being made.

Thus the corona's nature remains uncertain.

- Sandwiching the disk?
- Base of a jet?

But empirically it is found to be robust (with some notable exceptions).

Robustness of the X-ray Emission from the Corona

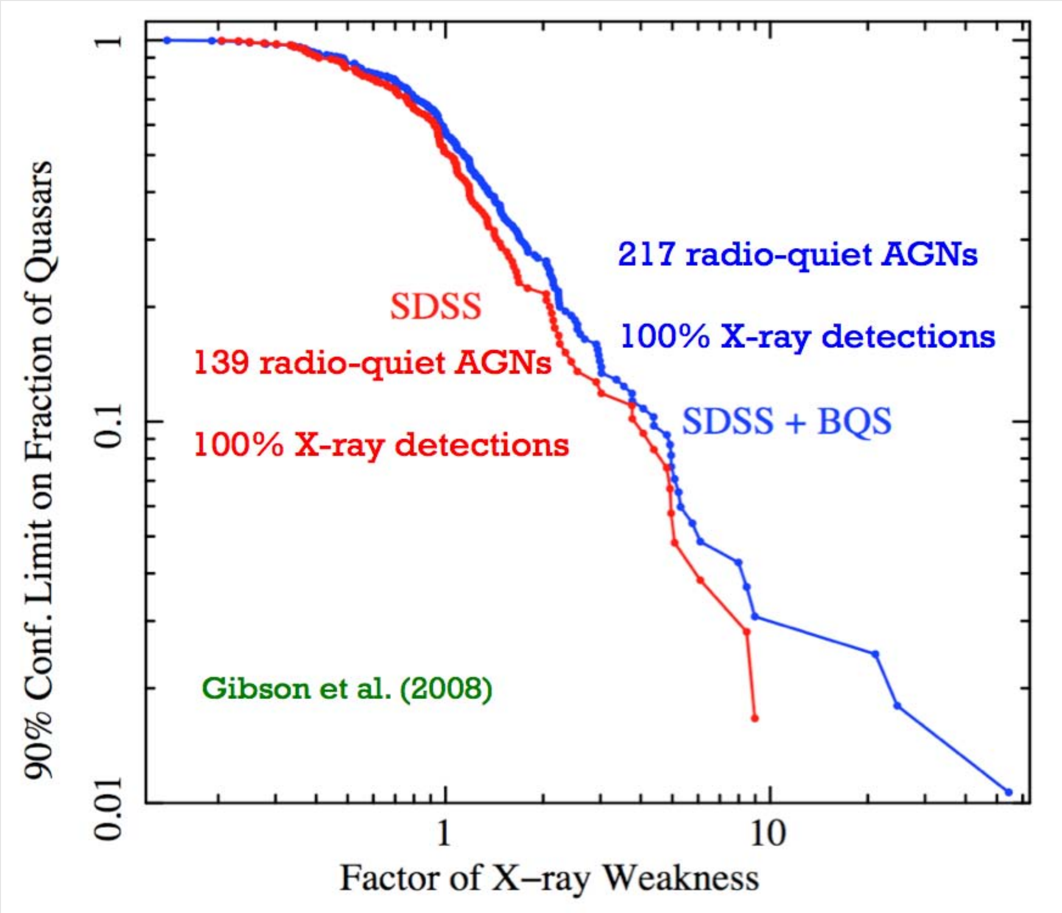

Soft X-ray Excess

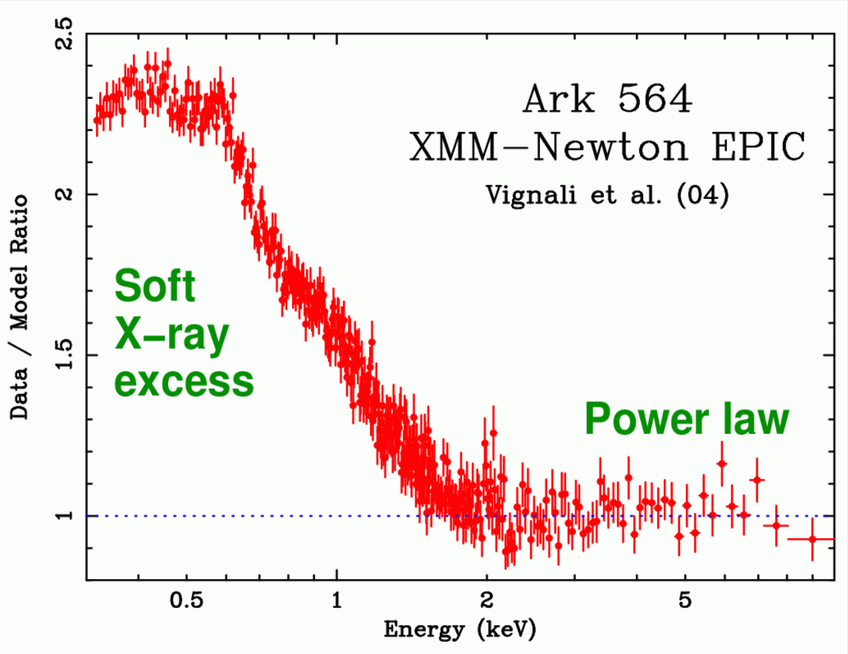

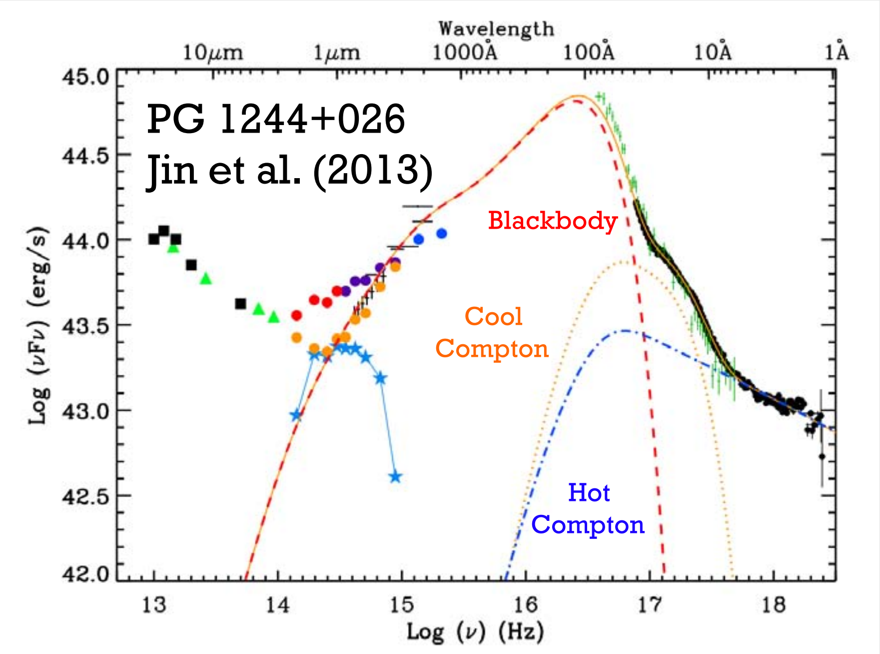

Strong soft emission of a ~ blackbody spectral form seen from some objects below ~ 1.5 keV.

Too hot and too variable to be entirely from standard accretion disk.

Likely a combination of disk emission at lowest energies plus a cool Compton-scattered component and disk reflection.

Compton Reflection Hump

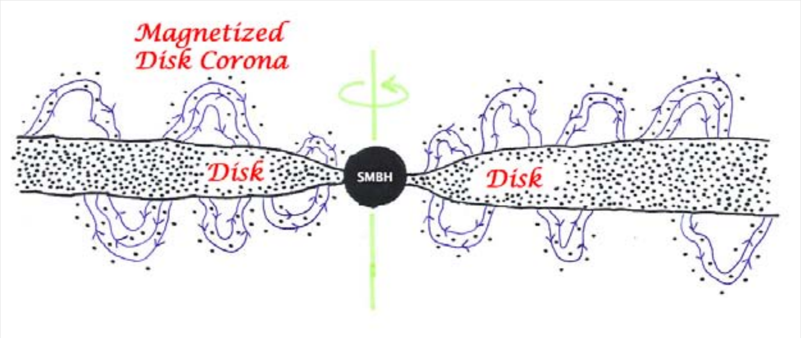

Broad band hump peaking at 20-40 keV.

Produced when X-rays shine upon the accretion disk or other material.

At low energies have a competition between Compton scattering and photoelectric absorption.

At high energies drops off due to Compton recoil, the Klein-Nishina cross section, and the power-law cutoff.

Affected by Doppler shifts, beaming, GR.

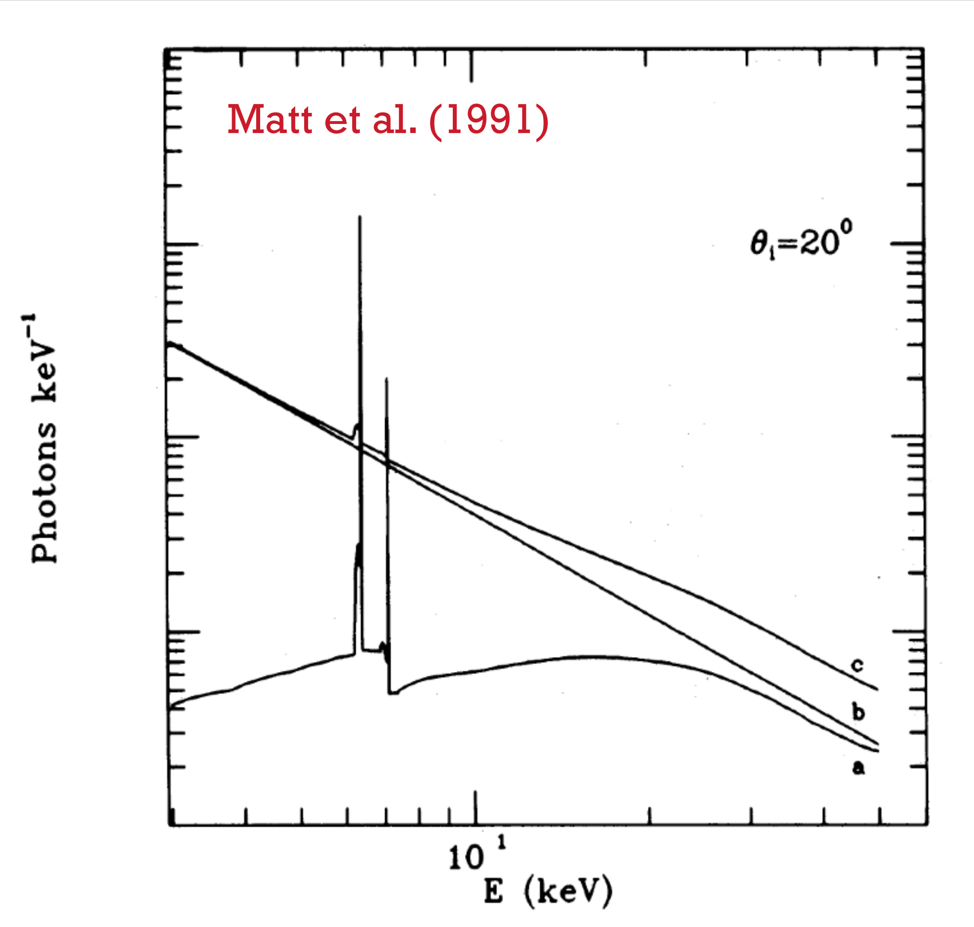

Iron Kα Line

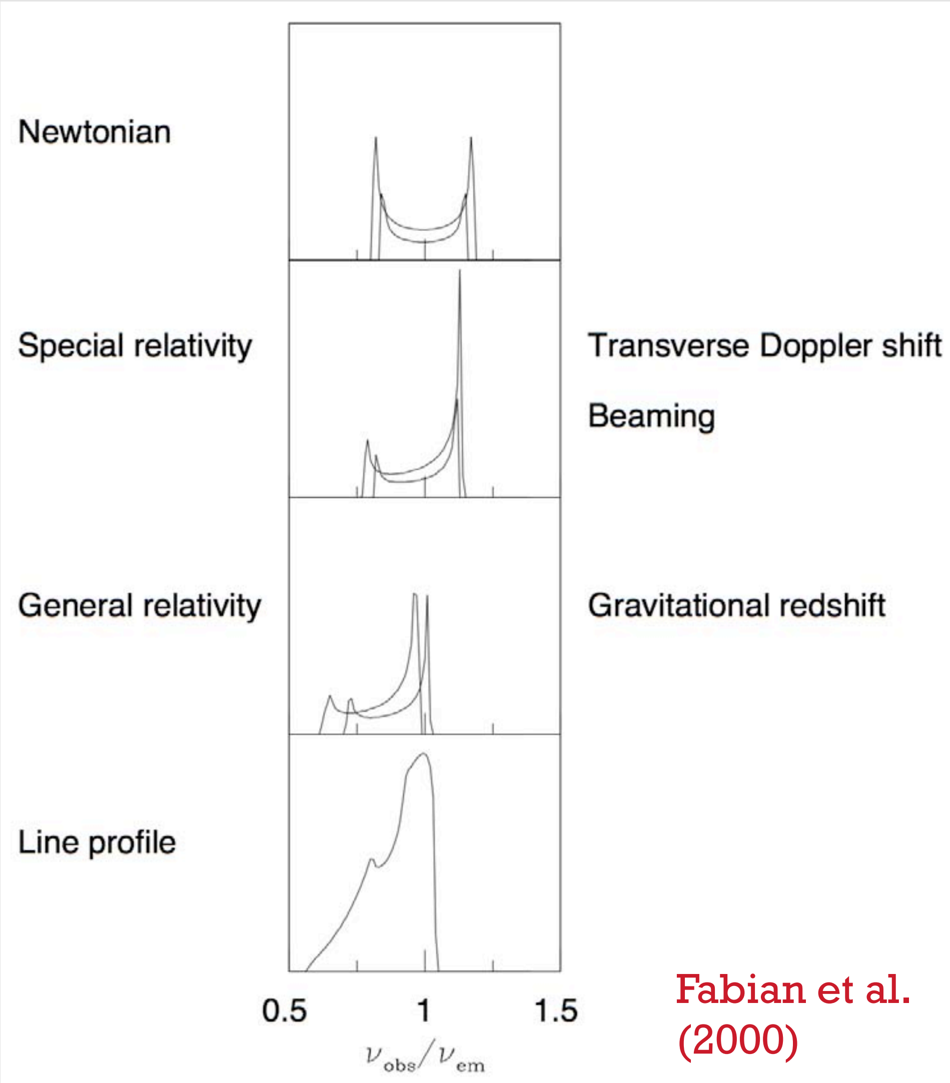

Fabian et al. (2000)

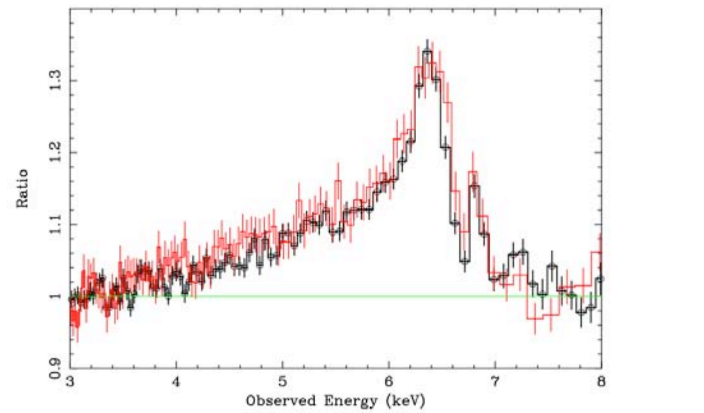

Figure 4: The figure above shows the relativistic disk line profile revealed in MCG-6-30-15 after fitting for the continuum. (Adapted from Miniutti et al. 2007 and Reeves et al. 2006.) The line in MCG-6-30-15 is the best example known presently, and these spectra above are the best yet obtained. The spectrum in black was obtained with *Suzaku*, and the spectum in red was obtained with *XMM-Newton*.

Made via iron fluorescence when disk irradiated by X-rays.

Iron has best product of abundance and fluorescent yield.

With very high-S/N data, can use to estimate disk inclination, disk emissivity, and black-hole spin.

Other Line Emission

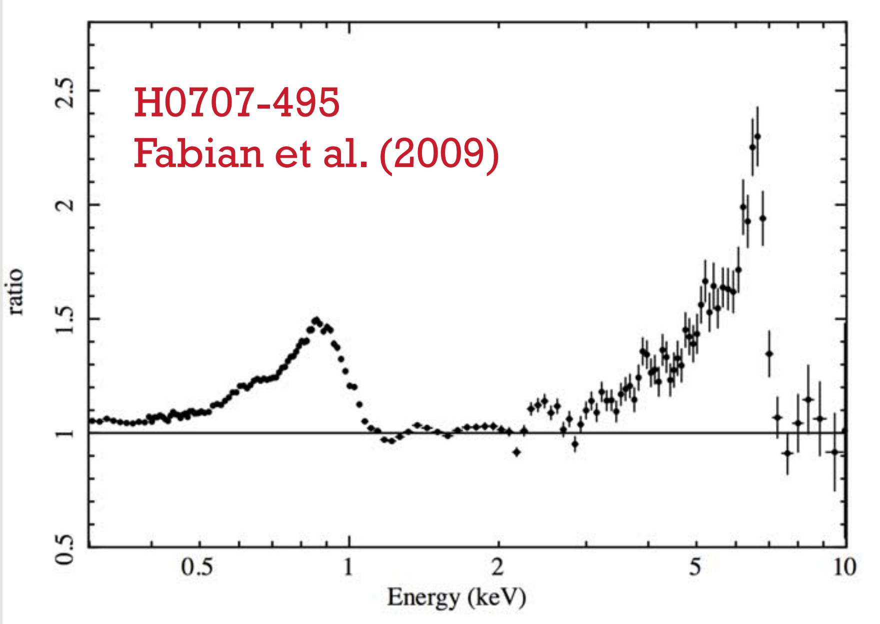

In some cases, broad iron L emission is also seen (probably from a line and absorption complex).

Contribute to the observed soft X-ray excess, and blending with other soft-excess components makes detailed modeling difficult.

Quantifying X-ray Variability

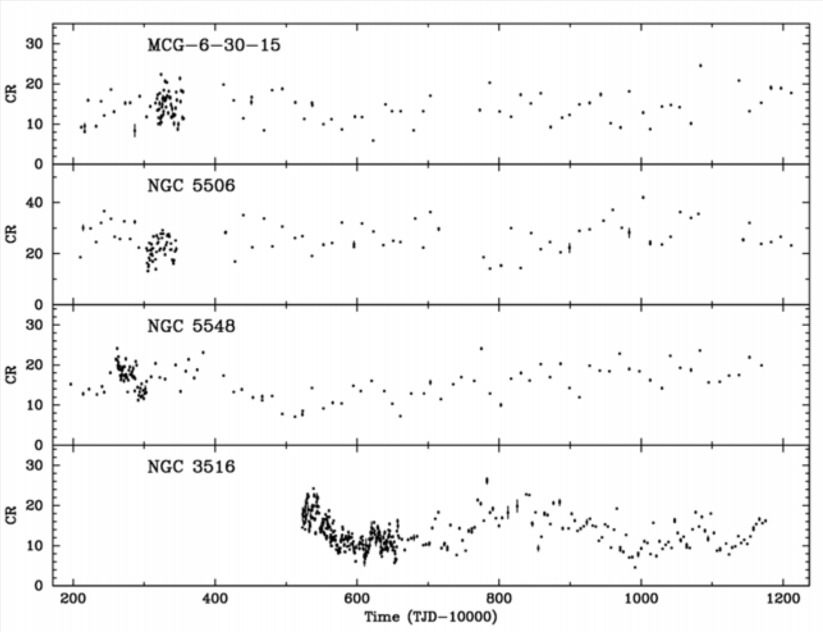

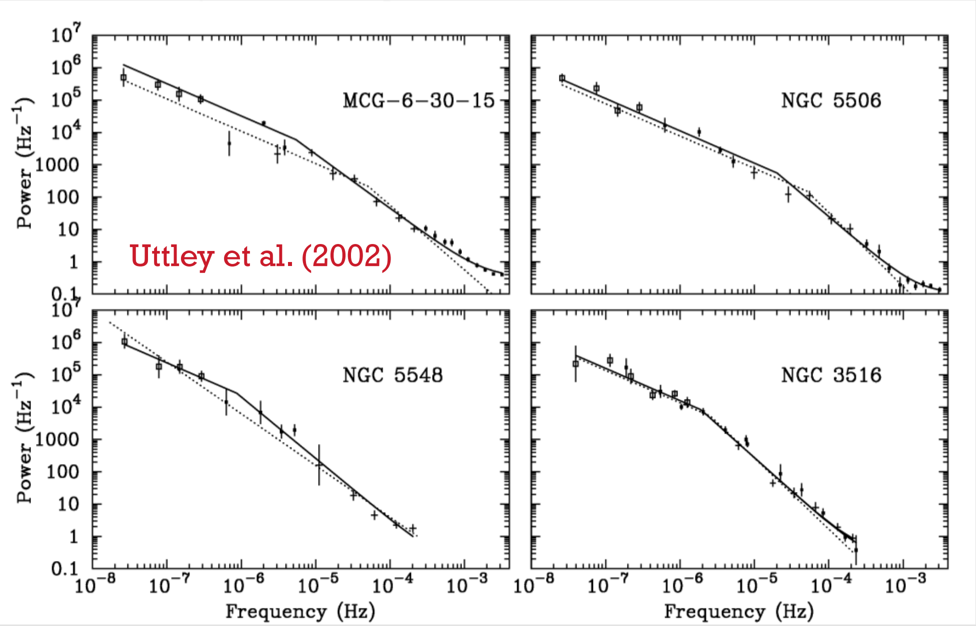

AGN variability power spectra usually do not show periodicity or quasi-periodicity.

Observe red noise power spectra with a bend/break at ~ 0.1-100 days.

The power spectra can be compared with those for Galactic black holes (the AGNs studied usually resemble soft-state Galactic black holes).

The bend/break timescale can be correlated with other AGN physical properties.

Mass and Eddington Fraction Scaling

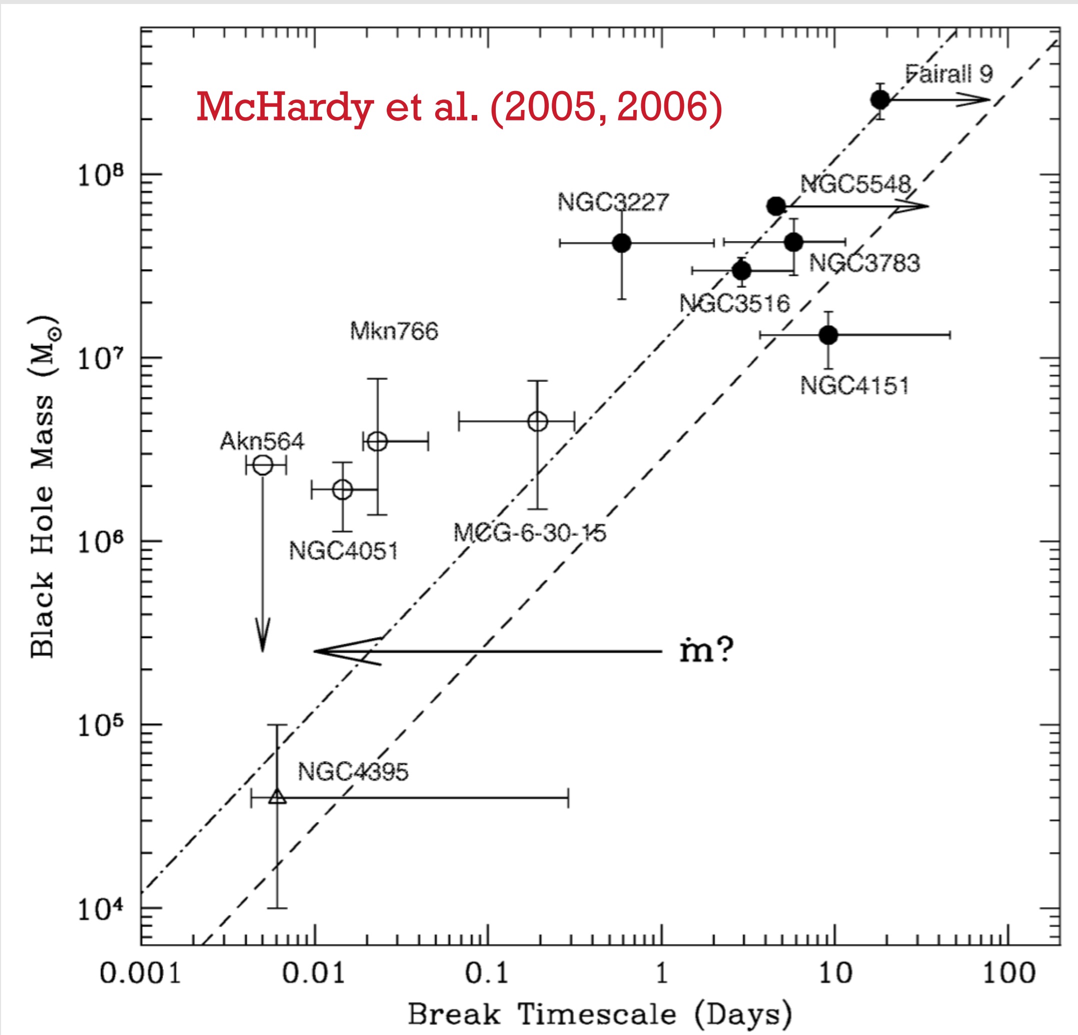

More detailed analyses find

$$T_{\rm B} \sim M^{1.17} \dot{m}_{\rm E}^{-0.9}$$

This simple formula describes well both Galactic black holes and AGNs.

AGNs behave like scaled-up Galactic black holes.

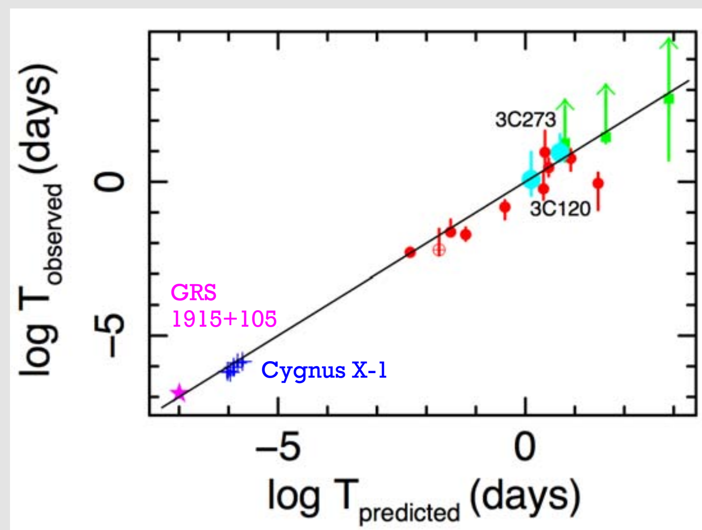

Extreme Variability Events: Example of PHL 1092

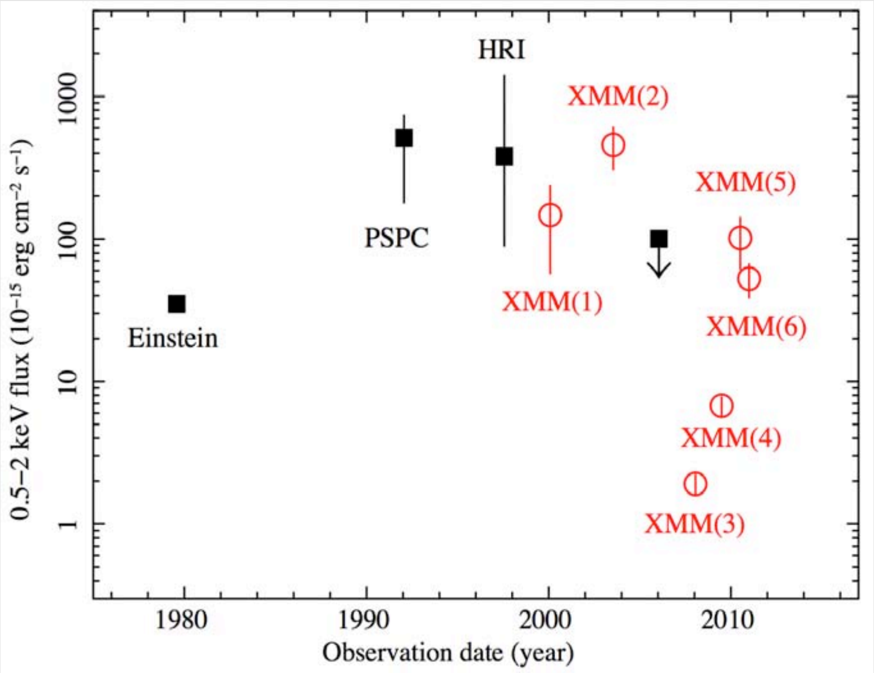

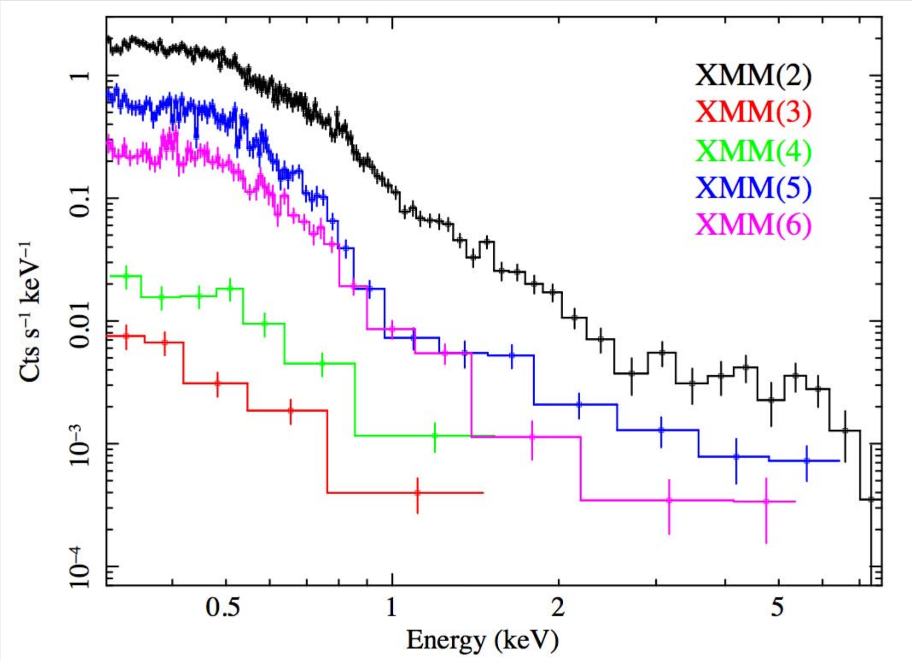

Miniutti et al. (2012)

X-ray luminosity drop by a factor of ~ 260 without strong X-ray spectral changes or correspondingly strong optical/UV changes.

Variable X-ray Absorption

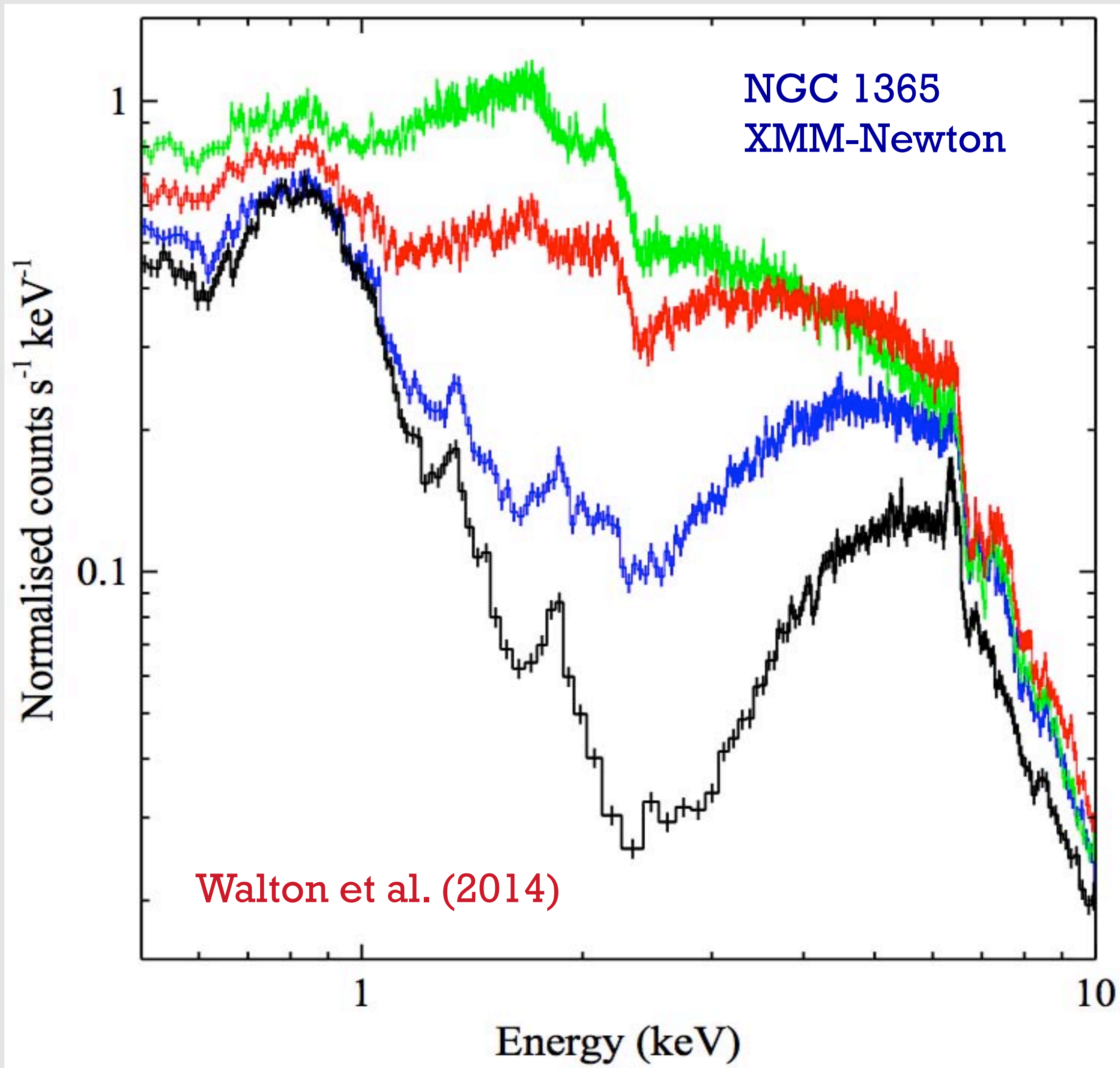

Examples of Iron Kα Line Variability

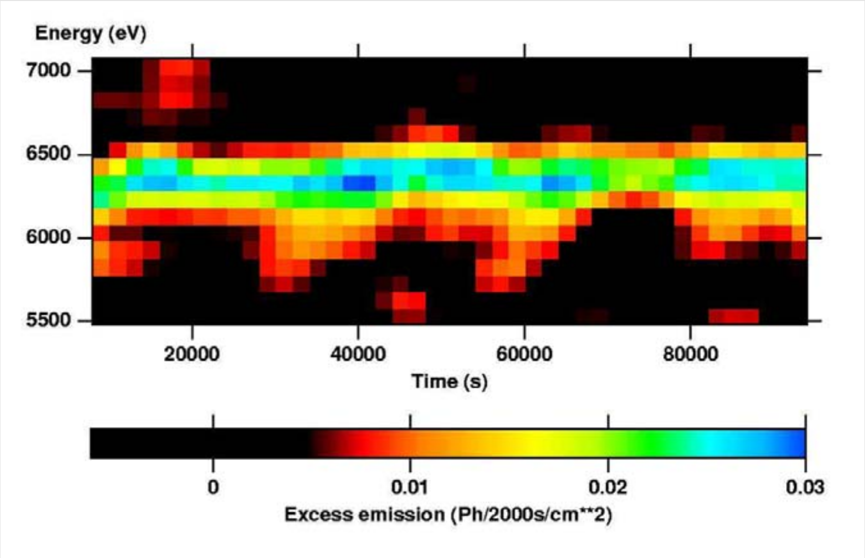

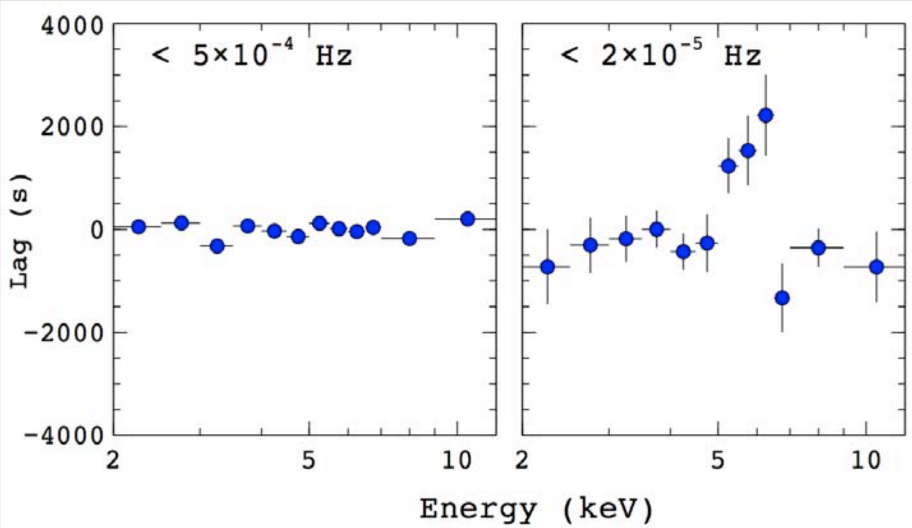

NGC 3516
Iwasawa et al. (2004)

NGC 4151
Zoghbi et al. (2012)

Iron Kα variability in a possibly periodic manner?

Iron Kα variability lagging the continuum by ~ 2000 s – reverberation?

The Broad Line Region (BLR)

Strong and Broad Optical/UV Emission Lines

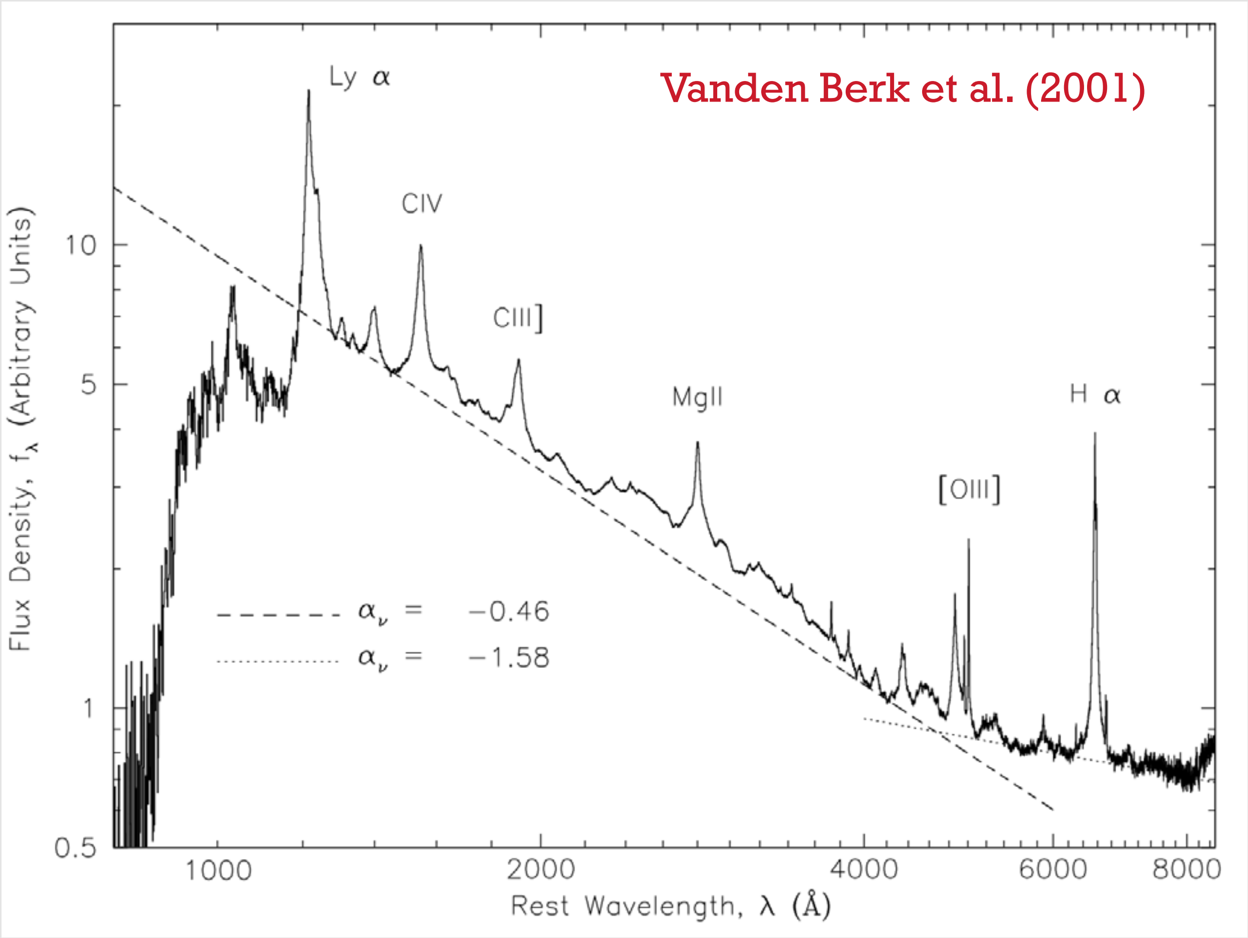

Ionization and Abundances

Relative strengths of emission lines in AGN spectra indicate we are observing gas in photoionization equilibrium at ~ 10^4 K.

Observed EWs of emission lines imply a global covering factor of ~ 10-20%.

Abundances about solar or slightly supersolar.

Lines are Kinematically Composite

Broad components

- Doppler widths of 1000-25000 km s^{-1}.
- Arise in gas with density $n_e \sim 10^9$-10^{11} cm^{-3} (as determined from strengths of certain density sensitive lines like [O III] and CIII]).
- From the "Broad Line Region".

Narrow components

- Doppler widths typically less than 900 km s^{-1}.
- Arise in relatively low-density gas ($n_e \sim 10^3$ cm^{-3}).
- From the "Narrow Line Region".

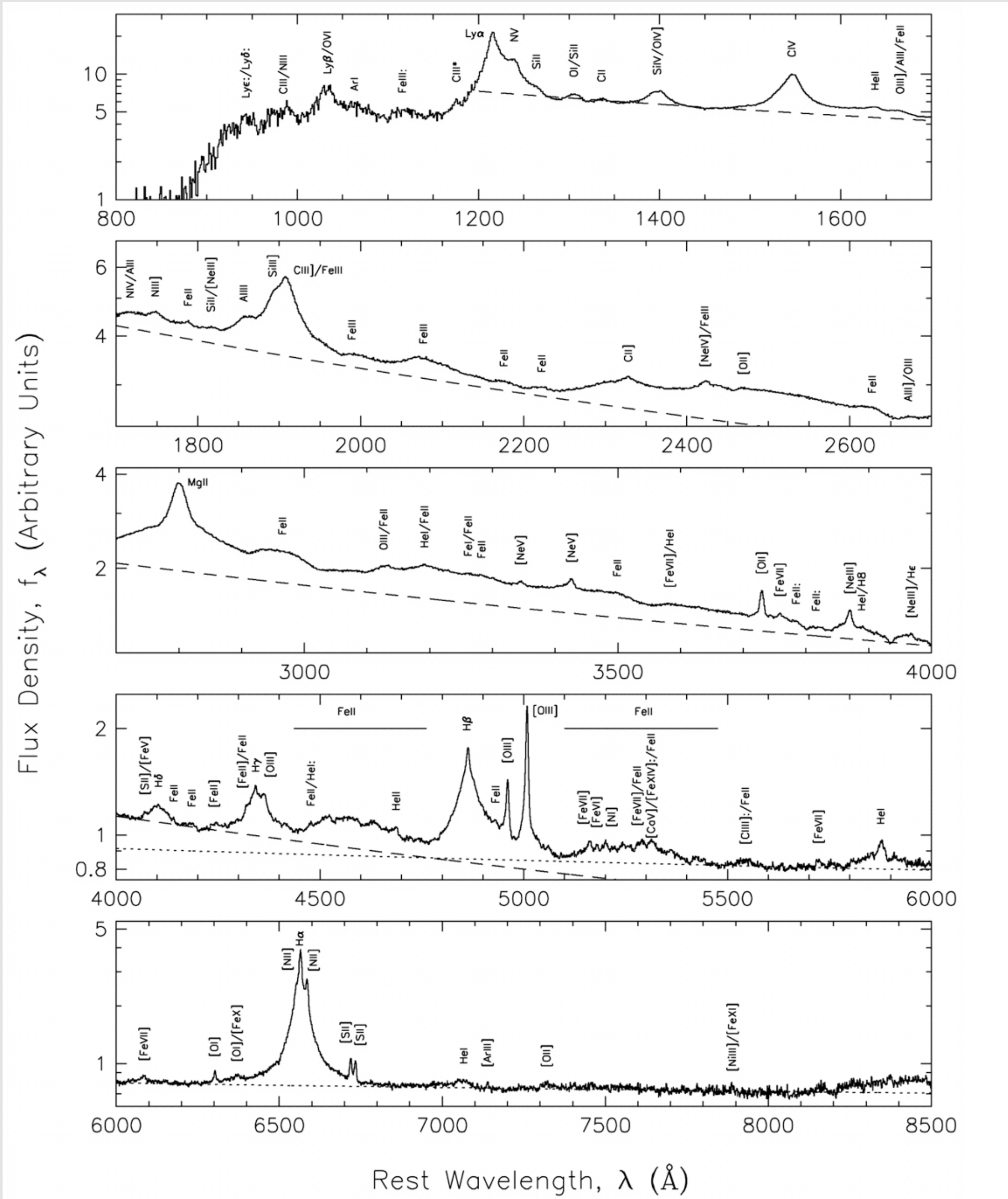

Vanden Berk et al. (2001)

Strong and Broad Lines Common

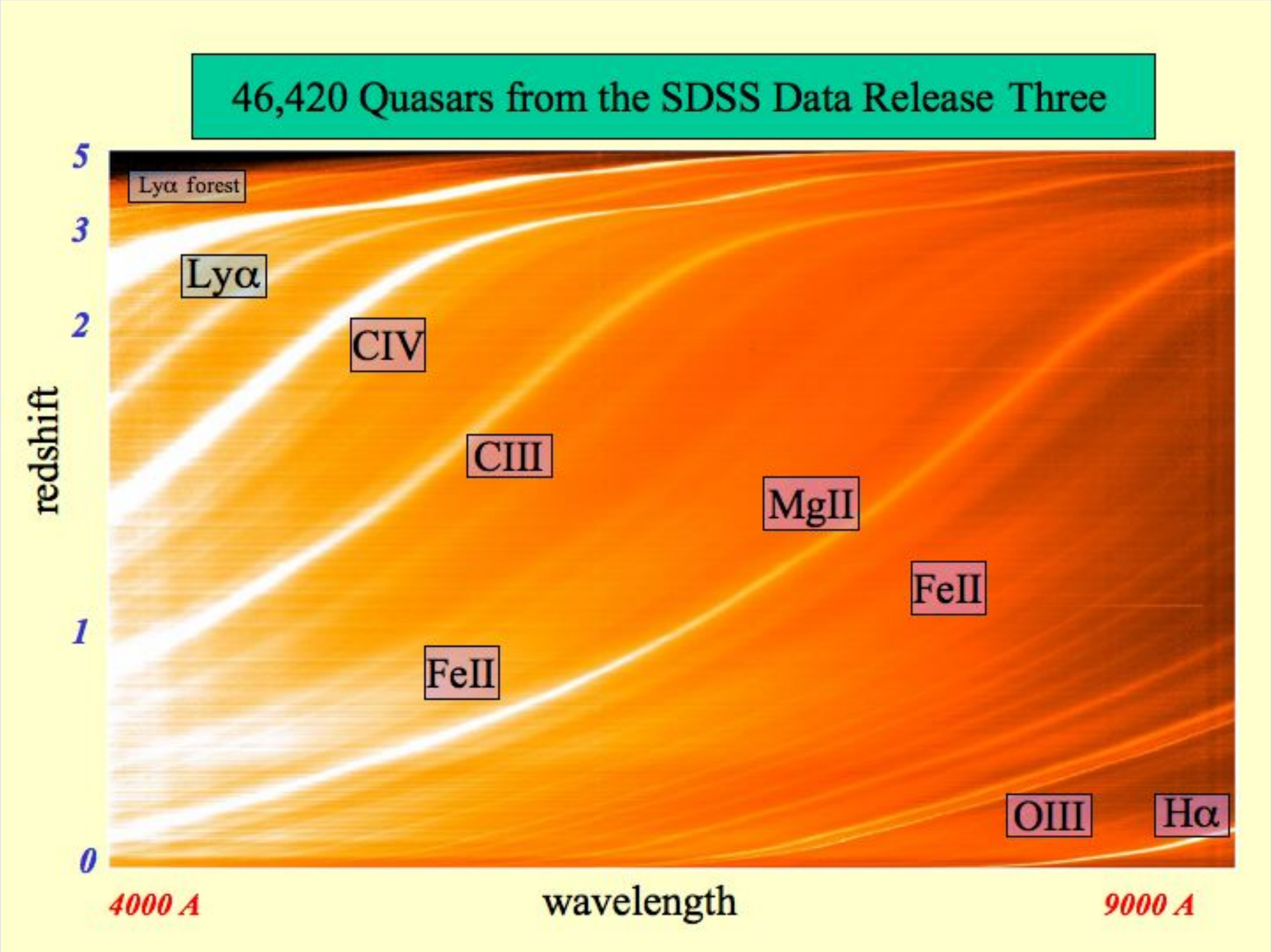

Fan et al.

Nature of the Doppler Widths

These motions are not thermal ($\sim$10 km s^{-1} for 10^4 K).

Rather are supersonic bulk motions.

The larger Doppler widths of the broad lines indicate they arise deeper in the gravitational potential.

Basic Variability Properties

The broad lines vary on short timescales, usually following the continuum variations with a time delay.

Thought to be the light travel time across the BLR, leading to the idea of "reverberation mapping".

Provides a way to measure the BLR size, which is ~ 5-500 light days depending upon luminosity.

The narrow lines do not vary on short timescales, indicating they are from a much larger region.

Broad Lines Lag Continuum

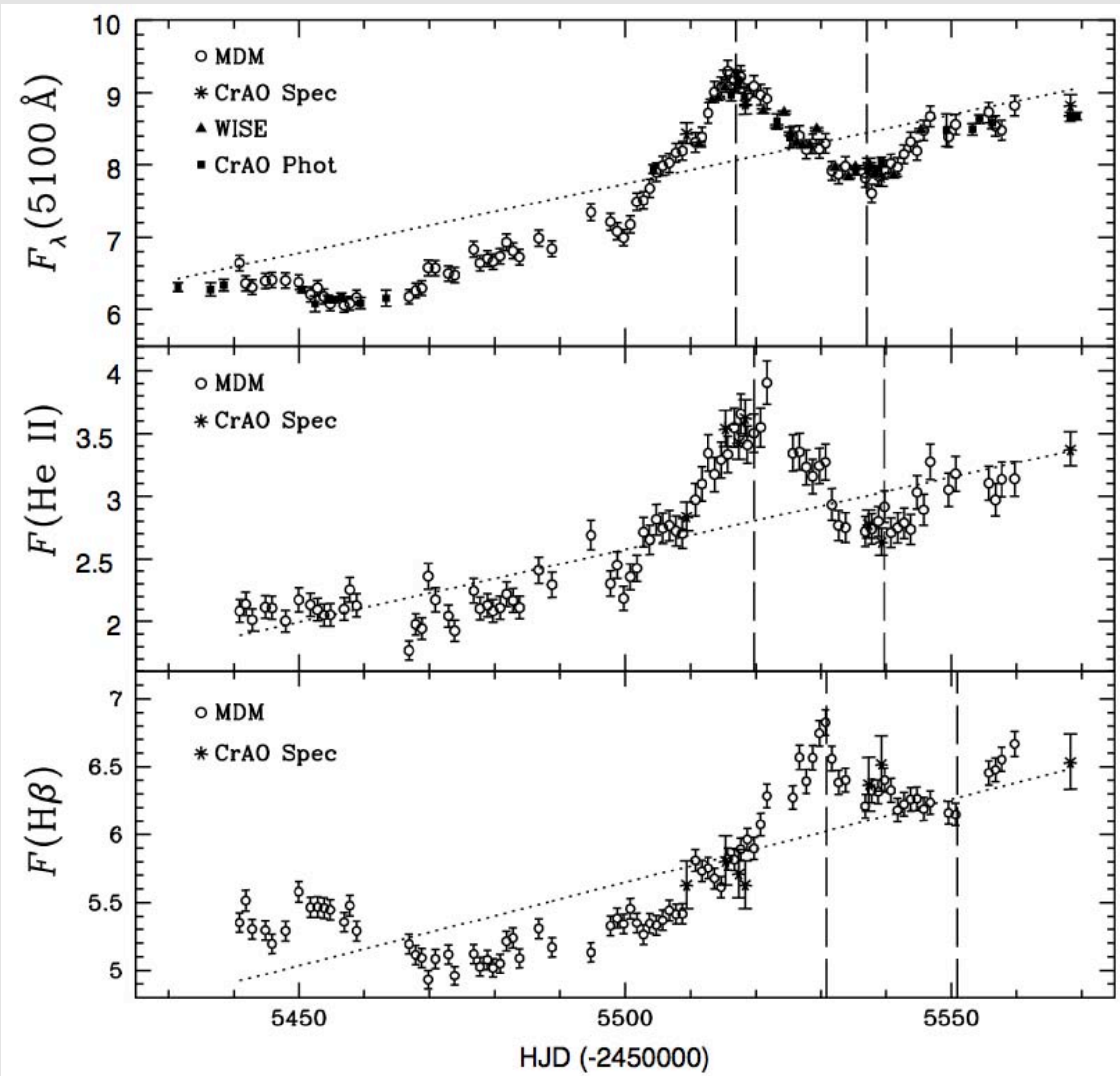

Figure 2. Complete light curves for Mrk 335 from our observing campaign. The top panel shows the 5100 Å flux in units of 10^{-15} erg s^{-1} cm^{-2} Å^{-1}, the middle panel shows the flux in the He II λ4686 region in units of 10^{-13} erg s^{-1} cm^{-2}, and the bottom panel shows the integrated H$\beta\lambda$4861 flux, also in units of 10^{-13} erg s^{-1} cm^{-2}. Open circles denote observations from MDM Observatory and asterisks represent spectra taken at CrAO. Closed squares show the photometric observations from CrAO, and closed triangles represent photometric observations from WISE Observatory. Vertical dashed lines have been placed at two obvious features in the continuum to aid the eye. The vertical lines have been shifted by the measured He II and Hβ lag values (2.7 days and 13.9 days, respectively) to aid the eye in identifying the correct lag values for each emission line. Dotted lines show the trends that were subtracted before performing the cross-correlation analysis.

Grier et al. (2012)

Size of the Broad Line Region

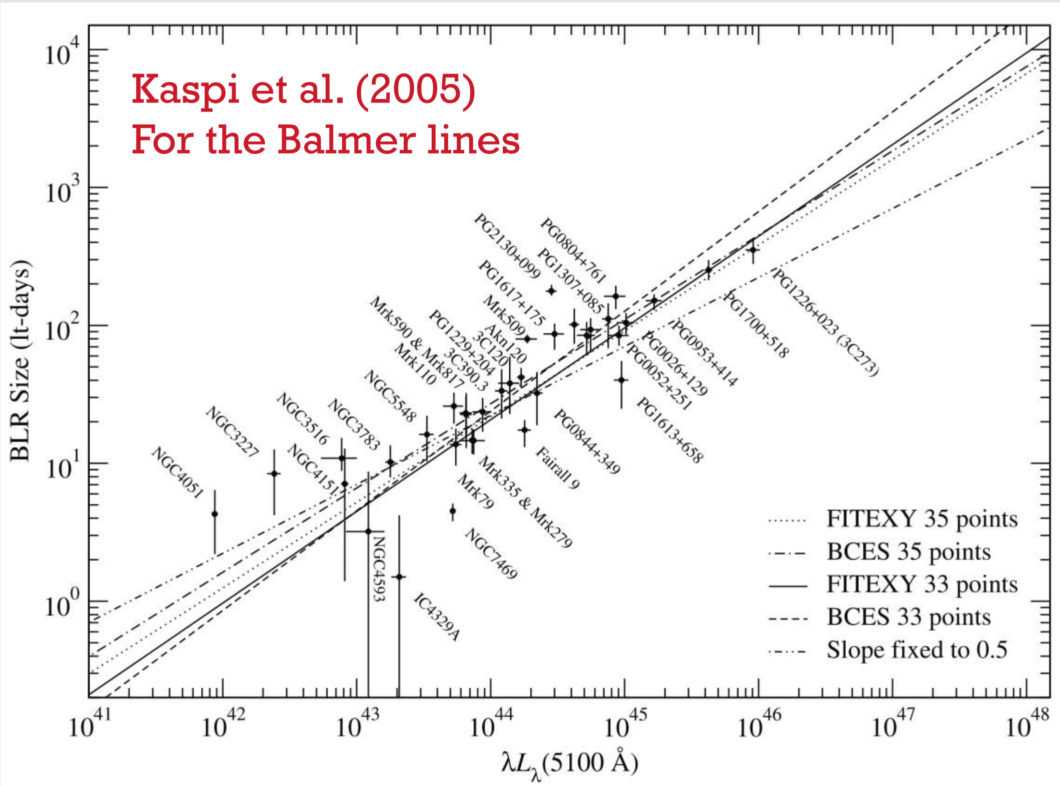

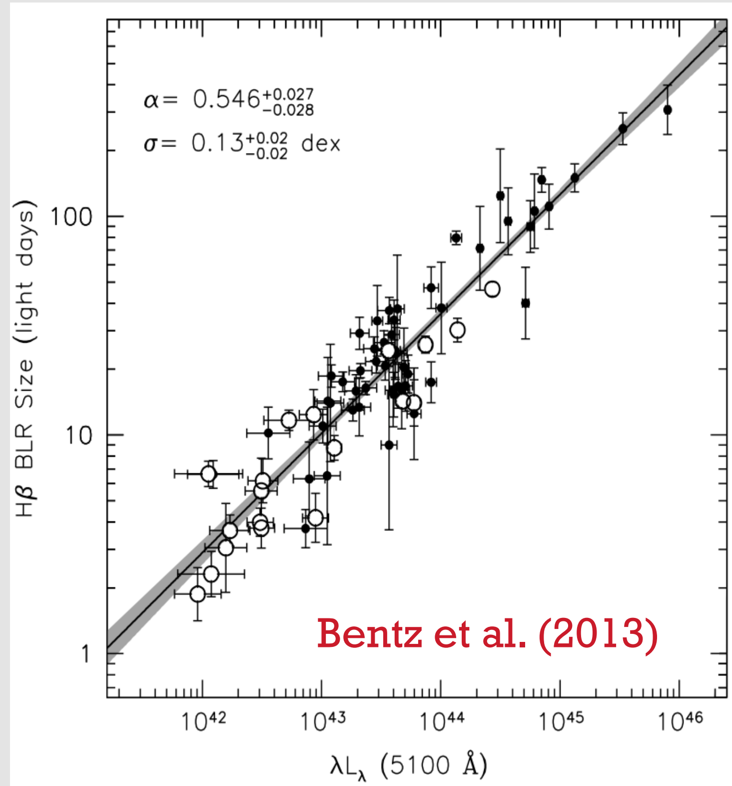

The BLR radius is found to scale as $R_{\rm BLR} \sim L^{0.5\text{-}0.7}$.

The slope is about as expected if all AGNs have similar ionization parameters and densities in their BLRs ($r \sim L^{0.5}$).

Broad-Line Profiles

Broad-line profiles are non-Gaussian.

Sometimes described as "logarithmic", where the flux at some offset $\Delta\lambda$ from the line center is proportional to $-\ln \Delta\lambda$ (for $\Delta\lambda$ not too close to line center).

Sometimes fit with 2-3 Gaussian components, or Gaussian + Lorentzian.

In a single source, the profiles of different broad lines show diversity; lines of more ionized species tend to be broader.

Some lines, particularly those of high ionization (e.g., C IV), can show significant blueshifts in the AGN rest frame.

In many cases the line profiles have additional structure; e.g., bumps, humps, asymmetric wings. Double-peaked BLR lines are a rare, extreme example.

Double-Peaked BLR Lines

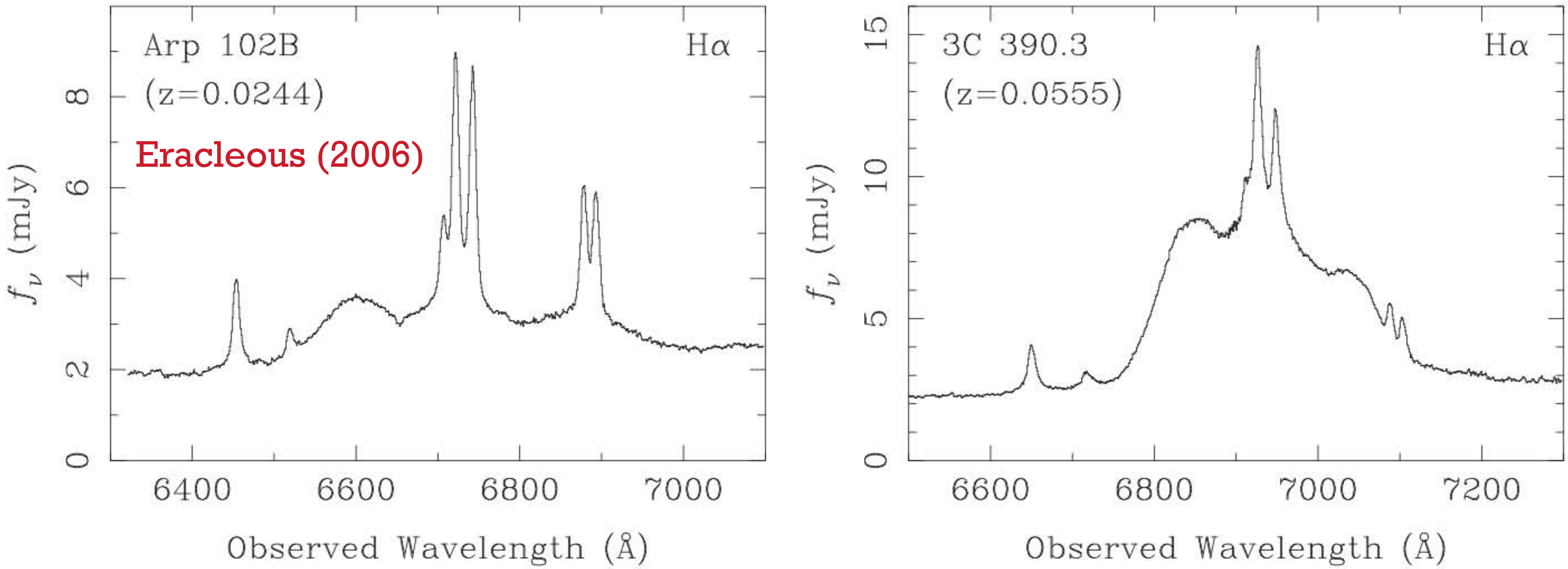

Figure 2. The observed Hα spectra of Arp 102B and 3C 390.3 as examples of double-peaked Balmer emission lines. The approximate full widths of the lines at half maximum are 16,000 km s^{-1} and 12,000 km s^{-1}, respectively.

Characteristic of rotating disks – some of the BLR emission from a disk?

Double-peaked BLR lines can show complex variability patterns.

Broad-Line Profiles

Unfortunately, modeling the profiles usually does not strongly constrain how the BLR gas is moving, owing to modeling degeneracies.

Infall? Outflow? Orbital motion?

But constraints upon the "microstructure" in line profiles suggest the number of discrete "clouds" must be large, more than ~ 10^6-10^8.

Suggests that there may well not be "clouds" at all, but rather a continuous flow.

High-S/N Microstructure Search

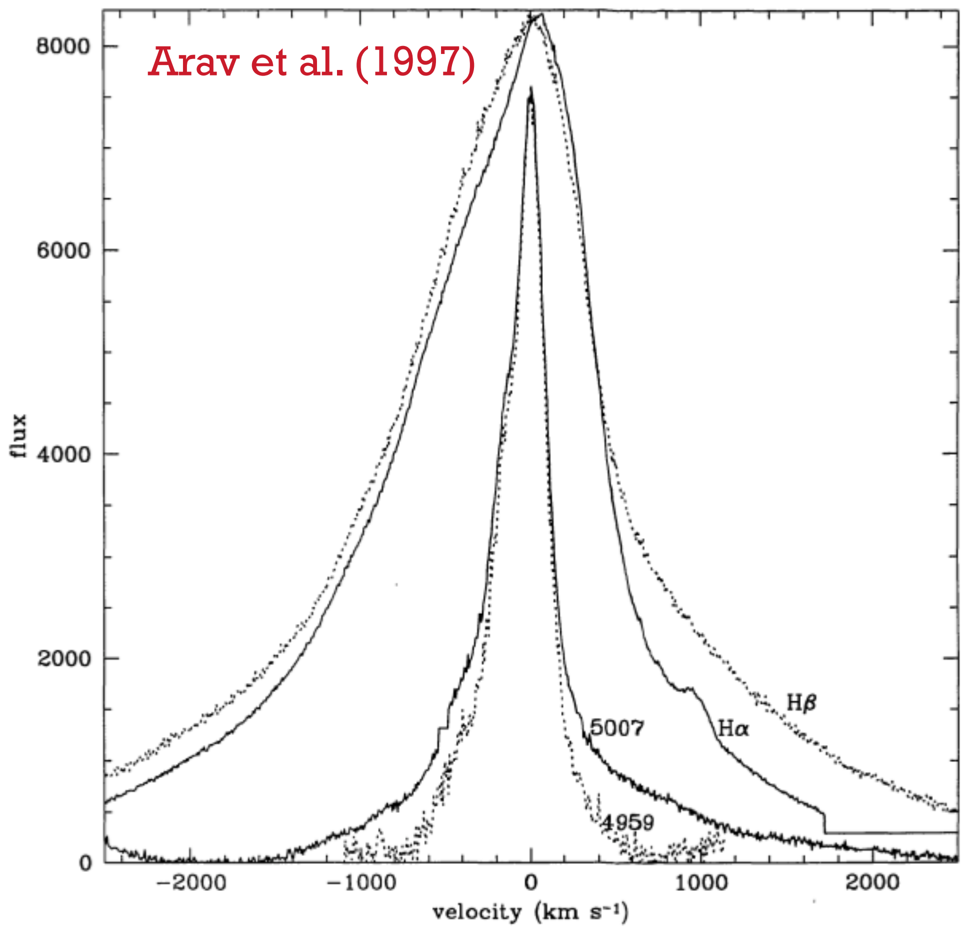

Figure 1. The observed line profiles of Mrk 335 (continuum subtracted) in arbitrary scaling that matches the peaks of Hα and Hβ, and separately the peaks of the O III lines (5007 and 4959 Å). The profiles of the 5007 and 4959 Å lines do not match owing to blending with Hβ.

Object-to-Object Differences in Broad Line Properties

There are significant object-to-object differences in broad-line properties.

Some emission lines, such as C IV, show lower EWs (on average) as luminosity increases. Known as the "Baldwin effect".

There is a set of emission-line properties that vary in a correlated manner called "Eigenvector 1". Likely related to L / L_{Edd}.

Eigenvector 1 from PCA

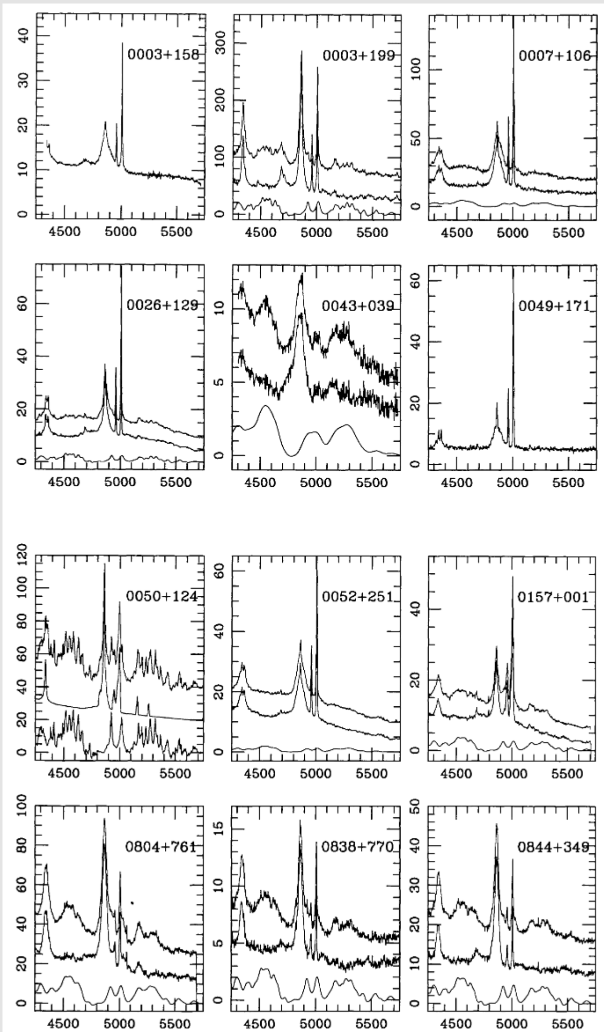

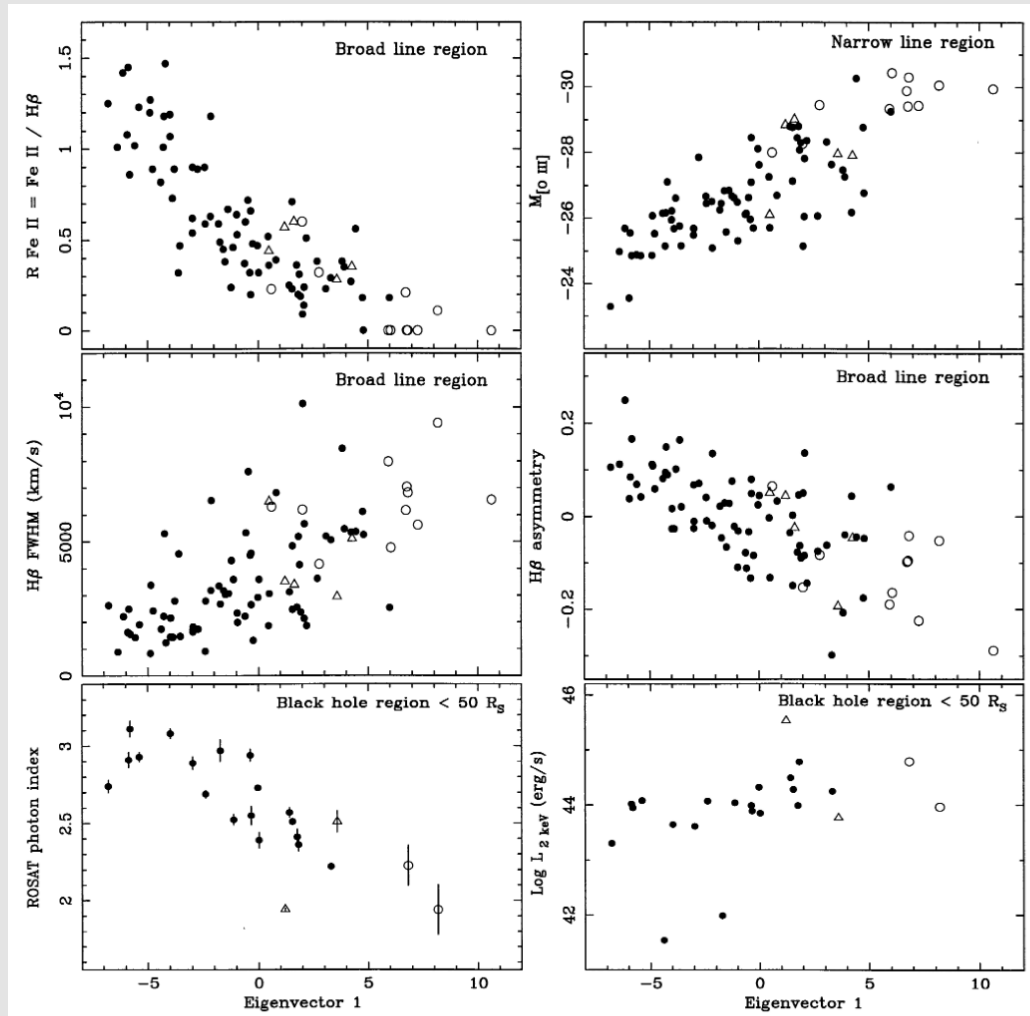

Boroson & Green (1992)

Reverberation Mapping: Stratification and Virialization

Reverberation lags have now been measured for ~ 50 AGNs.

The current sample is biased toward AGNs with relatively strong lines.

Mostly measured for Hβ, but in some cases for multiple lines.

The highest ionization emission lines respond most rapidly to continuum changes, indicating ionization stratification.

A plot of line width vs. lag (τ) shows that $v \sim \tau^{-0.5}$, as expected for virialized gas dominated by the gravitational potential of the central source.

But must still worry about other effects, especially radiation pressure.

Evidence for Virialization

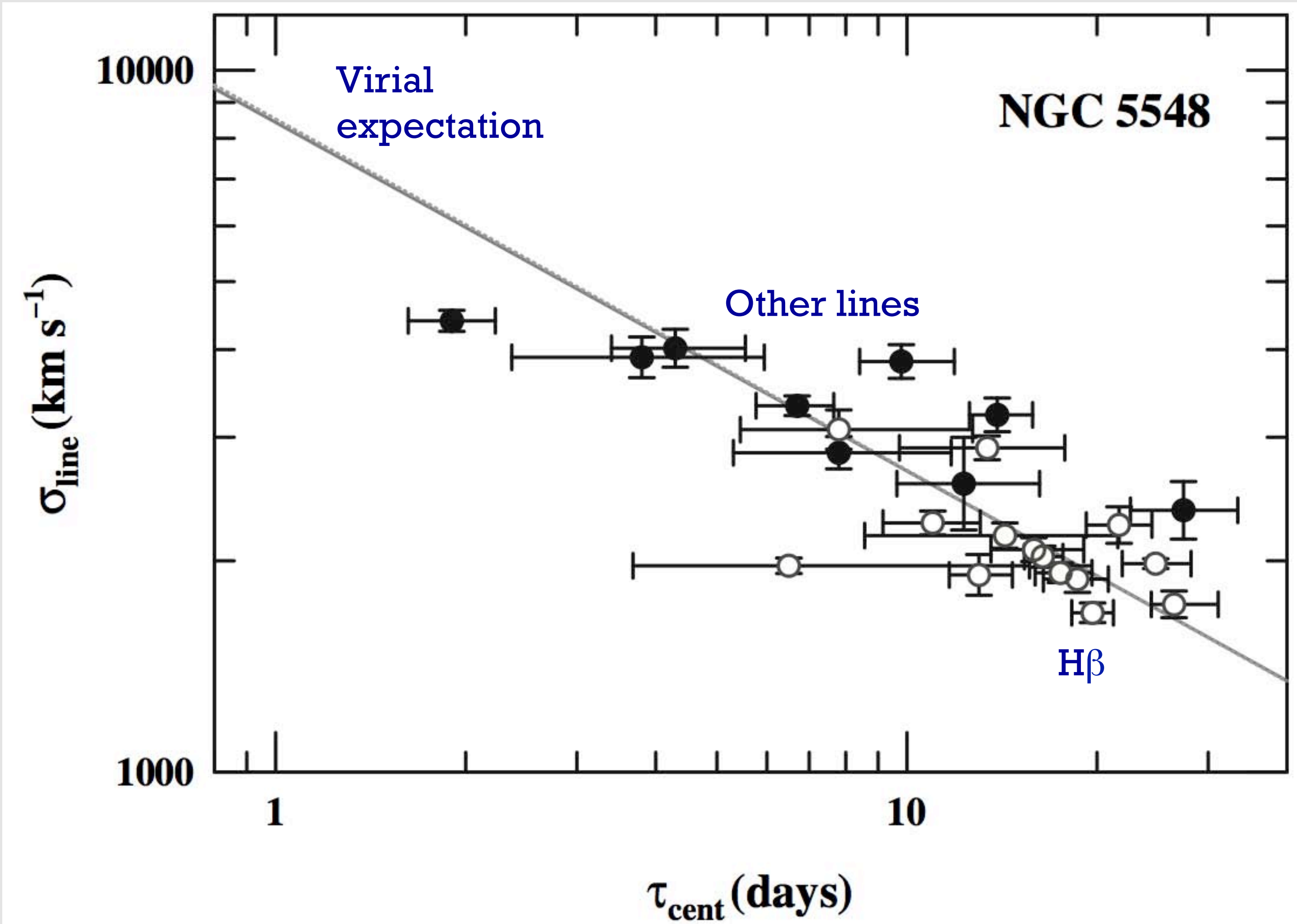

Peterson et al. (2004)

BLR "Breathing"

In a few well-studied objects the BLR has been observed to "breathe" over ~ year timescales, appearing to become larger as a source varies to high luminosities.

The BLR gas itself does not expand and contract under such "breathing". It is moving much too slowly for this.

Rather, there is gas everywhere in the line-emitting region, and what changes with luminosity is the distance from the continuum source where conditions are optimal for line emission.

This idea is called the "local optimally emitting cloud" (LOC) model.

Total reservoir of gas present is ~ 1000-10000 $M_{\odot}$, though only a small fraction of this (less than ~ 1%) radiates lines efficiently at a given time.

Example of BLR "Breathing"

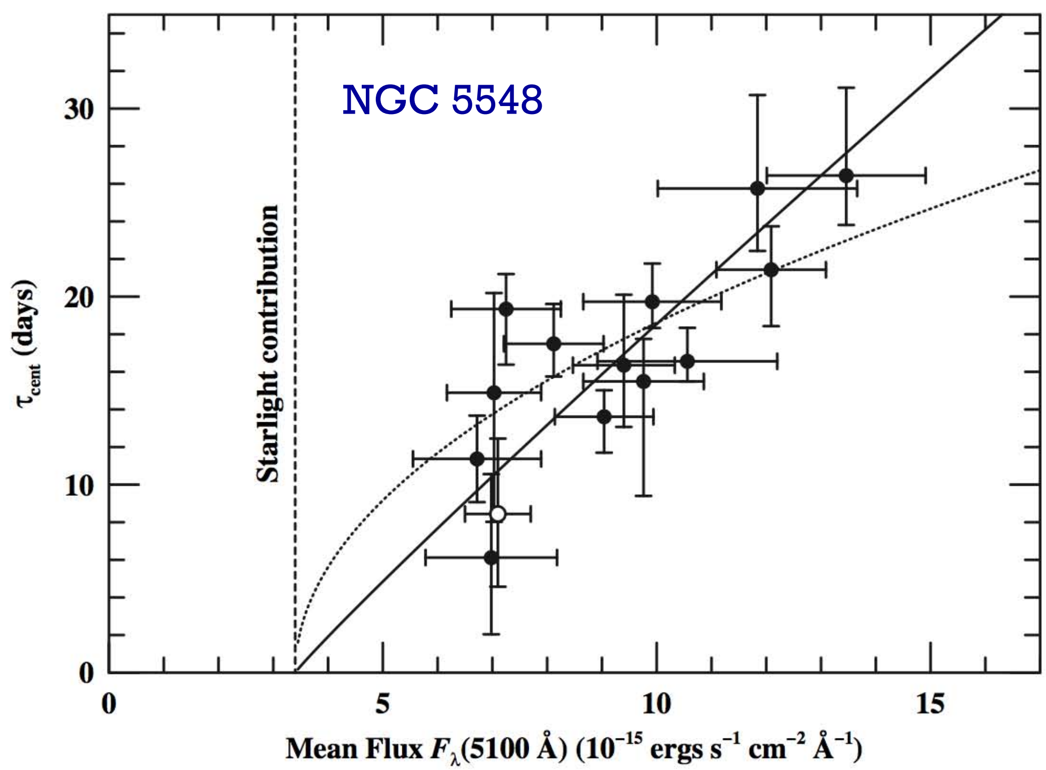

Fig. 7. Measured time delays for Hβ in NGC 5548 versus optical continuum flux for 14 independent experiments. The vertical line shows the constant stellar contribution to the measured continuum flux. The best-fit slope to this relationship is shown as a solid line $\tau(\mathrm{H}\beta) \propto F_\lambda^{0.9}$ and the dotted line shows the naive prediction $\tau(\mathrm{H}\beta) \propto F_\lambda^{1/2}$. From [27]

Peterson et al. (2002)

Estimating Black Hole Masses

Can estimate black-hole masses following the virial theorem:

$$M_{\mathrm{BH}} = \frac{f c\tau \Delta V^2}{G}$$

Where *f* is a factor that includes (unknown) BLR geometry and inclination.

Comparison with other mass-estimation methods indicates an average value of *f* ~ 4-5.

Masses measured this way appear accurate to within a factor of ~ 3 when Hβ is used.

Note this method can be used, if patient, for masses at high redshifts.

Mass-Luminosity Relationship

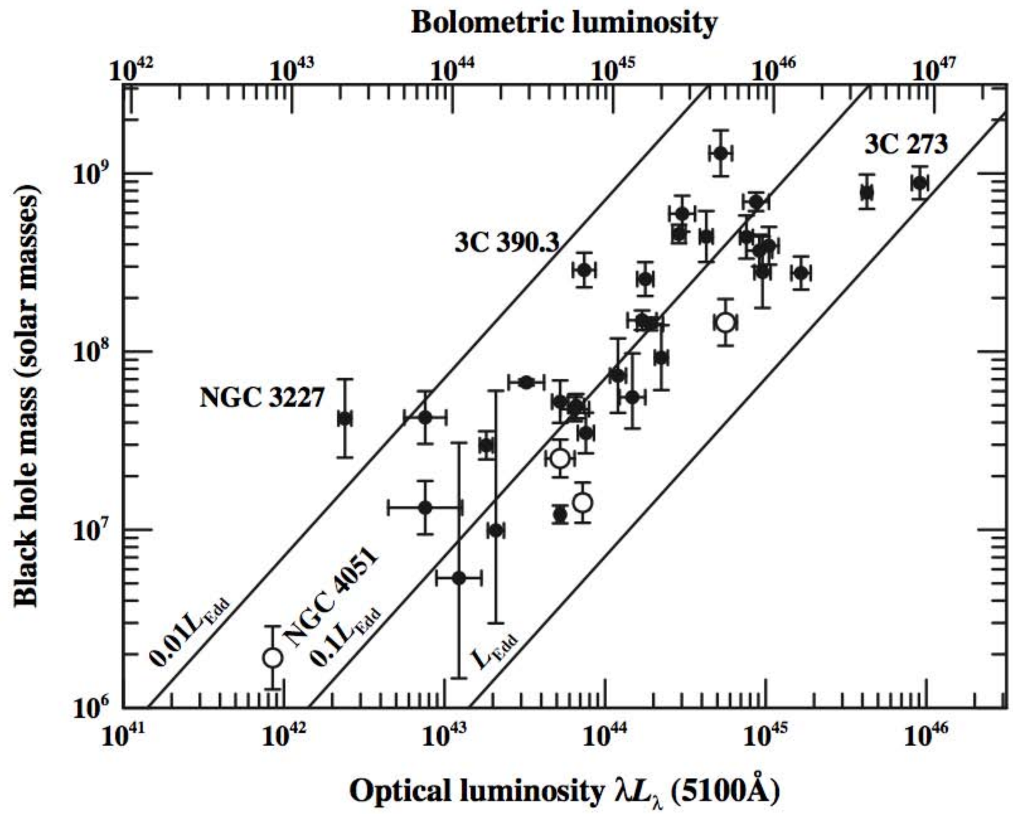

Fig. 9. The mass–luminosity relationship for reverberation-mapped AGNs. The luminosity scale on the lower x-axis is $\log \lambda L_\lambda$ in units of ergs s^{-1}. The upper x-axis shows the bolometric luminosity assuming that $L_{bol} \approx 9\lambda L_\lambda(5100\,\text{Å})$. The *diagonal lines* show the Eddington limit L_{Edd}, $0.1L_{Edd}$, and $0.01L_{Edd}$. The *open circles* represent NLS1s. From [25]

Peterson et al. (2004)

Single-Epoch Masses

Can combine the $R_{\rm BLR}$-L relation with the virial theorem to estimate single-epoch masses. For example…

$$\frac{M_{\rm BH}}{10^6\ M_\odot} = 4.35 \left[\frac{\nu L_\nu(5100\ \text{Å})}{10^{44}\ \text{ergs s}^{-1}}\right]^{0.7} \left[\frac{\text{FWHM(H}\beta)}{10^3\ \text{km s}^{-1}}\right]^2$$

Similar relations exist for Mg II and C IV.

These allow quick estimates for large AGN samples, but their accuracy is no better than a factor of several. The main challenge is characterizing the line widths, where caution is needed.

Statistical use of such masses in large samples is probably OK, but individual mass estimates may be unreliable.

Velocity Resolved RM

Ideally would study how the full line profile varies over time, instead of just the integrated line flux.

Observationally challenging, but some progress recently.

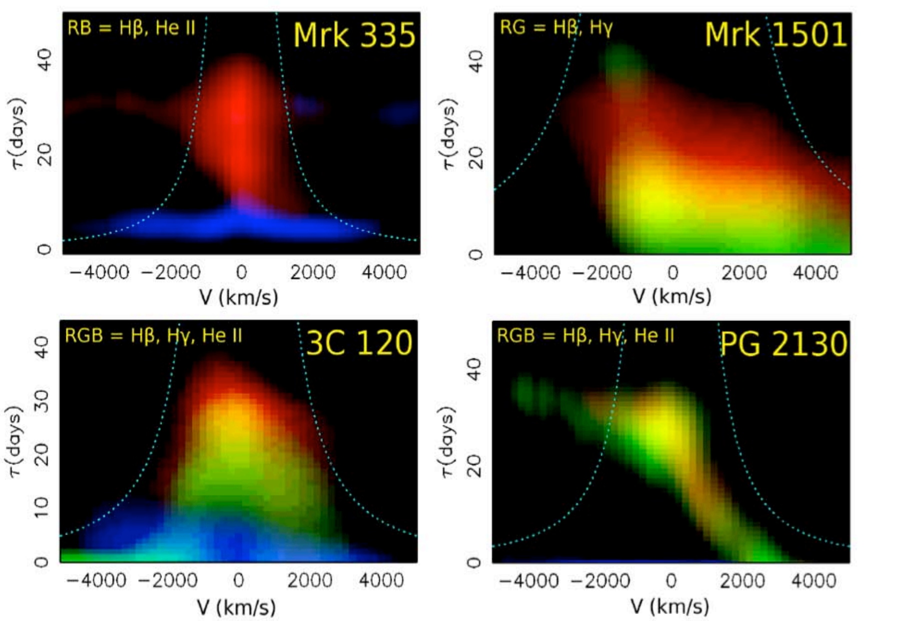

Fig. 5 Velocity–delay maps for four AGNs. 3C 120 has a disk-like structure and evidence for infall is apparent in each of these. Grier et al. (2013).

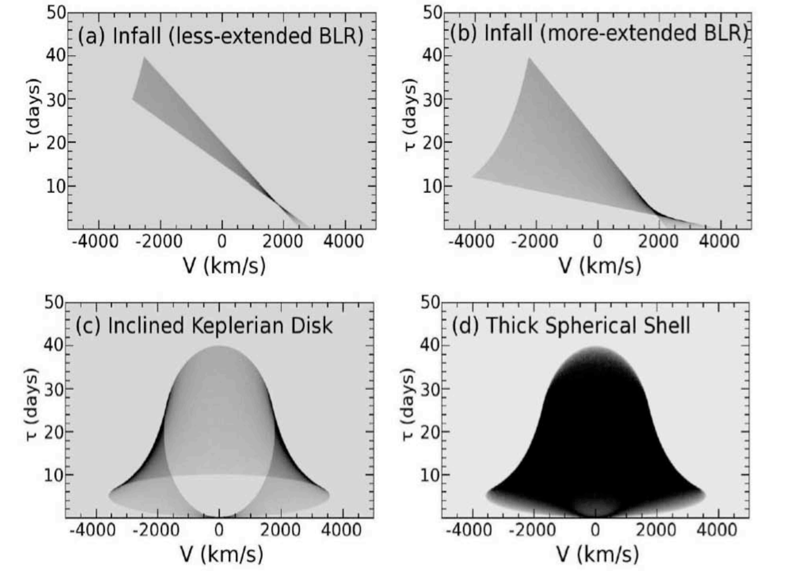

Fig. 6 Toy models of velocity–delay maps for spherical infall (top two panels) and a Keplerian disk (lower left) and a thick shell of randomly inclined circular Keplerian orbits (lower right). Grier et al. (2013).

Grier et al. (2013)

What is the Nature of the BLR?

After much research, it is appearing increasingly likely that the BLR itself has a composite nature:

Moderate-ionization and high-optical-depth region

- Largely responsible for the Balmer-line emission and Mg II
- Accretion disk itself?
- A disk with a large line-emitting region can make single-peaked profiles consistent with most objects

High-ionization and moderate-optical-depth region

- Largely responsible for the high-ionization lines
- Accretion-disk wind?
- Helps explain blueshifts of high-ionization lines and blueward line asymmetries

Outflowing Winds

Blueshifted UV Broad Absorption Lines in Quasars

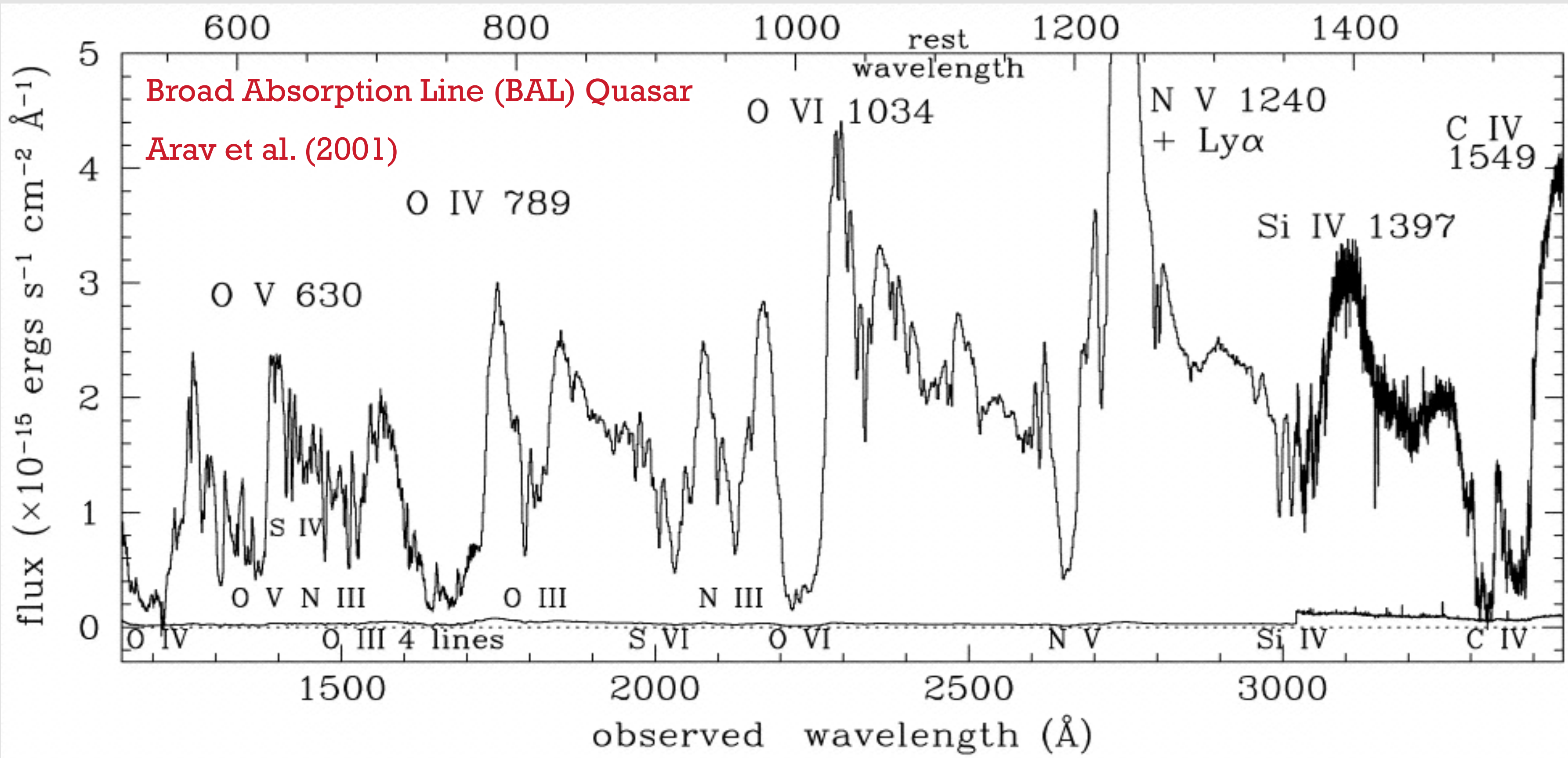

Bona-fide BALs seen in about 10-15% of optically selected quasars (true fraction higher).

Additional Examples of BAL Quasars

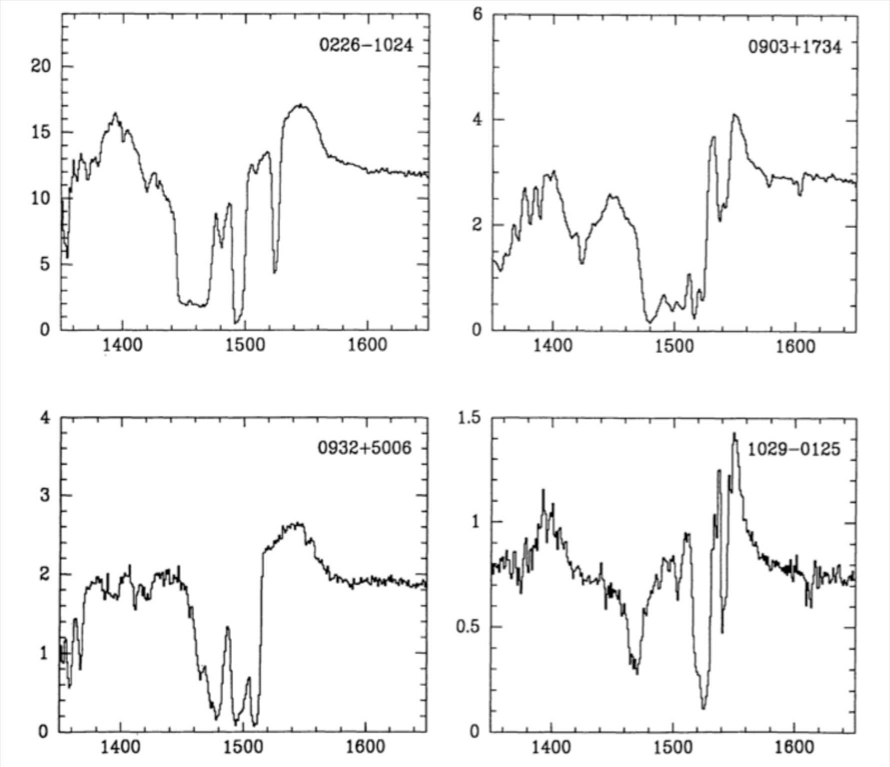

Korista et al. (1993)

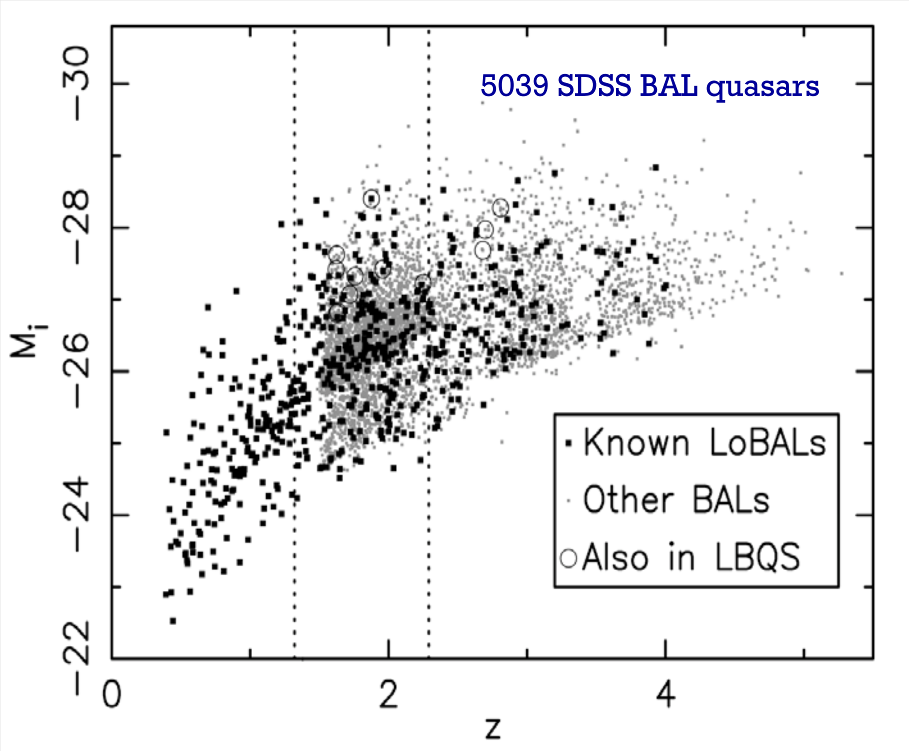

Gibson et al. (2009)

BAL profiles are complex and diverse. Also "mini-BAL" and "NAL" quasars.

Large samples of BAL quasars have now been identified from, e.g., SDSS.

UV Outflows Found Over a Wide AGN Luminosity Range

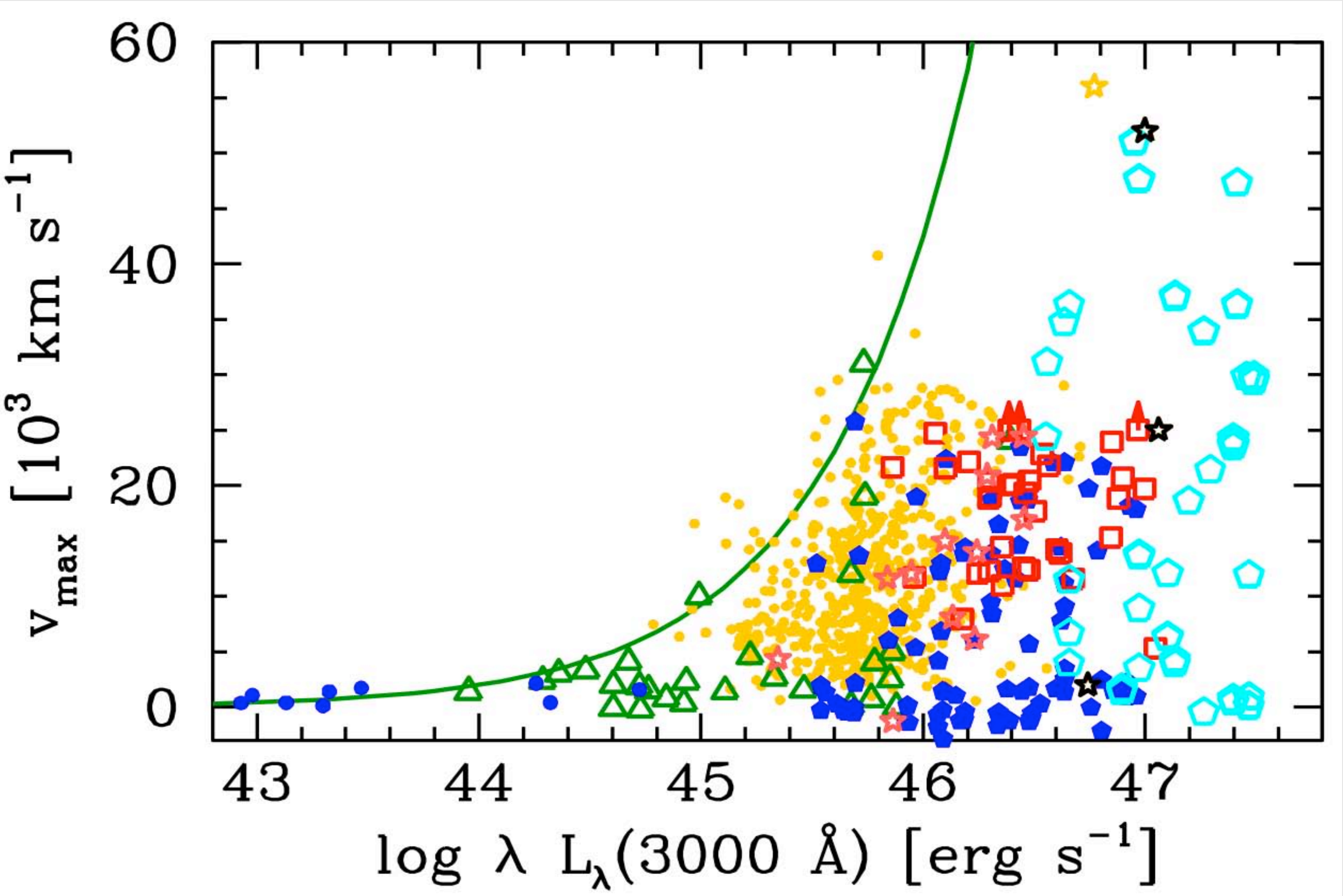

Ganguly & Brotherton (2008)

UV Absorption in Seyferts

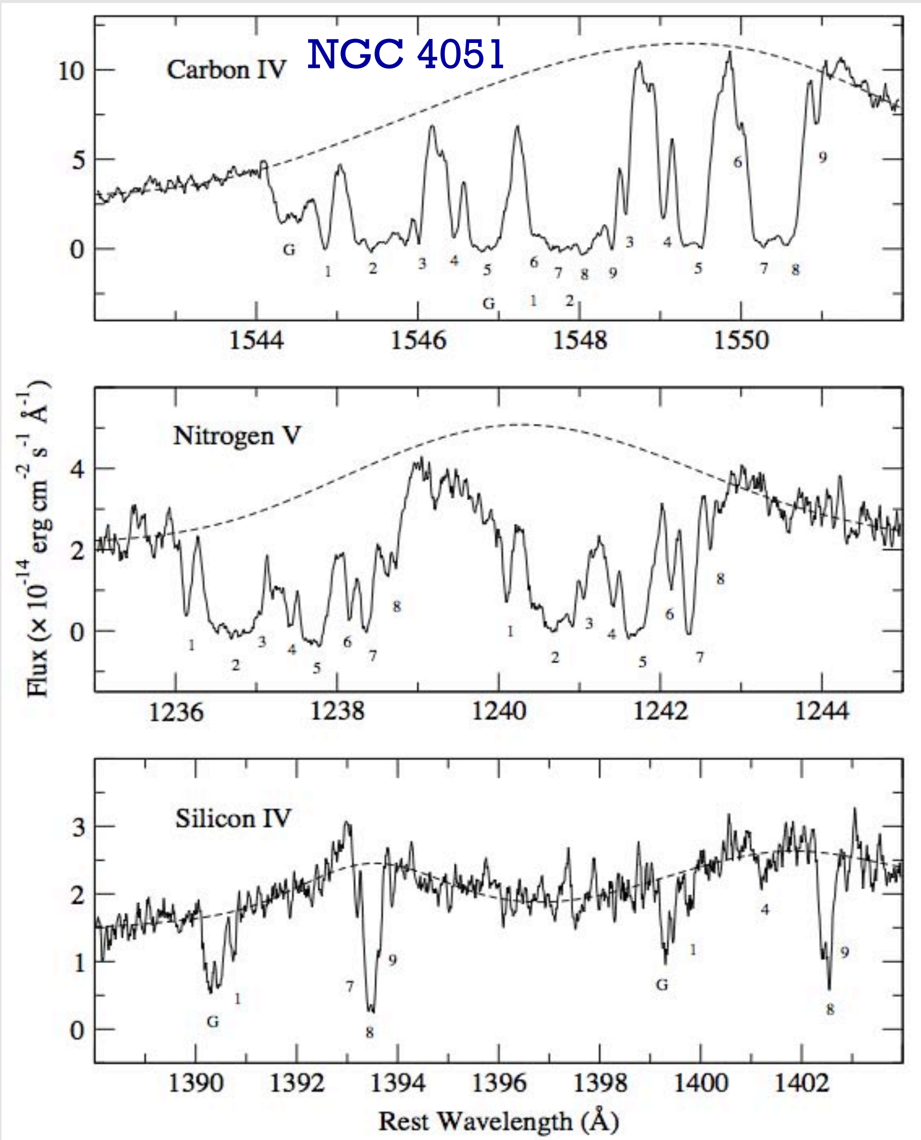

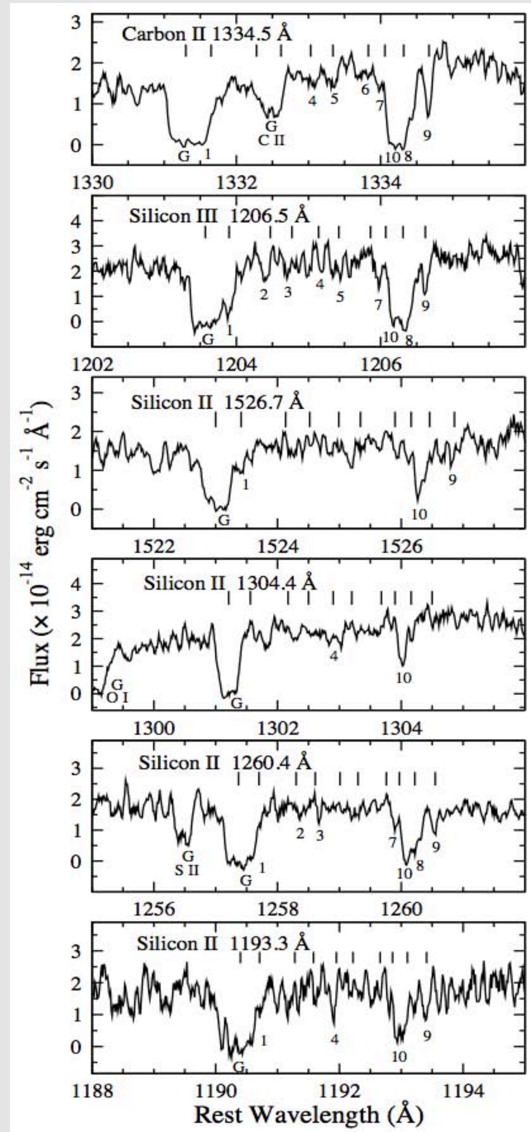

Collinge et al. (2001)

Slower and narrower than BALs in luminous quasars.

Blueshifted X-ray Absorption Lines / Edges in Seyferts

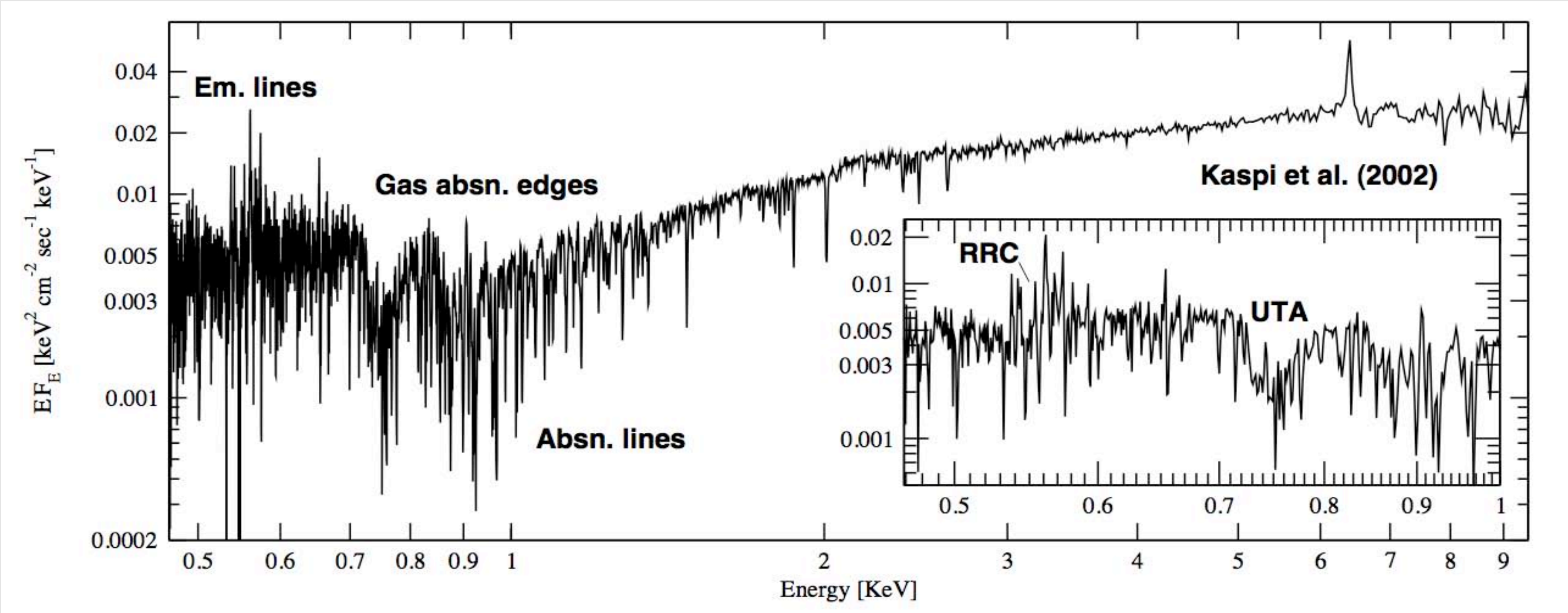

Called X-ray ionized absorbers or "warm" absorbers – seen in about half of Seyfert 1s.

Typical column densities of ~ 10^{21} – 10^{23} cm^{-2}, likely in multiple phases.

Likely related to some UV absorbers – specifically, some of those with high ionization.

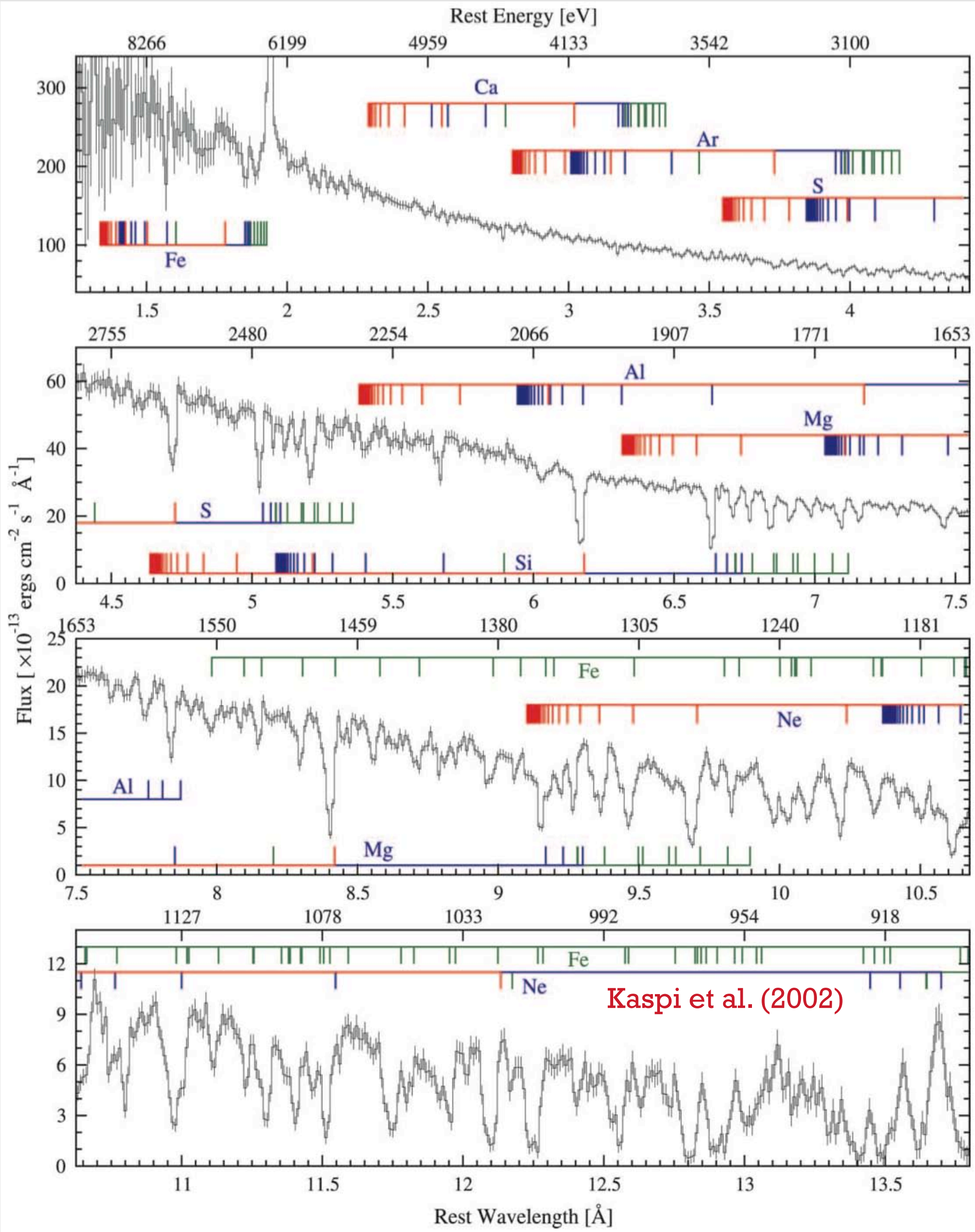
Rest Energy [eV]
Ca
Ar
S
Fe
Al
Mg
Si
Ne
Flux [×10^-13 ergs cm^-2 s^-1 Å^-1]
Rest Wavelength [Å]
Kaspi et al. (2002)

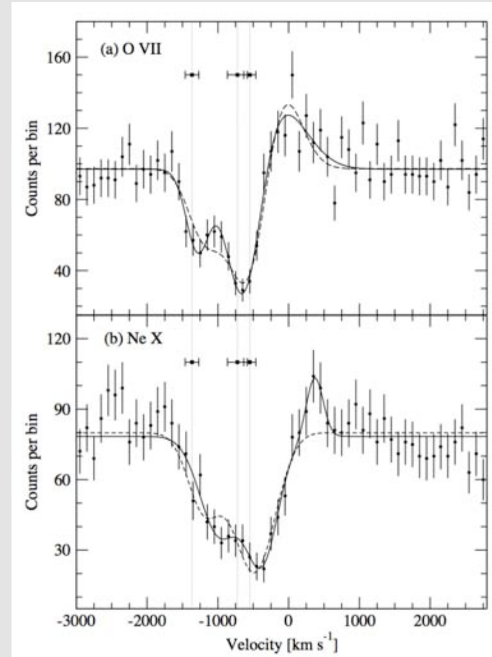
(a) O VII
(b) Ne X
Counts per bin
Velocity [km s^-1]

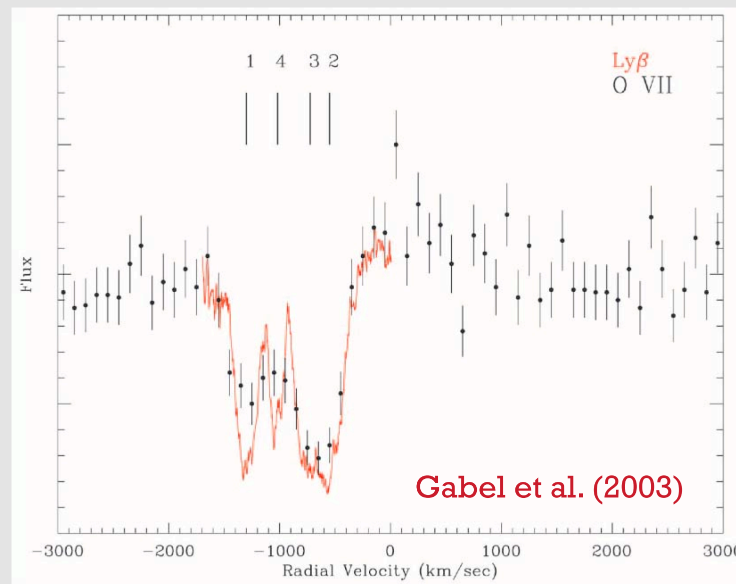
1 4 3 2
Lyβ
O VII
Flux
Radial Velocity (km/sec)
Gabel et al. (2003)

Wind Absorption Lines

Line-Driven Equatorial Accretion-Disk or Torus Wind with Velocities of ~ 100-30000 km s^{-1}

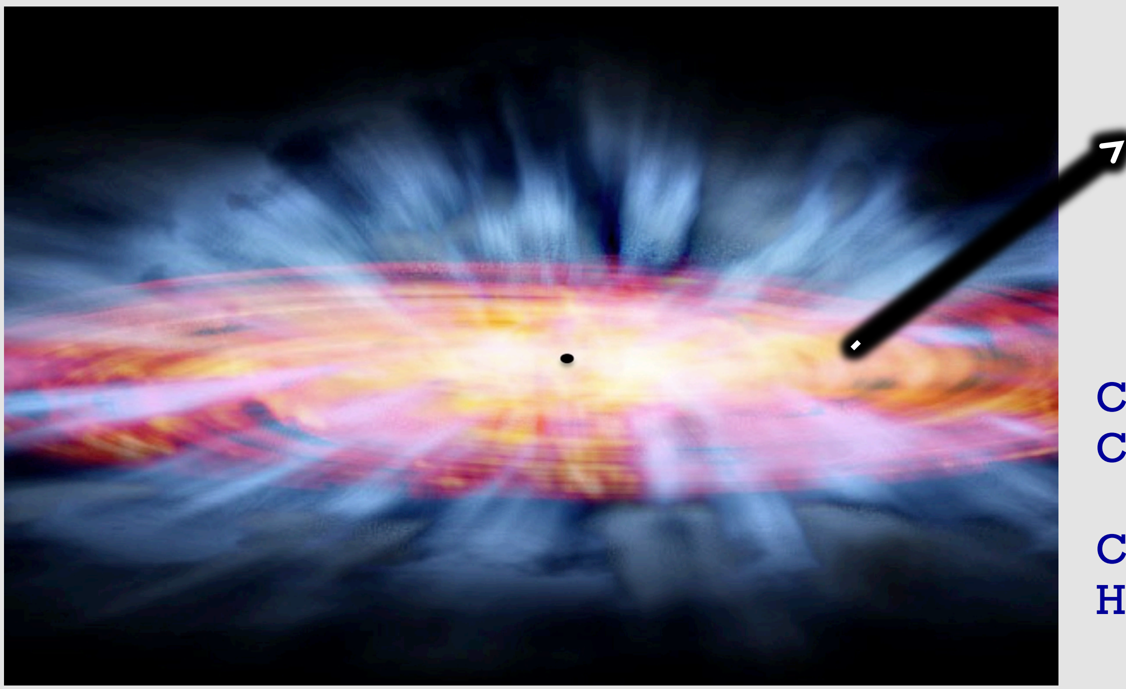

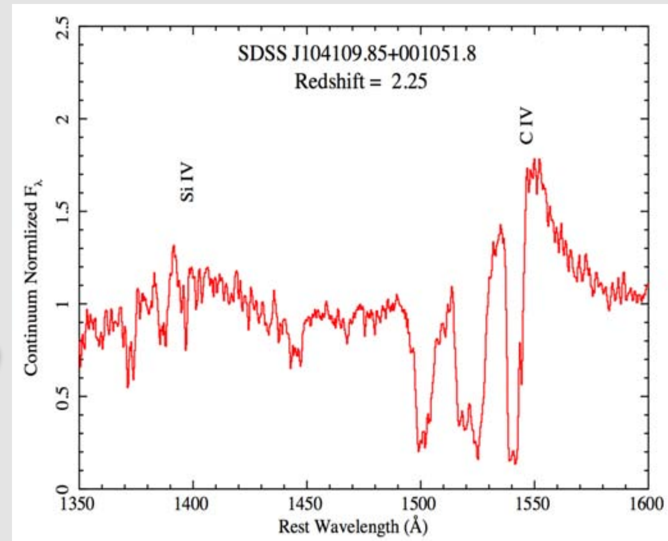

Most AGNs likely drive winds – orientation effect.

Wind material exists over a wide range of radii; 0.01 pc to kpc scales. Often outside the BLR.

Common UV transitions include C IV, Si IV, Mg II, Al III.

Common X-ray transitions include H and He-like C, N, O, Ne, Mg, Si, S, Fe.

Multiple lines from same transition probe distinct wind components.

Lines often saturated with partial covering.

Force Multiplier for Line Driving of Winds

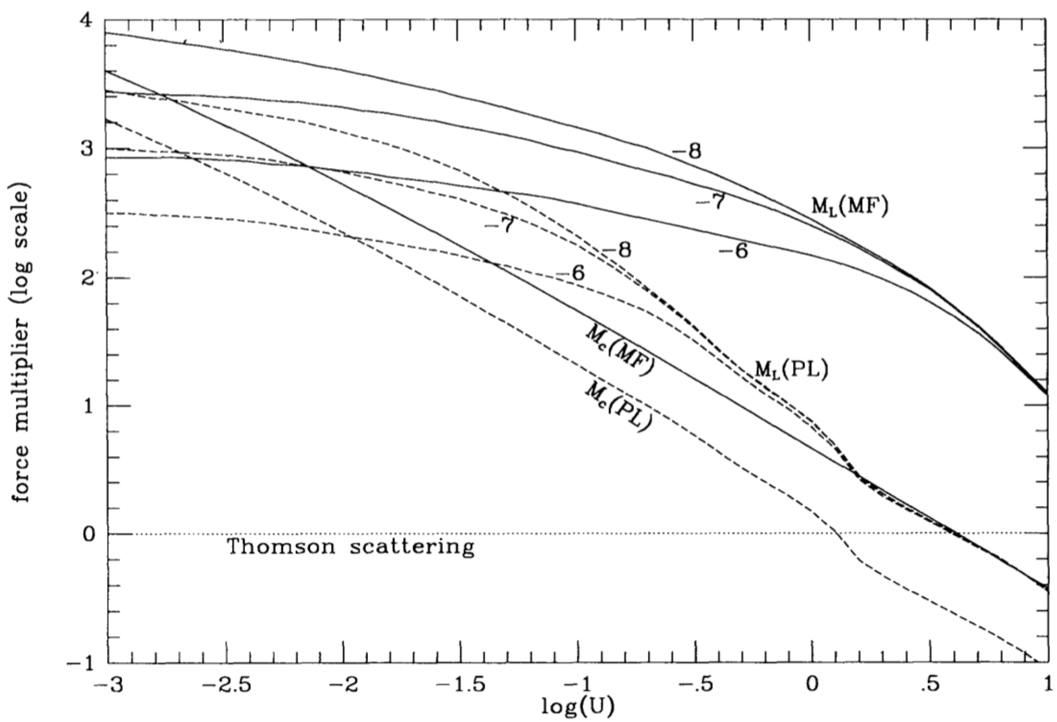

FIG. 2.—Force multipliers as functions of U. The line force multipliers (M_L) are calculated using eq. (2.8) and the continuum force multipliers (M_c) using eq. (2.11). MF stands for the Mathews-Ferland spectrum and PL for the power-law spectrum. The three curves for each line force multiplier are for different values of $\log(t) = -6, -7, -8$.

Arav et al. (1994)

AGN "Powers of Ten"

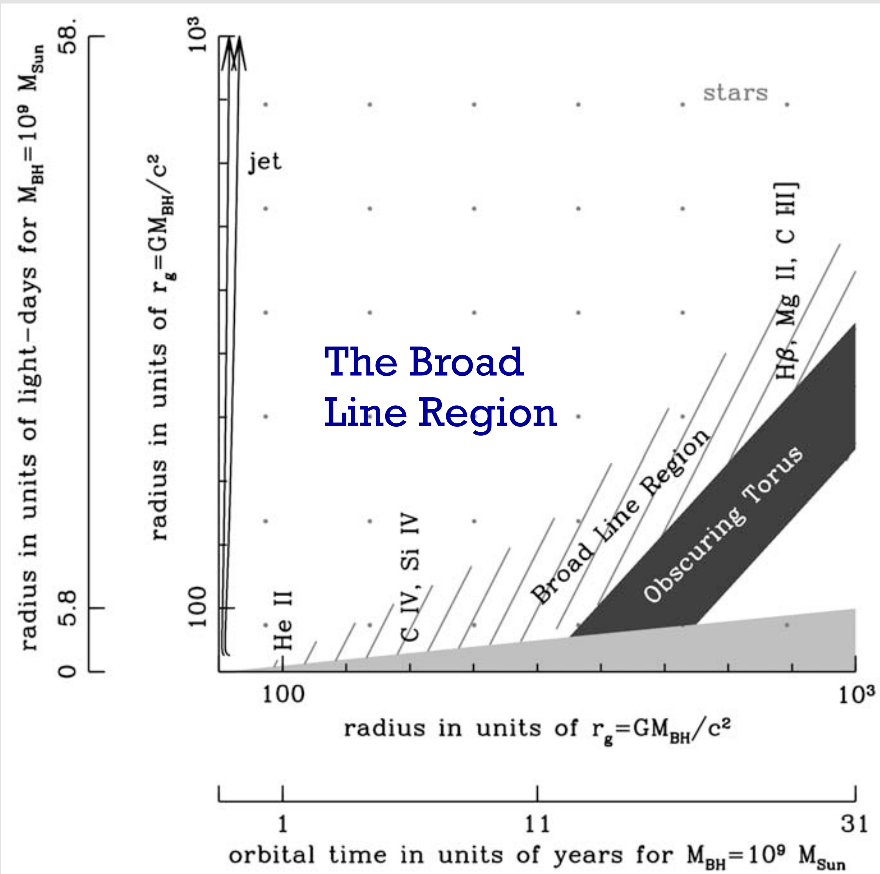

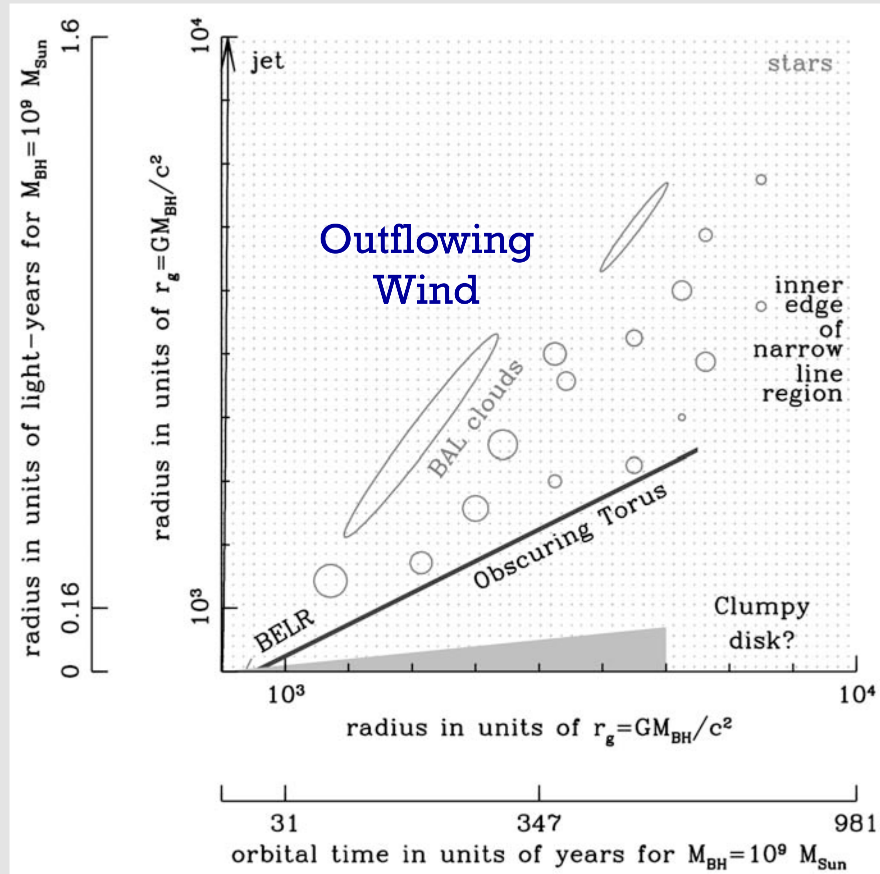

Courtesy of Pat Hall

Why Care About AGN Winds?

Significantly affect observed AGN properties (UV line absorption, high-ionization line emission, reddening, polarization, X-ray absorption).

Substantial part of typical AGN nuclear regions; seen in absorption in ~ 30+% of AGNs.

Help black-hole accretion to proceed by removing angular momentum from the disk.

Can evacuate gas from the host galaxy, perhaps affecting black-hole growth and galaxy evolution.

Why Care About AGN Winds?

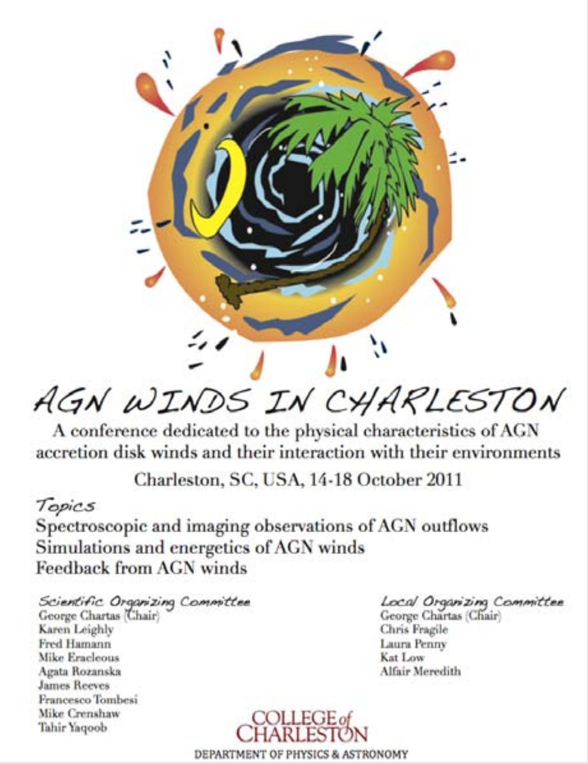

BAL Fraction Depends Upon Radio Power

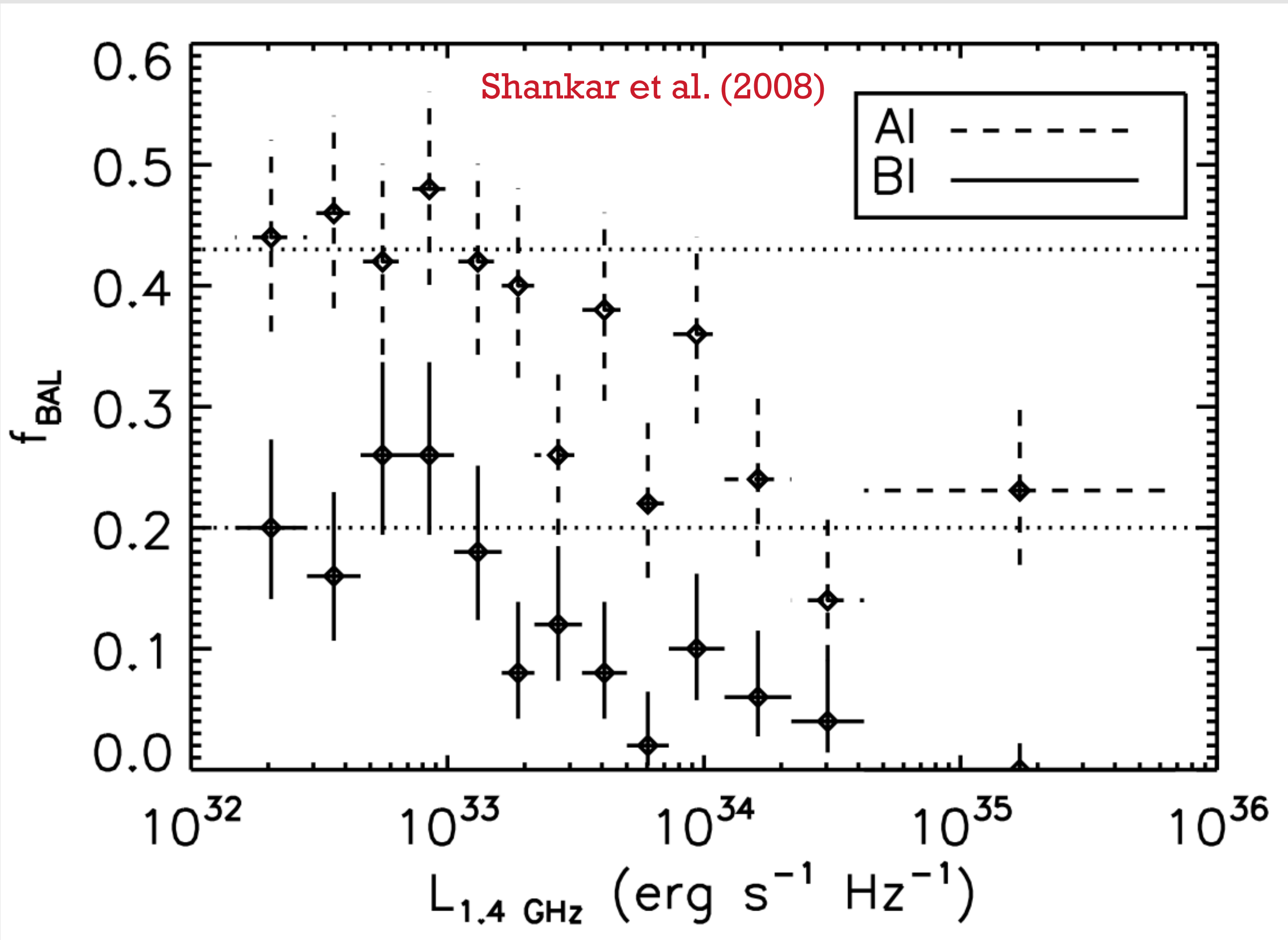

BALs generally avoid highly radio-luminous quasars (though not entirely).

Reason for this is still not entirely clear.

Wind-jet connection?

Orientation effects?

X-ray Absorption in BAL Quasars

Schematic Model of Equatorial BAL Outflow

e.g., Murray et al. (1995); Proga et al. (2000)

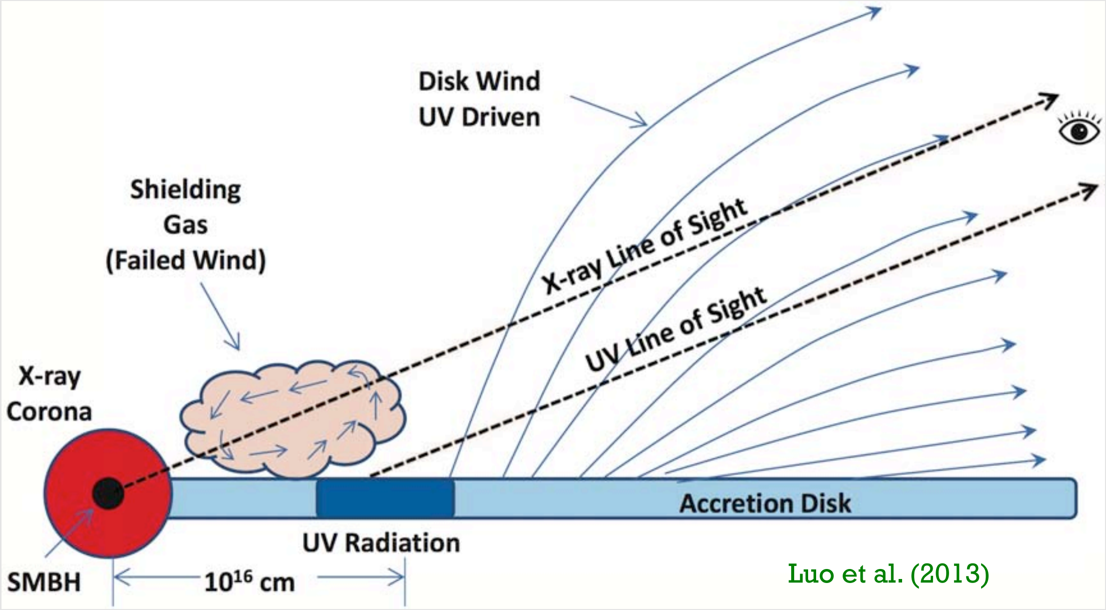

Proposed "shielding gas" is central to BAL wind driving - prevents wind over-ionization.

Such shielding gas is commonly observed in X-ray absorption with $N_{\rm H} \sim 10^{22}$-10^{24} cm^{-2}.

Relations found between level of X-ray absorption and UV absorption strength and velocity.

Variations of the X-ray shielding gas could lead to significant UV BAL variations, since they would affect the ionization level of the BAL gas.

An X-ray vs. UV Relation for PG Quasars

Basic Levels X-ray and UV Absorption Correlated Over Ranges of ~ 400 and ~ 1000: A Continuous Absorption “Spectrum”

C IV Absorption-Line Strength

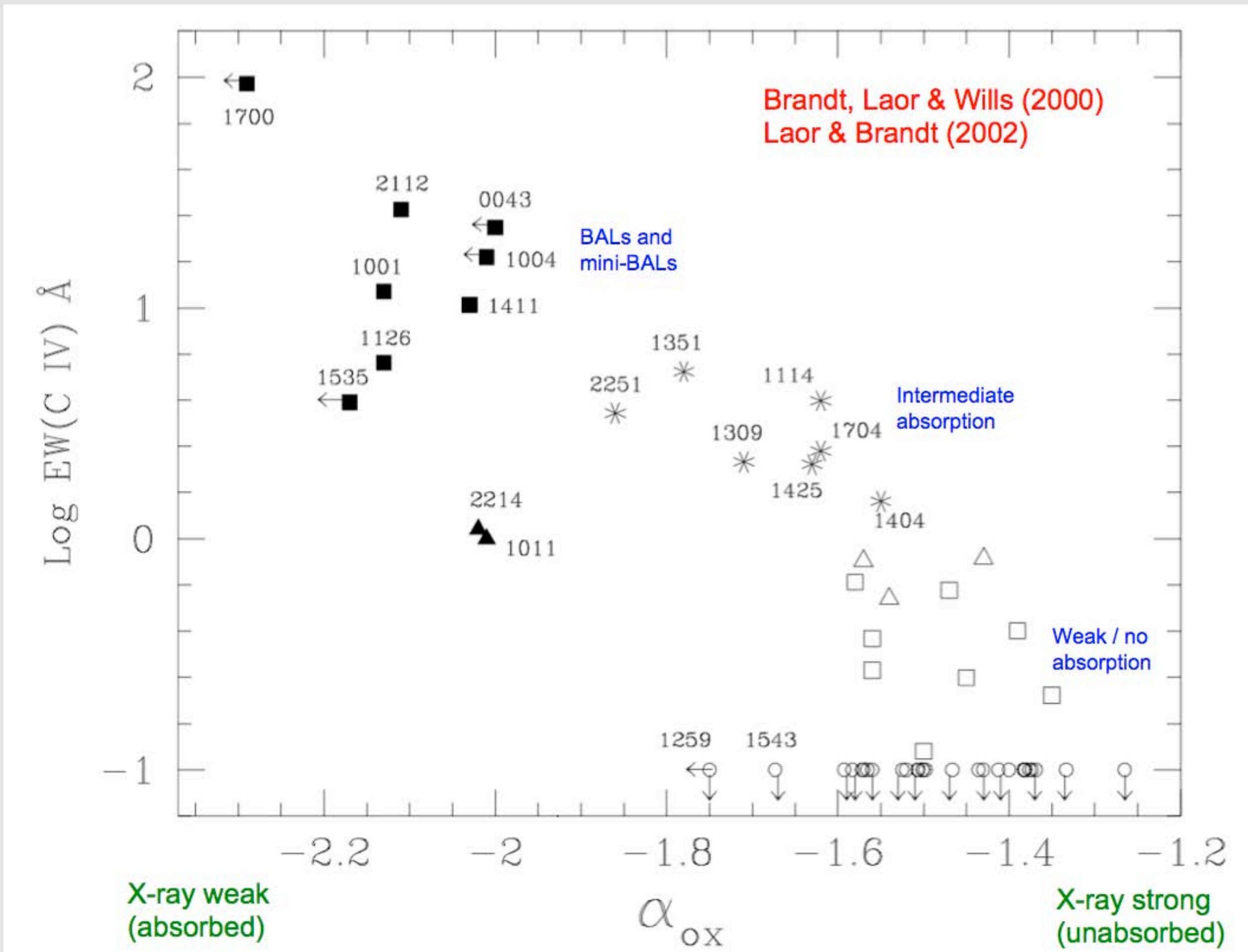

$$\alpha_{OX} = 0.3838 \log \left(l_{2\,\mathrm{keV}} / l_{2500\,\text{Å}} \right)$$

X-ray vs. UV Relations for BAL and mini-BAL Quasars

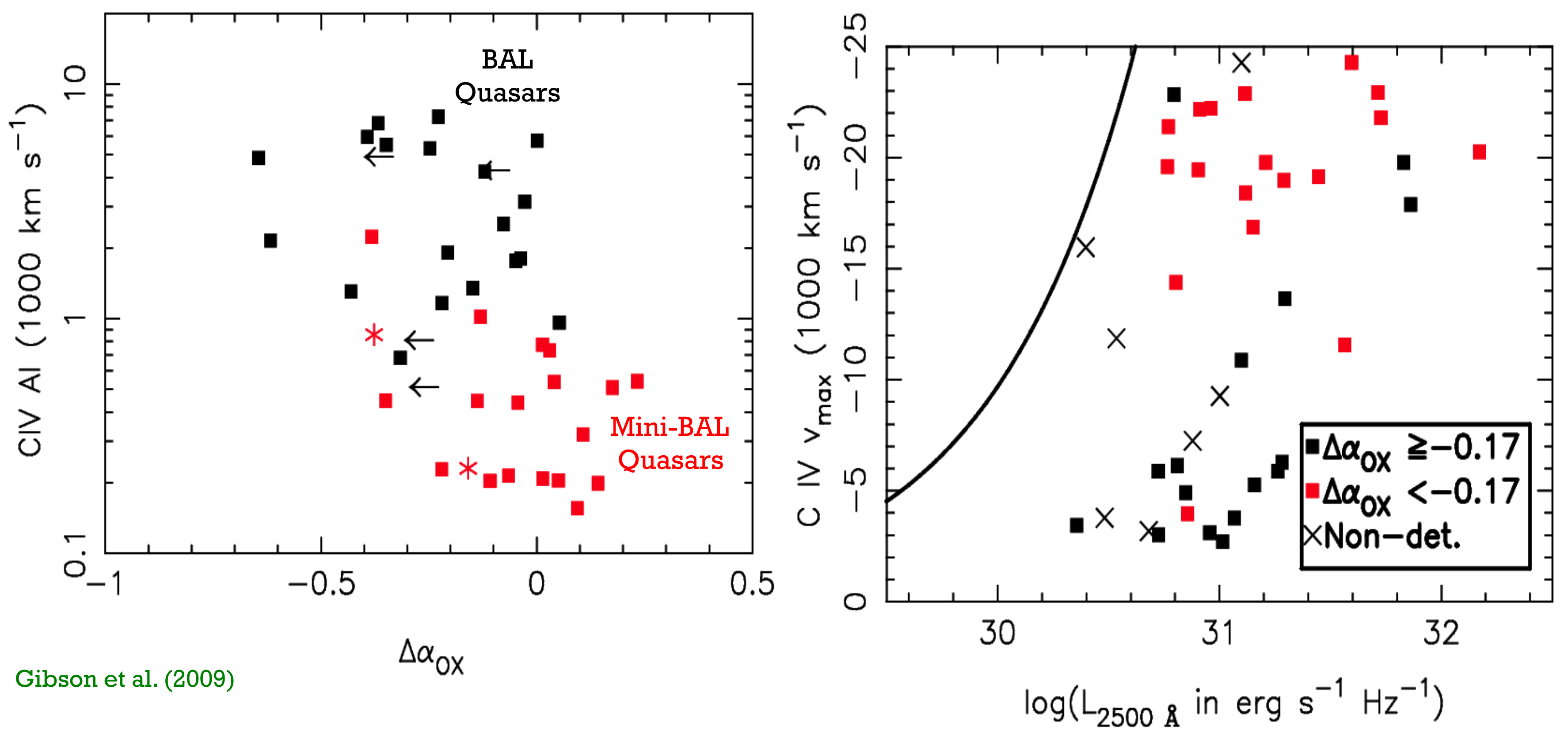

Gibson et al. (2009)

Dynamical Nature of Quasar Winds

Density Maps from BAL Quasar Wind Simulation

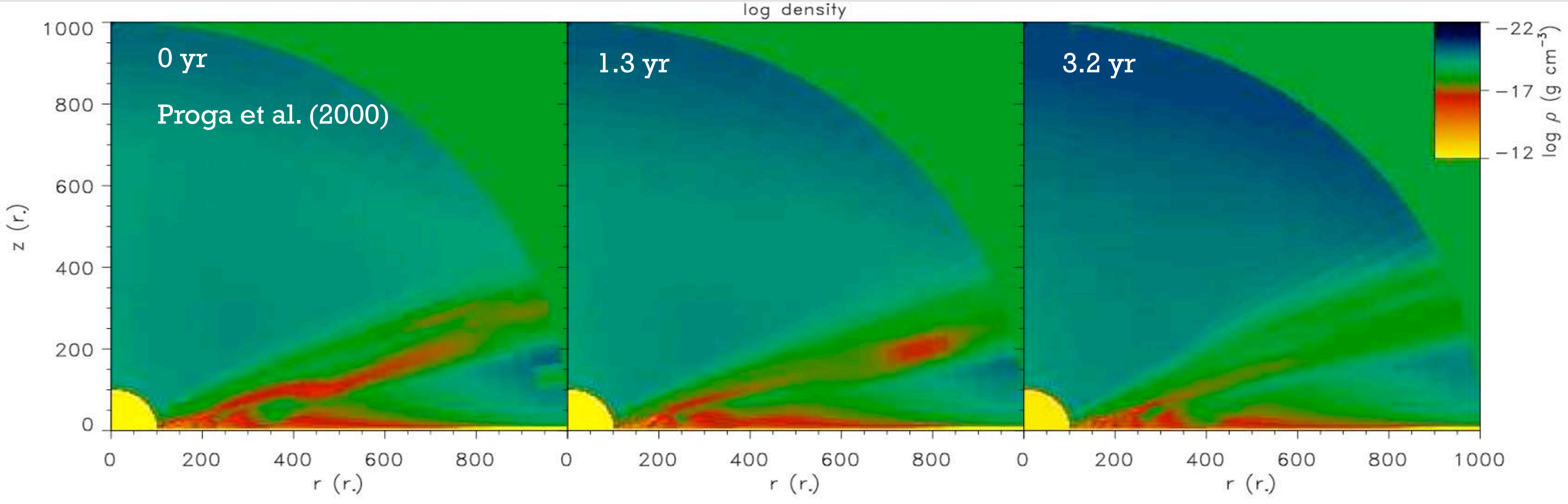

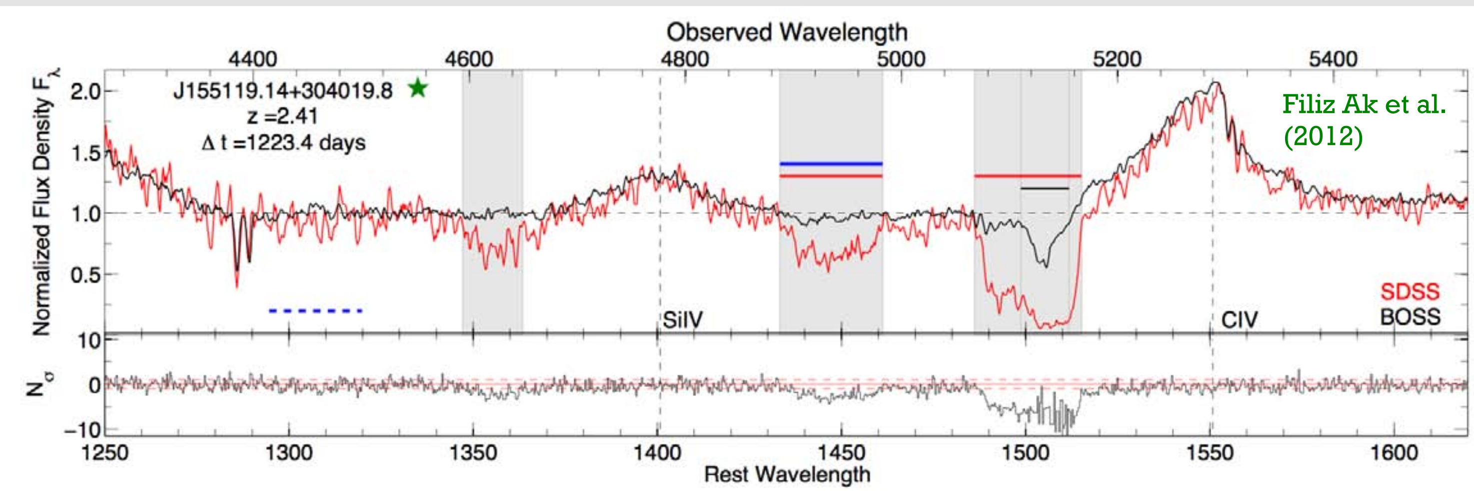

BALs commonly vary in EW on year timescales.

Acceleration or deceleration are rare

X-ray BALs from Iron K

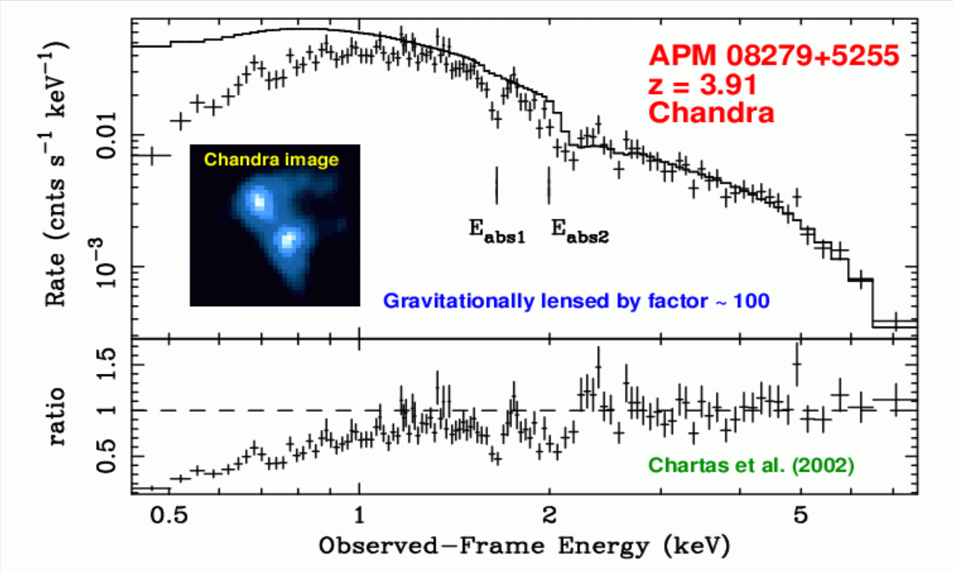

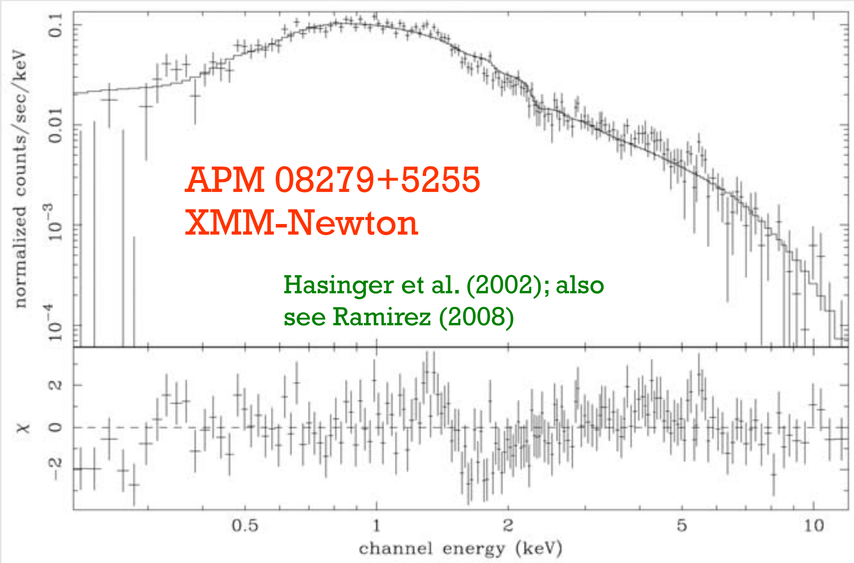

Absorption features at 8-12 keV in rest frame - X-ray BALs from ionized iron K.

Implied X-ray velocity is $v \sim 0.2\text{-}0.4c$ and higher. Much higher than for UV BALs.

X-ray absorber in some BAL quasars in state of outflow, as for Seyfert galaxies?

Implied mass-outflow rate is ~ 10-30 $M_\odot$ yr^{-1} and kinetic luminosity is ~ $10^{46\text{-}47}$ erg s^{-1}.

Such features could be present, but currently undetected, in many other BAL quasars.

Other Examples of X-ray BALs

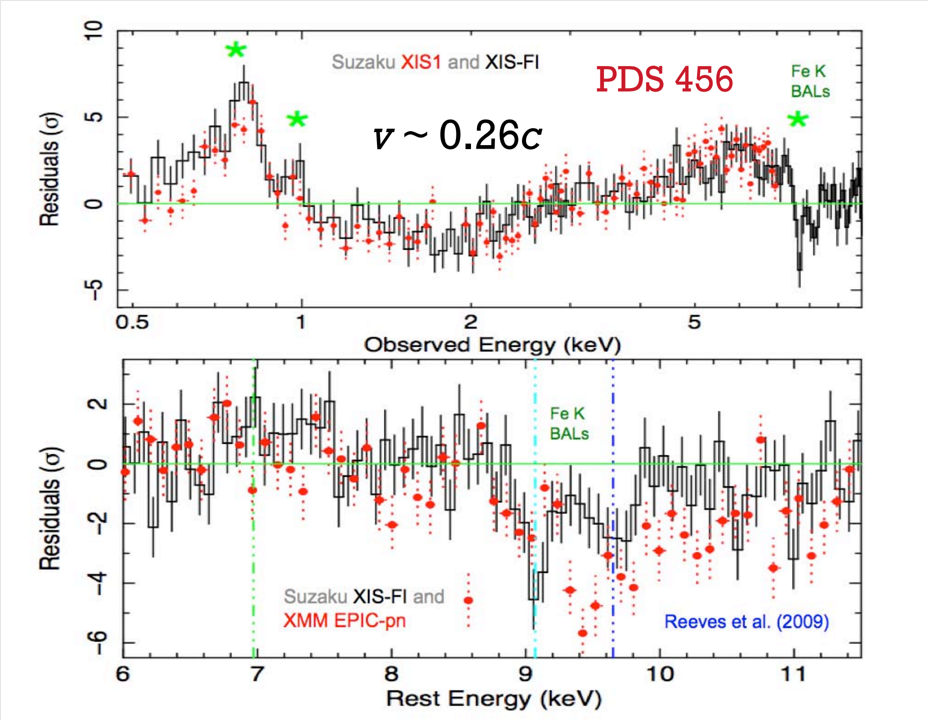

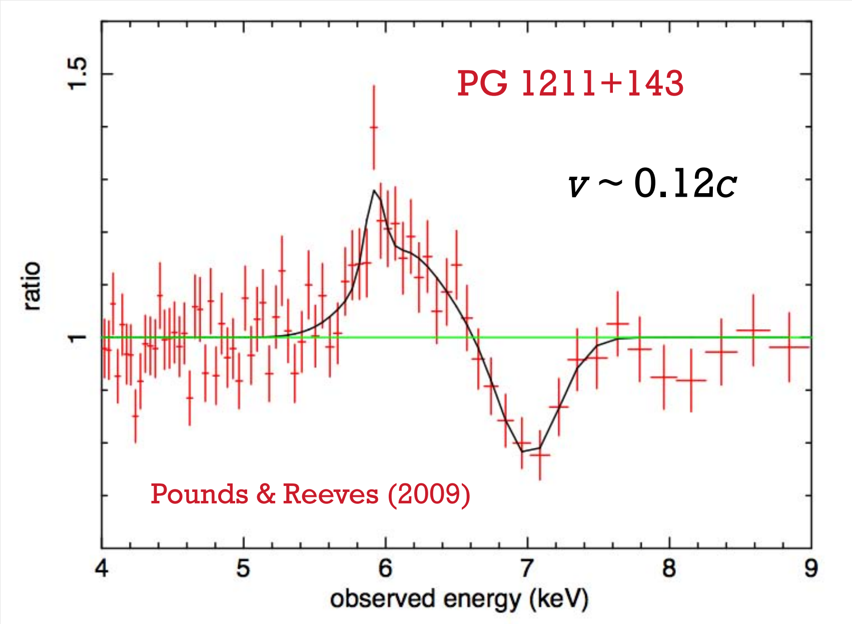

Other quasars and Seyfert galaxies also show X-ray BALs.

Interpretation of the data is often difficult, with significant debate - caution required.

Wind Feedback into the ISM

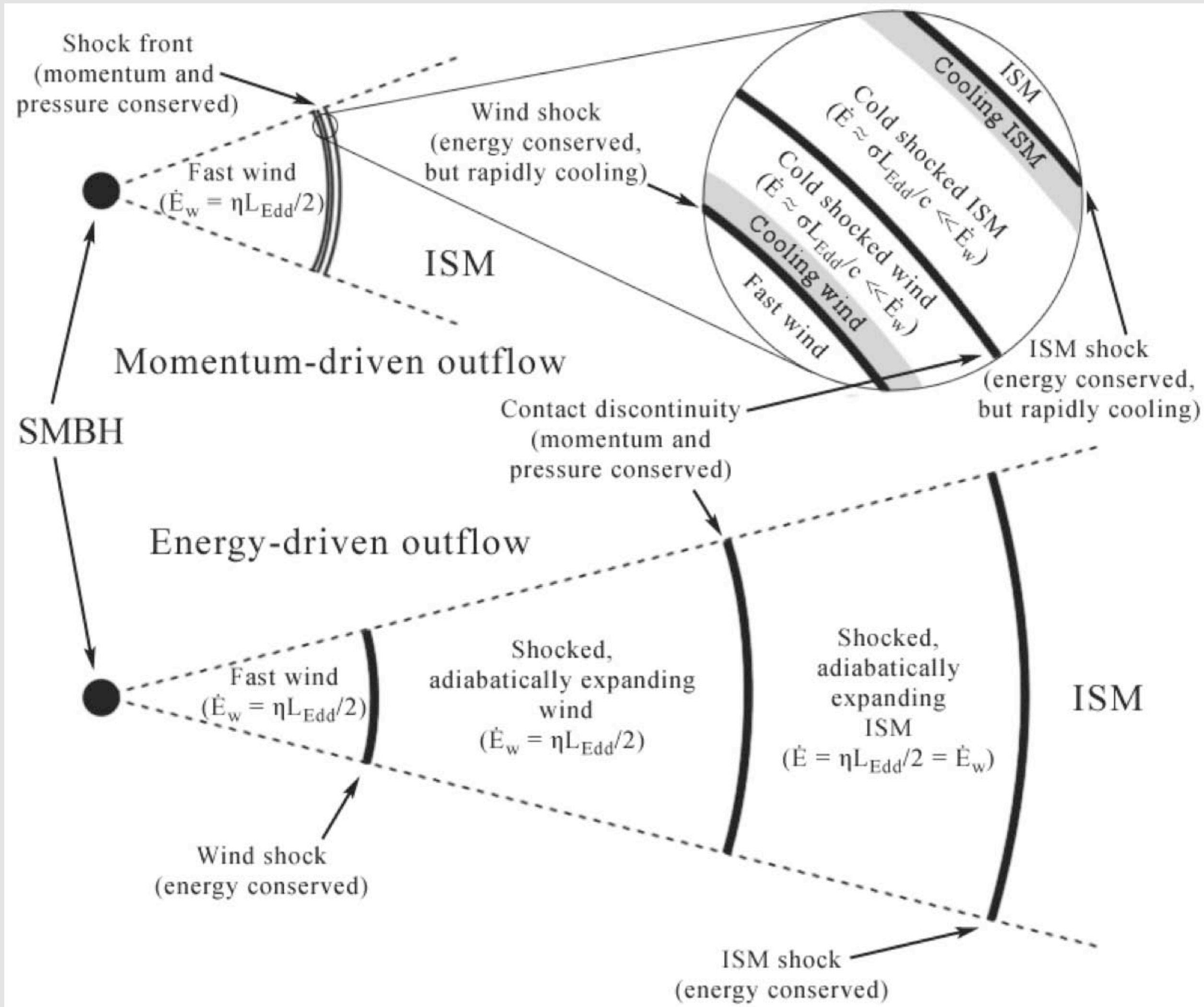

Courtesy of A. King et al.

The End

An Observational Overview of Active Galactic Nuclei

Niel Brandt (Penn State University)

Summary of Lectures

Introduction, AGN Basics, Finding AGNs, and Terminology

Observations on Small Scales: Black Hole Region, Broad Line Region, Outflowing Winds

Observations on Large Scales: Narrow Line Region, Torus, Jets

Summary of Lectures

Focused Lecture – AGN Demography, Physics, and Ecology from X-ray Surveys

Observations on Large Scales: Narrow Line Region, Torus, and Jets

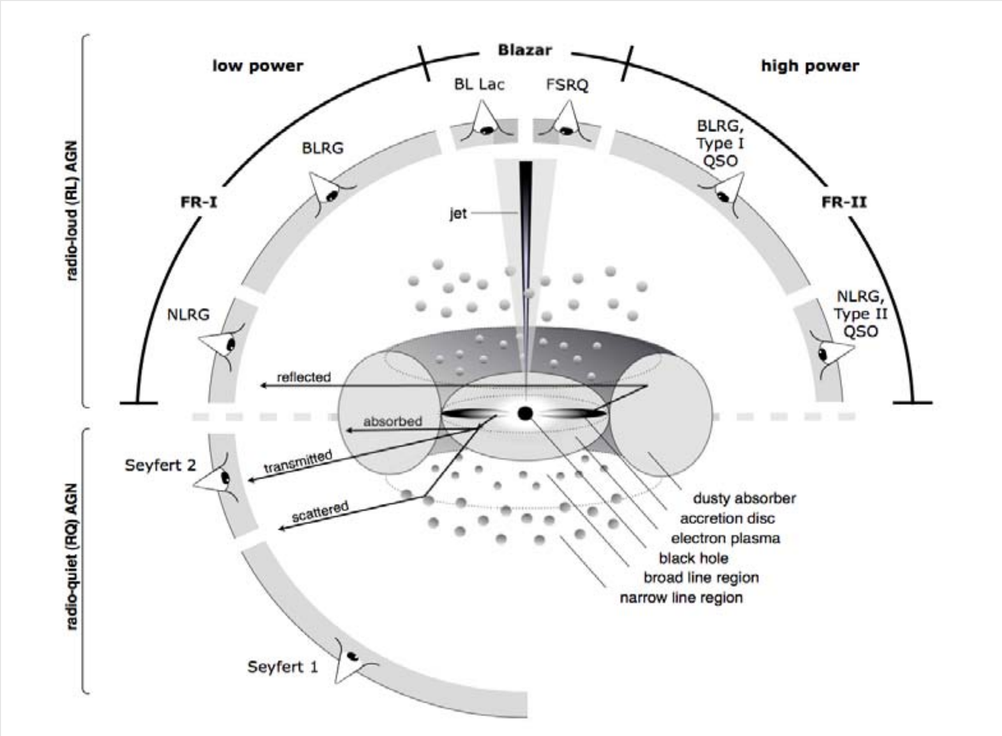

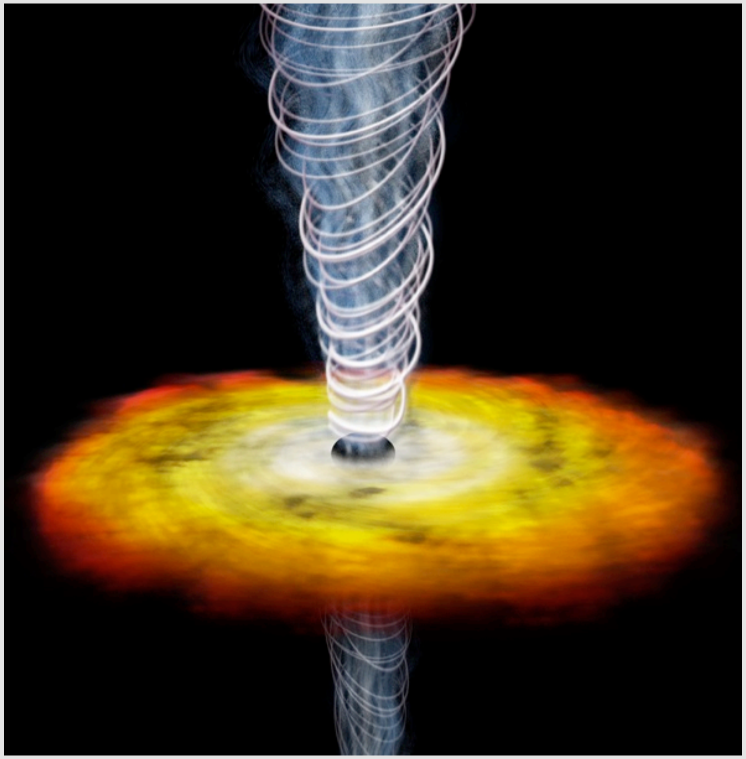

AGN "Powers of Ten"

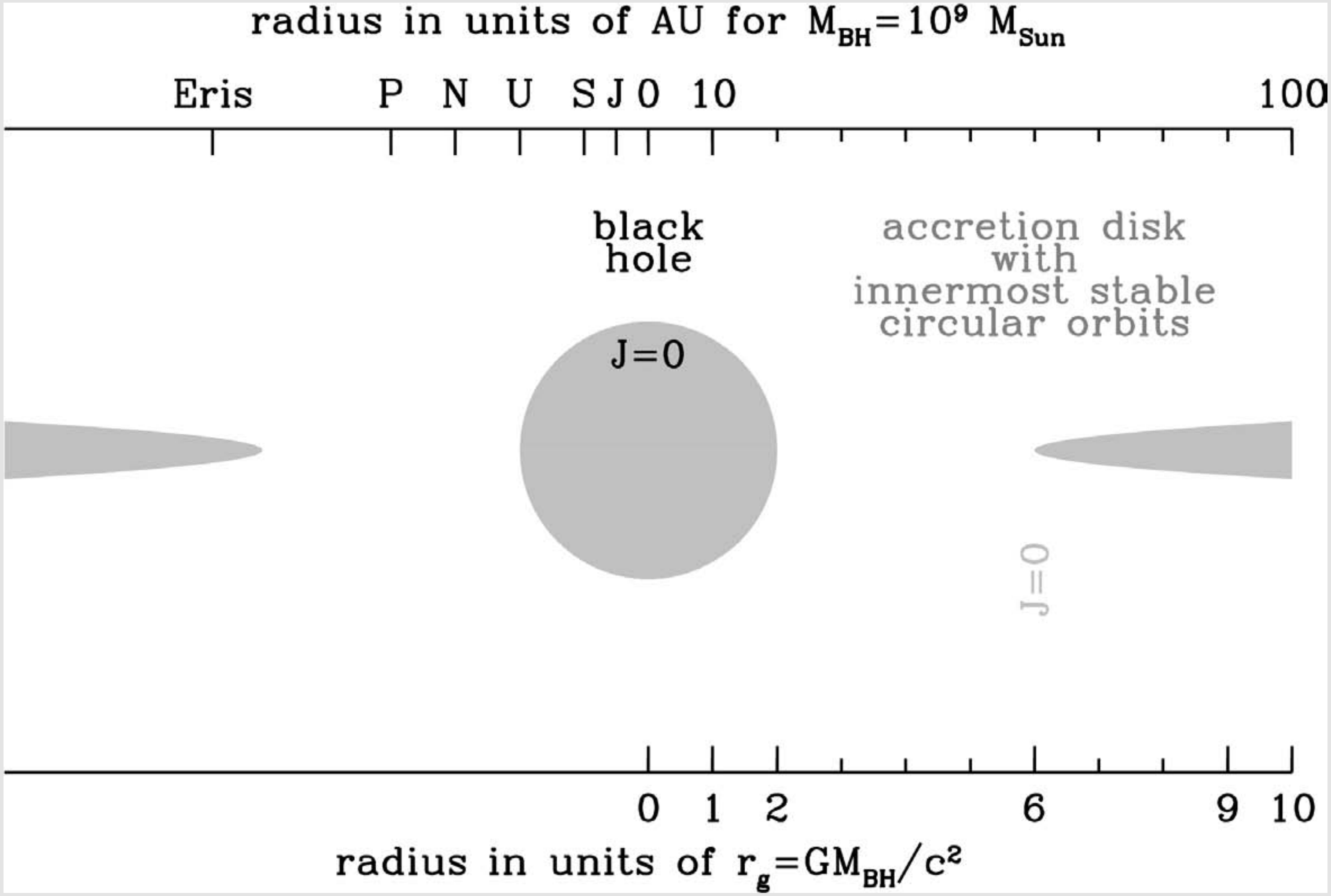

Courtesy of Pat Hall

AGN "Powers of Ten"

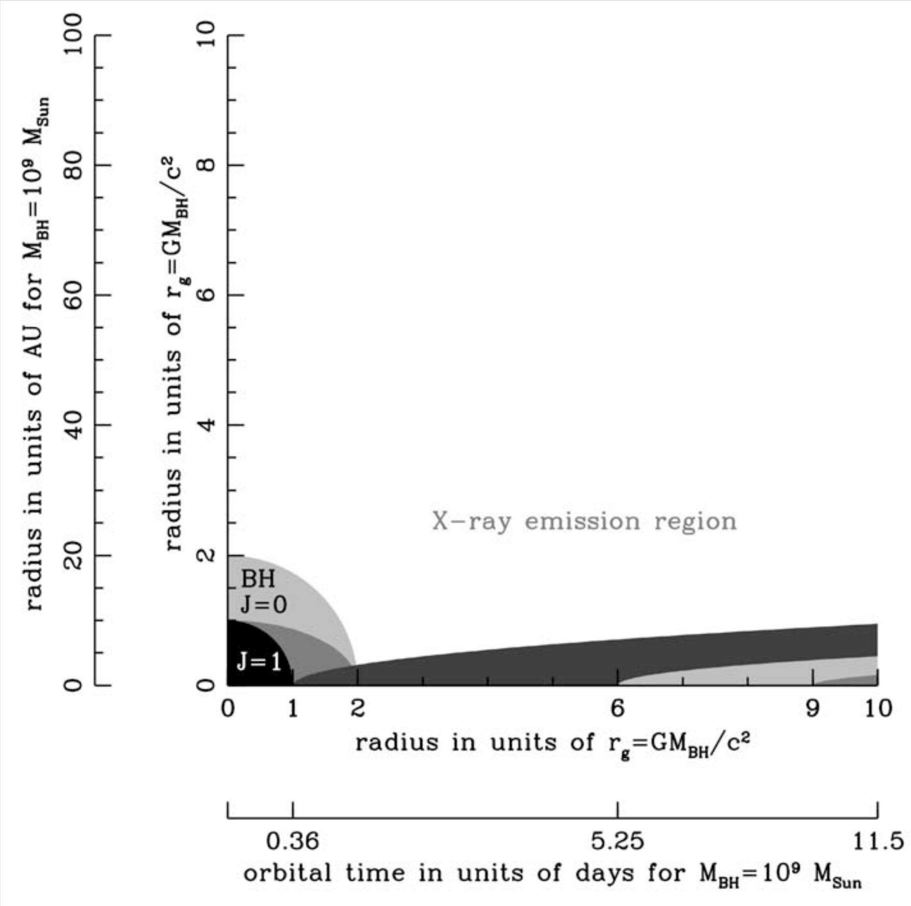

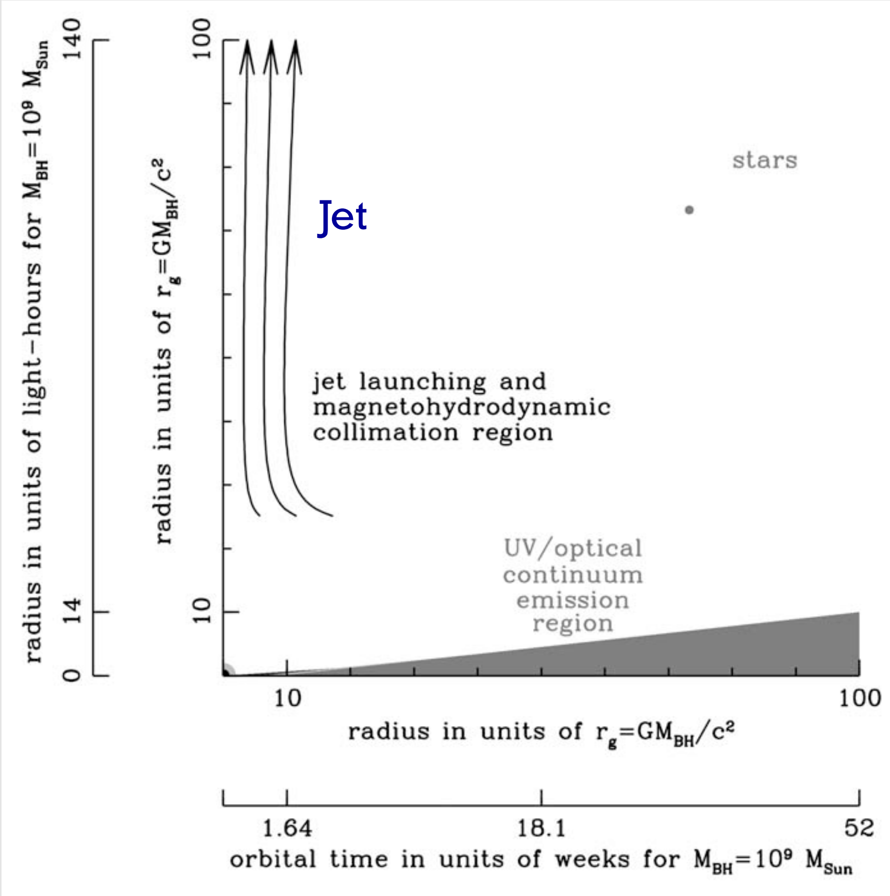

Courtesy of Pat Hall

AGN "Powers of Ten"

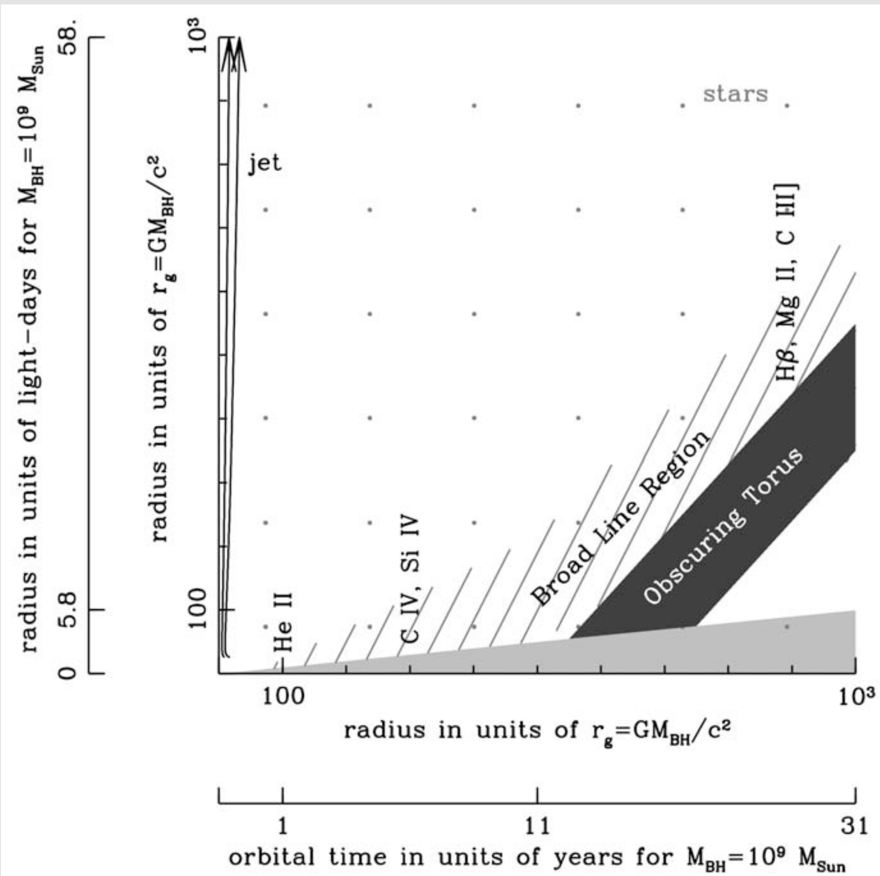

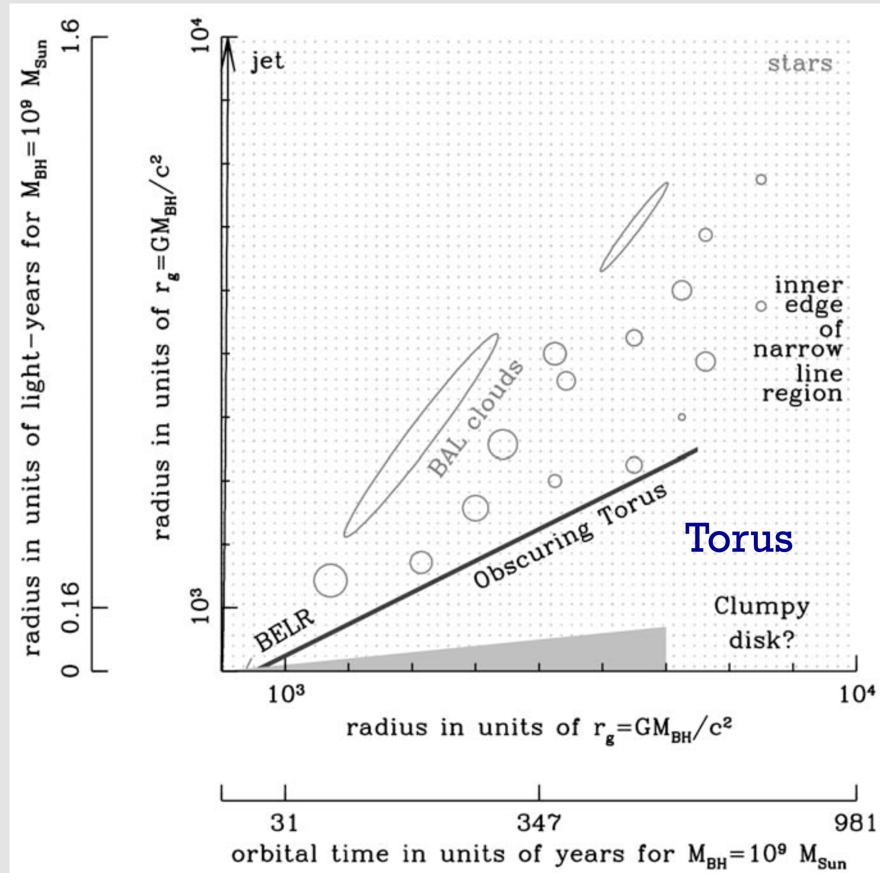

Courtesy of Pat Hall

AGN "Powers of Ten"

Jet and Lobes

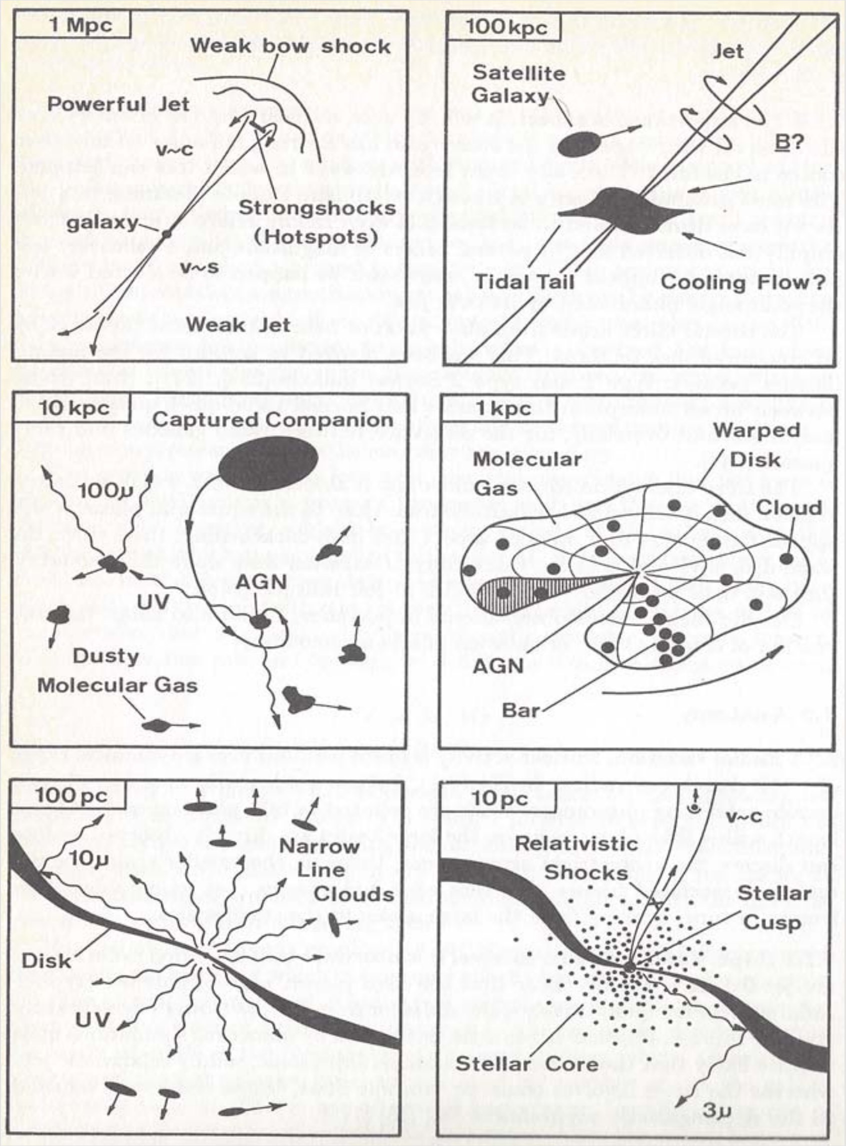

Jet

Host Galaxy

NLR

Jet

Blandford (1990)

The Narrow Line Region (NLR)

Lines are Kinematically Composite

Broad components

- Doppler widths of 1000-25000 km s^{-1}.
- Arise in gas with density $n_e \sim 10^9$-10^{11} cm^{-3} (as determined from strengths of certain density sensitive lines like [O III] and CIII]).
- From the "Broad Line Region".

Narrow components

- Doppler widths typically less than 900 km s^{-1}.
- Arise in relatively low-density gas ($n_e \sim 10^3$ cm^{-3}).
- From the "Narrow Line Region".

Optical/UV Emission Lines

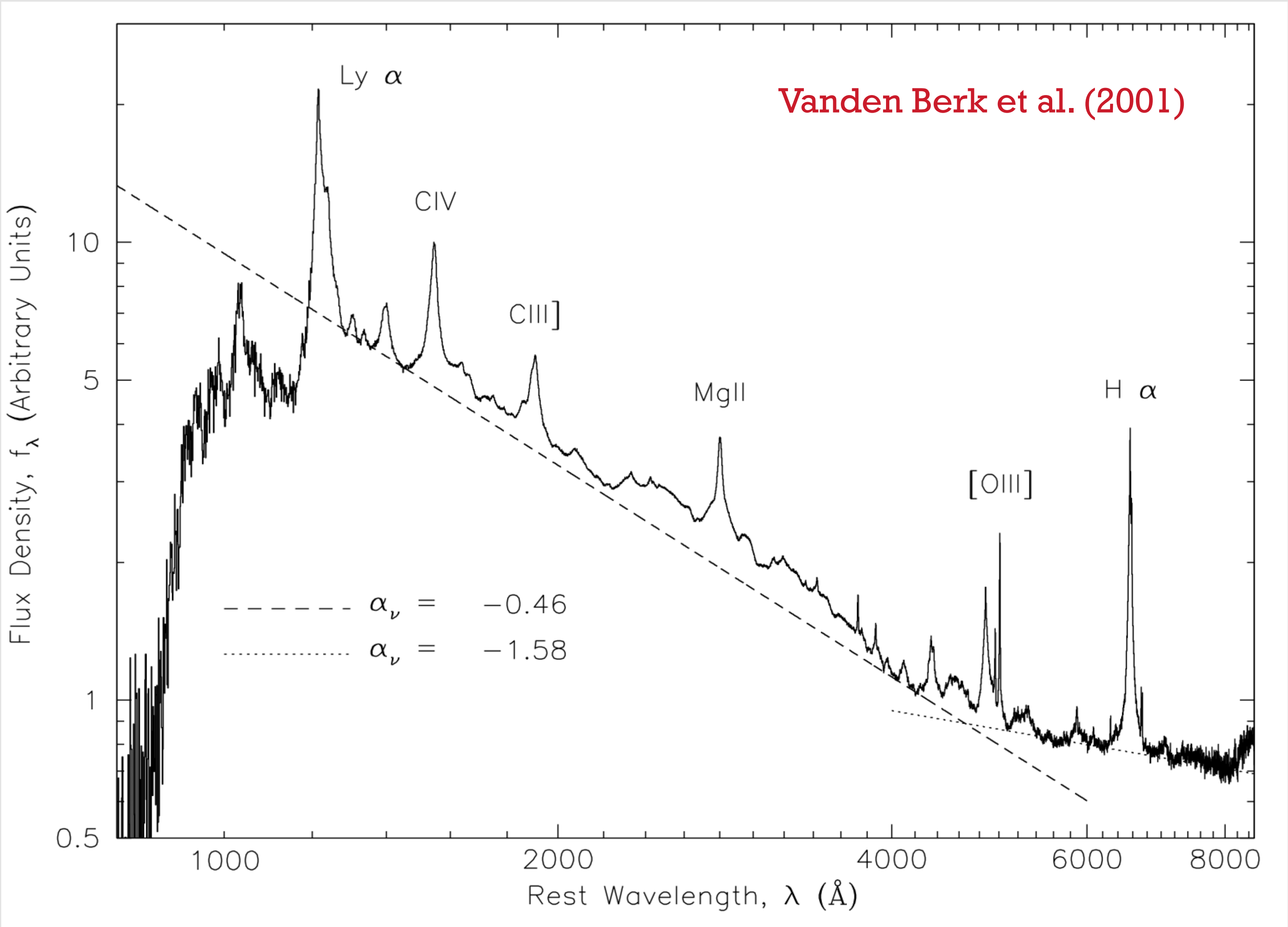

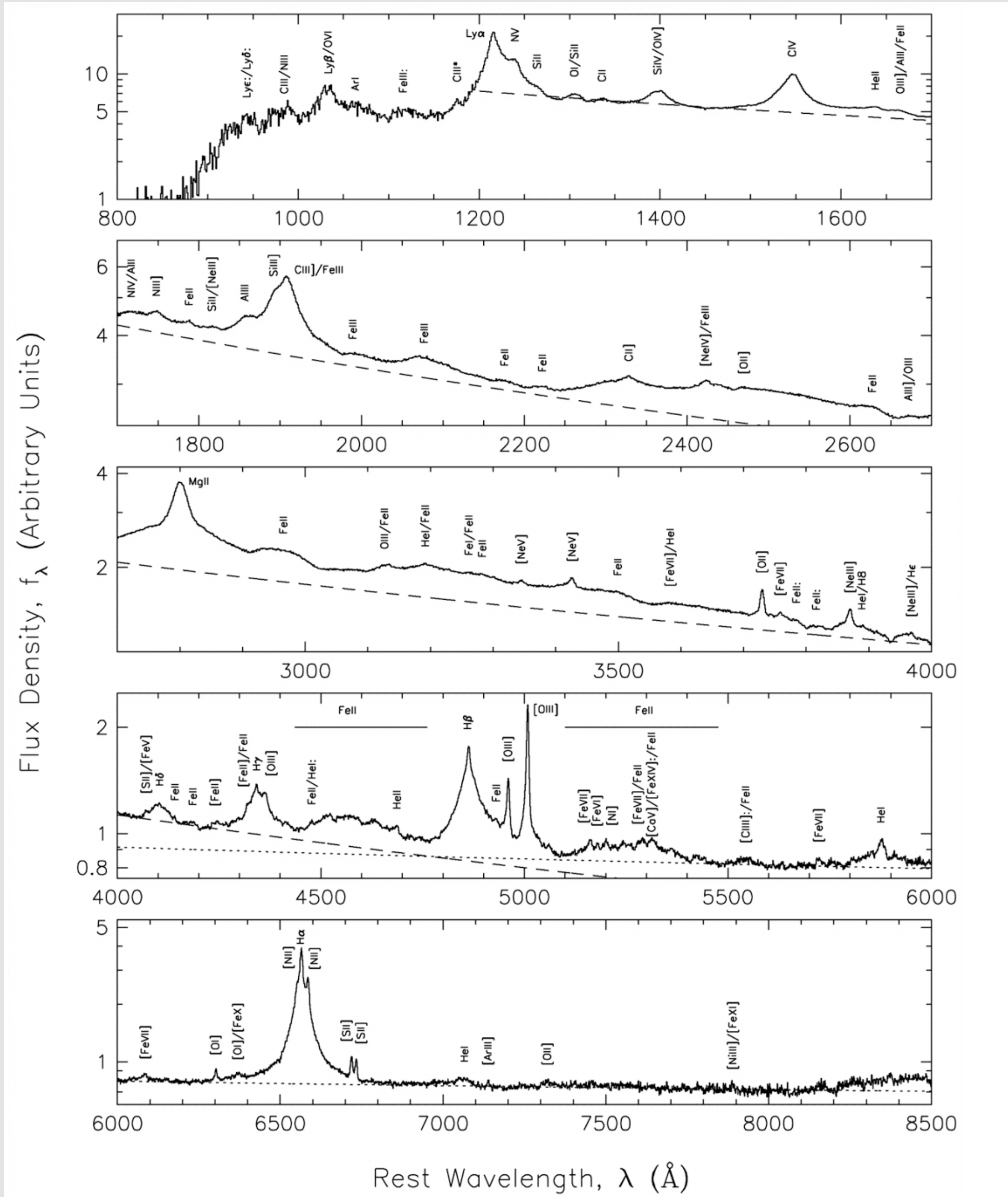

Vanden Berk et al. (2001)

Basic Points about the NLR

Largest spatial scale where ionizing radiation from the AGN dominates.

NLR can be spatially resolved in the optical; has sizes of ~ 100+ pc in local Seyferts (and even larger in quasars).

Can map out physical and kinematic properties directly to some extent.

Imaging the NLR with HST

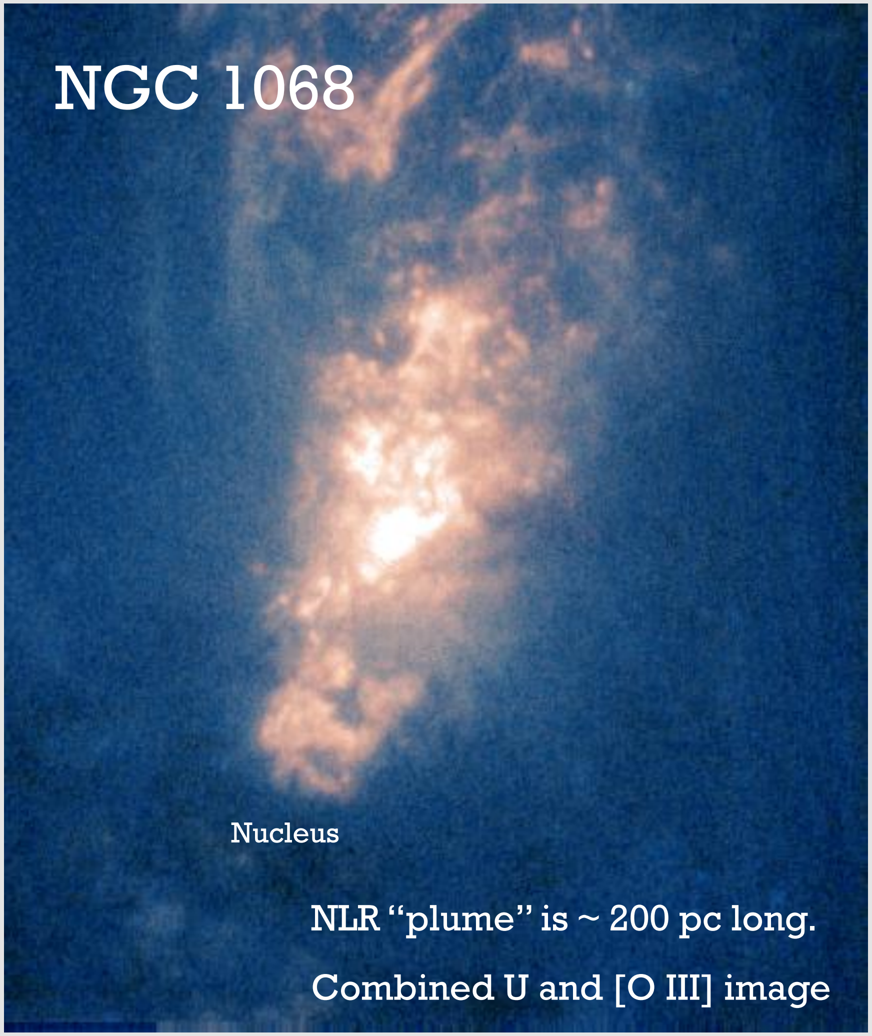

Macchetto et al. (1994)

The line emission region is clumpy and complex.

NLR is clearly not spherically symmetric, but rather is roughly axisymmetric.

NLR axis generally coincides with radio axis in cases where extended linear radio emission is detected.

In some sources, we see strong line emission from regions where the radio jet is colliding with the ISM and causing shocks – an additional source of ionization.

NLR: Basic Properties

FWHM values are 200-900 km s^{-1}, with line profiles varying across NLR.

See a wide range of ionization states:

- Low ionization (e.g., [O I] λ6300)
- High ionization (e.g., [O III] λλ4959, 5007)
- Sometimes even very highly ionized species (e.g., iron coronal lines)

From line ratios, infer that the NLR is mostly photoionized by the AGN continuum (with some likely additional ionization by shocks from radio jets).

Optical/UV Spectrum of Obscured AGN

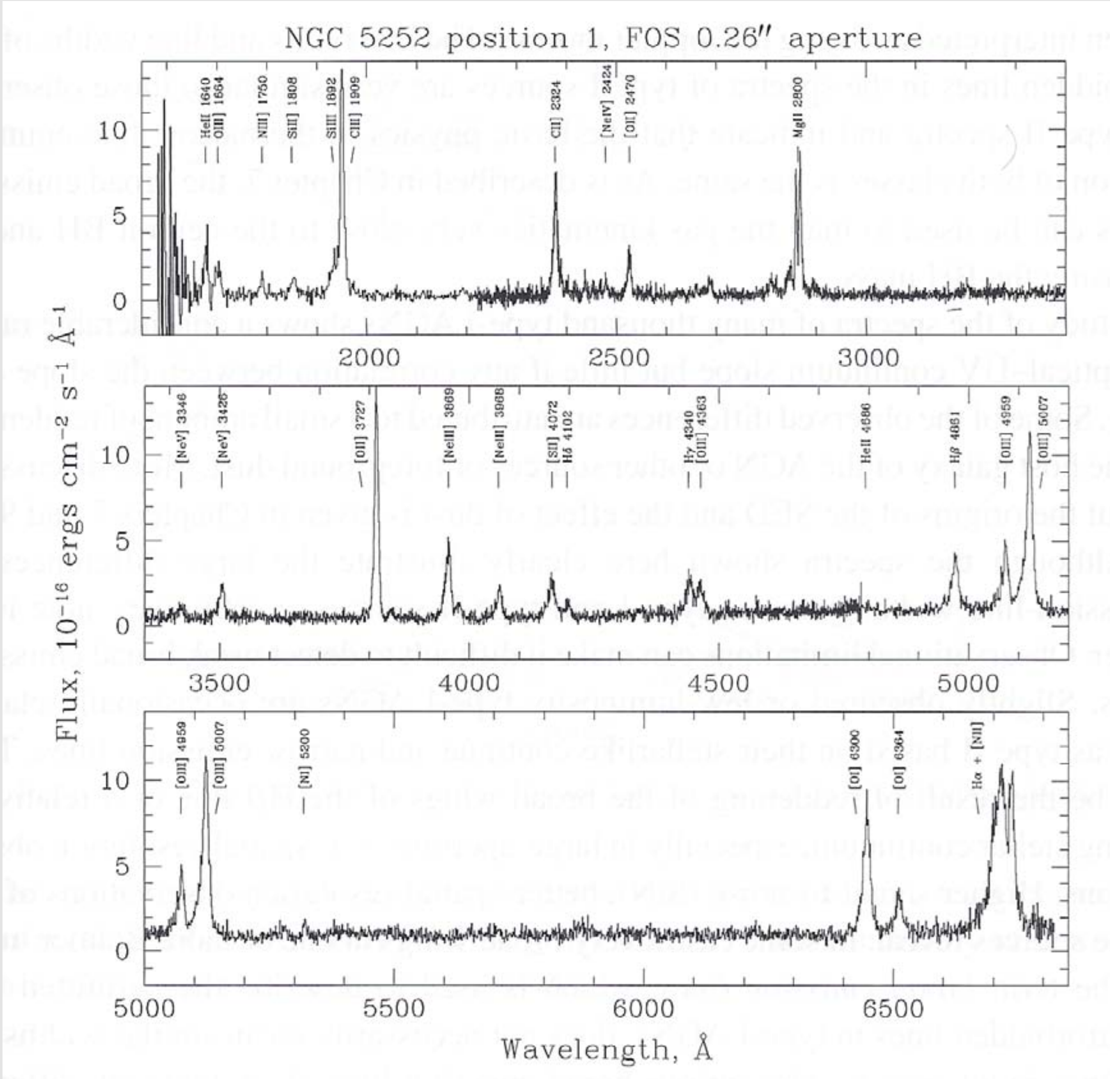

Figure 1.3. The spectrum of the low-luminosity, low-redshift type-II AGN NGC 5252 (courtesy of Zlatan Tsvetanov).

Only NLR lines visible.

NLR: Basic Properties

Density is sufficiently low to allow forbidden transitions. Varies from 10^2-10^5 cm^{-3} across the NLR.

From line ratios, infer temperatures of ~ 10000-25000 K, again varying across the NLR.

At these temperatures, dust can survive in the NLR and cause self-extinction. Can largely overcome using near-infrared lines.

Estimated total mass of the NLR in Seyferts is ~ 10^6 solar masses.

Emission-line strengths often comparable to those from BLR since emissivity (~ n_e^2) is much lower.

NLR Luminosity Dependence

NLR line EWs drop with increasing continuum luminosity, and are often undetectable in high-luminosity quasars.

NLR becoming larger than the host galaxy?

Why is the NLR Important?

Line peaks provide useful systemic redshifts for AGNs.

Useful spectral calibrator since NLR lines should not vary.

Useful as a bolometer for inferring AGN total power.

Connection with Eigenvector 1.

Dynamics tells us about AGN fueling and/or outflows.

Anisotropic illumination provides clues about AGN geometry and orientation.

The NLR as a Bolometer

NLR lines can be used to estimate rough bolometric luminosities, even for obscured AGNs.

Emitted from a region larger than any nuclear obscuration.

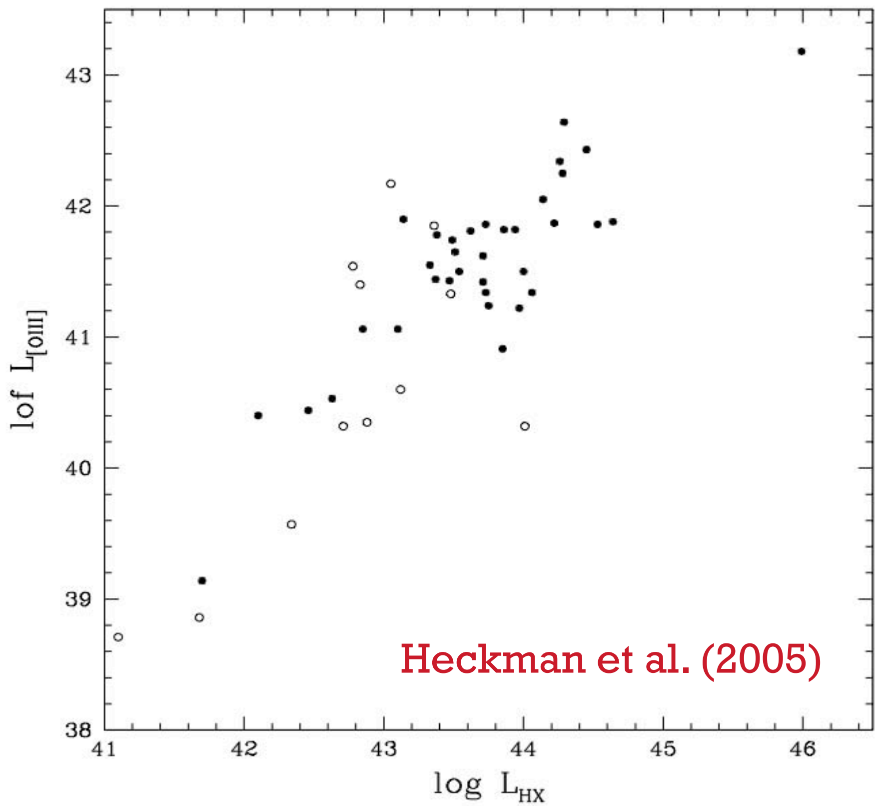

FIG. 2.—Plot of the hard X-ray (3–20 keV) vs. the [O III] λ5007 luminosities for the AGNs in Fig. 1. The Type 1 AGNs are plotted as filled circles and the Type 2 AGNs as hollow circles. Luminosities are in units of ergs s^{-1}.

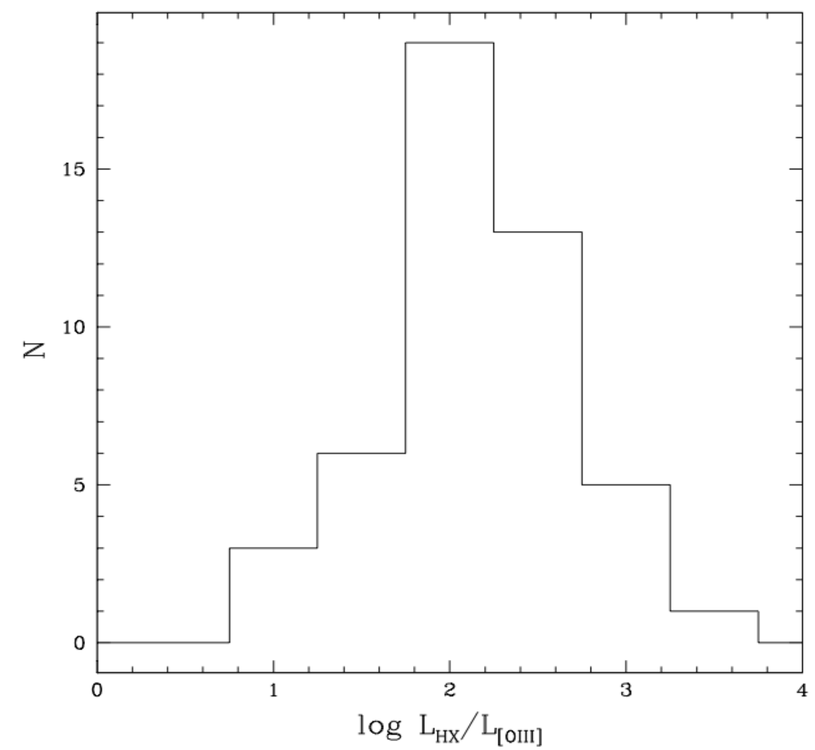

FIG. 1.—Histogram of the log of the ratio of the hard X-ray (3–20 keV) to [O III] λ5007 luminosities for a sample of 47 local AGNs selected on the basis of their hard X-ray flux (the SR04 sample). The distribution has a mean of 2.15 dex and a standard deviation of 0.51 dex. There is no significant difference between the Type 1 and 2 AGNs in this sample (see text for details).

NLR and Eigenvector 1

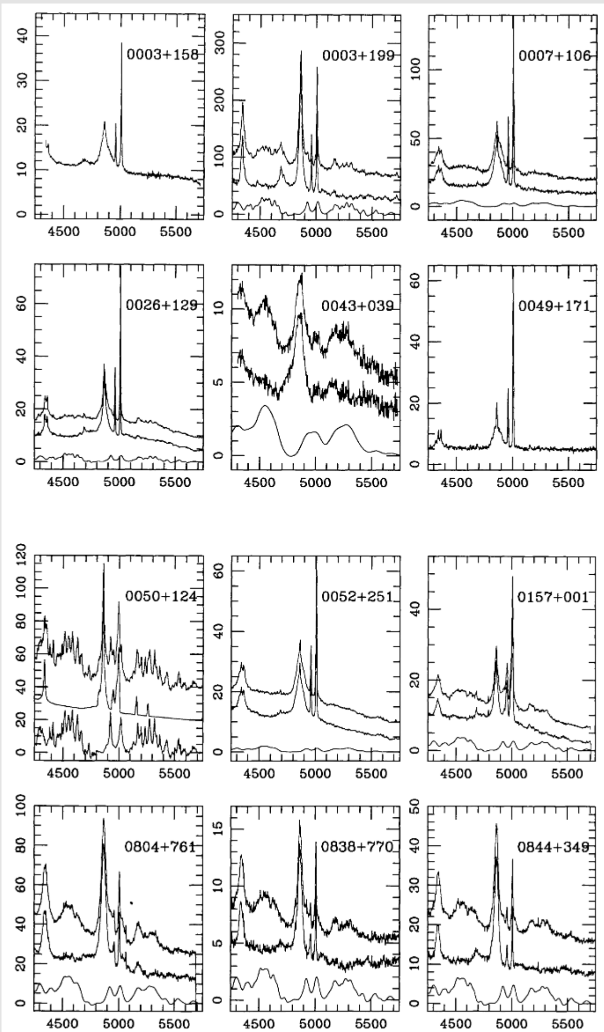

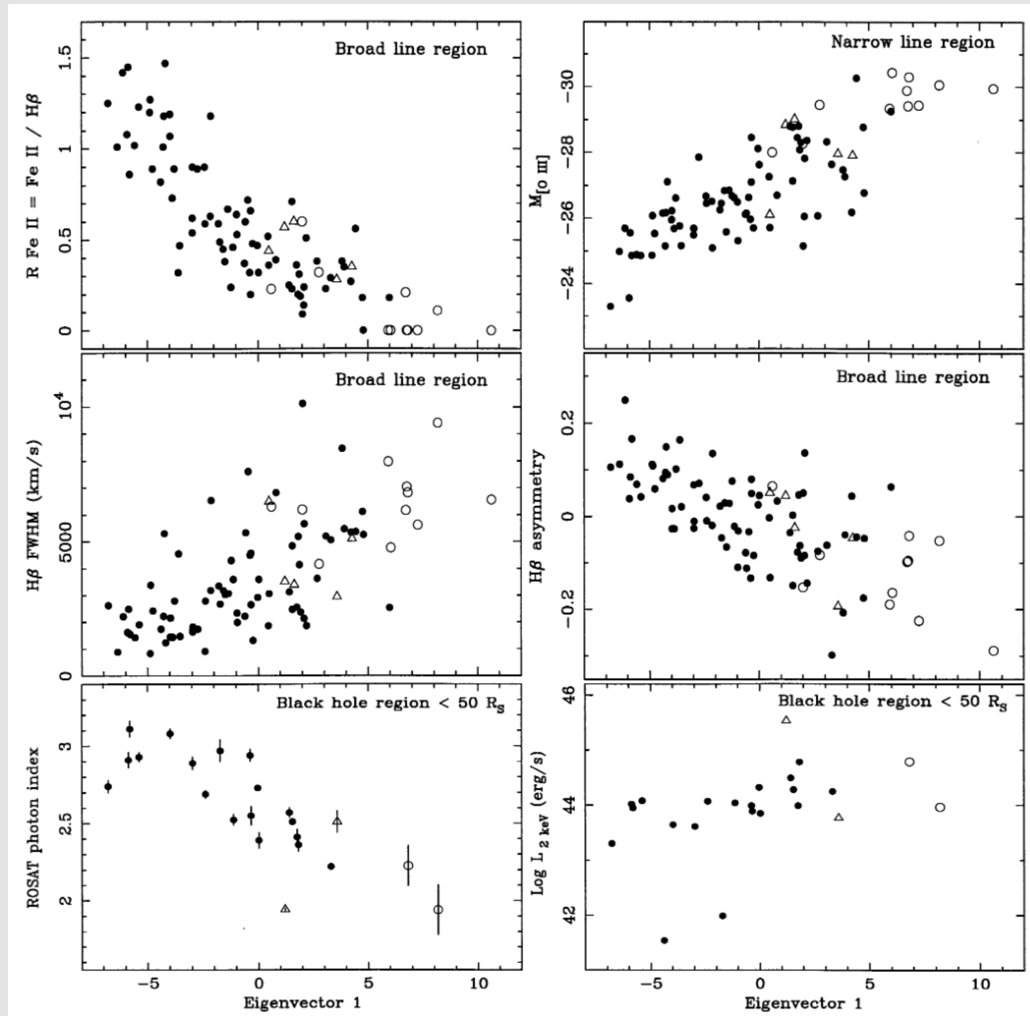

Boroson & Green (1992)

[O III] link indicates eigenvector 1 is not just orientation.

NLR Relation to Bulge

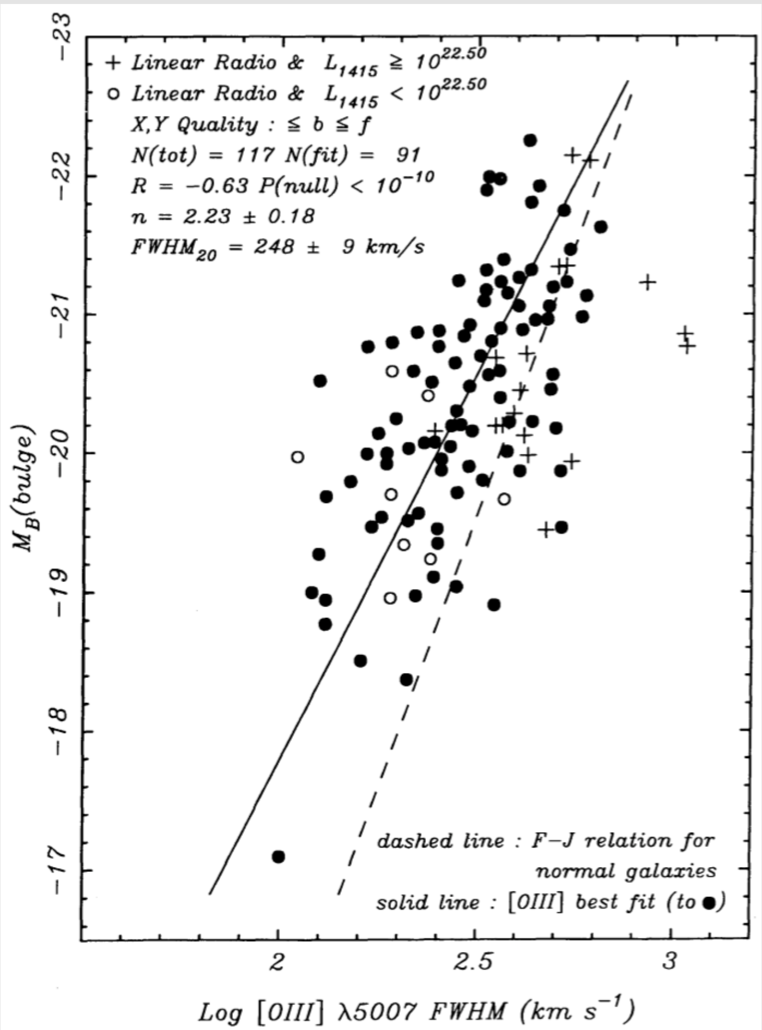

Whittle (1992)

NLR line widths are correlated with host-galaxy bulge luminosity (and bulge gravitational potential).

Indicates NLR widths are primarily virial in origin, reflecting the gravitational field of the stars (and not the black hole).

AGNs with powerful radio jets lie off the correlation, having larger widths than expected.

Apparently can also be some non-virial component to the velocities, such as shock interactions between the radio jets and NLR gas.

NLR Line Profiles

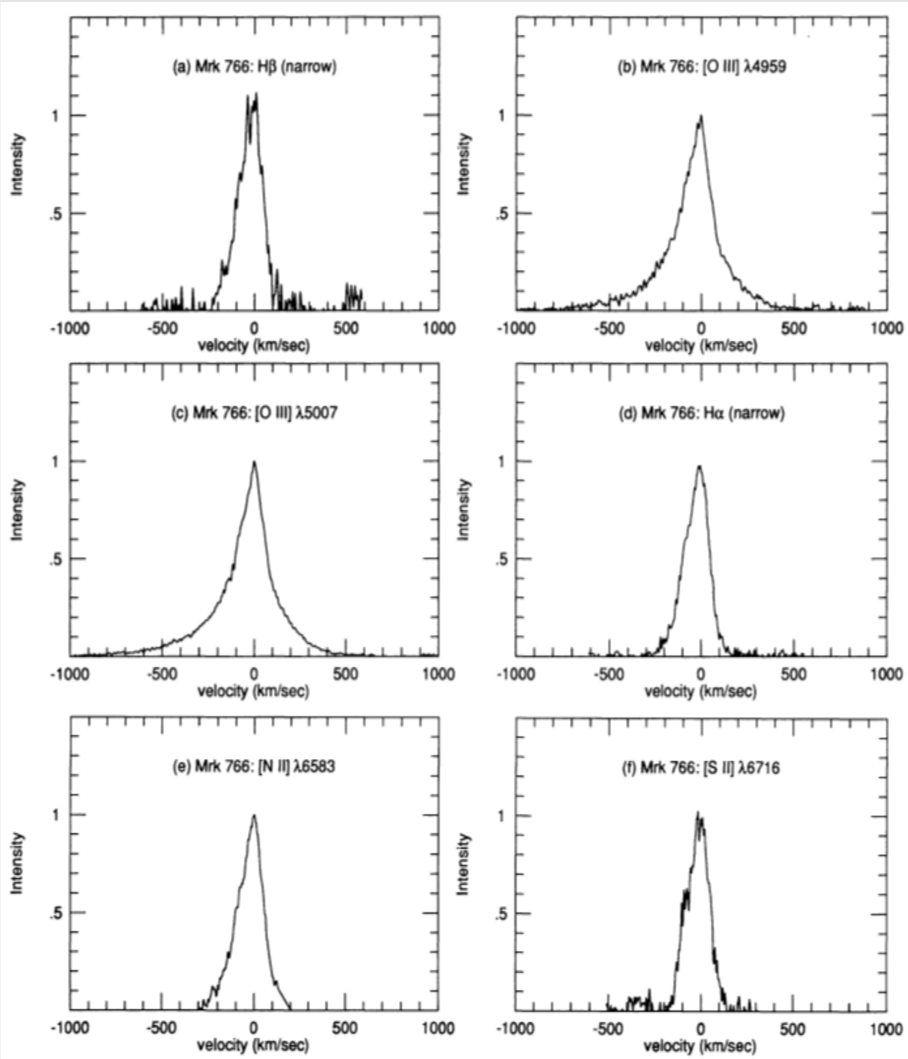

Veilleux (1991)

NLR line profiles are non-Gaussian

- Stronger bases than Gaussian
- Often blueward asymmetric, especially in the line base

Asymmetry arises from some combination of outflow motion plus dust extinction.

Redshifted side of outflow extincted, leading to the line asymmetry.

This is also seen in direct NLR mapping.

In a given object, NLR line widths are larger for higher ionization species; radial stratification of the NLR.

Flux and Velocity Maps of Brγ

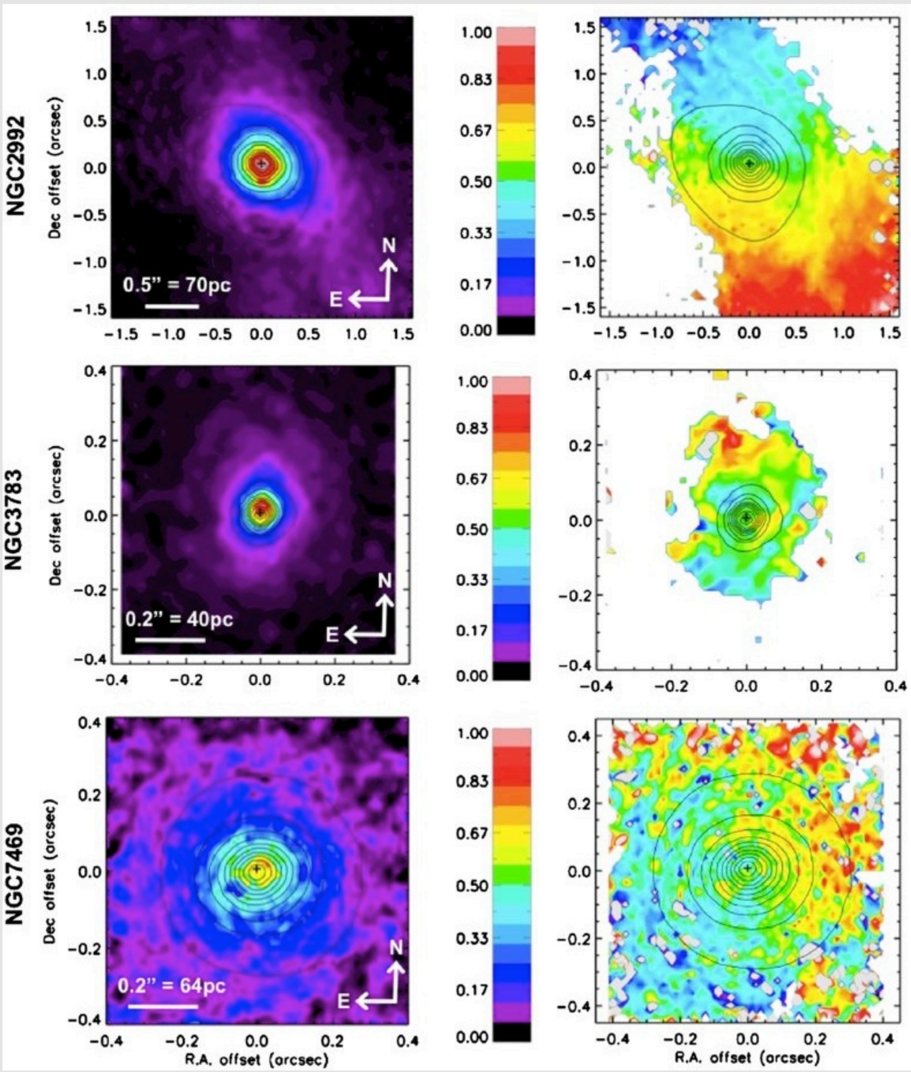

2.1655 μm, thereby minimizing extinction

Sometimes see ~ biconical outflow signatures

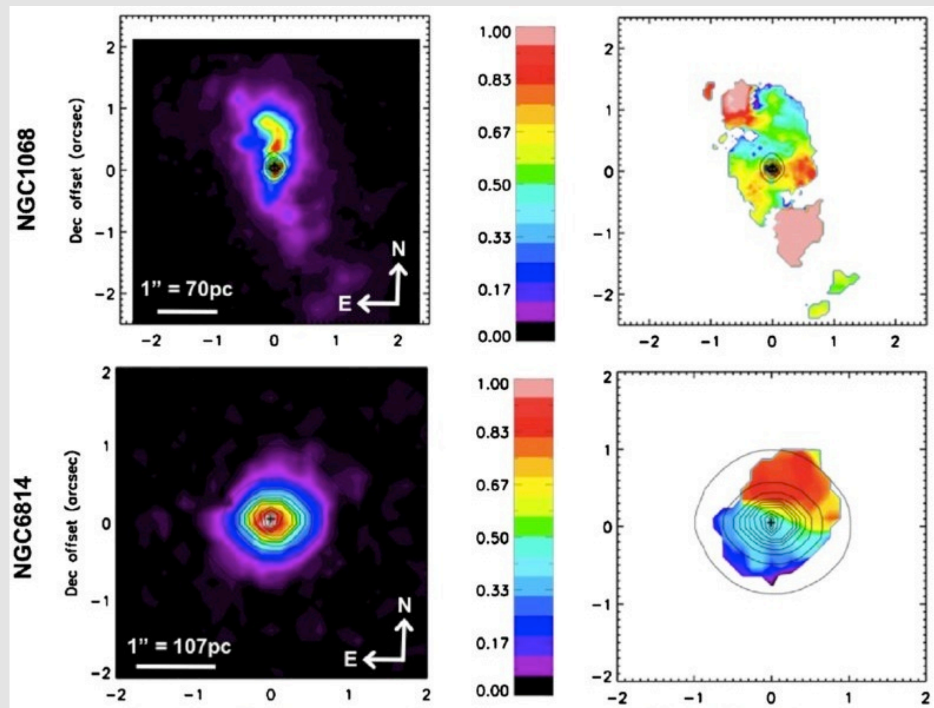

Muller-Sanchez et al. (2011)

Ionization Cones

Often see “ionization cones” in maps of high-excitation lines; wedge-shaped structures of gas ionized by the AGN continuum.

These often begin in the “classical” NLR, and can extend outward to ~ kpc scales, forming an “extended” NLR.

The fairly sharp edges of ionization cones are defined by the collimation of light from the AGN.

Collimation could be due to “shadowing” by the torus, or alternatively an inherently anisotropic ionizing continuum.

They come in single-sided and bi-conical types, with the single-sided ones presumably having an obscured counterpart on the other side.

Ionization Cone in the Circinus Galaxy

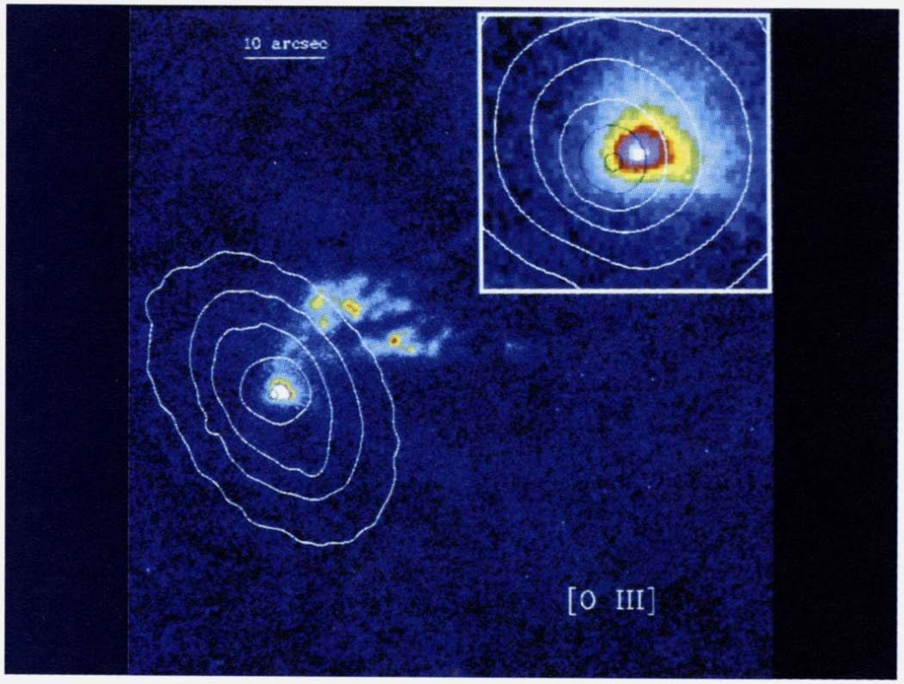

Figure 3: *Same as Figure 1 but in the [OIII] line. Note the clear cone-shaped structure and the displacement between the line and K' continuum peaks.*

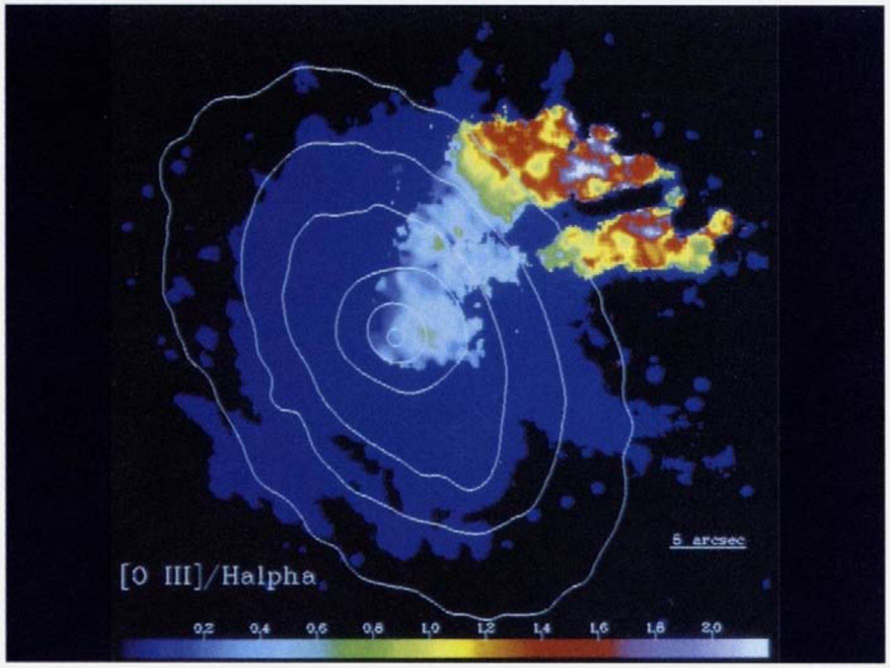

Figure 6: *[OIII]/(Hα+[NII]) showing the ionization structure of the cone. The uniform dark blue region is where Hα+[NII] but not [OIII] was detected at more than 10σ.*

Marconi et al. (1994)

Ionization Cone in NGC 5252

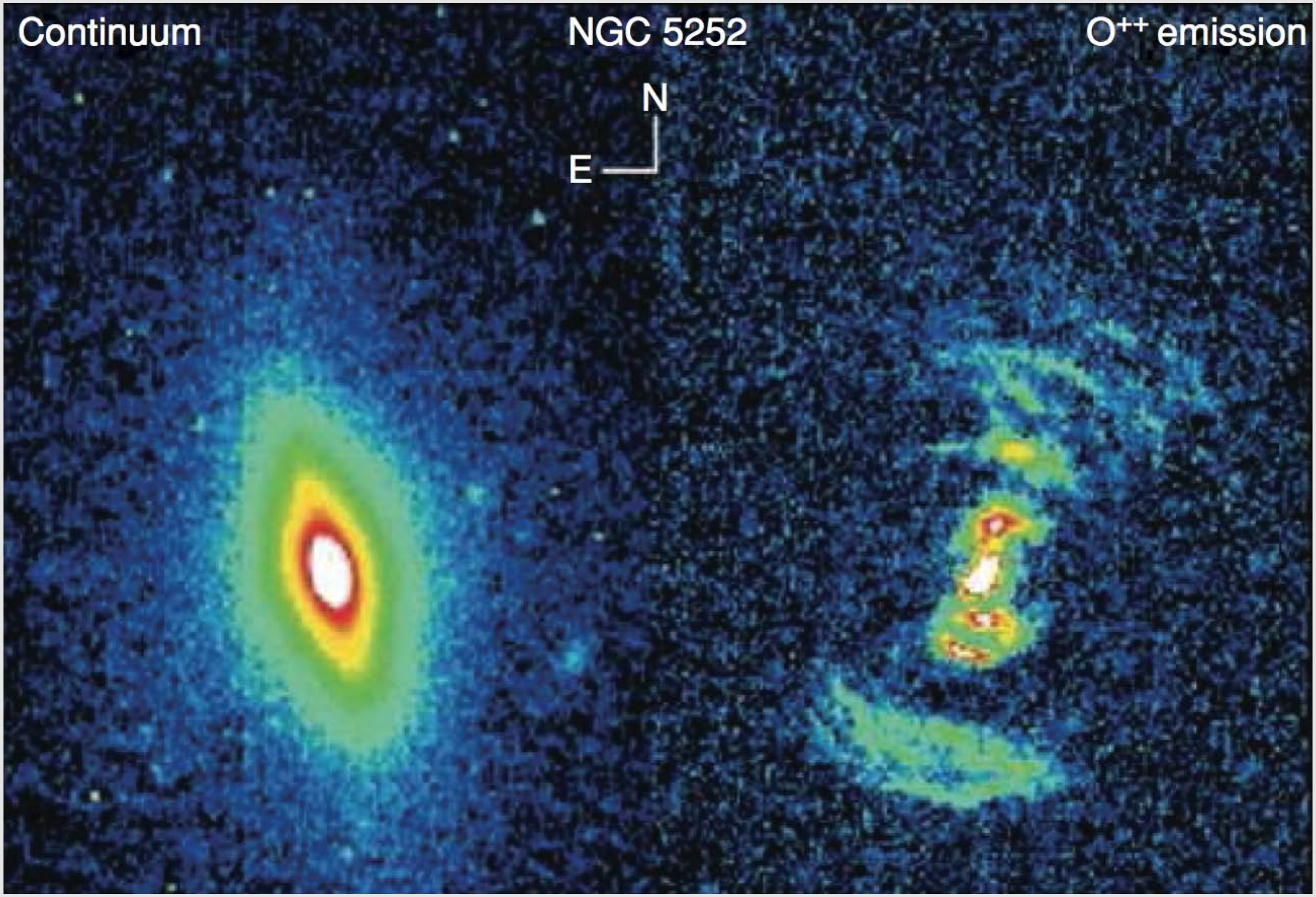

From Netzer (2013), courtesy of C. Tadhunter

Why Distinct BLR + NLR?

Line EWs from "Clouds" at Different Radii

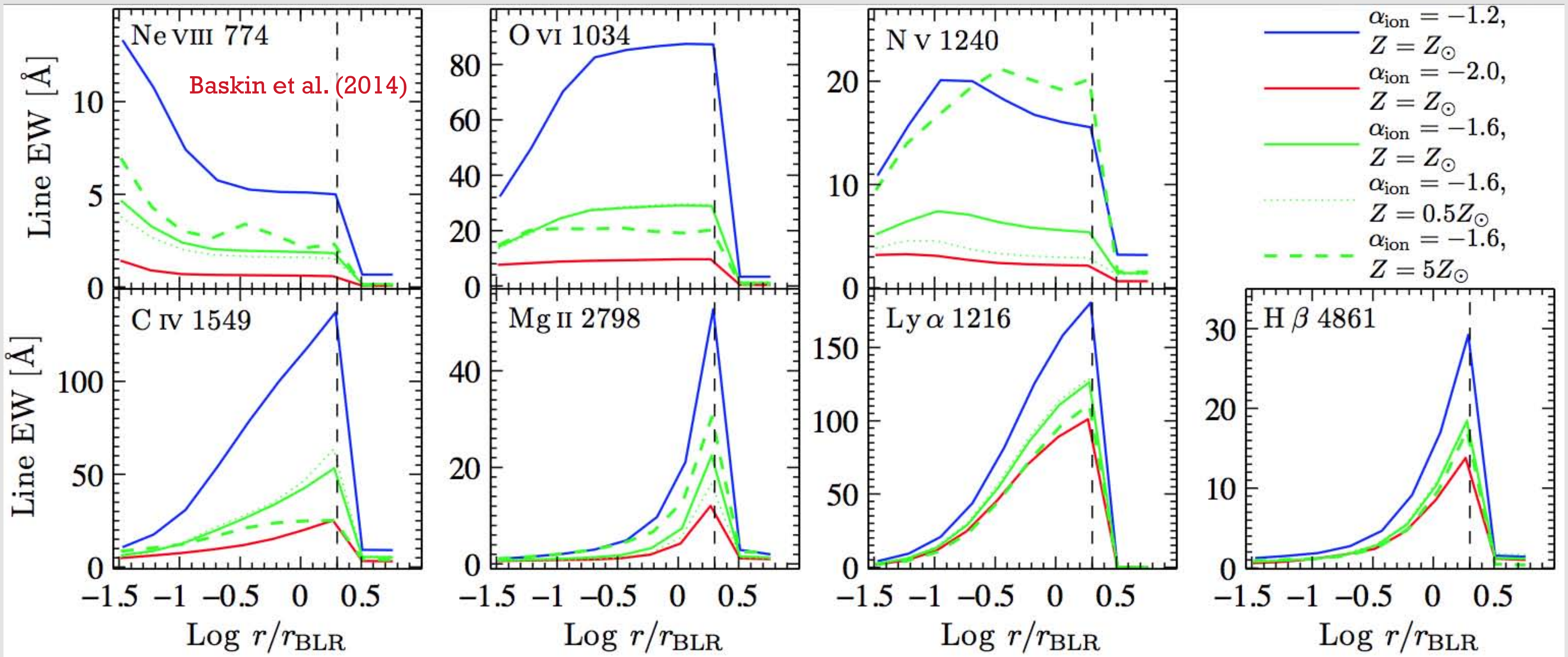

Beyond the dust sublimation radius (vertical dashed lines), about 80% of incident radiation is re-radiated by dust in the infrared.

The line emission drops sharply when dust is present, and then must go far out to accumulate sufficient emission from NLR gas. This is the likely cause of the distinct BLR + NLR structure.

The Torus

Type 1 vs. Type 2 AGNs

To first approximation, the optical/UV spectra of AGNs separate into two broad spectral types:

Type 1

- Broad permitted emission lines, particularly the Balmer lines
- Permitted lines clearly broader than forbidden lines
- Moderate EW forbidden lines

Type 2

- Narrow permitted emission lines, particularly the Balmer lines
- Permitted lines have similar widths to forbidden lines
- High EW forbidden lines

There are additional complications to this simple scheme (e.g., intermediate type classifications, narrow-line Type 1 AGNs).

And note that people unfortunately sometimes use these "Type 1" versus "Type 2" labels in inconsistent ways.

Type 1 vs. Type 2 AGNs

Example Type 1 AGN

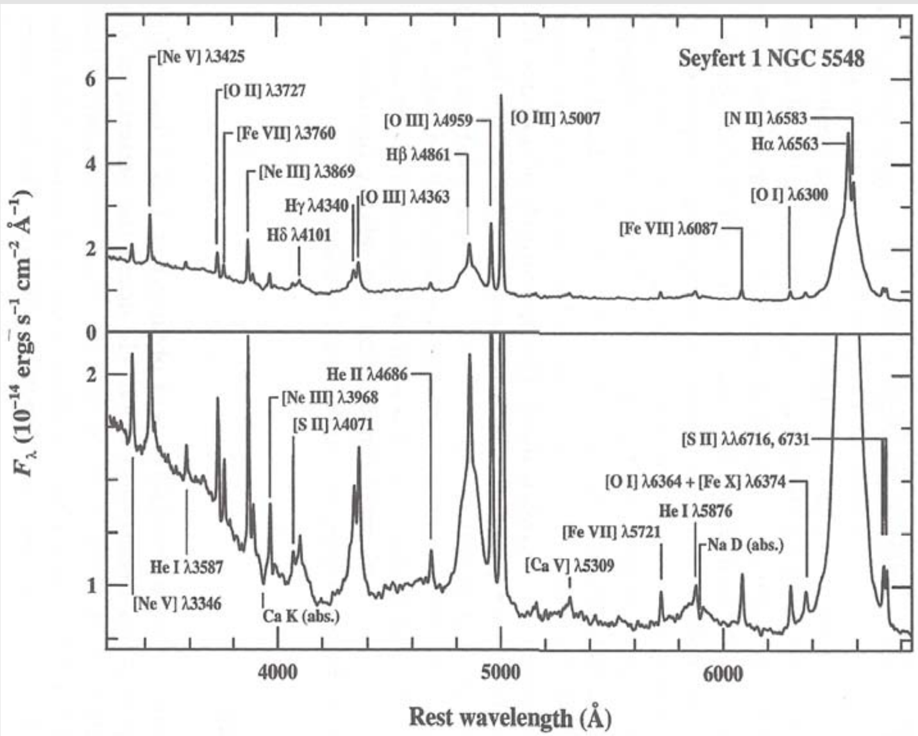

Example Type 2 AGN

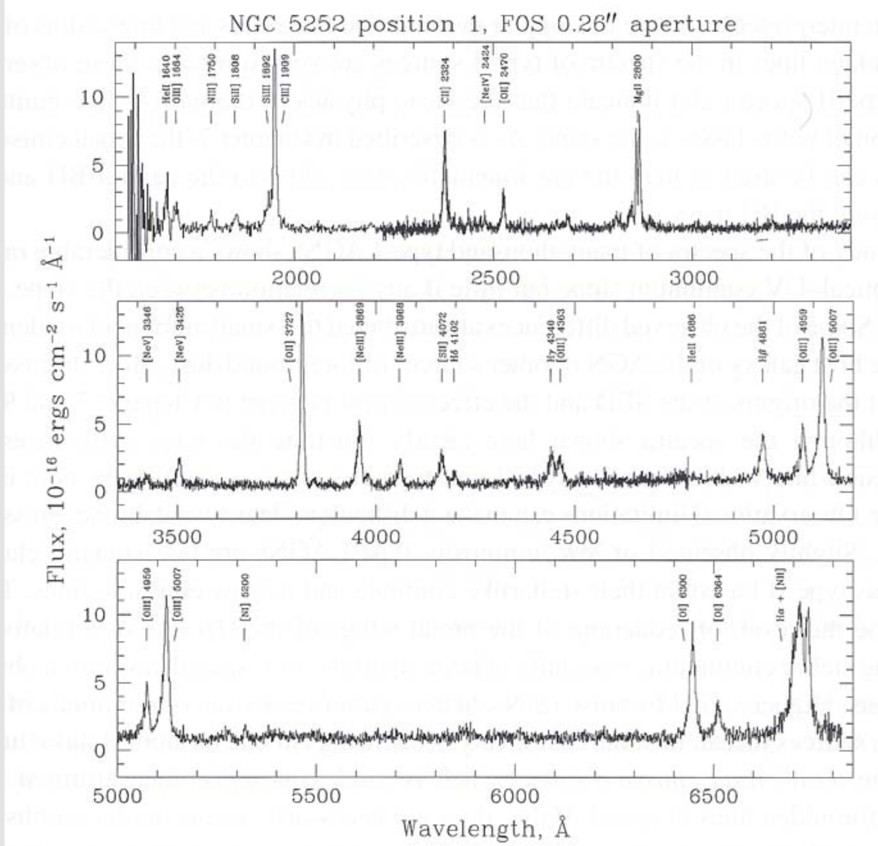

Figure 1.3. The spectrum of the low-luminosity, low-redshift type-II AGN NGC 5252 (courtesy of Zlatan Tsvetanov).

Peterson (1997)

The Torus and AGN Unification

These optical spectral differences have come to be understood as (often) due to orientation-dependent central obscuration by a so-called "torus".

The torus is presumed to be an axisymmetric structure of large height so that, at least at low luminosities, the majority of AGNs are obscured by it.

It is made of a combination of dusty atomic and molecular gas.

The dust causes large extinction in the optical/UV and sometimes even in the NIR.

The Torus and AGN Unification

The torus lies between the BLR and the NLR.

Type 2 AGNs are those obscured by the torus, and emission on the scale of the BLR and smaller is obscured by it.

Models explaining differences between Type 1 and Type 2 AGNs this way are referred to as "unification models".

These models have had much success, though they are not complete and there are likely exceptions.

There appear to be substantial object-to-object variations in the covering factor and geometry of the torus.

The Torus and AGN Unification

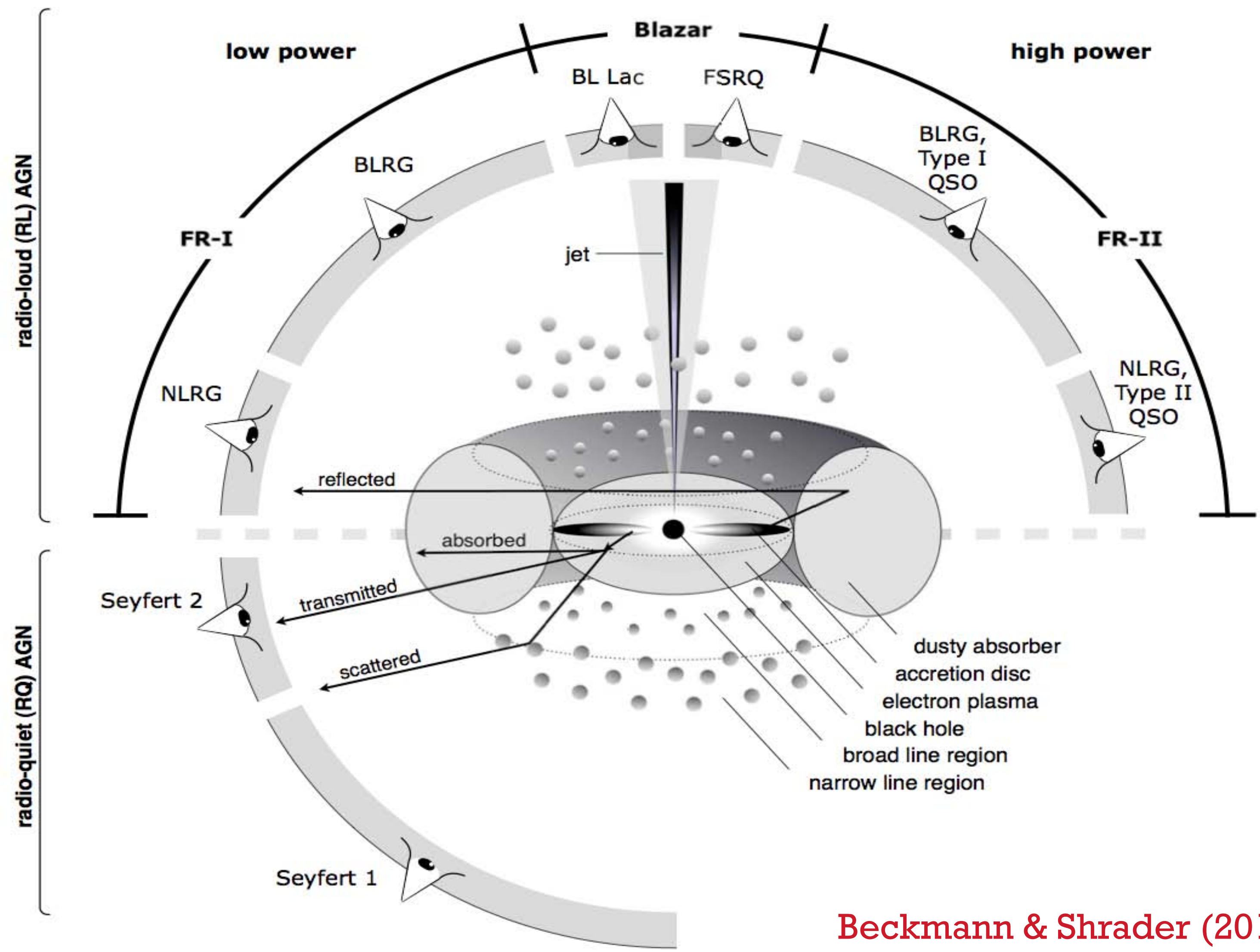

Beckmann & Shrader (2012)

Polarization by Scattering and the Unified Model

The early history of the unified model is complex, and several researchers put forward early ideas along these lines.

However, a significant breakthrough came from sensitive studies of the polarization properties of AGNs.

These found "hidden" BLRs in the polarized light from many Type 2 AGNs.

A "mirror" made of electrons or dust is able to scatter some of the small-scale emission around the torus, providing a "periscopic" view of the inner regions.

This scattering polarizes the relevant radiation.

Examples of Hidden BLRs

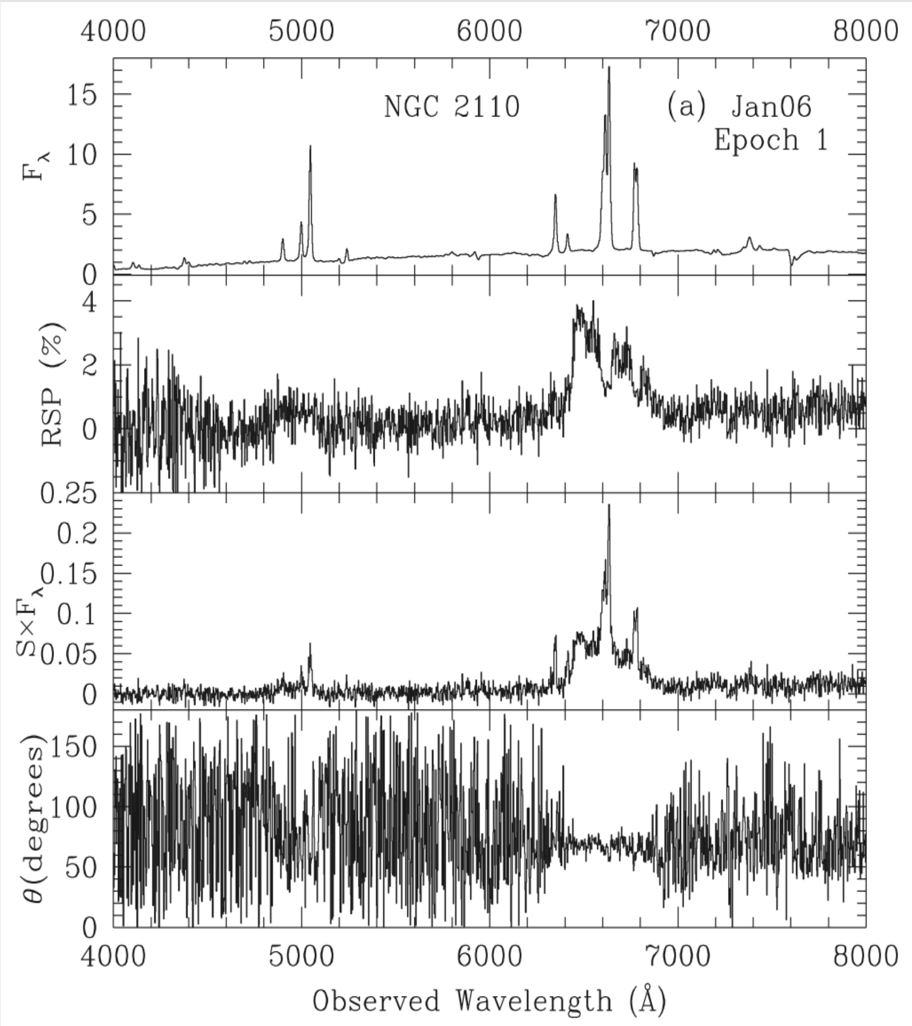

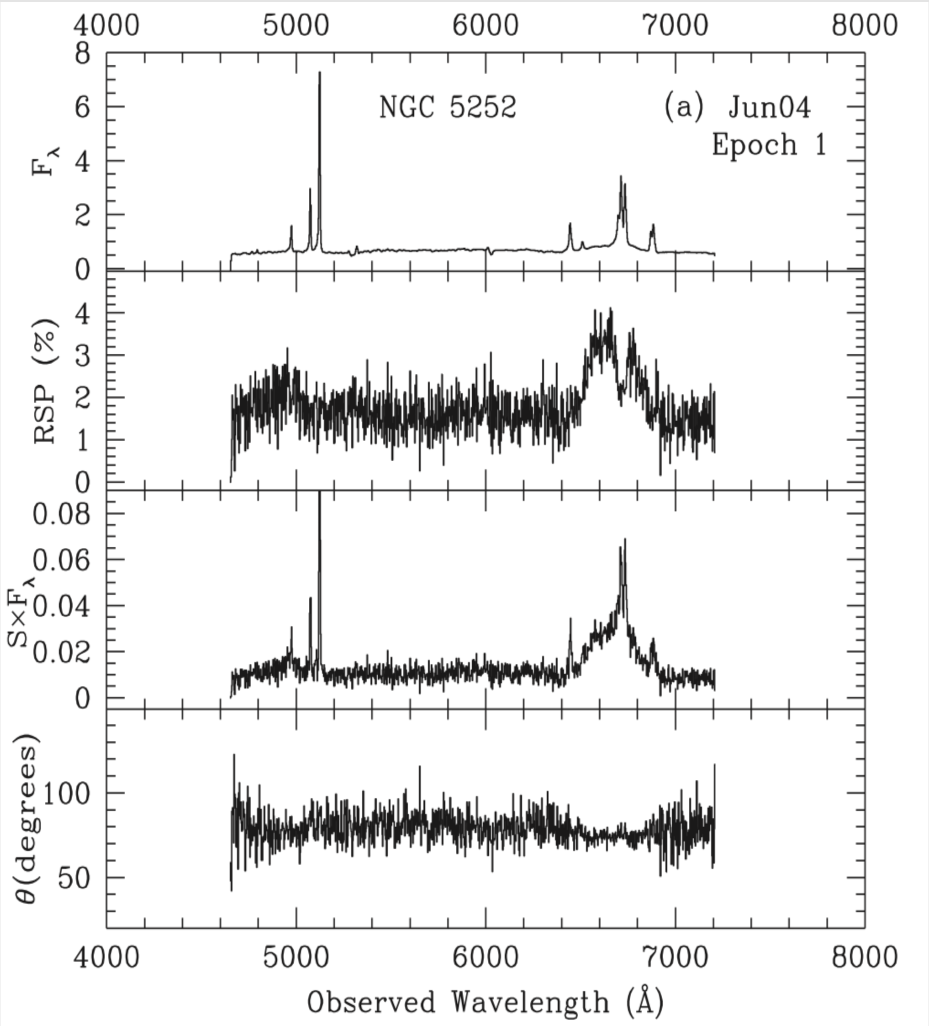

Tran (2010)

X-rays and the Unified Model

Additional evidence for the unified model comes from studies of X-ray absorption and iron K line emission in Type 2 AGNs.

The X-ray opacity of gas is strongly energy dependent, and high-energy X-rays can in many cases pierce through the torus.

This enables the column density through the torus to be estimated, with values of 10^{22}-10^{24} cm^{-2} often being found.

Some Type 2 AGNs have very large column densities that cannot be pierced even with high-energy X-rays – these are called "Compton-thick" AGNs.

Additional evidence for the unified model comes from the very high EWs of iron K line emission in some Type 2 AGNs. The large EW arises when the direct continuum is blocked but the torus and/or mirror are able to produce iron K lines.

Piercing the Torus with High-Energy X-rays

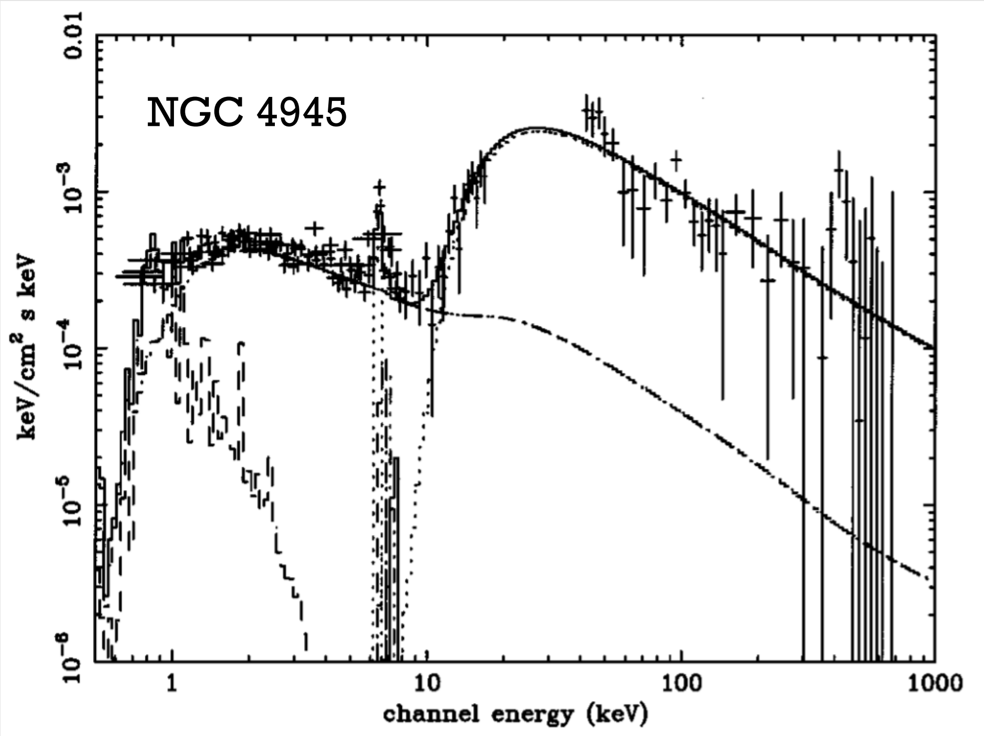

Done et al. (1996)

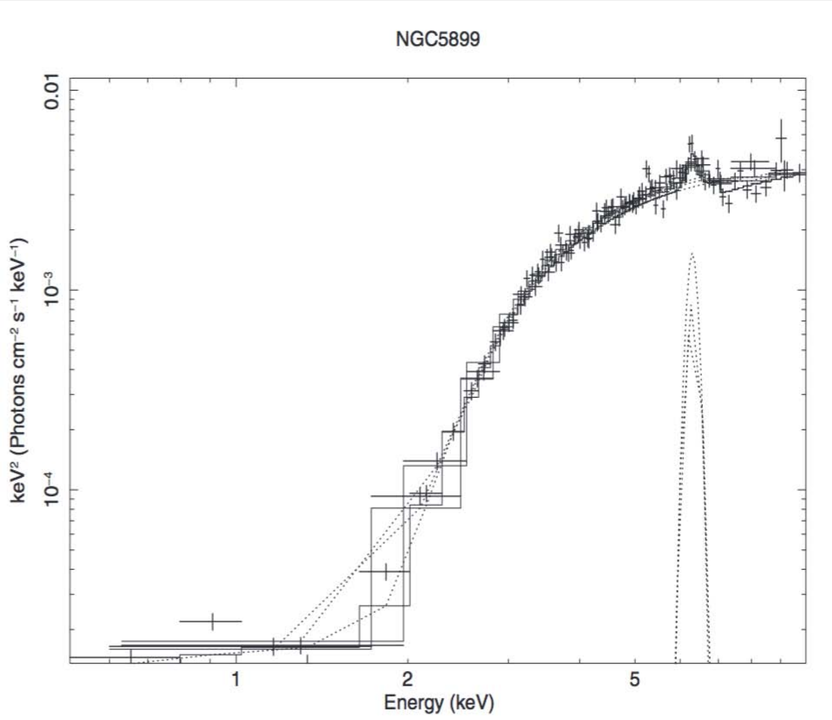

Vasudevan et al. (2013)

How Big is the Torus?

We know the torus must lie between the BLR and NLR, but we can be more specific.

We can now directly measure the size of the torus using

- Dust reverberation mapping between the *V*-band and *K*-band light curves.

- Interferometry in the NIR and MIR.

The size of the torus appears to scale as $L^{0.5}$.

The inner edge of the torus is at about 3 times the BLR radius for Hβ as determined from reverberation mapping.

Direct Measurements of the Torus Size

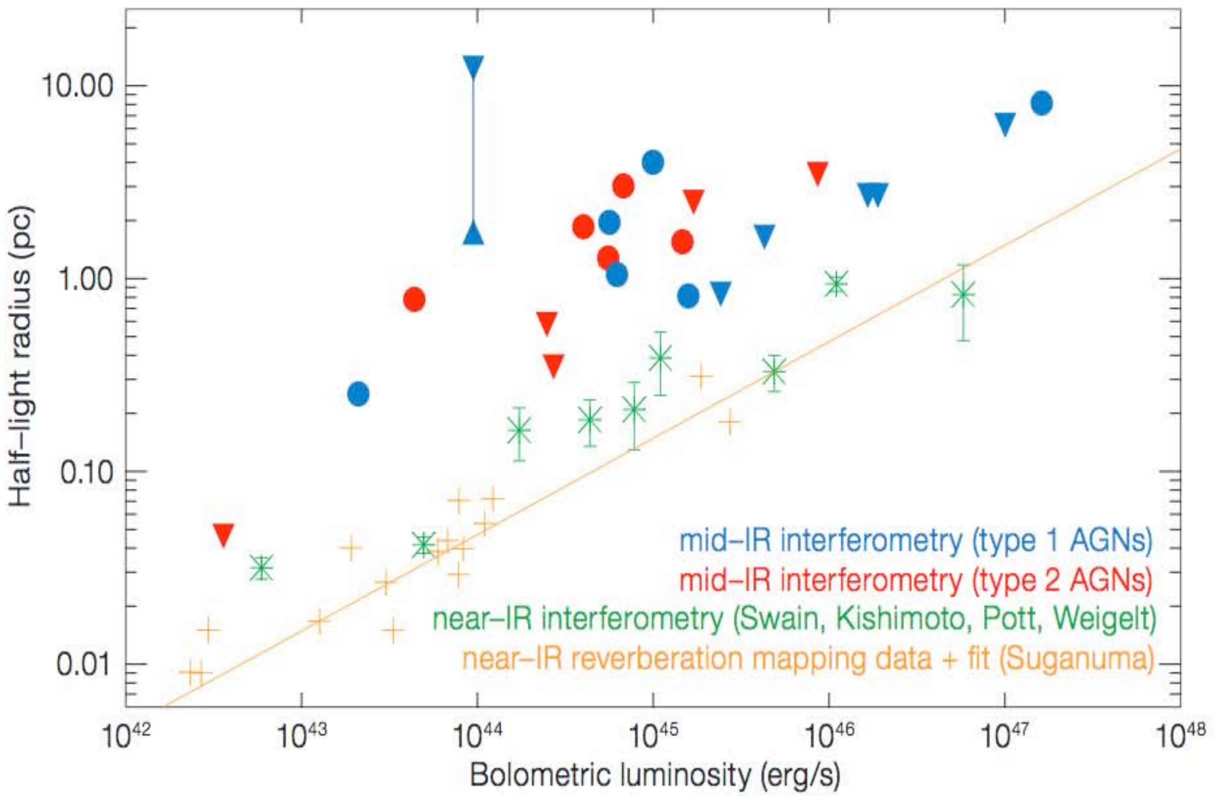

Figure 5. Size–luminosity relation for AGNs probing different regions of the torus: blue/ red points are MIDI measurements from the MIDI AGN Large Programme + archive for type 1/type 2 sources (statistical errors are smaller than symbol sizes); green crosses are NIR interferometry with both the Keck-Interferometer and AMBER/VLTI; orange pluses are from NIR dust reverberation mapping. Filled triangles show limits. Taking both the limits and the determined half-light radii into account shows that the mid-infrared size is less strictly correlated with luminosity than the innermost radius of dust that is seen in the NIR.

Burtscher et al. (2013)

NIR / MIR Torus Spectra

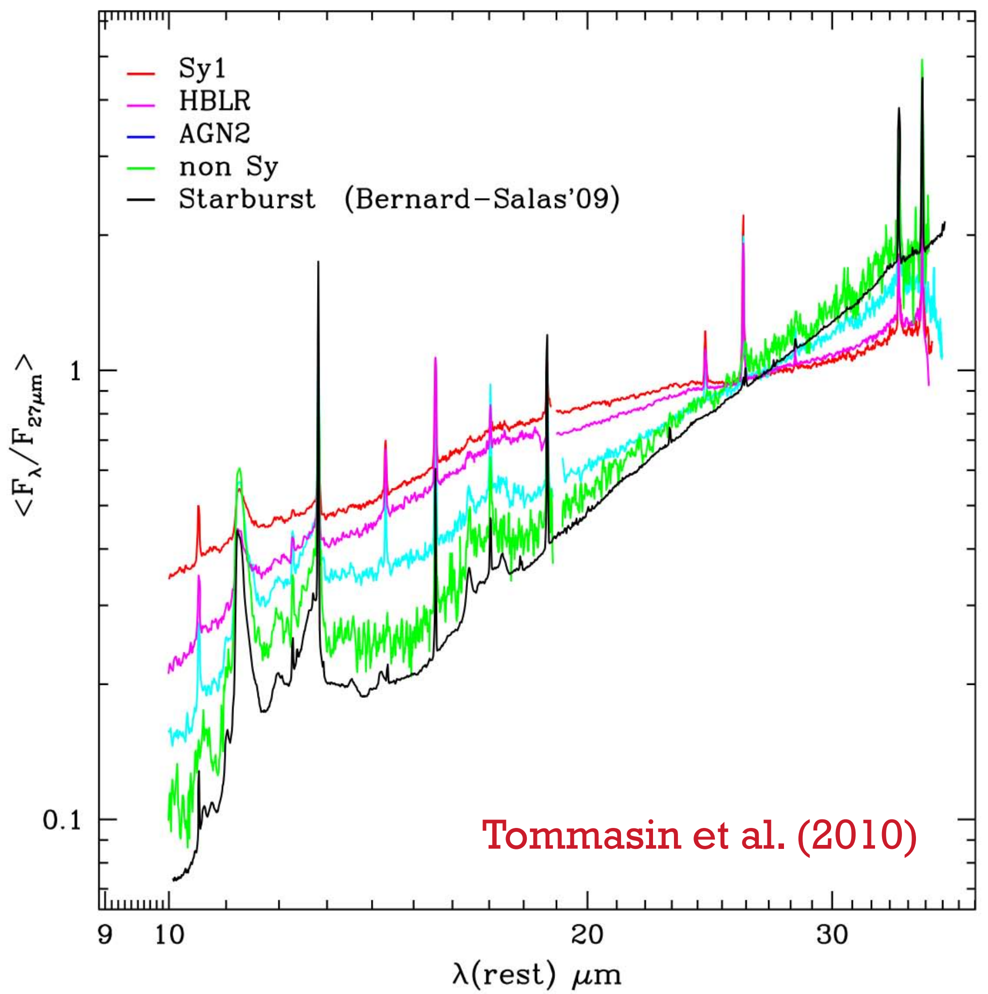

Figure 14. Average high-resolution spectra for our classes of galaxies, compared with the mean high-resolution spectrum of starburst galaxies.

NIR / MIR spectroscopy of dust emission places further constraints upon the torus properties.

If the torus were continuous over the range of radii observed, one would expect substantially hotter dust emission in Type 1 AGNs than Type 2 AGNs.

In Type 1 AGNs one could see the hot inner wall of the torus, while in Type 2 AGNs one could only see cooler dust at large radii.

But this is not observed. This result and others have led to a preference for "clumpy" torus models.

A Clumpy Torus

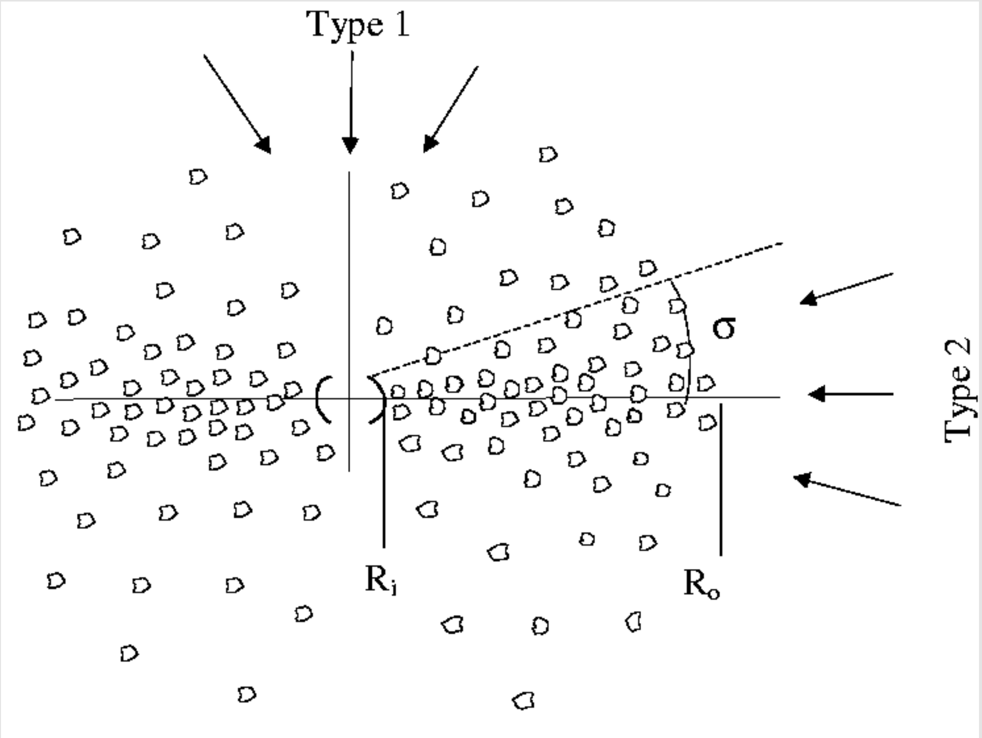

Nenkova et al. (2002, 2006)

Clumpy torus models break the strict correlation between dust temperature and distance, allowing clumps further out to be heated by the central radiation.

They improve agreement with the data.

AGN type would then be an orientation-dependent probability.

To explain the full NIR / MIR spectrum, one must also include NLR dust emission and a detailed treatment of the hot (1500-2000 K) graphite dust at the inner wall of the torus.

Some Characteristic Torus Properties

Keplerian velocities at the torus distance are ~ 1000 km s^{-1}.

Density of torus "clumps" are ~ 10^5-10^7 cm^{-3}.

The estimated mass of the torus is only a small fraction of the SMBH mass.

The Nature of the "Torus"

The torus is likely a dynamic system, being part of the general flow of matter from the galaxy's center to the SMBH.

This can help explain its large H/R, resolving stability issues.

But the details remain unclear.

One attractive idea is that the torus is part of an outer disk wind where dust is able to form – large disk required.

Another idea is that the torus may actually a warped outer accretion disk – large disk required.

The Torus as a Disk Wind

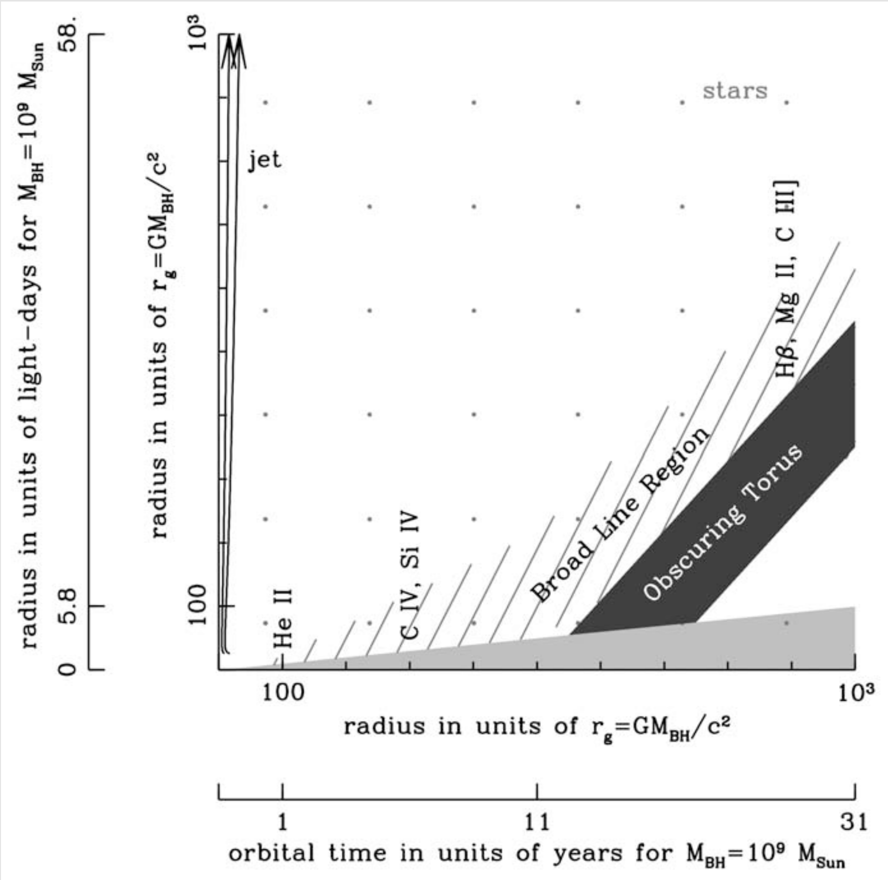

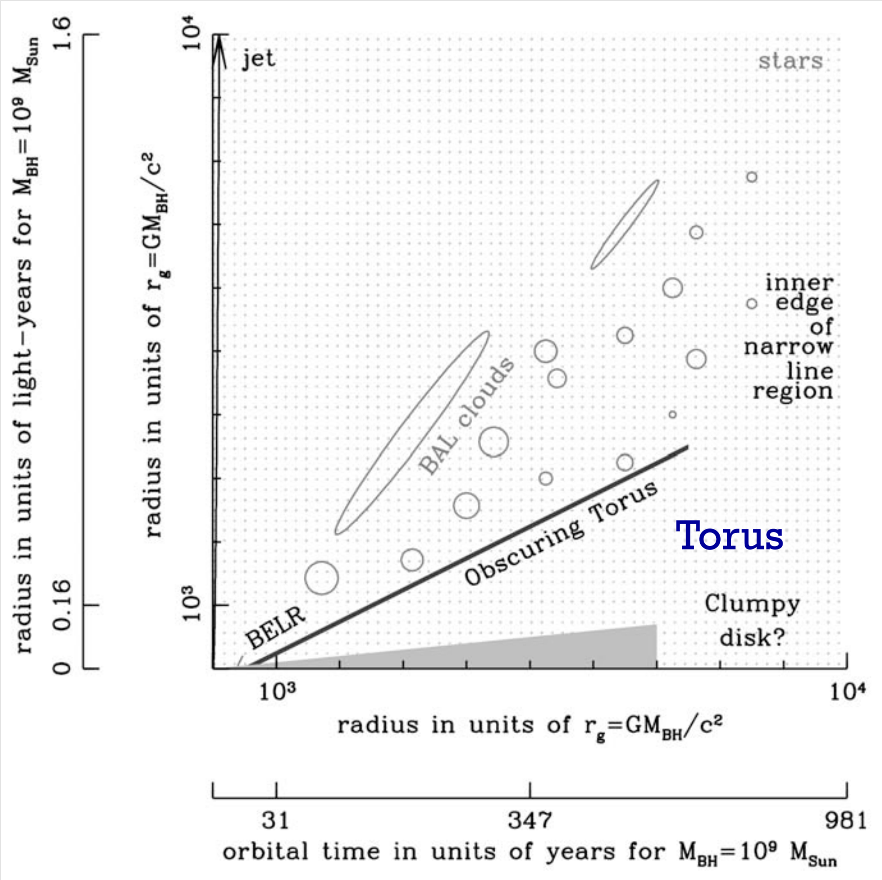

Courtesy of Pat Hall

Jets

A Warning / Apology

Studies of jets and radio-loud AGNs are an *enormous* field with a long history (since H. Curtis 1918).

Could have a great 5-lecture series just on them!

Even though radio-loud AGNs are a minority of the luminous AGN population, they have fascinating physical processes accessible at many wavelengths.

So their coverage here must inevitably be even less complete than for most other topics.

An Entire Conference on Jets

A Useful Working Hypothesis

At least to first order, we can adopt many of the findings about radio-quiet AGNs for radio-loud AGNs.

RL AGN ~ RQ AGN + Strong Jets

For example, they have accreting SMBHs, they have BLRs, they have NLRs, etc.

A tremendous simplification, and often seems to work well to first order of approximation (but not to higher orders).

Radio-Loud AGNs

AGNs are often divided into radio-loud vs. radio-quiet using

$$R = L_\nu(5\ \mathrm{GHz})\ /\ L_\nu(4400\ \mathrm{A})$$

where $R = 10$ is the typical (arbitrary) separator value.

About 10% of luminous AGNs are radio loud.

But no strong R bimodality, and perhaps none at all.

Even nominally radio-quiet quasars can have weak jets.

Radio-loudness is generally associated with strong particle jets emitting a synchrotron power-law continuum in the radio.

Radio-Loud vs. Radio-Quiet SEDs

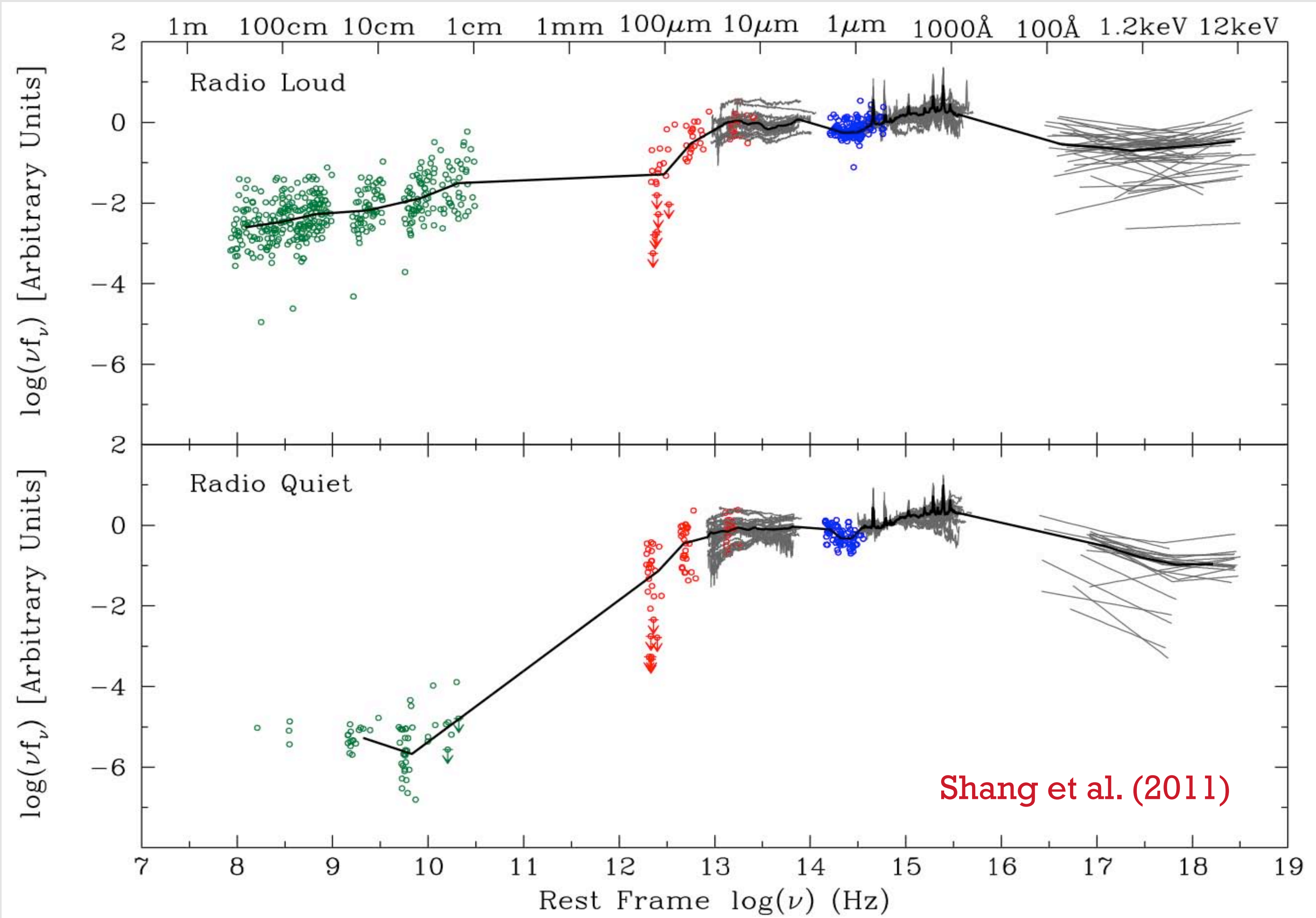

Components of a Radio Source

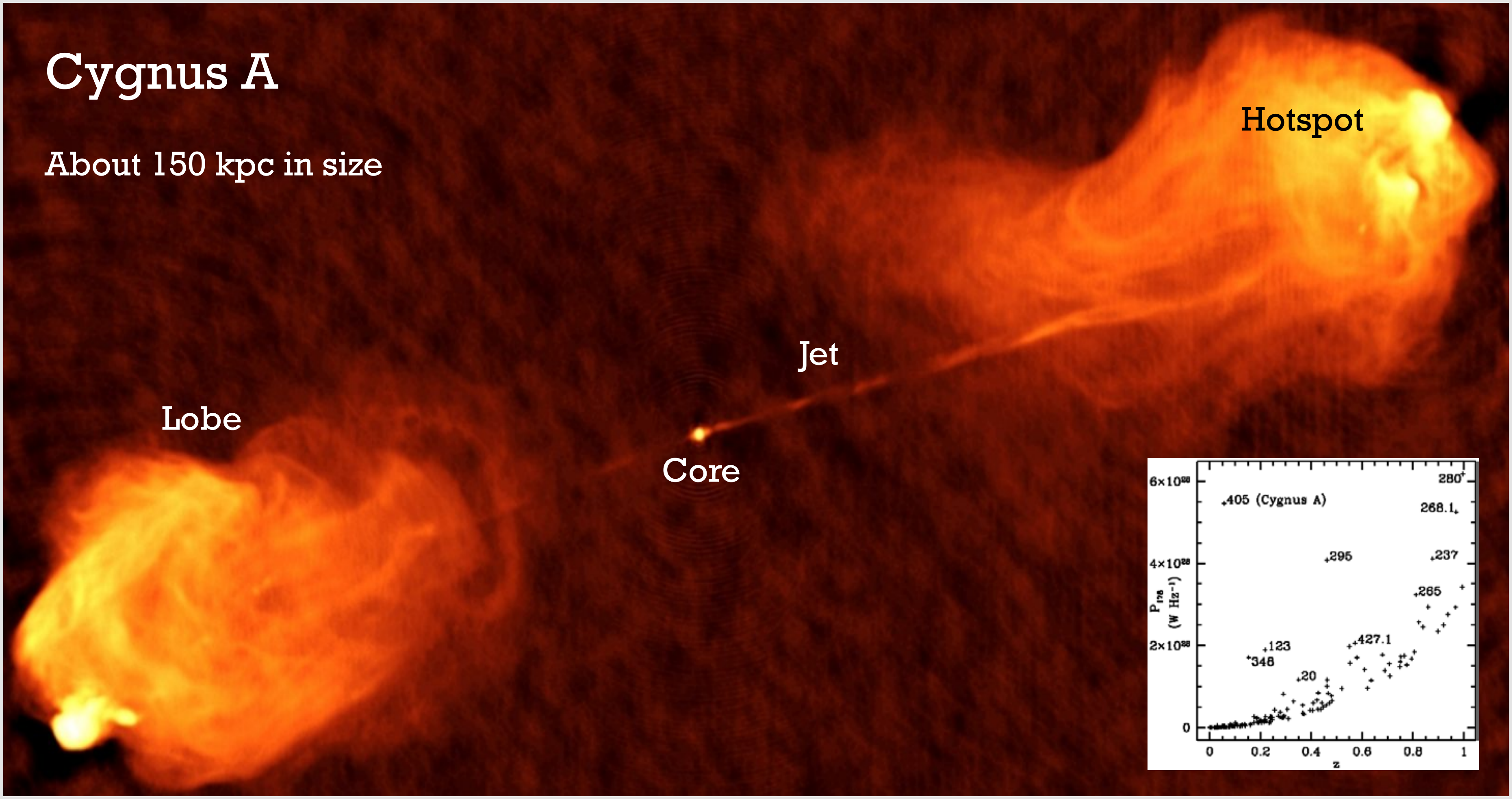

Carilli & Barthel (1996)

A 3 Mpc Size Radio Galaxy

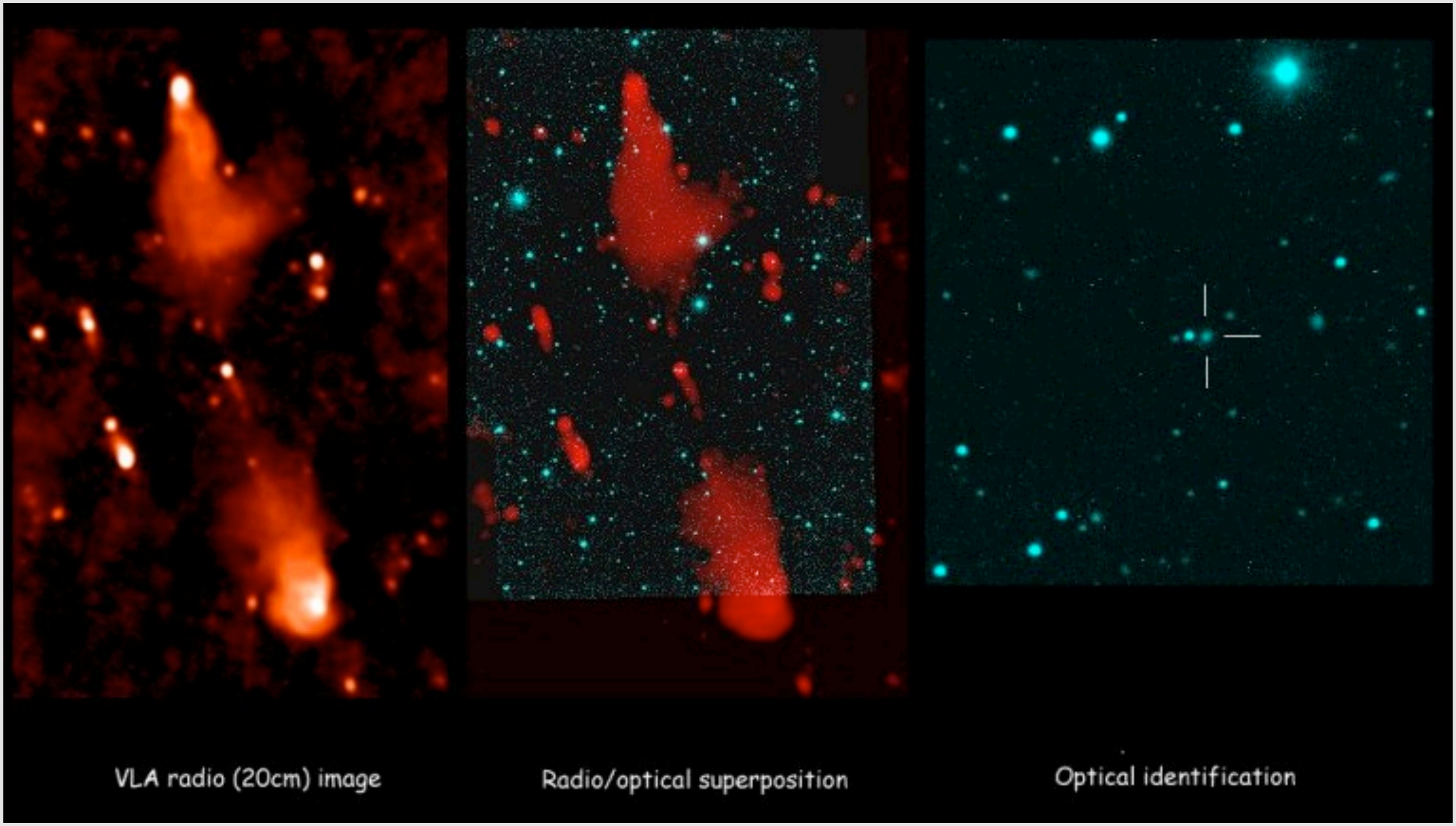

Palma et al. (2000)

Diverse Radio AGN Morphologies

Radio Galaxy Images at 74 MHz from the VLA Low-Frequency Sky Survey

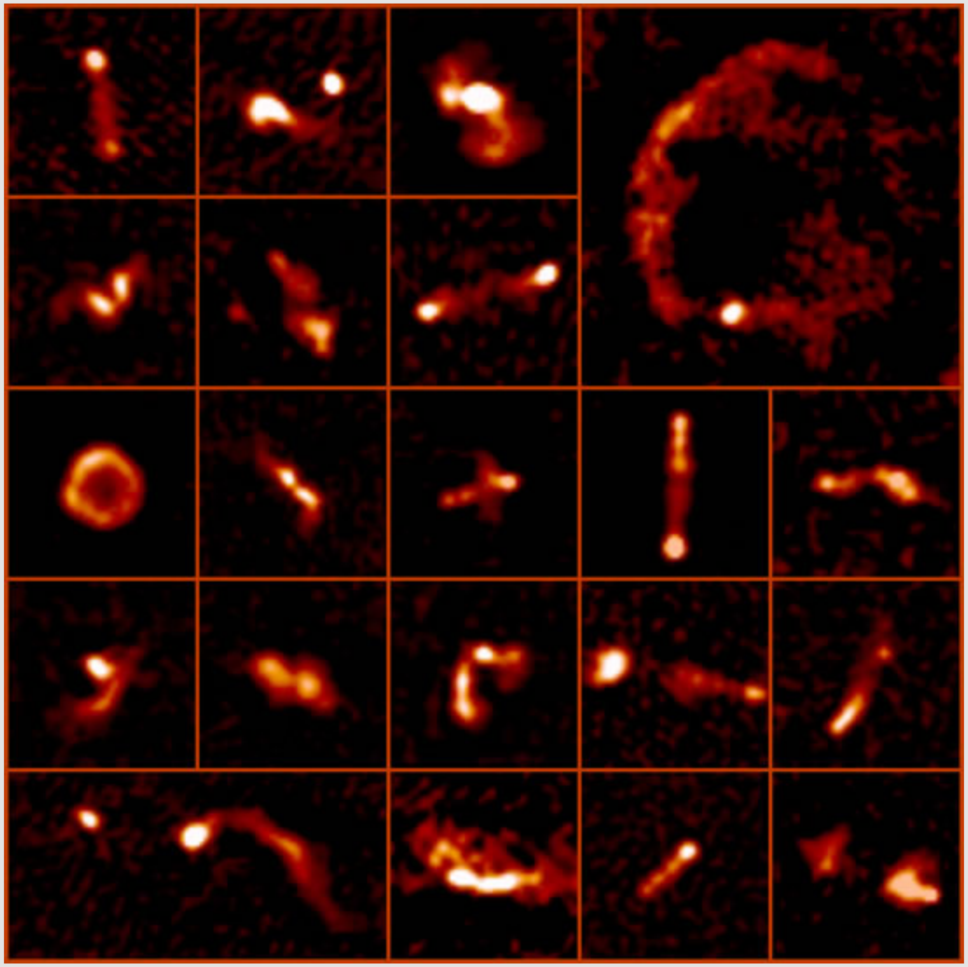

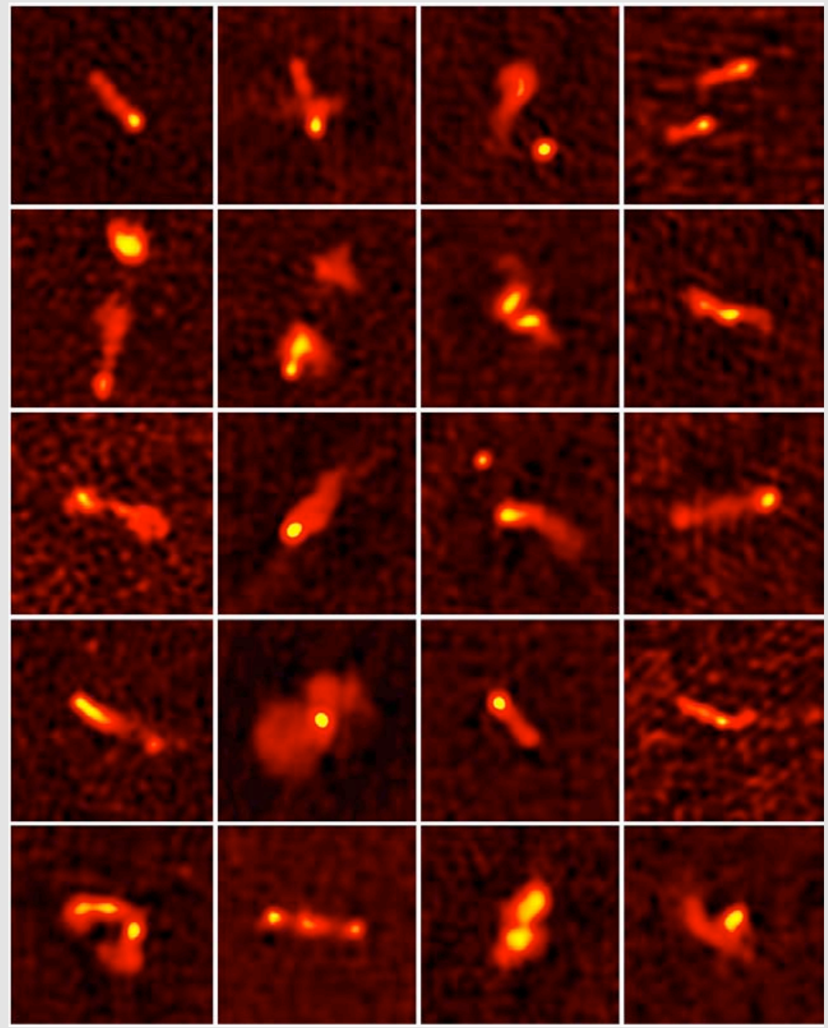

Cohen et al. (2007)

Some Basic Properties of Radio Jets

Jets often appear relativistic based on beaming, apparent superluminal motions on sub-pc scales, and variability.

Thus, the apparent properties of a jet depend *strongly* upon orientation.

At least in some cases, jets are launched on very small scales (making much of the "core" radio emission). And they can be collimated over a huge range of scales.

Jets are often seen in the X-ray and also the optical.

Launching of the M87 Jet

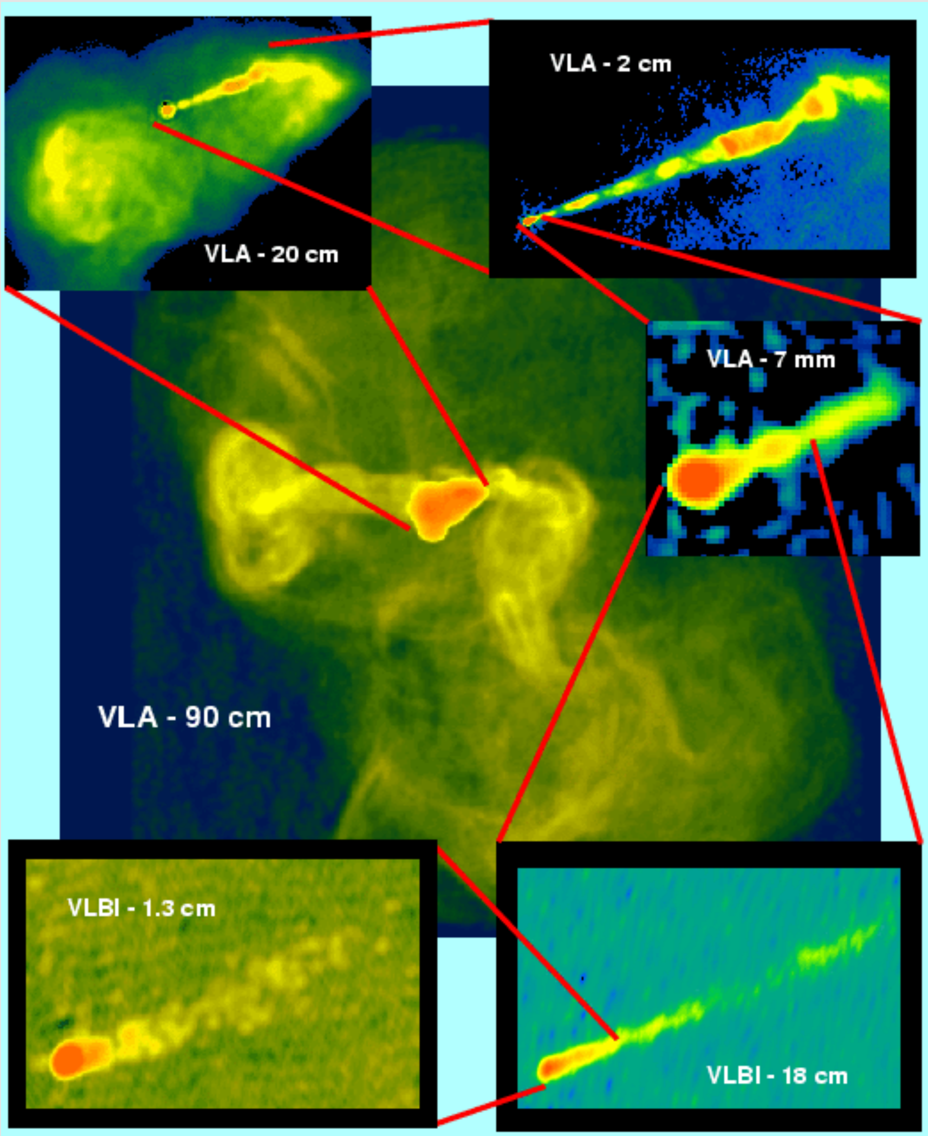

We can directly observe the M87 jet down to a few hundred R_S.

Structure of the Inner Jet

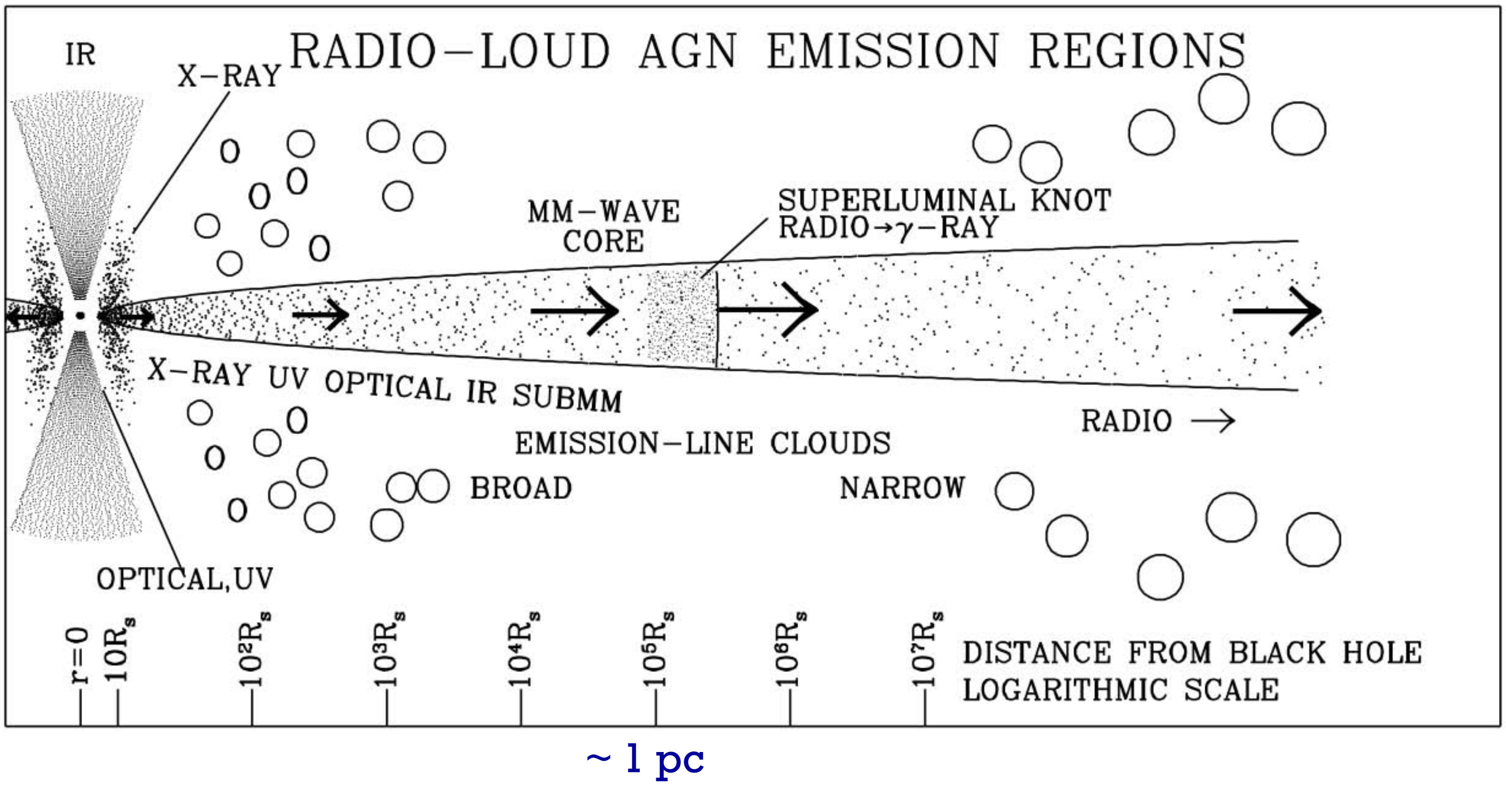

FIGURE 1. Sketch of the various sites of emission in an active galactic nucleus with a relativistic jet. The density of dots signifies in a qualitative way the intensity of the emission. The radiation produced in the jet is relativistically beamed, while the emission from outside the jet is not. It is not clear whether the emission from the ambient jet between the black hole (small black circle near the base of the jet) and the core is visible. The length of the arrows indicates the Lorentz factor of the flow. Note the logarithmic scale of approximate distance from the black hole, measured in Schwarzschild radii. (Adapted from Marscher, 2005)

Optical Jet Emission from 3C273

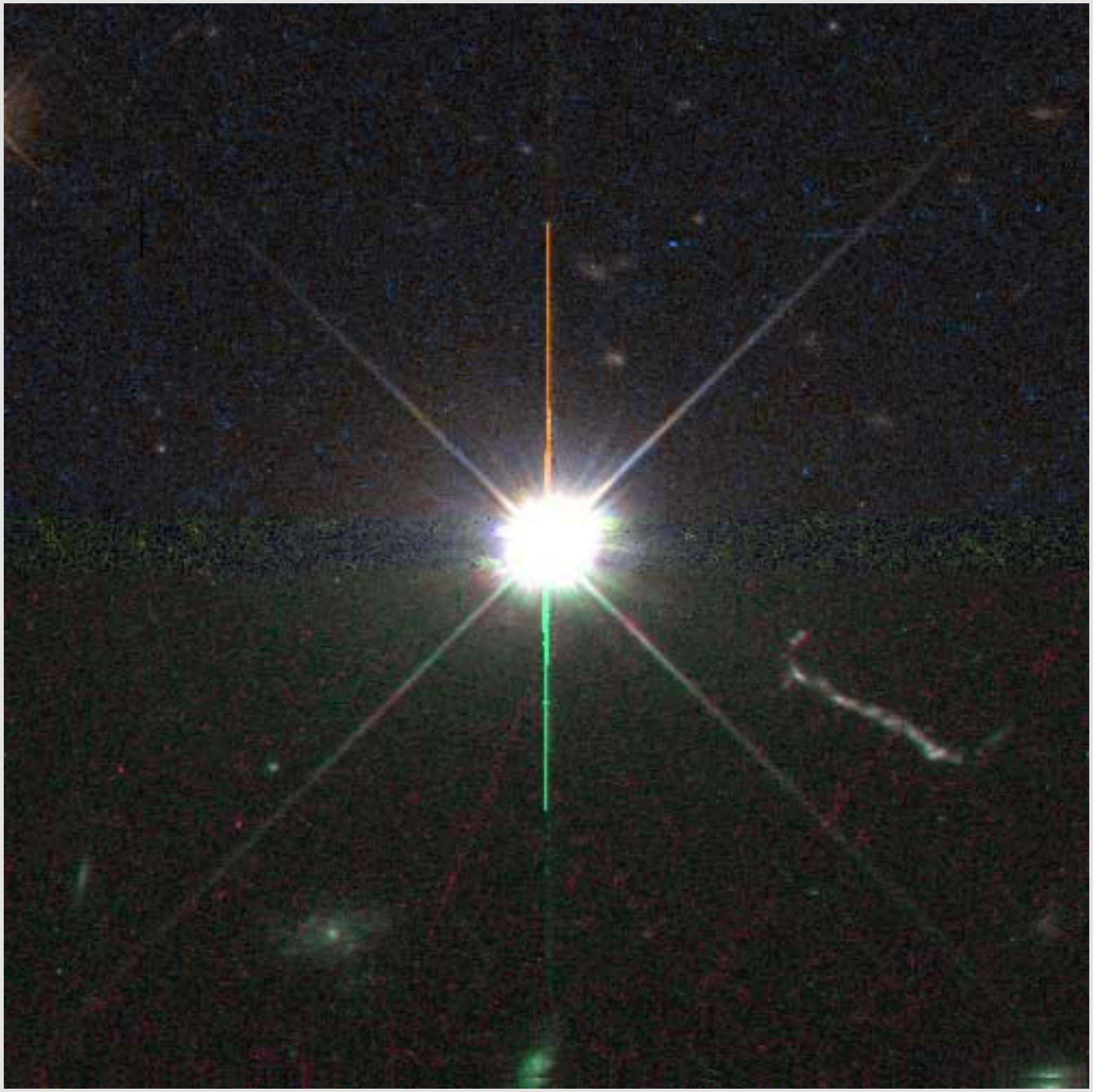

Multiwavelength Jet Emission

M87

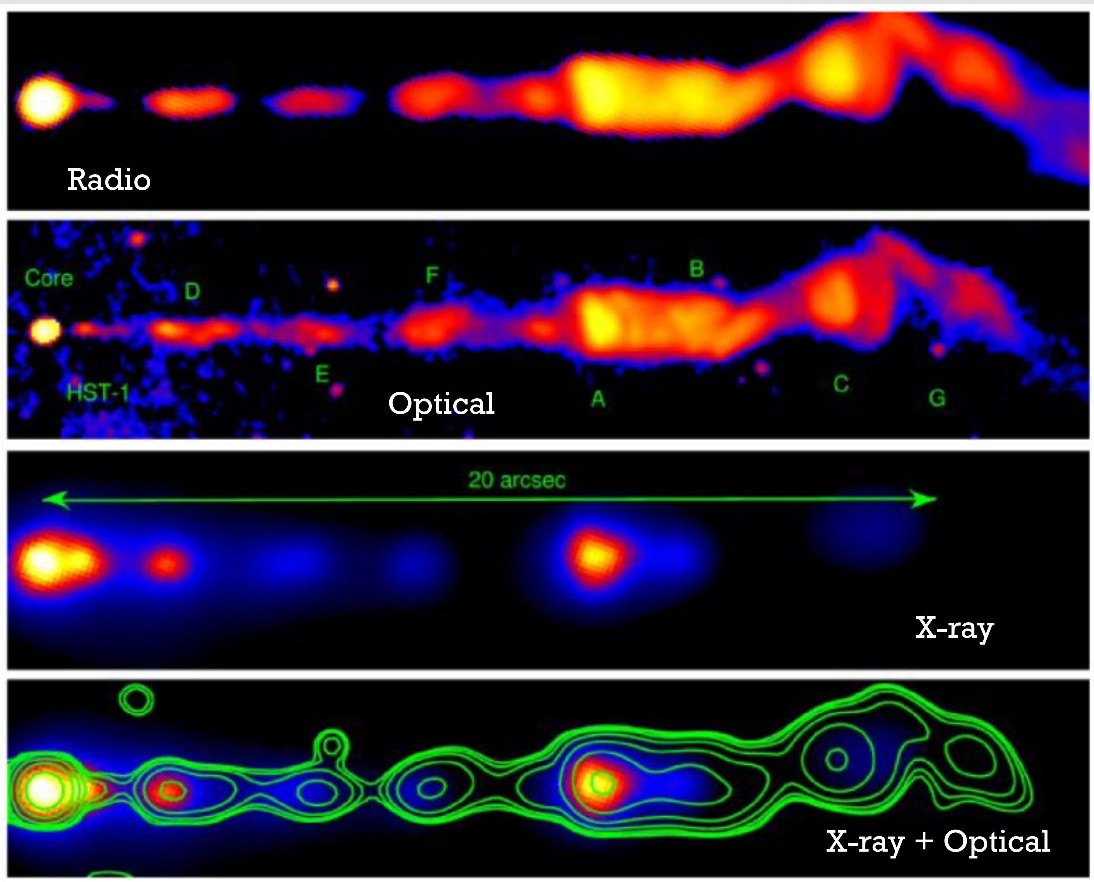

Marshall et al. (2002)

3C273

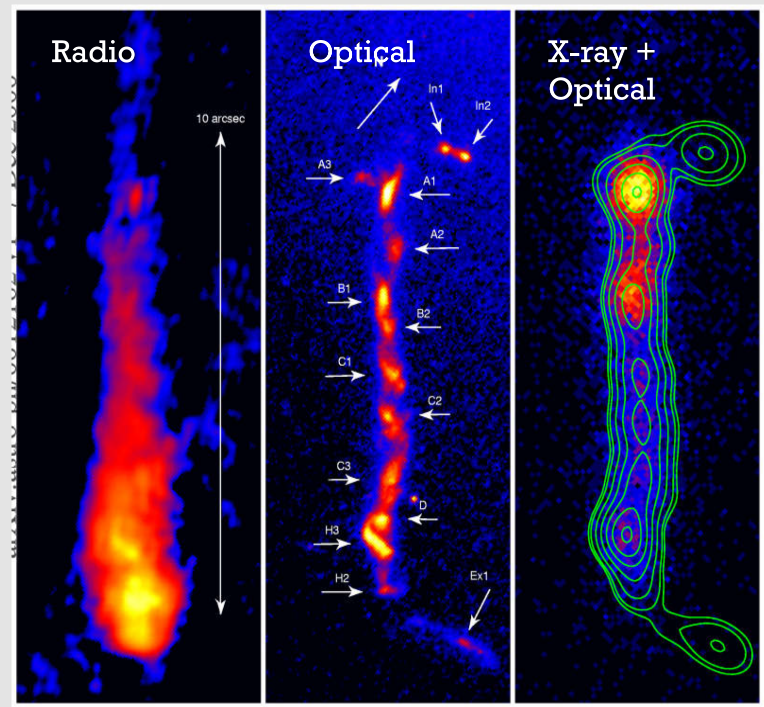

Marshall et al. (2001)

Multiwavelength Jet Emission

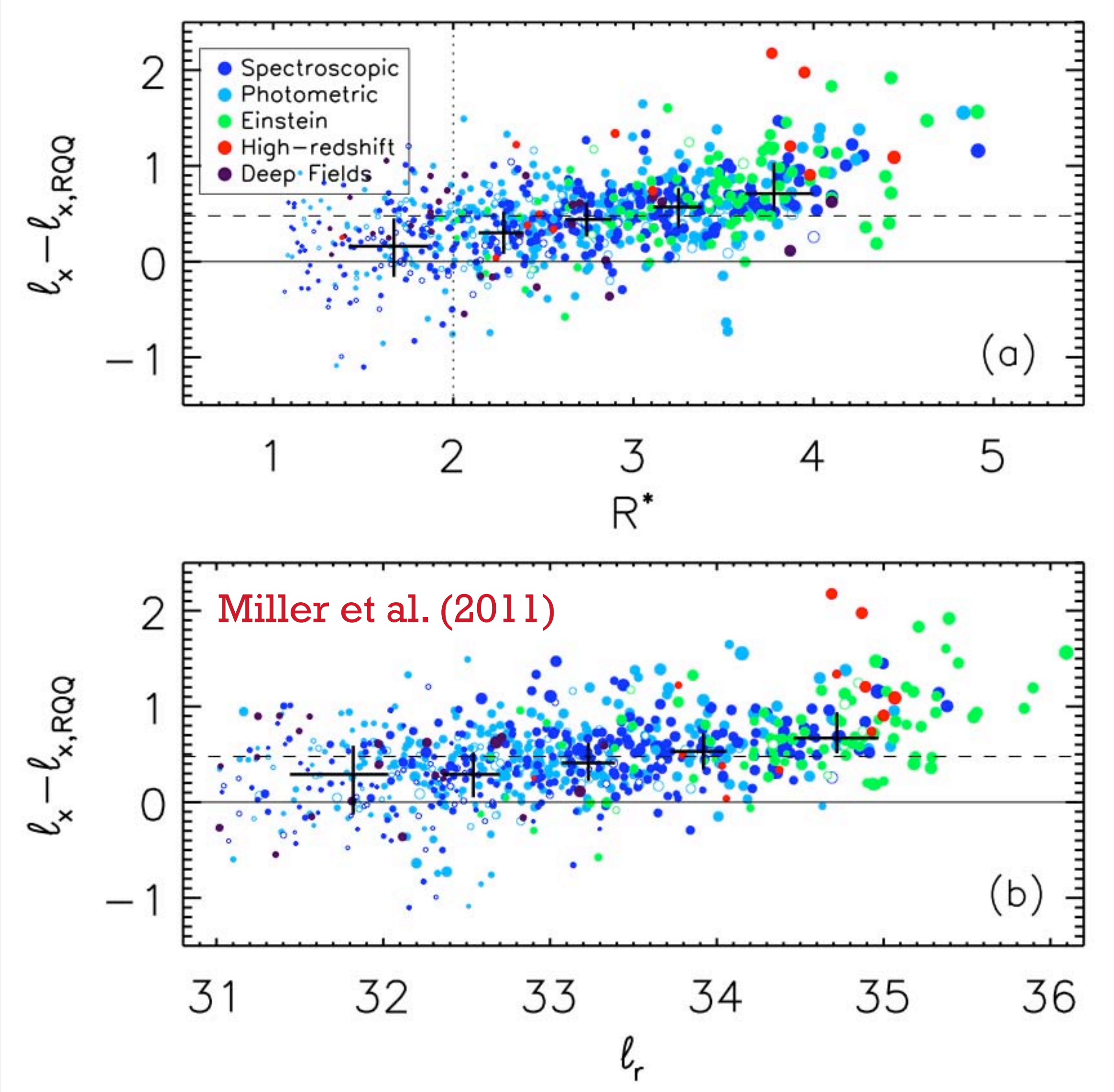

X-ray emission from radio-loud quasars increases as the radio volume control is dialed upward.

Radio-Loud Type Classification

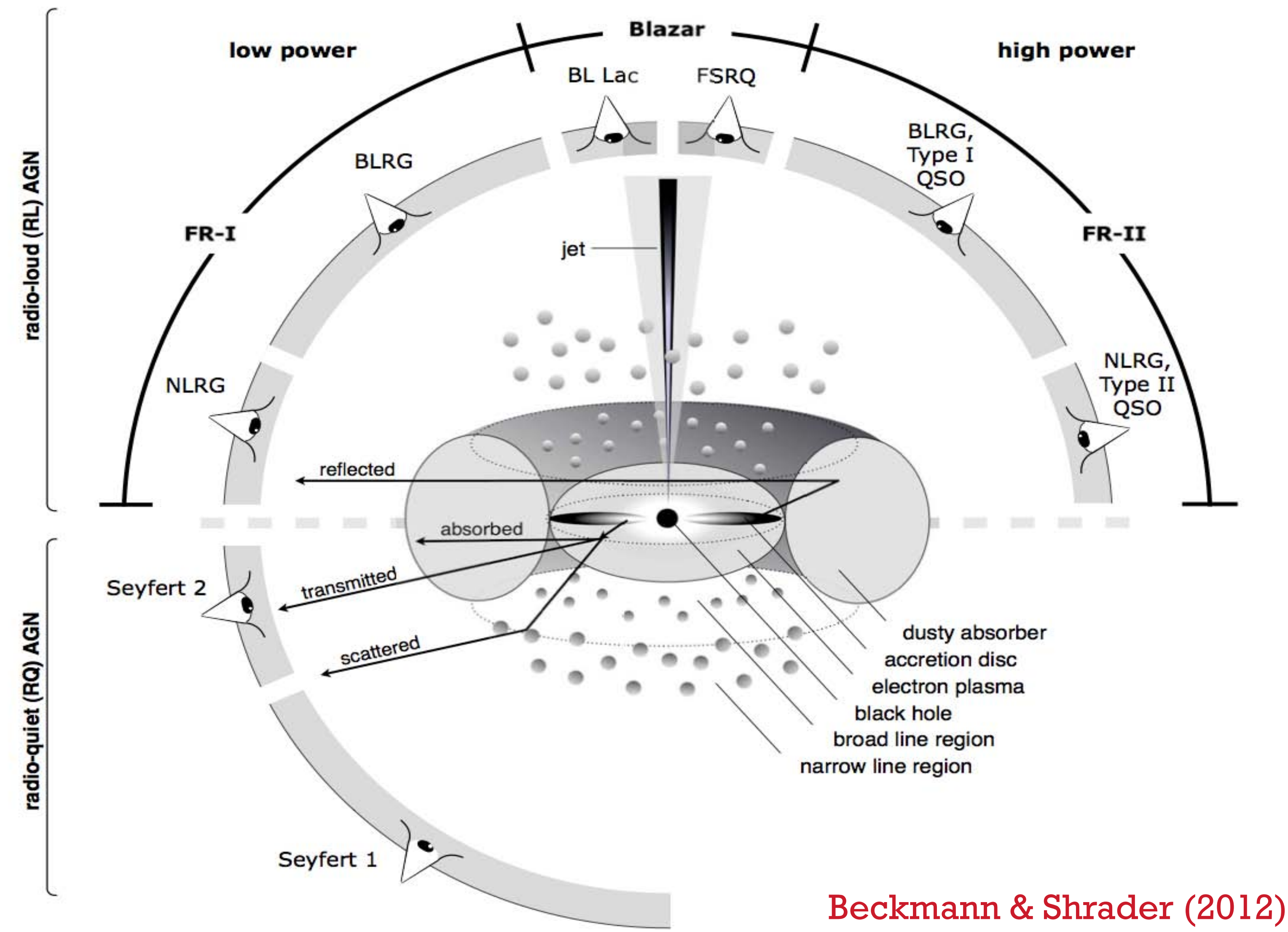

Beckmann & Shrader (2012)

Fanaroff-Riley Types

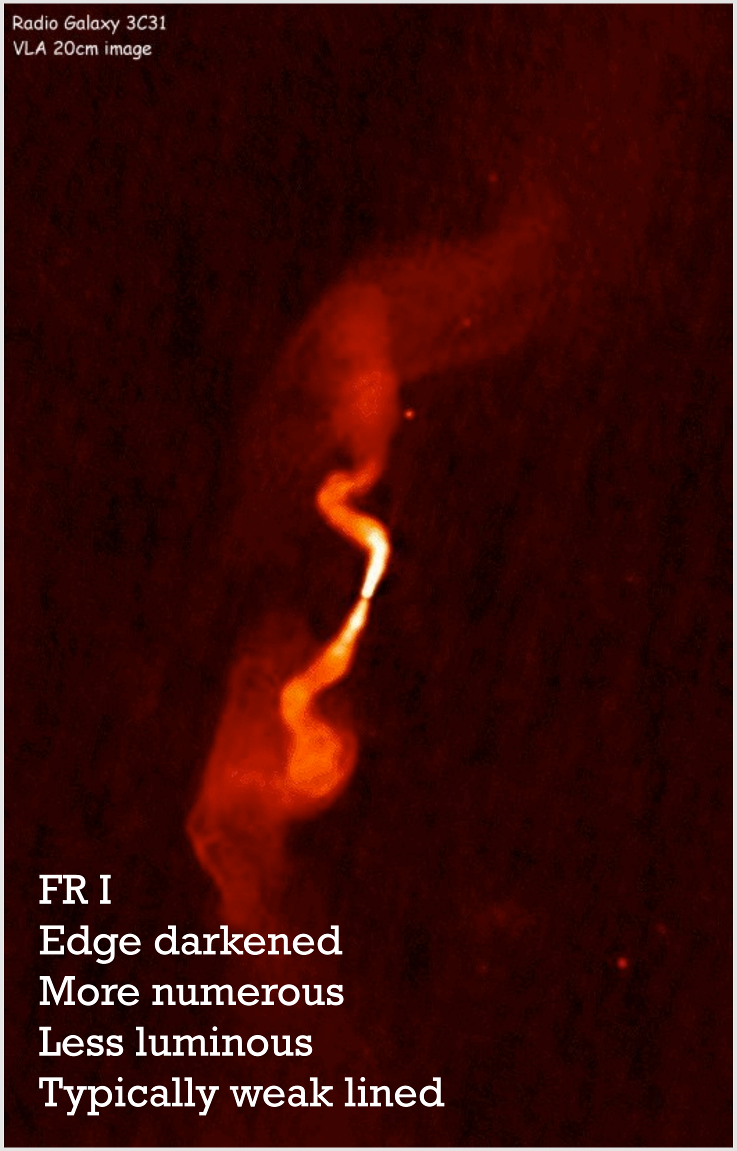

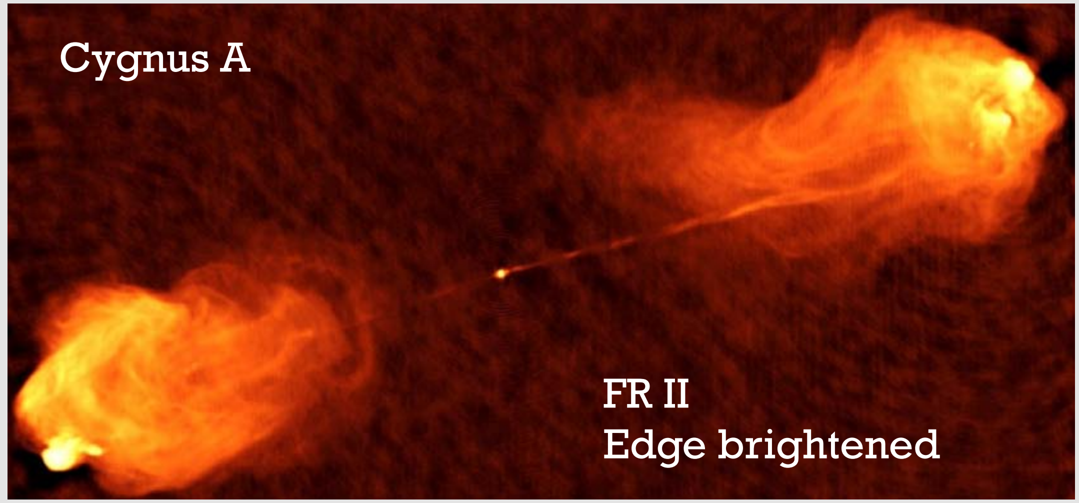

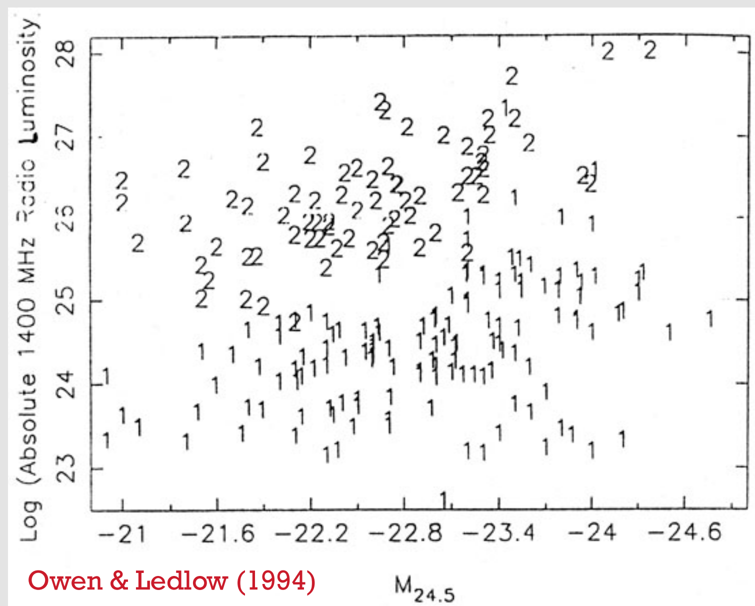

Cause of this dichotomy still debated.

Large-scale environment vs. small-scale launching.

Flat vs. Steep Spectrum Radio Sources

Often observe radio power-law spectra: $L_\nu \sim \nu^{-\alpha r}$

Radio-loud AGNs with dominant radio cores usually show "flat" radio spectra with $\alpha_r < 0.5$

Radio-loud AGNs with dominant lobes usually show "steep" radio spectra with $\alpha_r > 0.5$

Much of the difference in measured value of α_r is due to inclination of radio jet to our line-of-sight.

Broad-Band Blazar Emission

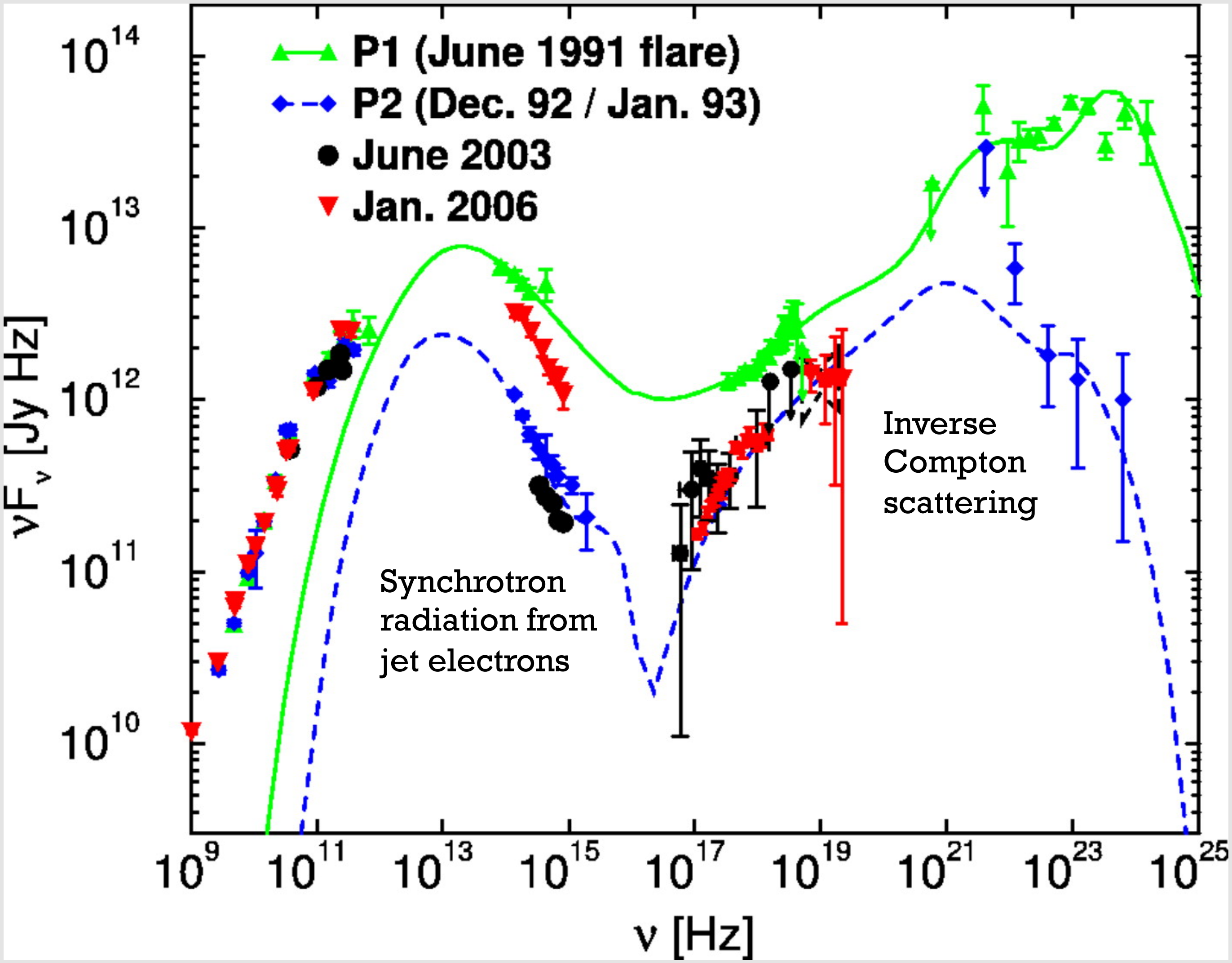

Bottcher et al. (2007)

Typical blazar properties:

Flat radio spectra

SEDs dominated by jet emission at many wavelengths

Intense and highly variable emission in γ-rays and radio

Polarization

Sometimes apparent superluminal motion

Sometimes weak emission lines

TeV Gamma-Rays from Blazars Detected with Cherenkov Light from Air Showers

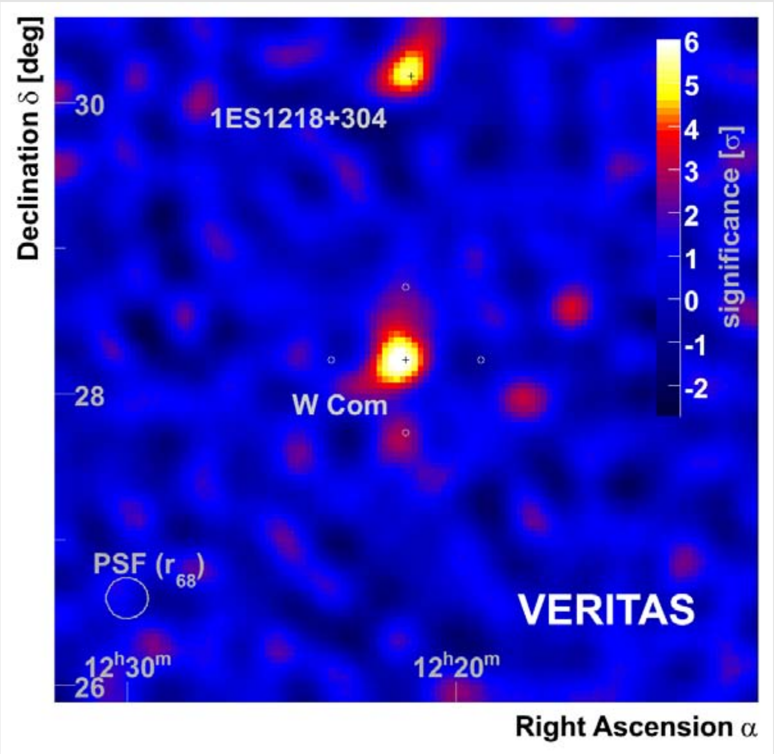

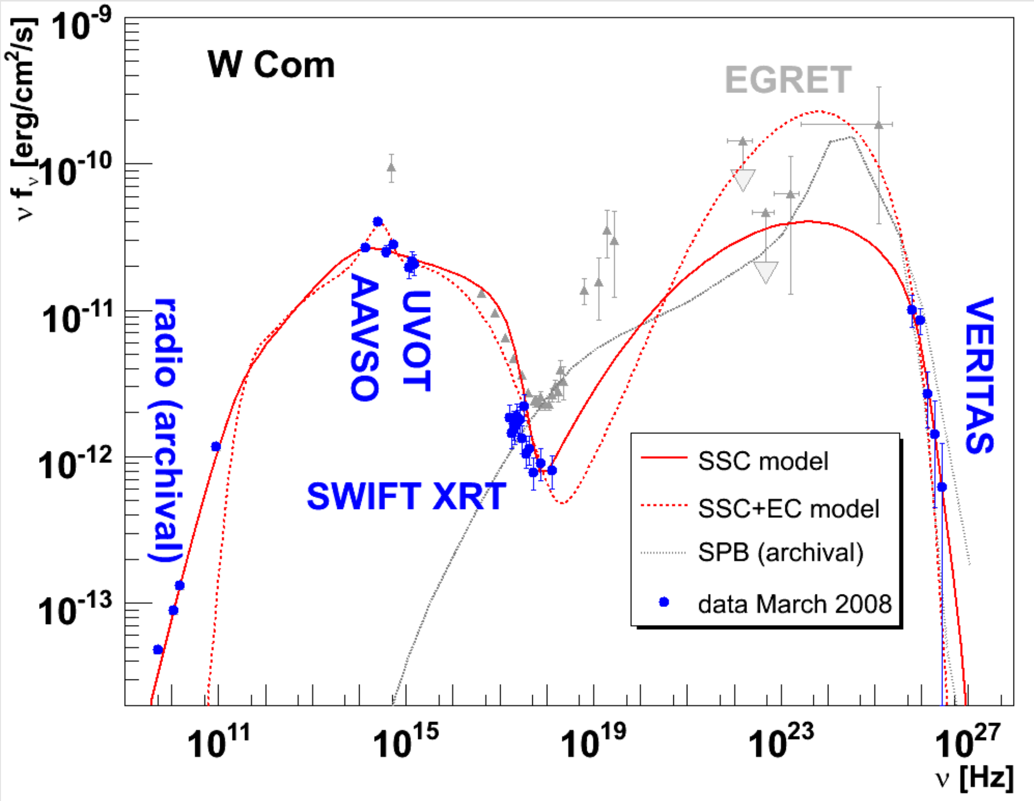

Cogan et al. (2009)

Mean Spectrum of BL Lacs

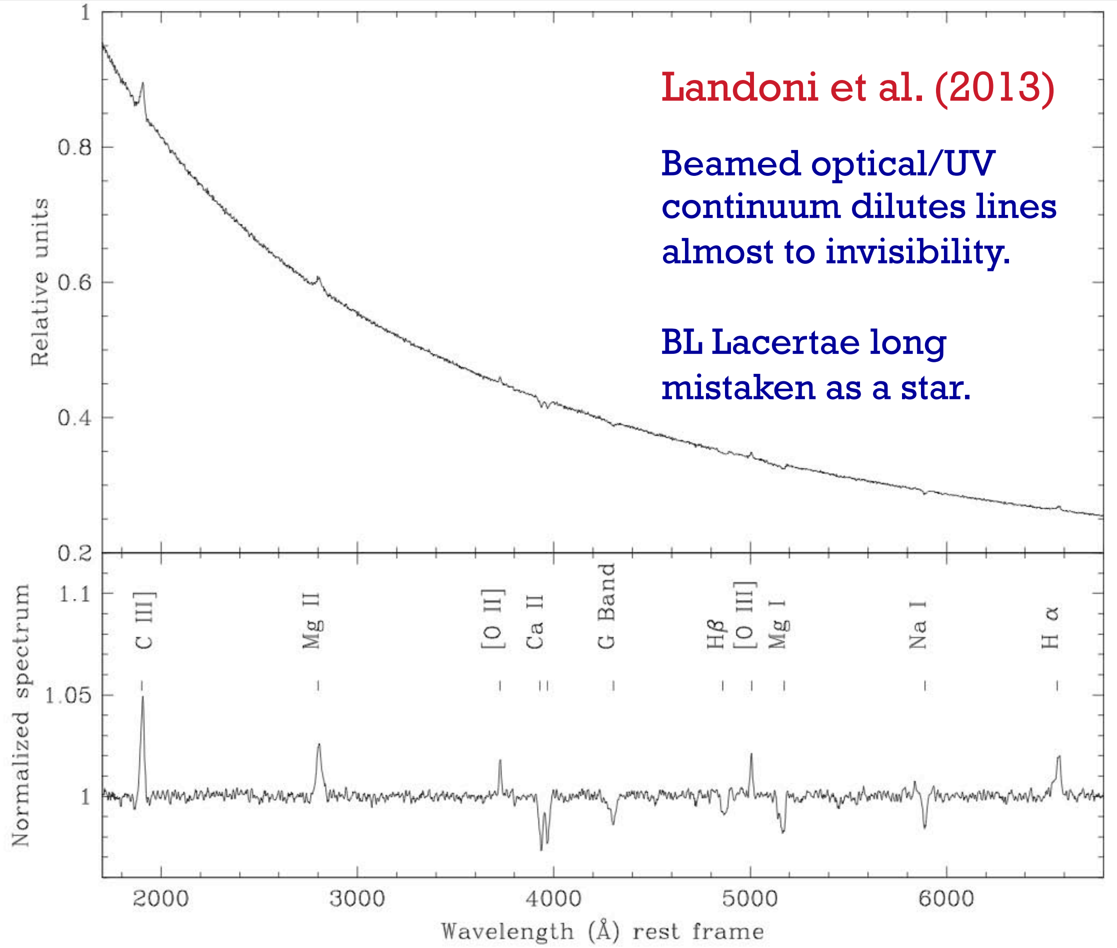

Fig. 3.— Mean spectrum of BL Lac objects obtained combining the 23 objects of our campaign in which intrinsic spectral features are detected. The first panel reports the mean spectrum assuming for the continuum a power-law with index $\alpha = 0.90$ (which corresponds to the mean spectral index of the whole BL Lac sample). In the second panel normalised spectrum is shown.

How Are Jets Made?

An accreting SMBH model has promising "ingredients" for making jets:

- Preferred axis that is stable
- Relativistically deep potential well
- Magnetic fields in orbiting plasma

Generally invoke MHD processes to divert some of the inflowing plasma outward and then keep it collimated.

How Are Jets Made?

But exactly how to combine the "ingredients" remains poorly understood.

See, e.g., Meier (2013) for a review.

What sets if a strong jet will be launched

- SMBH spin?
- Magnetic geometry?
- Environment?

Simulations of Jet Formation

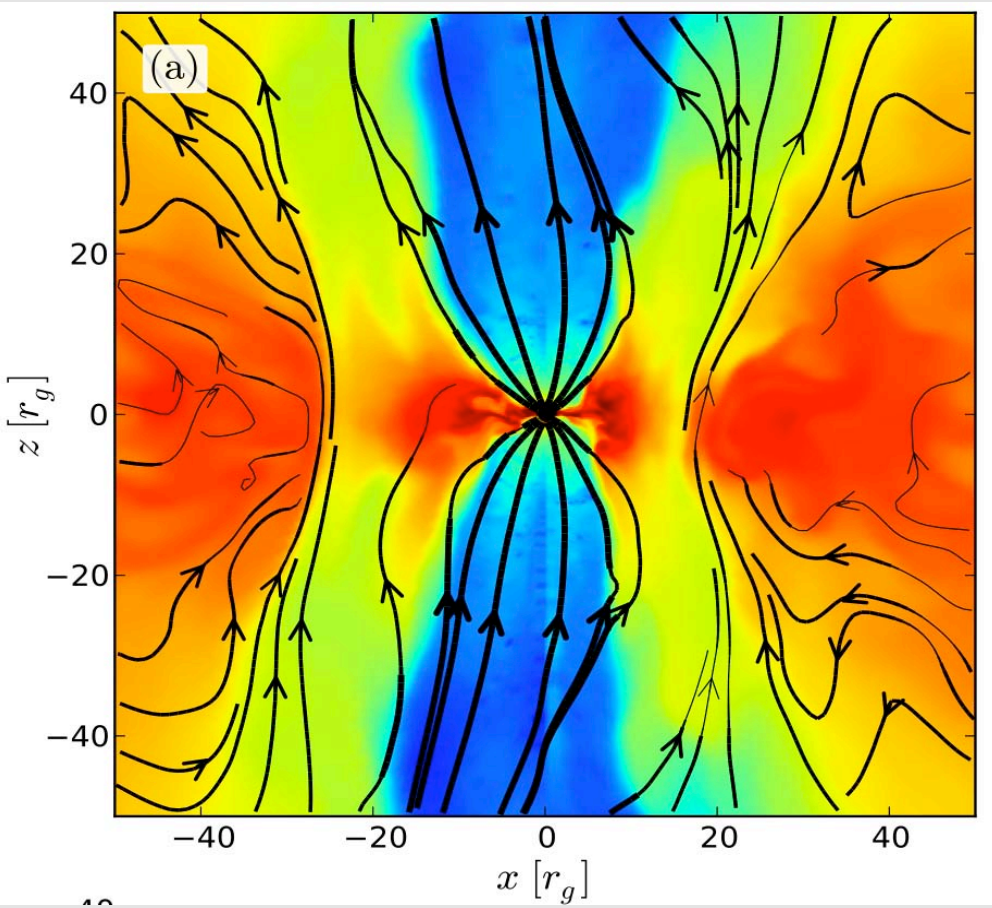

Color shows density, and black lines are magnetic-field lines.

Tchekhovskoy et al. (2012)

Simulations of accretion flows now allow the jet power to be determined as a function of SMBH spin in some regimes.

At high spins, differences found from the classical BZ formula:

$$P_{\rm BZ} = \frac{\kappa}{4\pi c} \Phi_{\rm BH}^2 \frac{a^2}{16 r_g^2}$$

Much work on jet formation remains, especially in the regime of high accretion rate.

Jet Feedback in Clusters

Jets can do substantial work against the hot gas in galaxy clusters

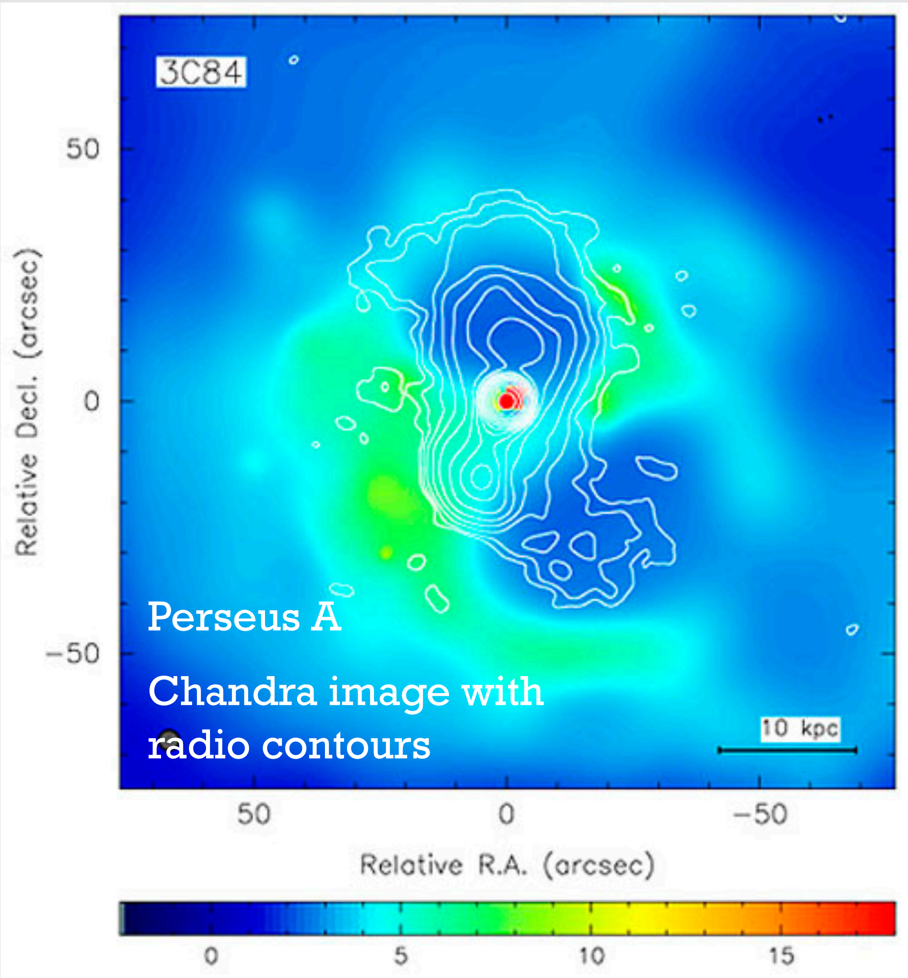

Fabian et al. (2003)

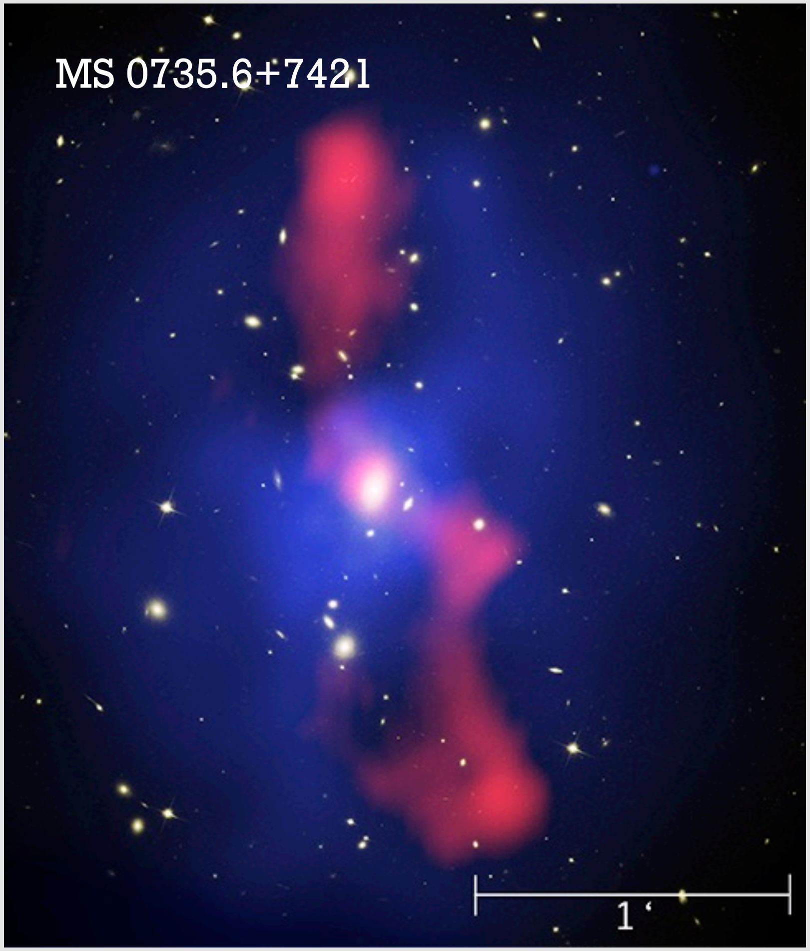

McNamara et al. (2005)

The End

An Observational Overview of Active Galactic Nuclei

Niel Brandt (Penn State University)

Summary of Lectures

Introduction, AGN Basics, Finding AGNs, and Terminology

Observations on Small Scales: Black Hole Region, Broad Line Region, Outflowing Winds

Observations on Large Scales: Narrow Line Region, Torus, Jets

Summary of Lectures

Focused Lecture – AGN Demography, Physics, and Ecology from X-ray Surveys

AGN Demography, Physics, and Ecology from X-ray Surveys

Now more than 600 substantial papers from ~ 25 ongoing surveys!

Will describe some highlights, but cannot be complete.

Outline

Utility of X-ray AGN Surveys

Current X-ray Surveys and Follow-Up Work

Selected AGN Science Results

Some Future Prospects

Utility of X-ray AGN Surveys

(Three Reasons)

(1): X-ray Emission is Nearly Universal from Luminous AGNs

X-ray Luminosities of Optically Selected AGNs

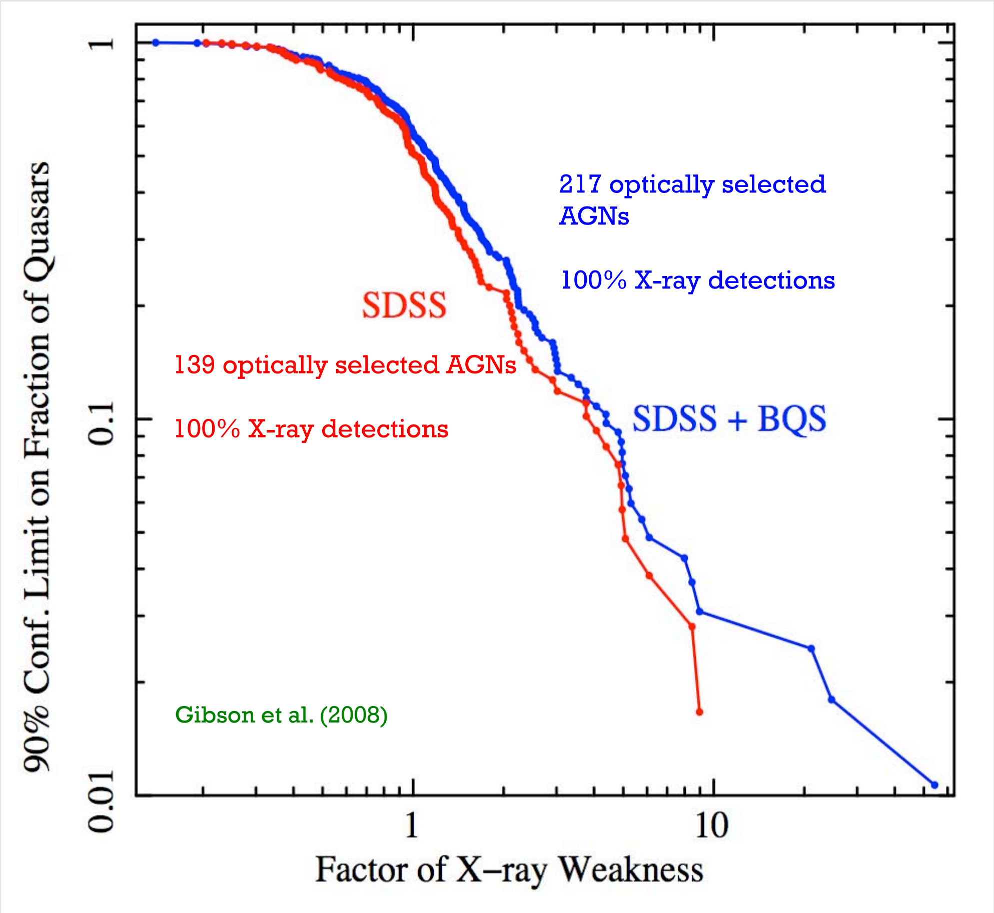

Optically, infrared, and radio-selected AGNs almost always show strong X-ray emission.

Accretion-disk corona is empirically *robust*, even if poorly understood.

(2): X-ray Emission is Penetrating with Reduced Absorption Bias

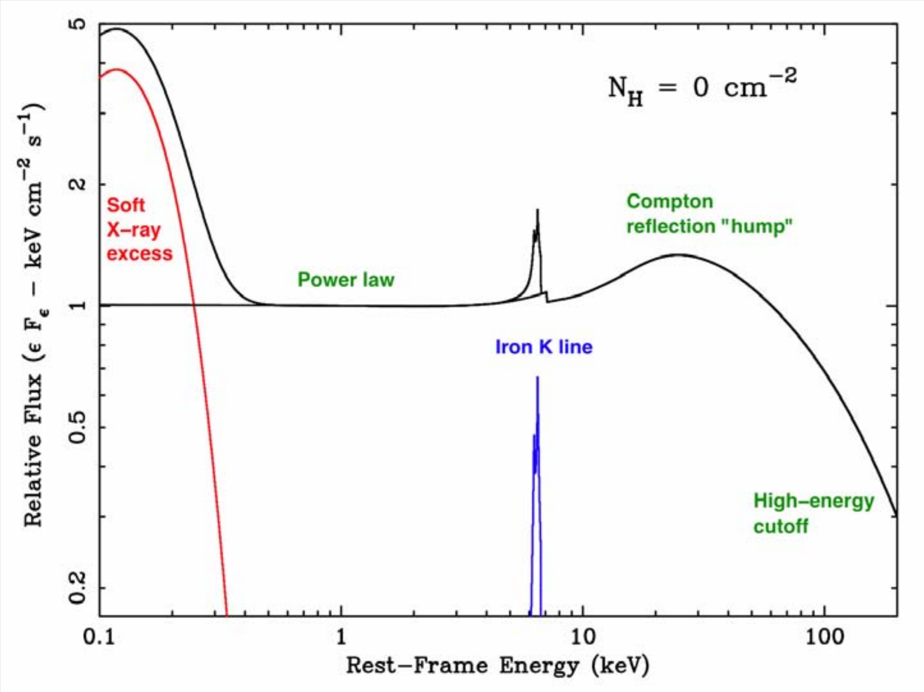

X-ray emission can penetrate and measure large column densities.
Hand ($10^{23}\ cm^{-2}$), chest ($10^{24}\ cm^{-2}$).

Absorption bias drops going to high redshift.

Hard X-ray Imaging with NuSTAR

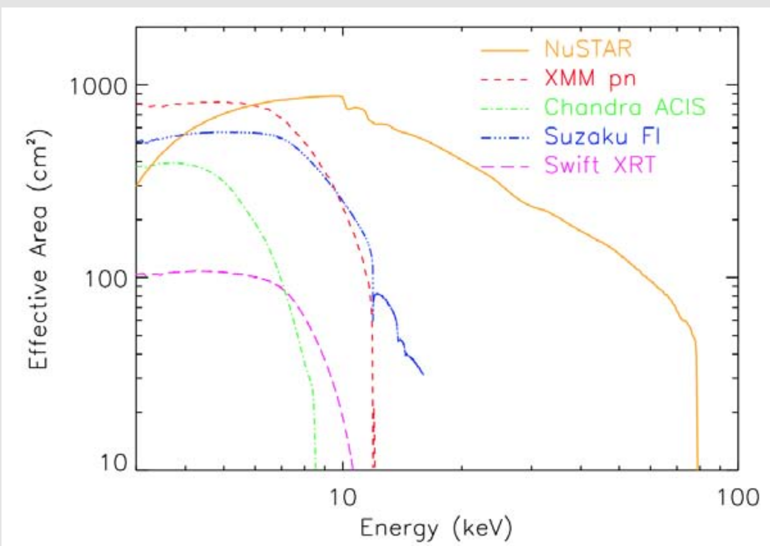

KEY OBSERVATORY PERFORMANCE PARAMETERS.

Parameter	Value
Energy range	3 – 78.4 keV
Angular resolution (HPD)	58″
Angular resolution (FWHM)	18″
FoV (50% resp.) at 10 keV	10′
FoV (50% resp.) at 68 keV	6′
Sensitivity (6 – 10 keV) [10^6 s, 3σ, $\Delta E/E = 0.5$]	2×10^{-15} erg cm^{-2} s^{-1}
Sensitivity (10 – 30 keV) [10^6 s, 3σ, $\Delta E/E = 0.5$]	1×10^{-14} erg cm^{-2} s^{-1}
Background in HPD (10 – 30 keV)	1.1×10^{-3} cts s^{-1}
Background in HPD (30 – 60 keV)	8.4×10^{-4} cts s^{-1}
Spectral resolution (FWHM)	400 eV at 10 keV, 900 eV at 68 keV
Strong source ($> 10\sigma$) positioning	1.5″(1σ)
Temporal resolution	2 μs
Target of opportunity response	$<$ 24 hr
Slew rate	0.06° s^{-1}
Settling time	200 s (typ)

(3): X-rays Have Low Dilution by Host-Galaxy Starlight

Optical vs. X-ray Emission from a Local AGN (NGC 3783)

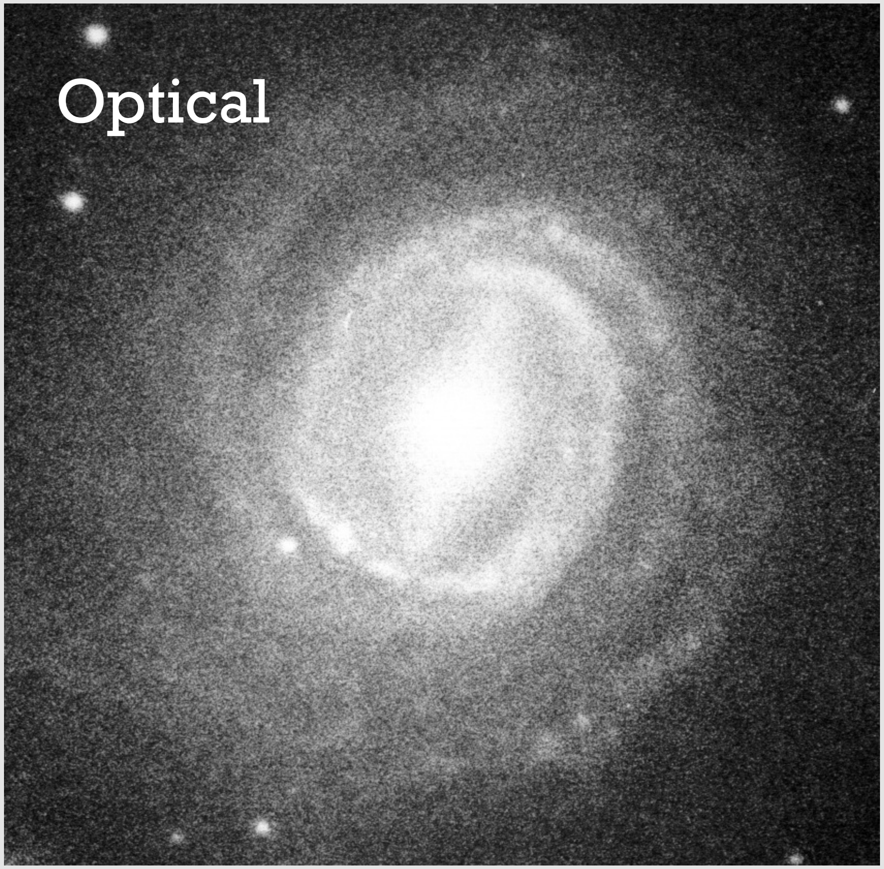

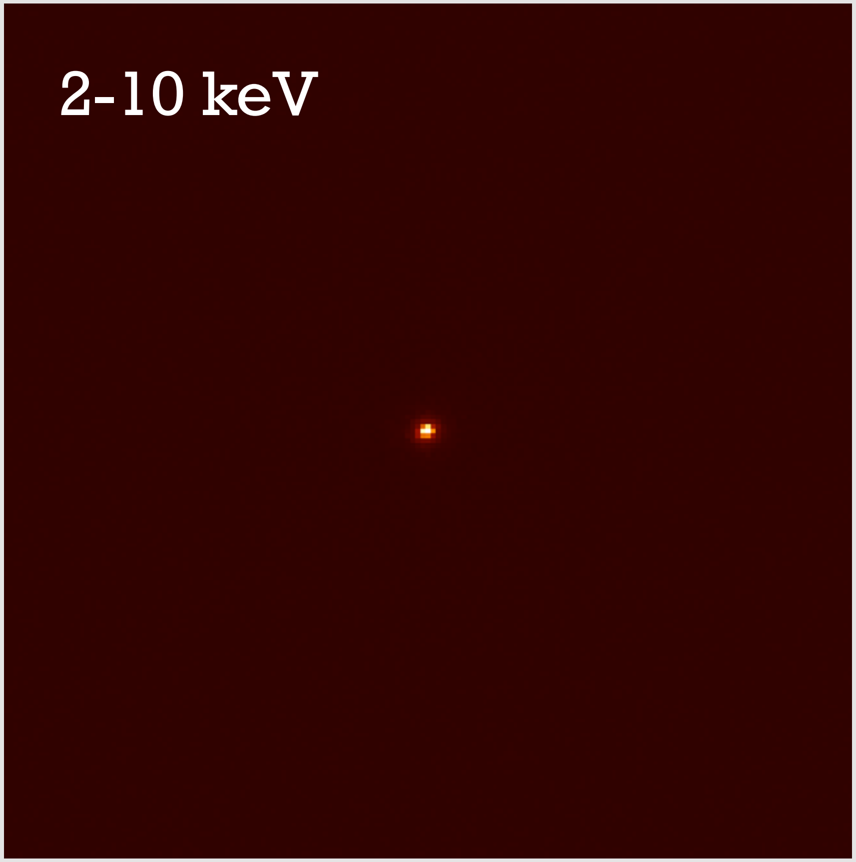

(3): X-rays Have Low Dilution by Host-Galaxy Starlight

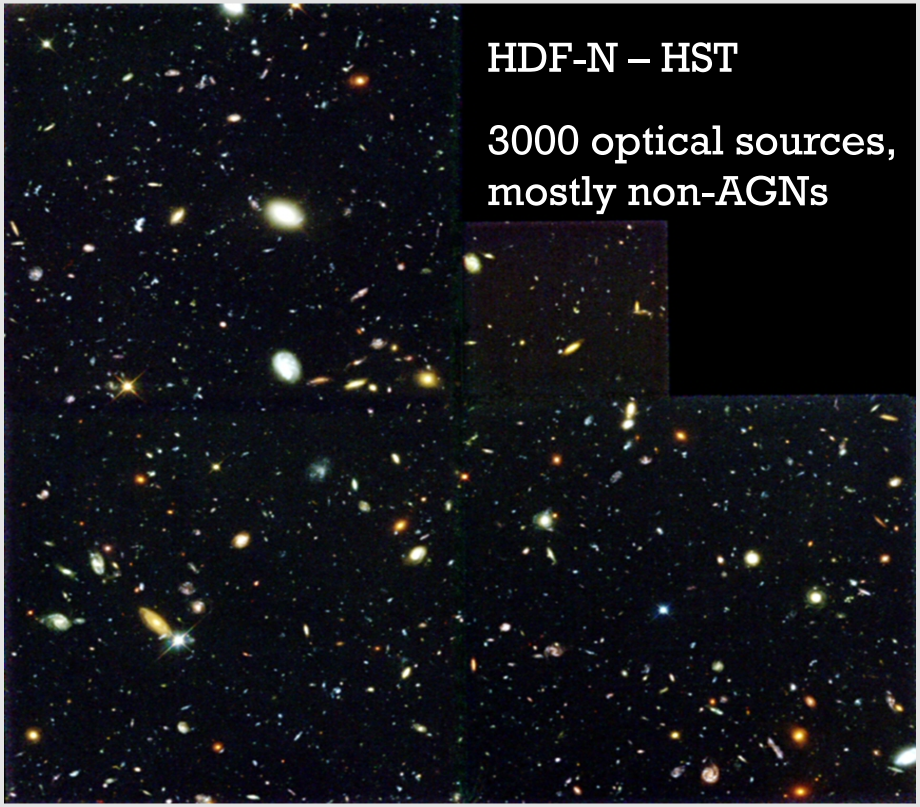

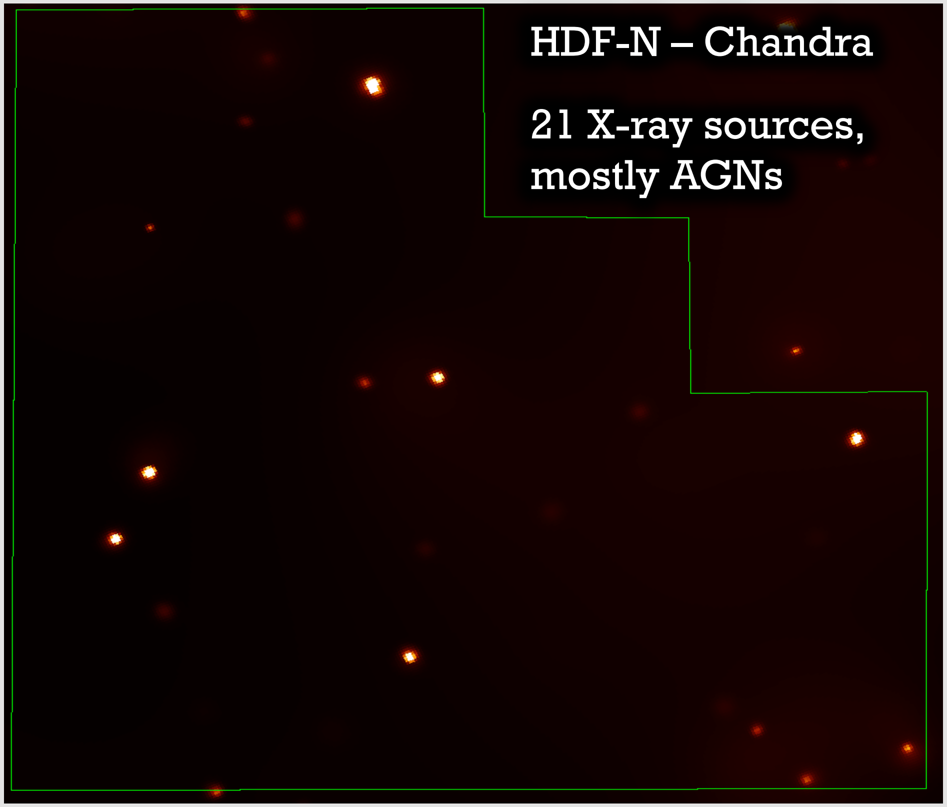

At high redshift cannot spatially resolve AGN light from host-galaxy starlight.

X-rays maximize contrast for "cleanest" samples.

Best of all is X-ray + multiwavelength surveys.

Current X-ray Surveys and Their Multiwavelength Follow-Up

Capabilities of Chandra and XMM-Newton for Surveys

Good-to-great angular resolution (0.8-15'') – Broad bandpass – Respectable FOVs

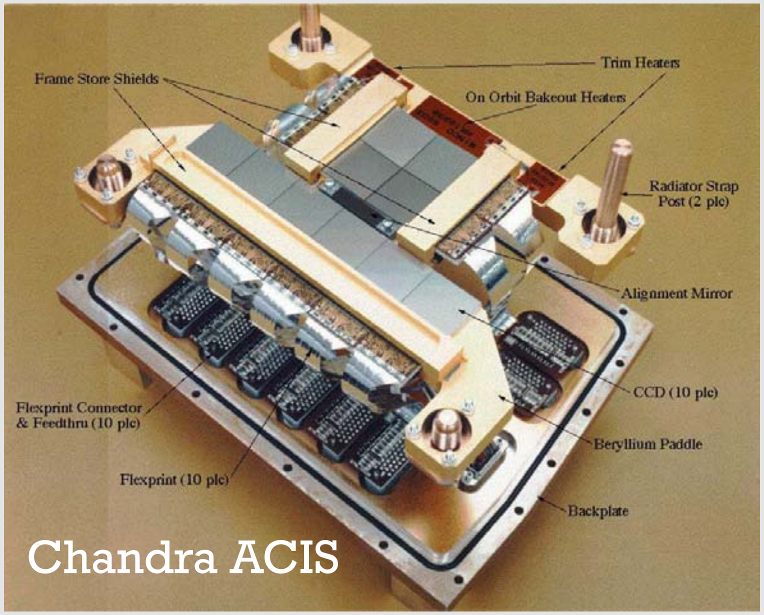

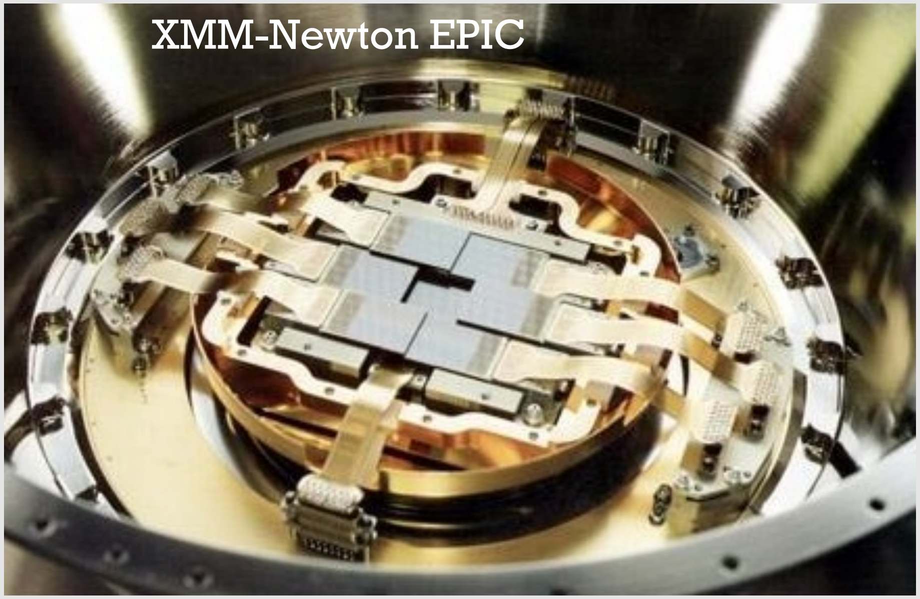

Great sensitivity – Up to 80-400 times that of previous missions.

Good-to-great positions – 0.2-2.5 arcsec. *Essential* for reliable follow-up work at faint fluxes.

Large samples – Hundreds-to-thousands of sources for powerful statistical studies.

Good archiving practices – Allows effective survey federation by anyone.

Multitude of X-ray AGN Surveys

Some Recent Contiguous Deep X-ray Surveys

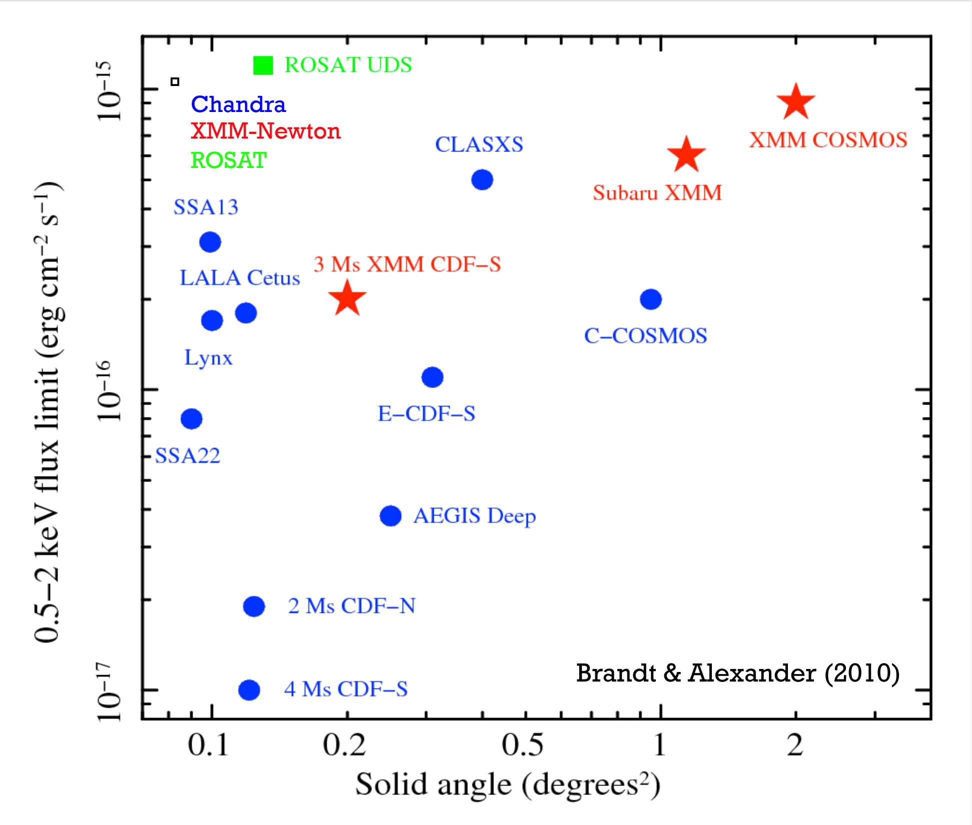

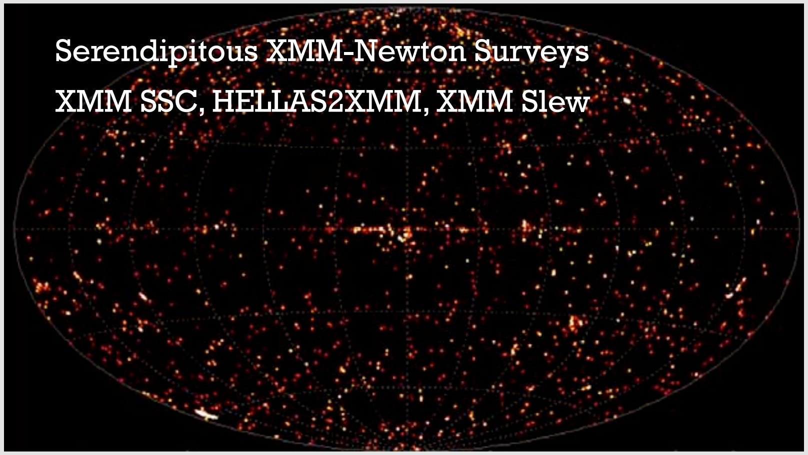

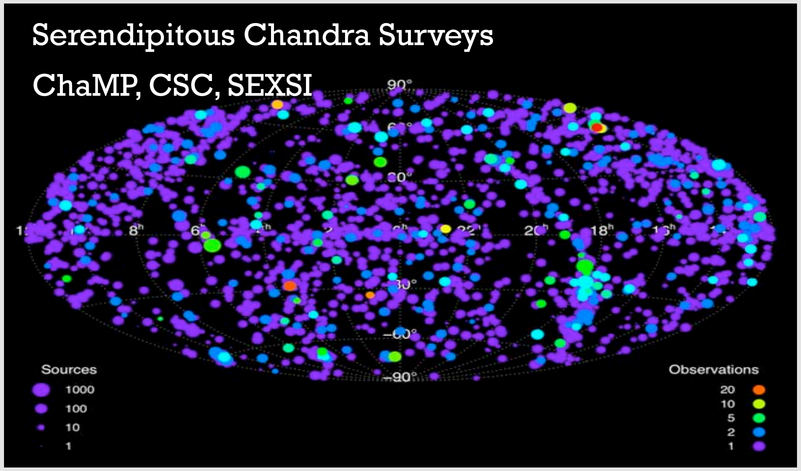

~ 25 ongoing Chandra and XMM-Newton surveys cover most of the practically accessible sensitivity vs. solid-angle "discovery space."

Together are providing a complete understanding of X-ray source populations.

The Chandra Deep Fields

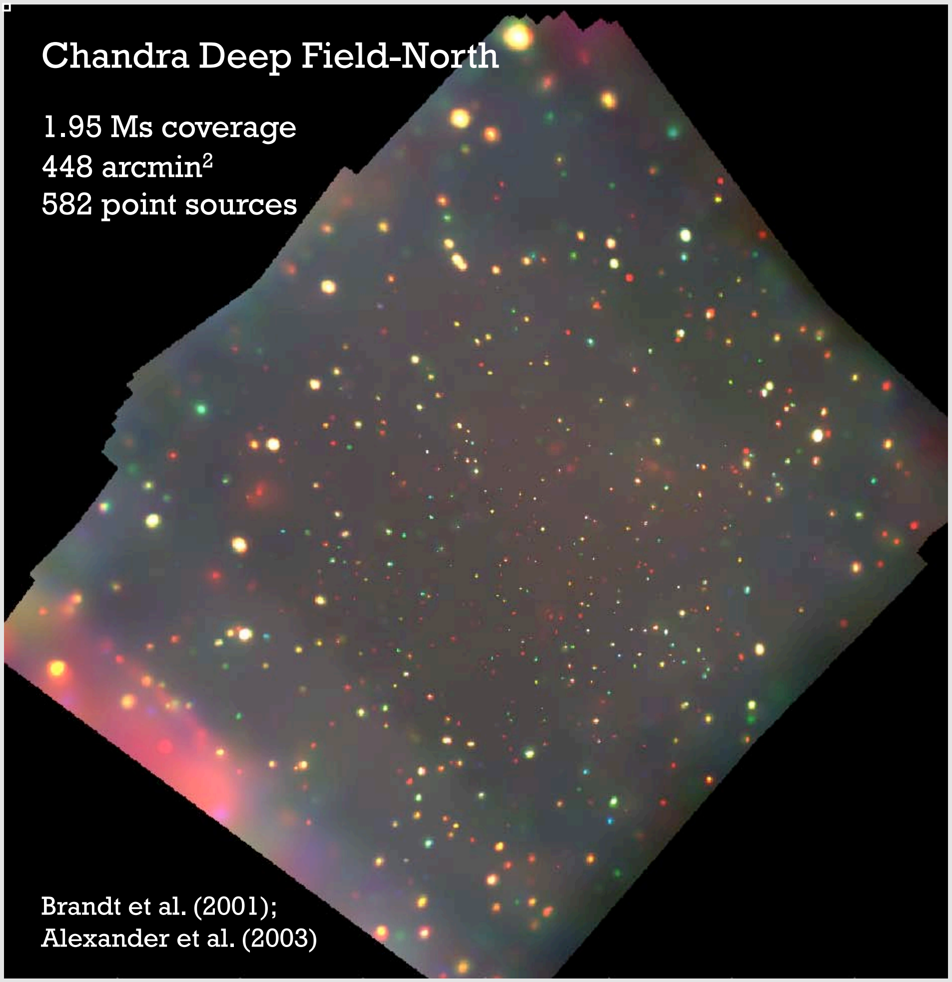

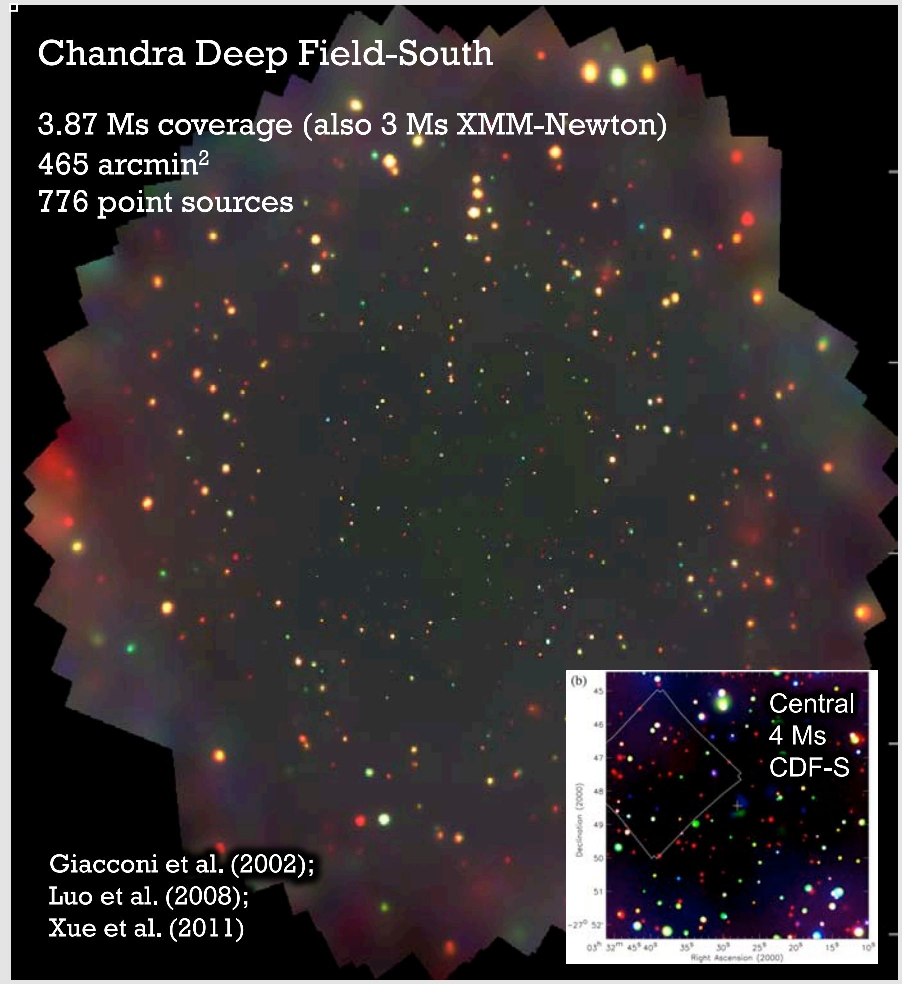

Faintest sources have 1 count per ~ 7 days!

The 3 Ms XMM-Newton CDF-S

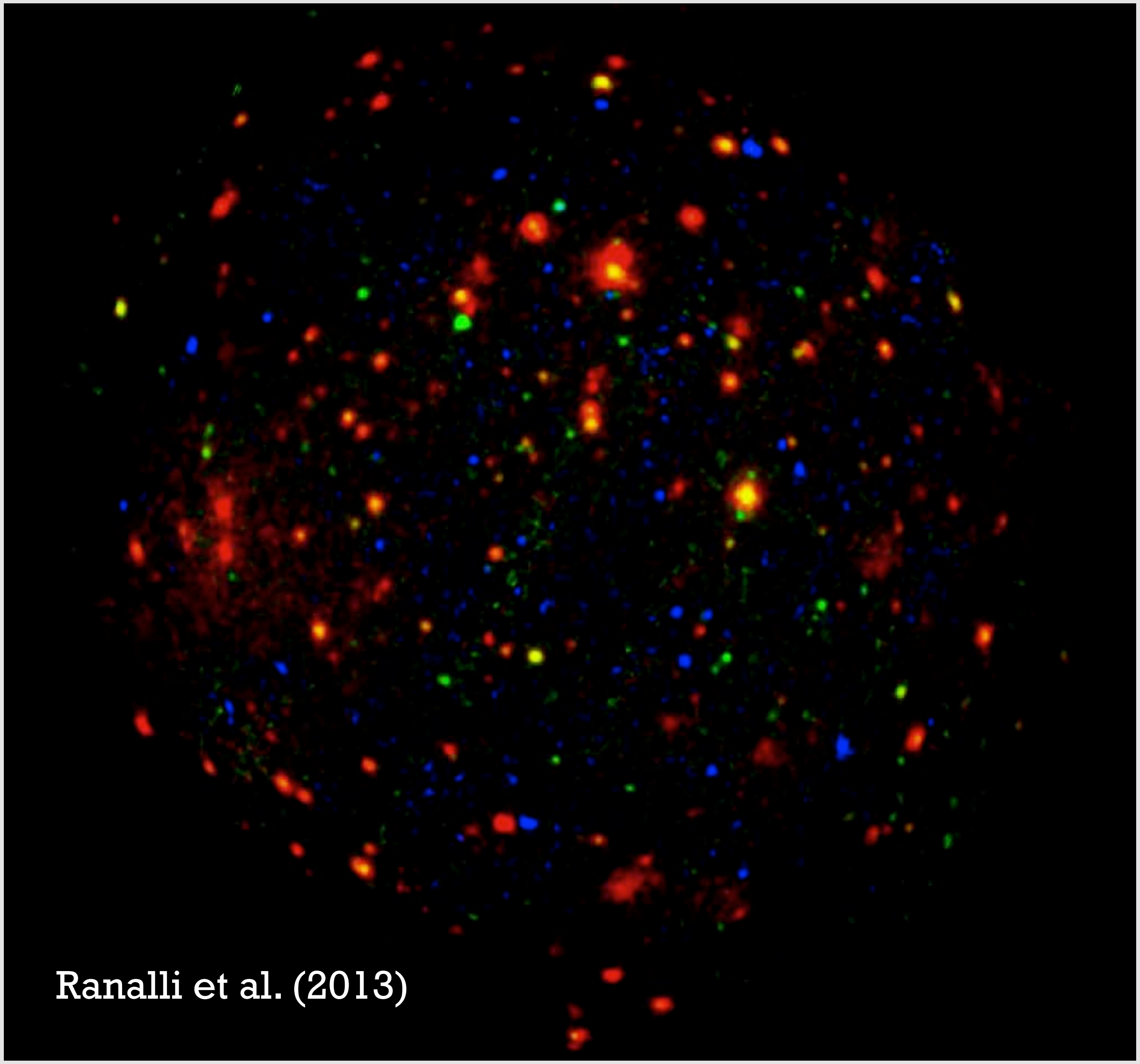

Chandra and XMM-Newton data are complementary

XMM-Newton provides spectroscopy & variability for bright sources, as well as somewhat higher energy coverage.

Confusion and background affects XMM-Newton at fainter fluxes.

The XMM-Newton COSMOS Field

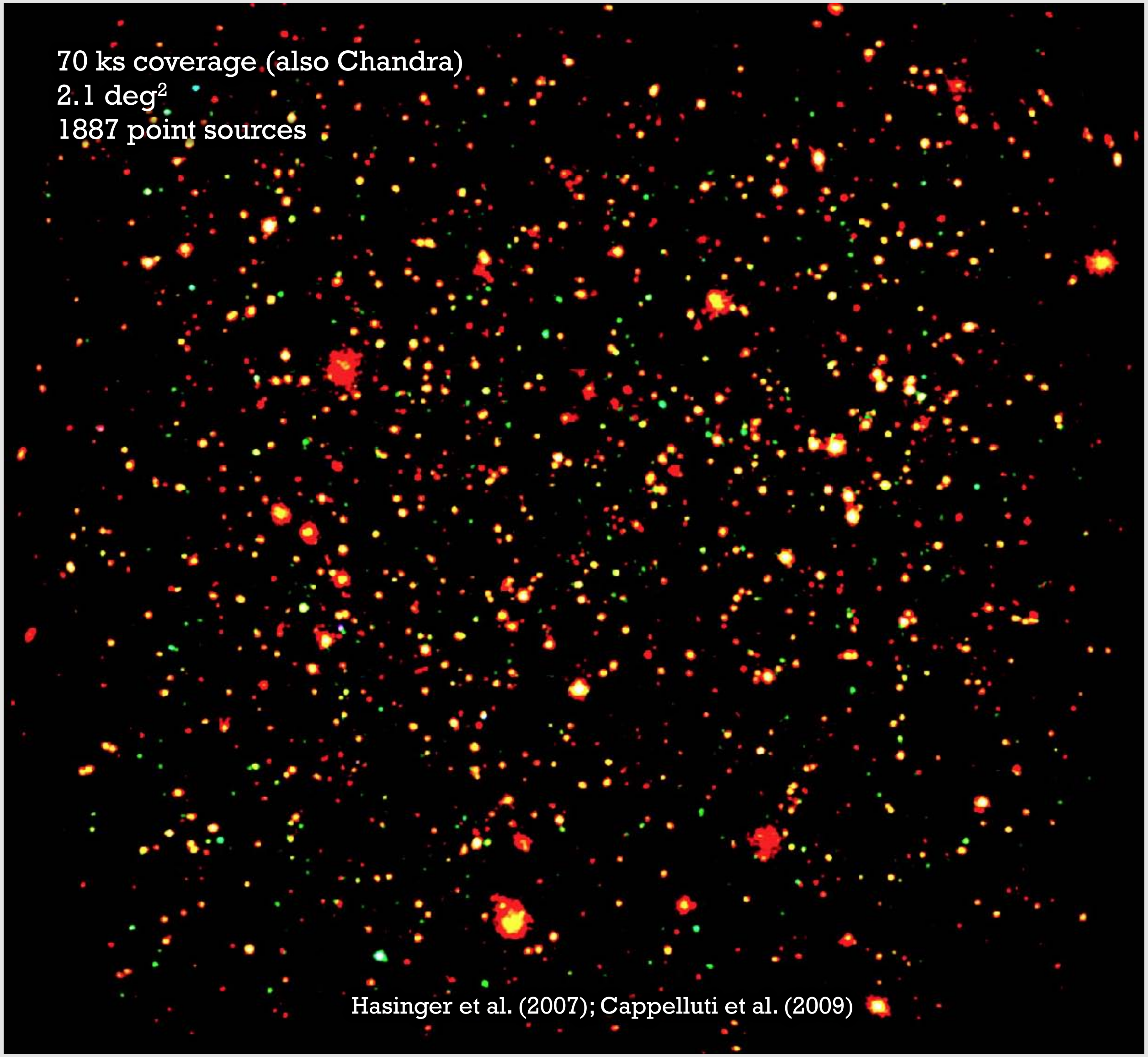

Ultradeep Multiwavelength Coverage (CDF-S)

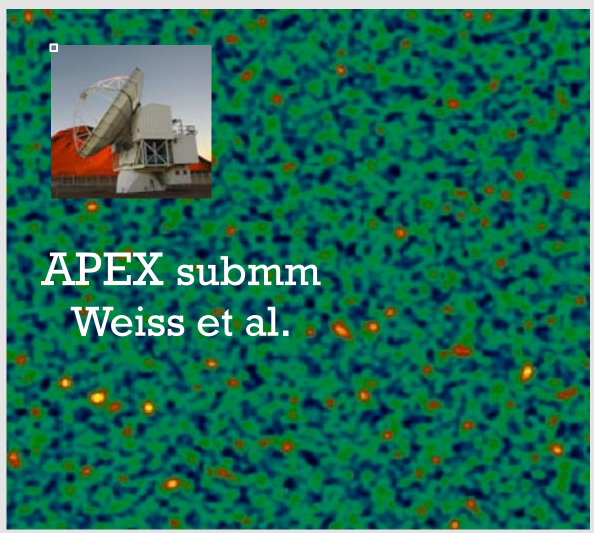

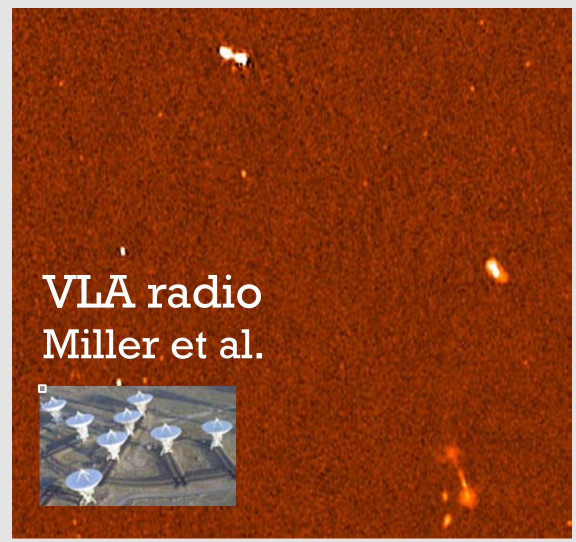

Extraordinary multiwavelength supporting data continue to grow - NuSTAR, ALMA, EVLA, JWST, LSST, ELTs.

Roles of the Multiwavelength Data

Example IR-to-UV SED with Fitted Template

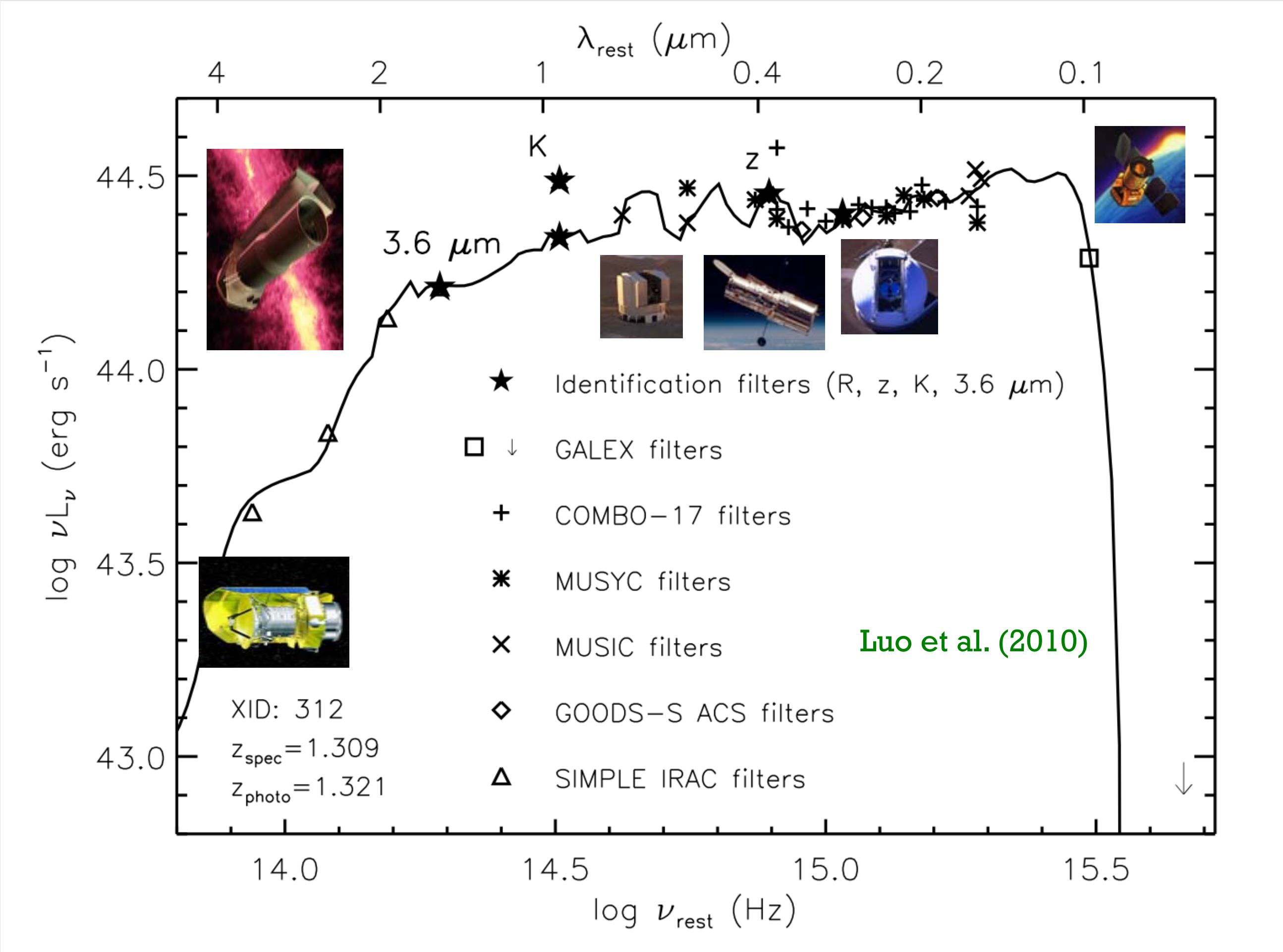

Source identification

Photometric redshifts (often 15-40 bands)

AGN accretion physics

Host-galaxy properties

X-ray missed AGNs

X-ray Source Spectroscopic IDs

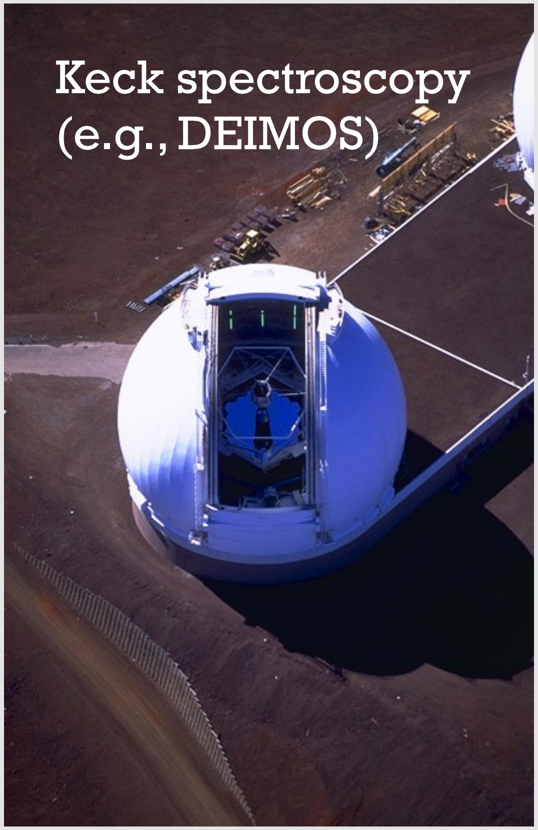

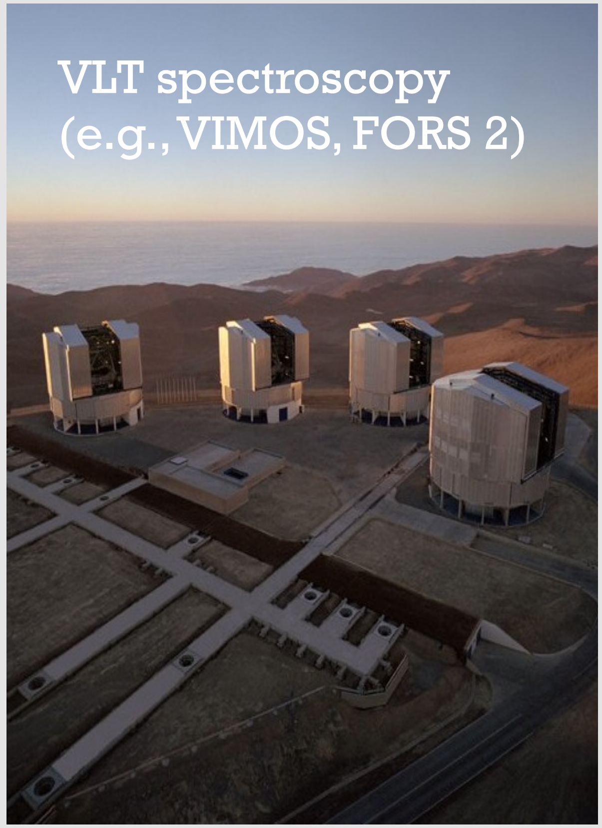

Enormous progress over the past decade using multi-object spectrographs, but remains a persistent challenge and bottleneck (especially at $R \sim$ 24-28).

Driver for future large spectroscopic facilities (e.g., ELTs).

Good photometric redshifts often derived to $R \sim 27$.

Selection of AGNs from the X-ray Source Population

X-ray Luminosity Distribution for CDF-S Sources

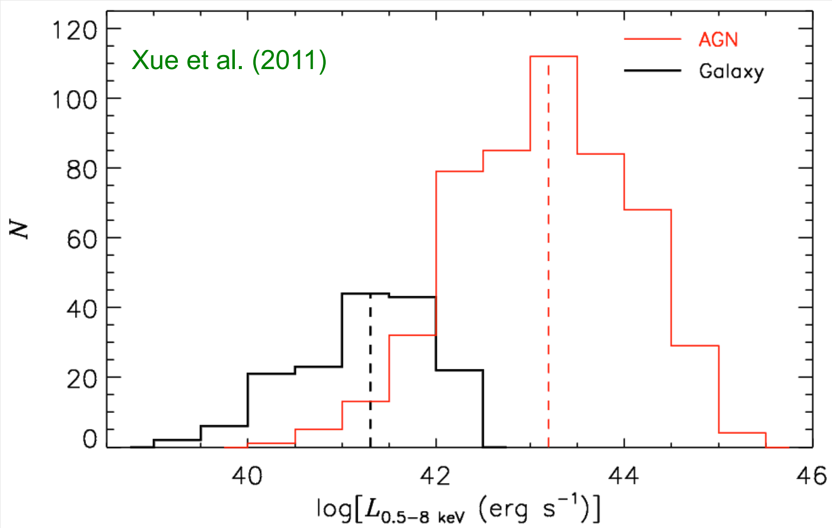

Select AGNs using

- X-ray luminosity
- X-ray-to-optical flux ratio
- X-ray spectral shape
- X-ray variability
- Follow-up spectroscopy
- SED fitting

Multiple independent cross-checks provide "purest" possible AGN selection.

Typically 75-90% of the X-ray sources are AGNs.

Other X-ray point source populations are starburst galaxies, normal galaxies, and stars.

Active Galactic Nucleus Selection

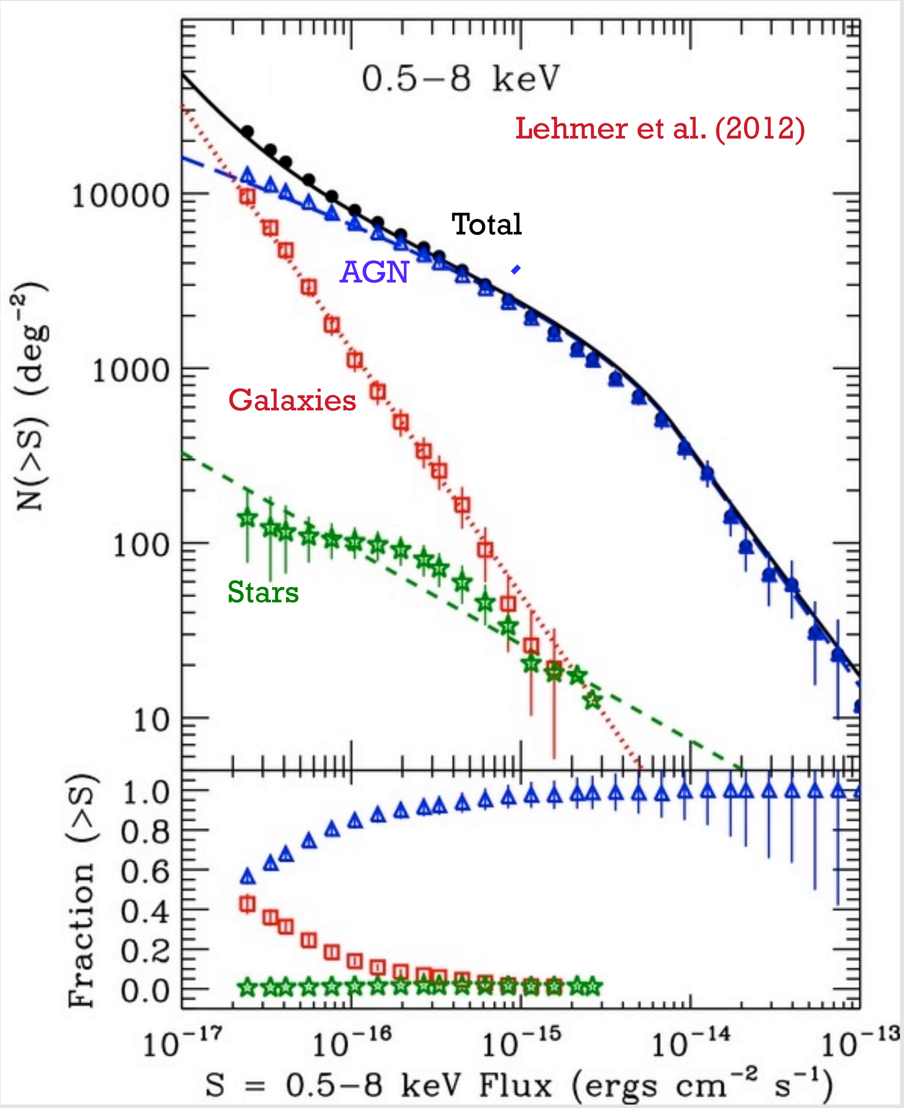

AGN number counts now reach about 15000 deg^{-2} in Chandra Deep Fields.

600 million across sky.

About an order of magnitude higher than deepest optical AGN surveys.

X-ray AGN selection compares *very* well with selection at other wavelengths, particularly considering purity.

But it's not perfect - highly obscured AGNs.

Cosmologically Distant Galaxies

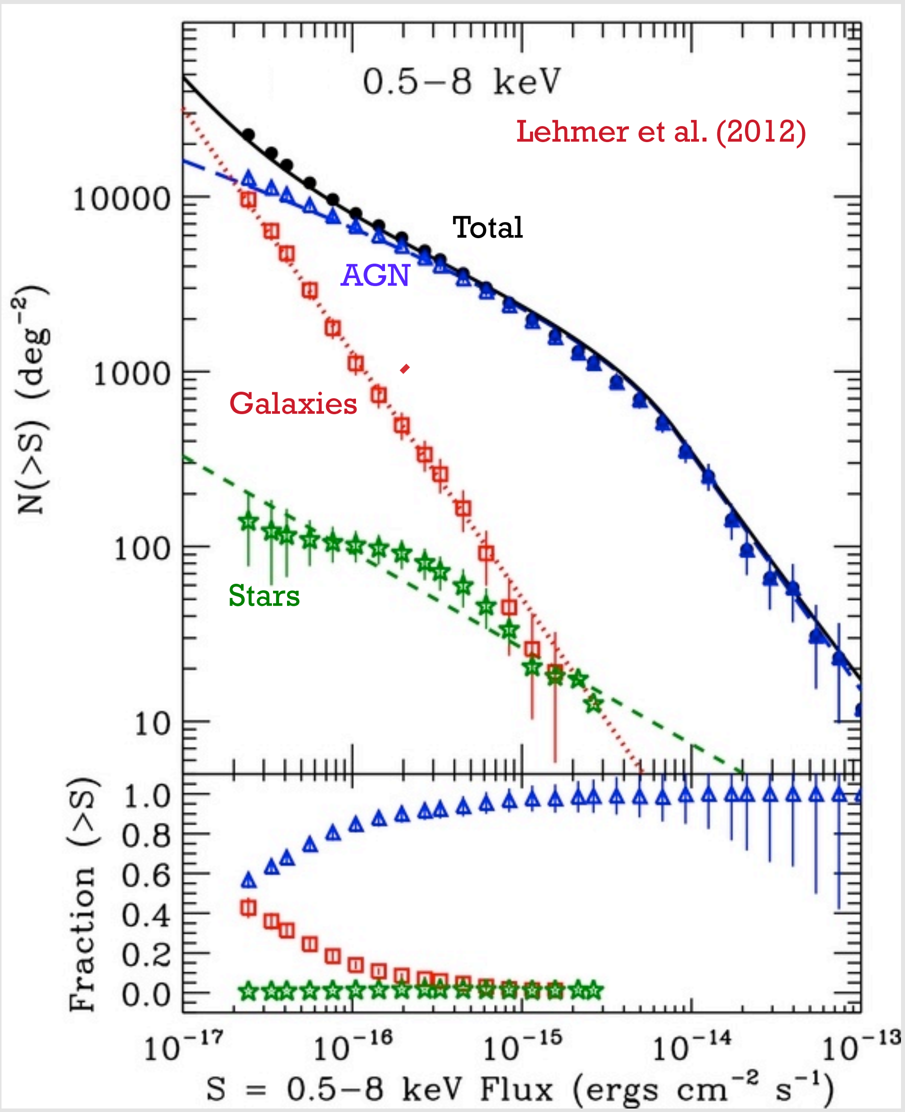

At the faintest fluxes, galaxies make a comparable contribution to the number counts (mainly X-ray binaries).

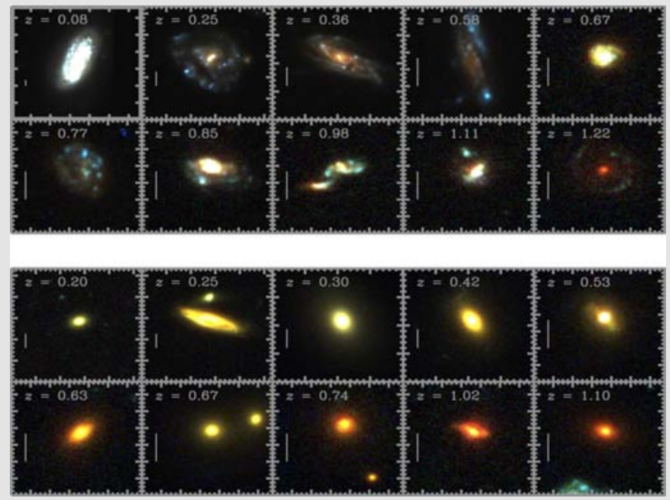

Late-Type Galaxies (often starburst)

Early-Type Galaxies

And their number counts continue to rise rapidly.

We are presently just seeing the "tip of the iceberg".

Selected AGN Science Results

Demography

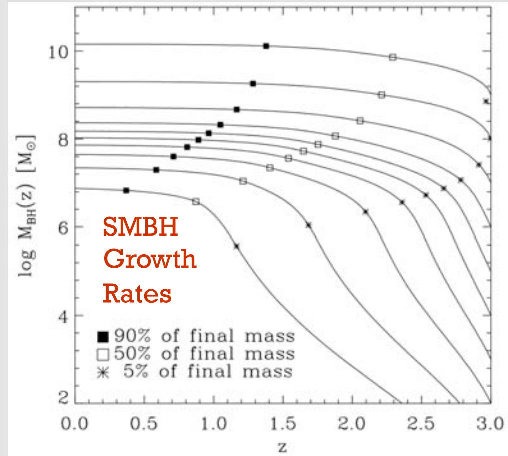

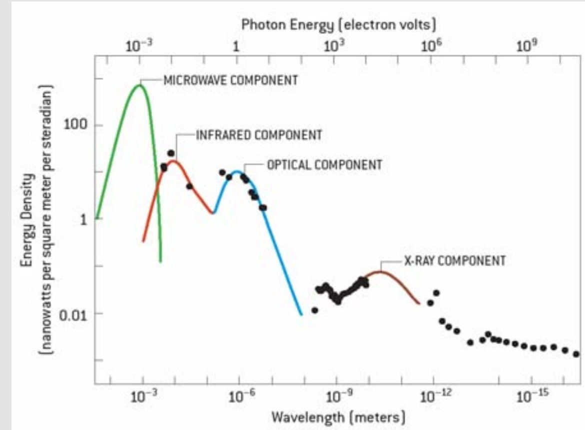

Physics

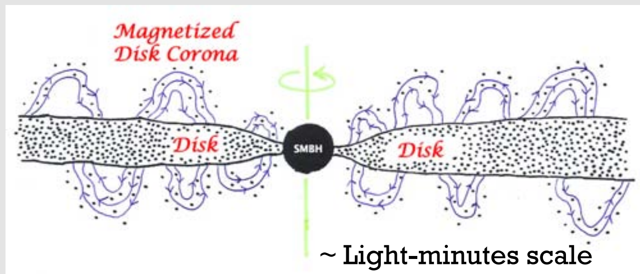

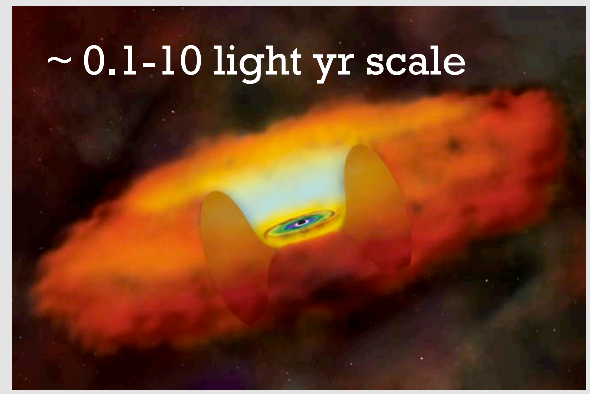

Ecology

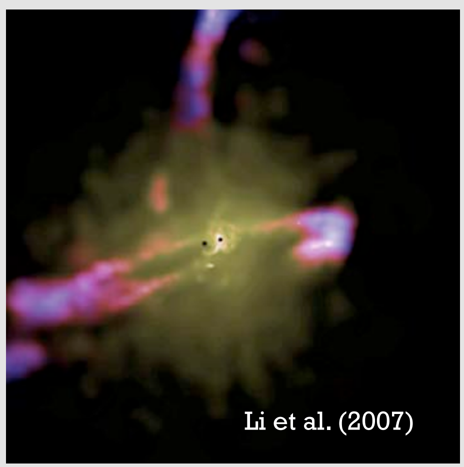

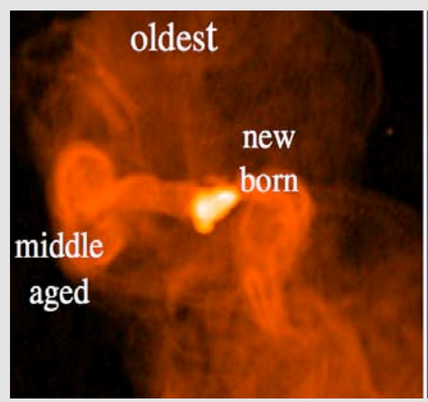

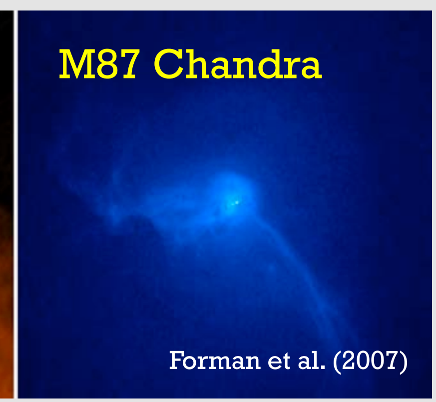

Demography

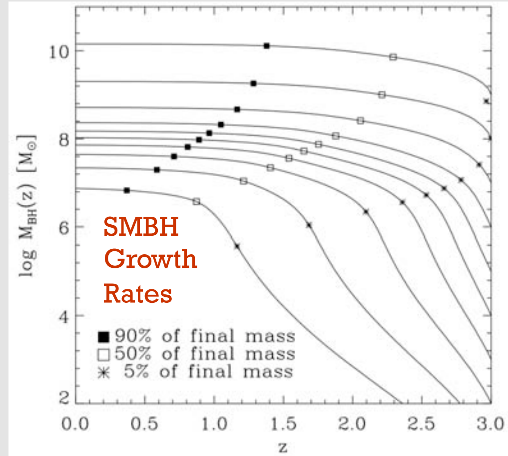

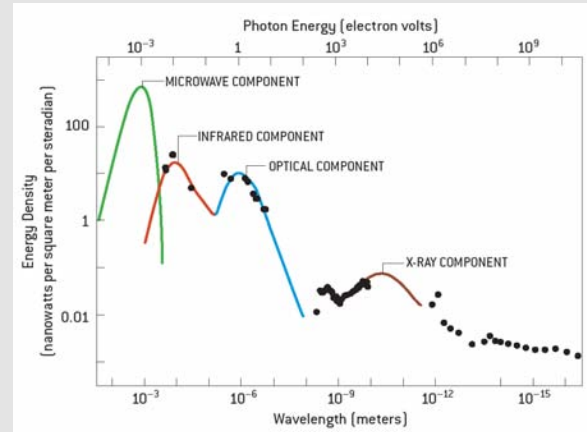

Physics

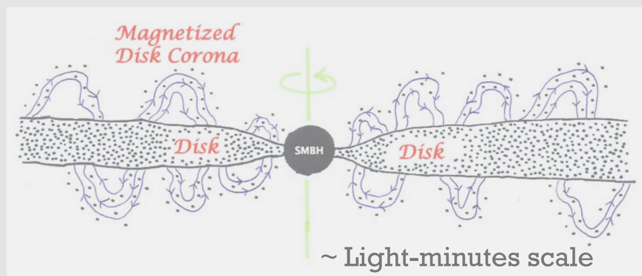

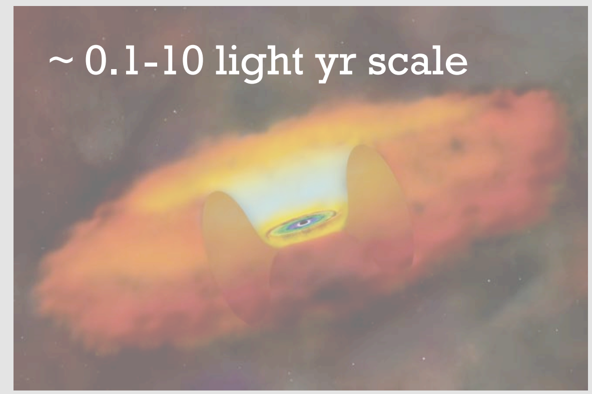

Ecology

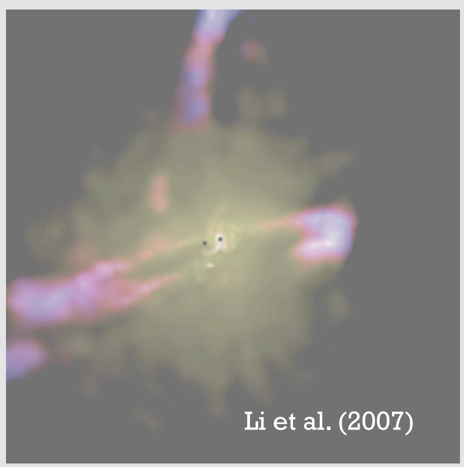

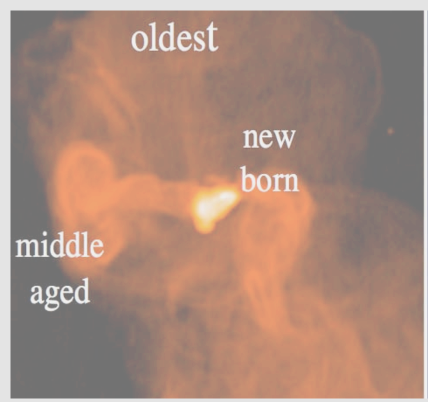

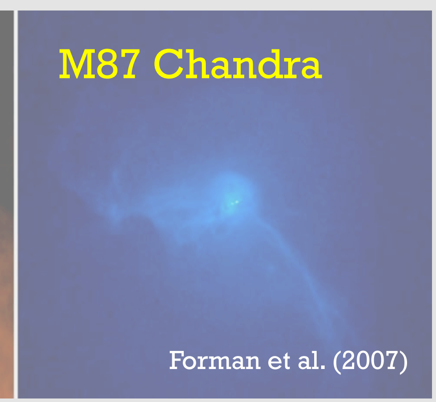

AGN Demography from Quasars

SDSS+2dF Luminous Quasar Evolution

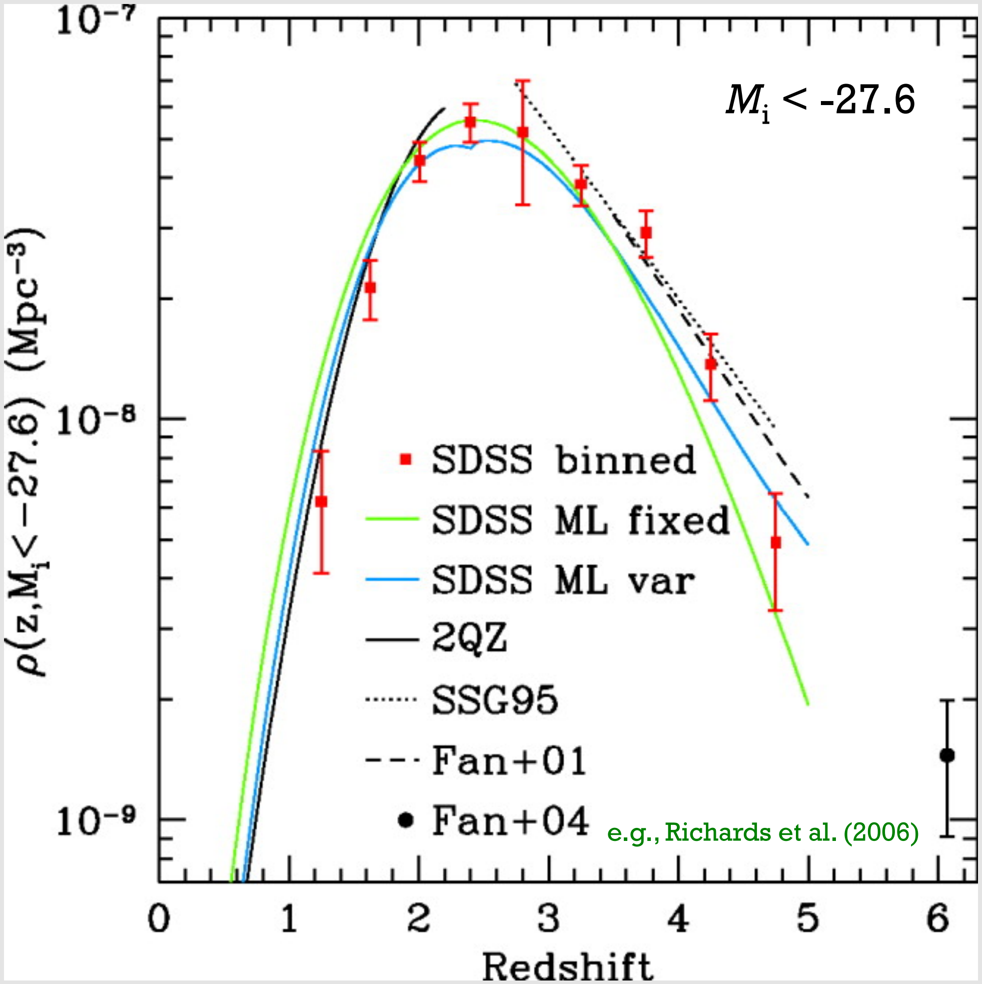

1960s–1990s: Dominated by wide-field surveys of rare, luminous quasars.

Luminous quasars *strongly* peak at $z \sim$ 2-3 (factor of ~ 1000 evolution).

We missed the party!

But how do *most* AGN evolve?

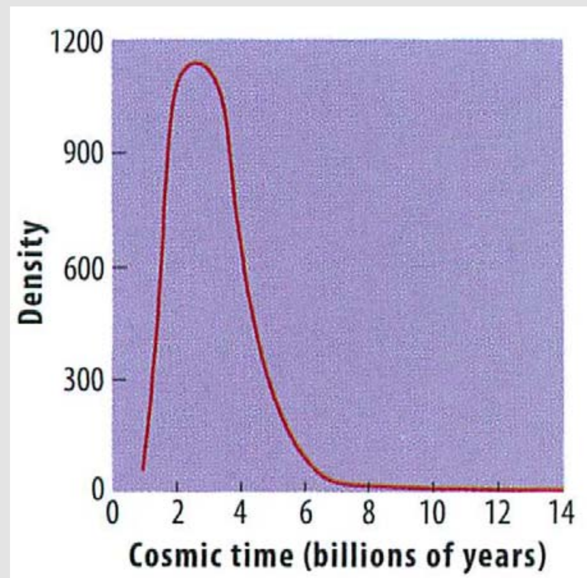

Typical AGNs in the High-Redshift Universe

Chandra Deep Fields AGNs vs. SDSS Quasars

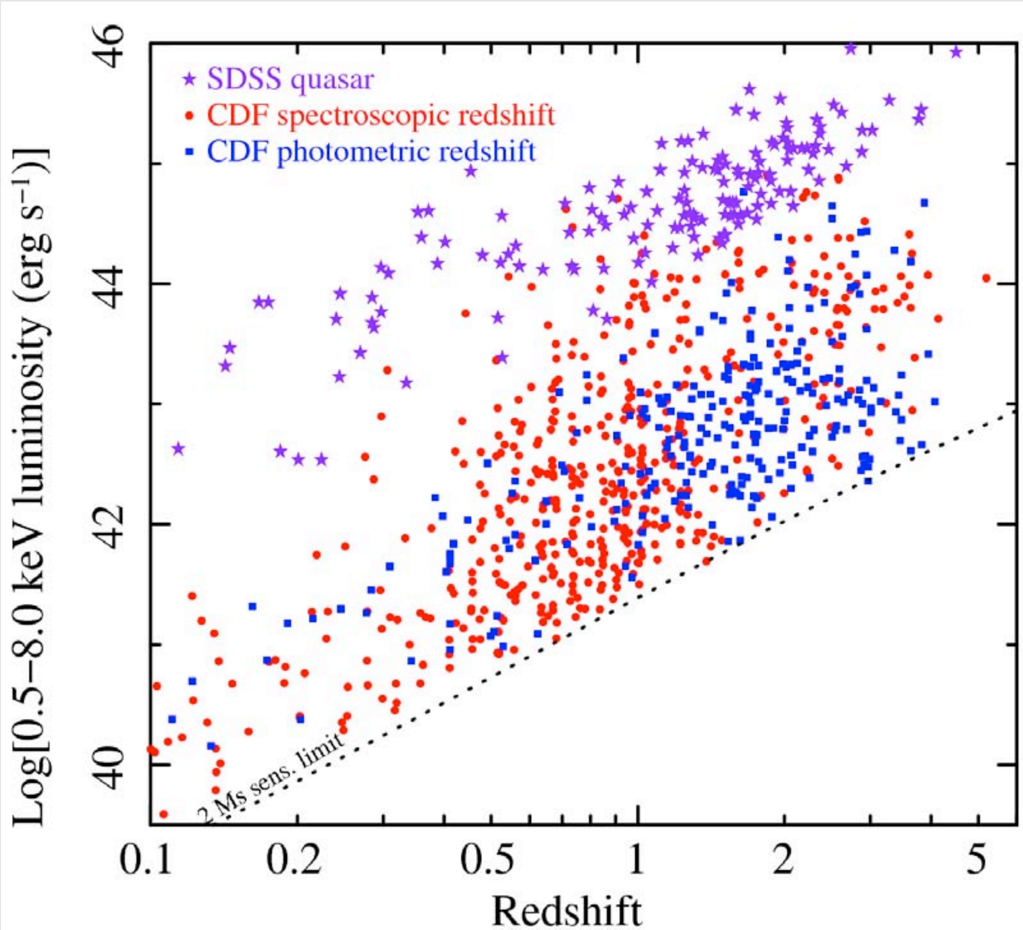

X-ray surveys allow AGN selection about 100 times fainter than wide-field optical surveys.

These AGNs are ~ 500+ times more numerous.

Equally important, do this with minimized obscuration bias.

The key new discovery space!

Luminosity Dependent AGN Evolution

Number-Density Changes with Luminosity

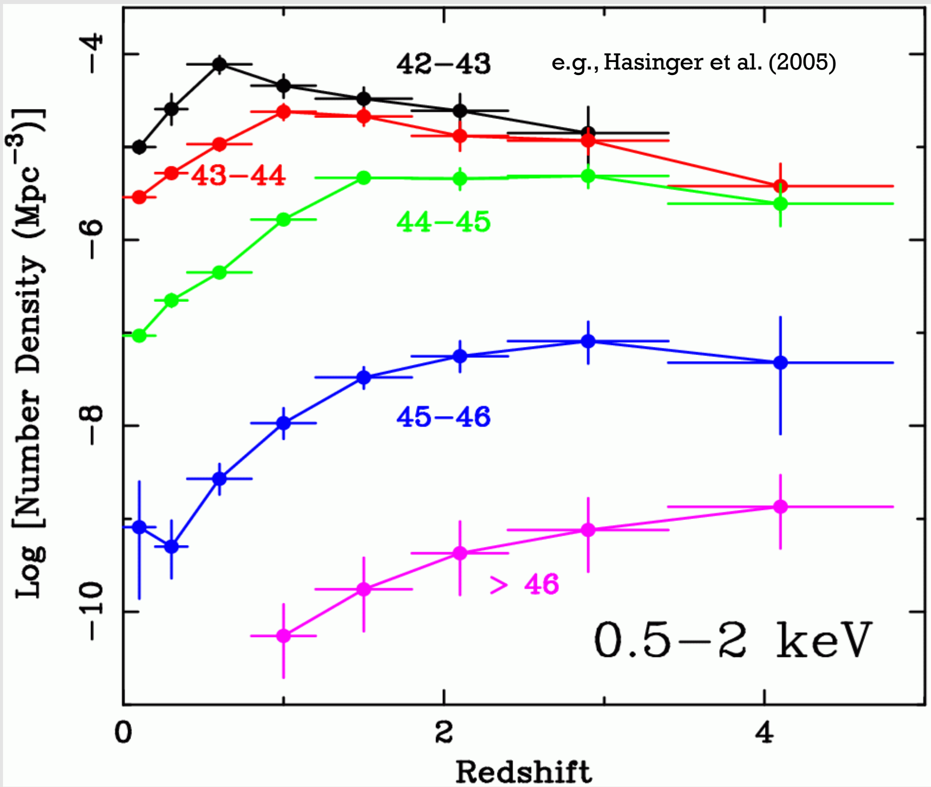

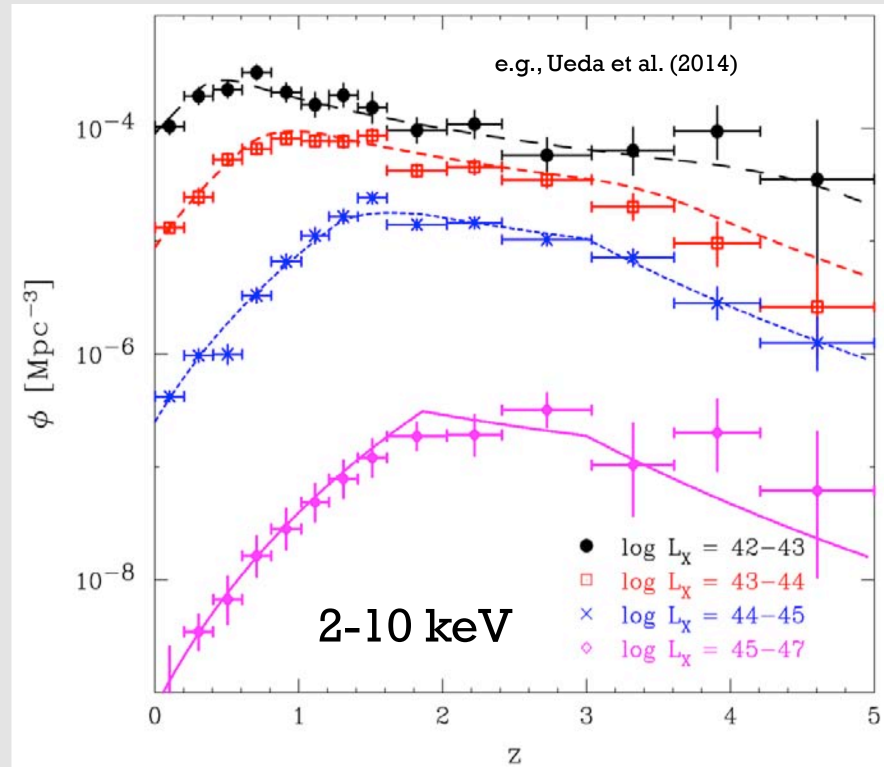

Lower luminosity AGNs peak at later cosmic times - “cosmic downsizing.”

Surprising anti-hierarchical behavior.

Peak of SMBH power production at $z \sim$ 1-1.5 and not $z \sim$ 2-3.

The Soltan Argument

The summed SMBH mass growth found in surveys should add up to the mass density of local SMBHs.

Mon. Not. R. astr. Soc. (1982) **200**, 115–122

Masses of quasars

Andrzej Sołtan *N. Copernicus Astronomical Centre, Bartycka 18, 00-716 Warsaw, Poland*

Received 1981 October 18; in original form 1981 August 19

Summary. Quasar masses are investigated assuming that accretion on to massive black holes is the ultimate source of energy produced by quasars. Lower limit for the total energy emitted and the mass accumulated in black holes in $1\,\mathrm{Gpc}^3$ is calculated using various data on quasar counts and bolometric luminosities. The energy produced is at least $8.5 \times 10^{66}\,\mathrm{erg\,Gpc^{-3}}$. This result is independent of the cosmological model. Assuming that quasars reside in nuclei of giant galaxies it is shown that minimum masses of dead quasars are of the order of $10^8 M_\odot$, close to the observational threshold for ground-based telescopes.

$$E = \eta M c^2$$

$$\epsilon_{\mathrm{rad}}(1+\bar{z}) = \eta \rho_\bullet c^2$$

Soltan Argument with X-ray AGNs

Local vs. Expected Black-Hole Mass Function

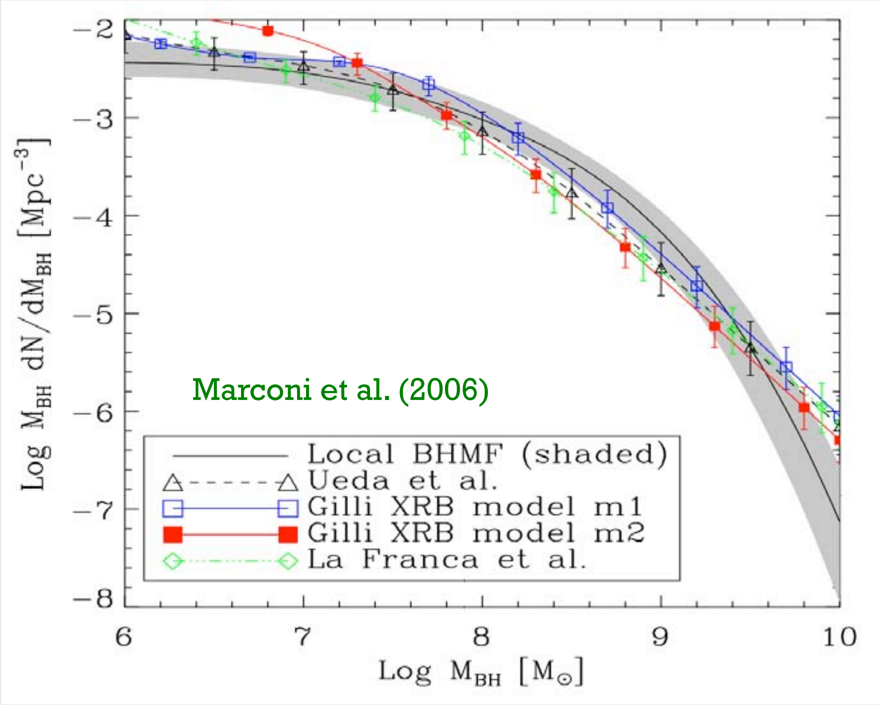

Growth History for Different SMBH Masses

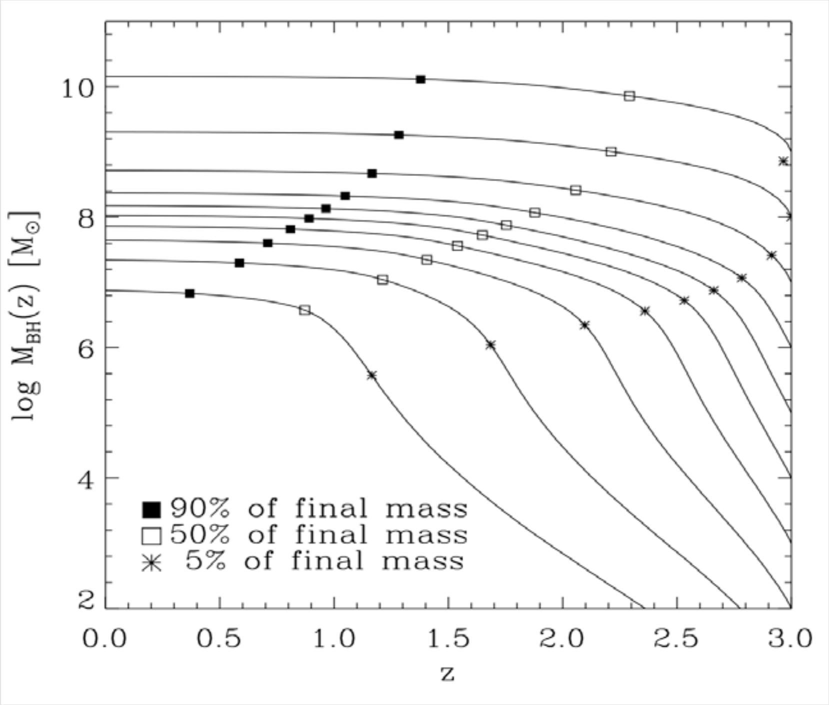

Soltan argument with X-ray luminosity function gives plausible agreement with local SMBH density (3-5 x 10^5 $M_\odot$ Mpc^{-3}).

Radiatively efficient accretion likely drives most SMBH growth.

More massive SMBHs generally grew earlier.

How Many AGNs Being Missed?

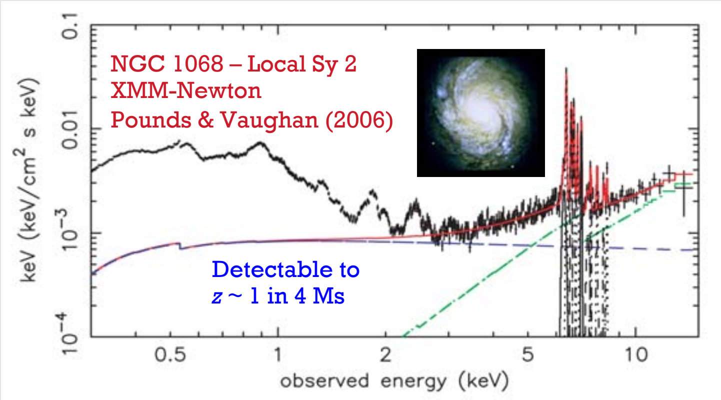

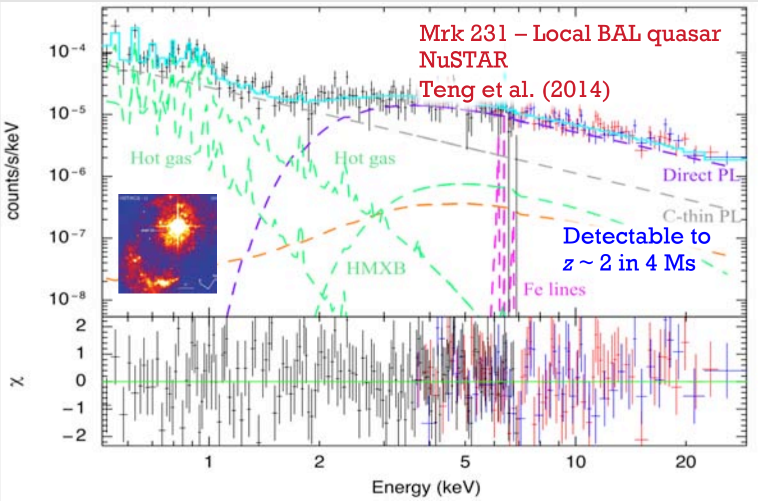

Column-Density Distribution for CDF-S

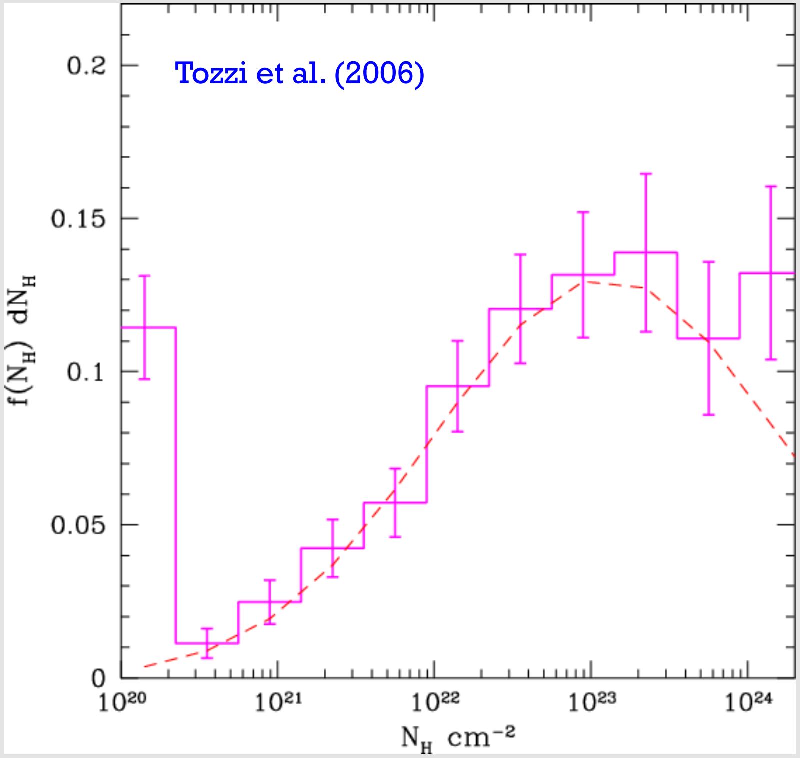

Not surprising – consider local luminous, but highly obscured, AGNs.

X-ray spectra show many highly obscured AGNs in deep fields. Expect many Compton-thick.

Missed obscured AGNs could add ~ 3000 deg^{-2} or more to the number counts.

How to Find Missed AGNs?

Home in on the waste heat – AGN heated dust.

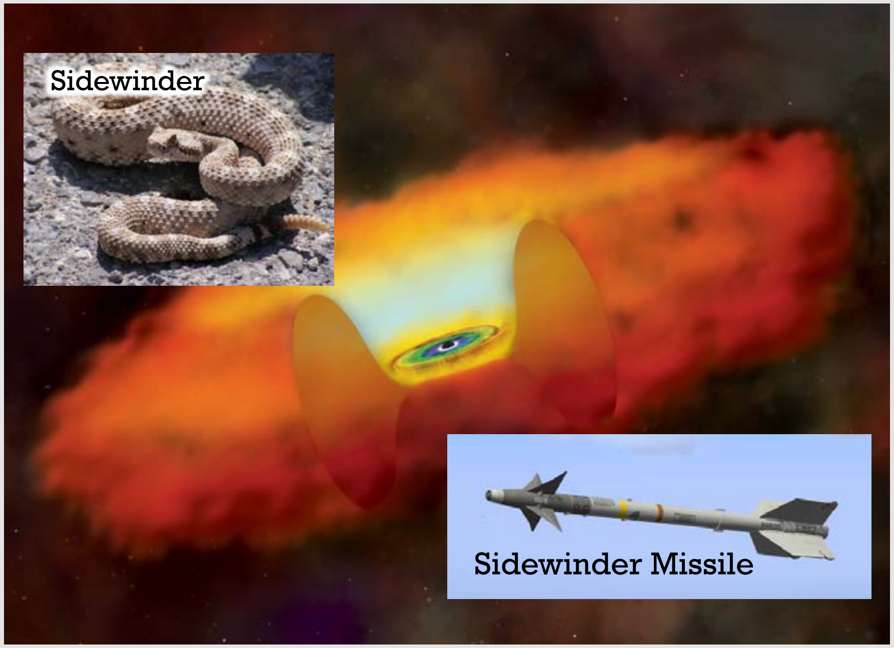

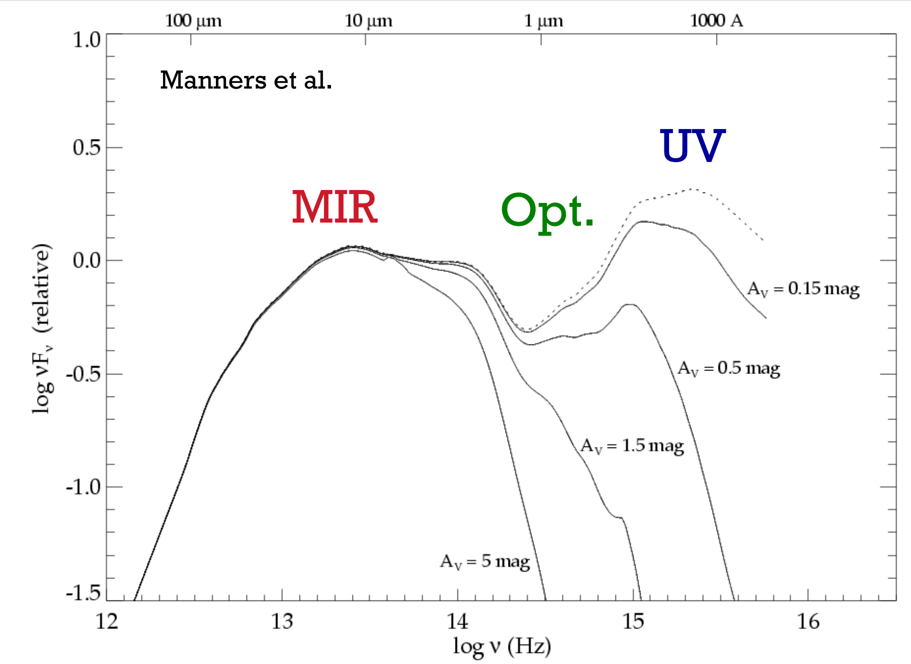

Also highly sensitive hard X-ray surveys.

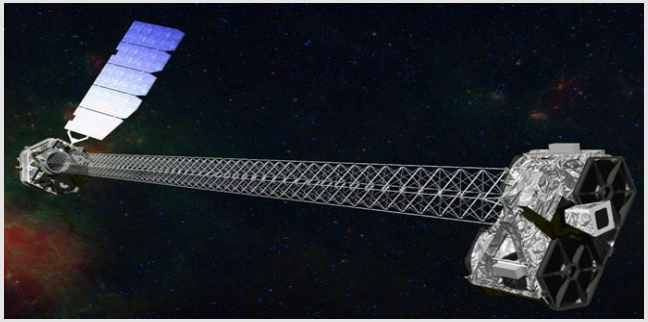

Infrared + X-ray AGN Selection Methods

Infrared Power-Law Selection

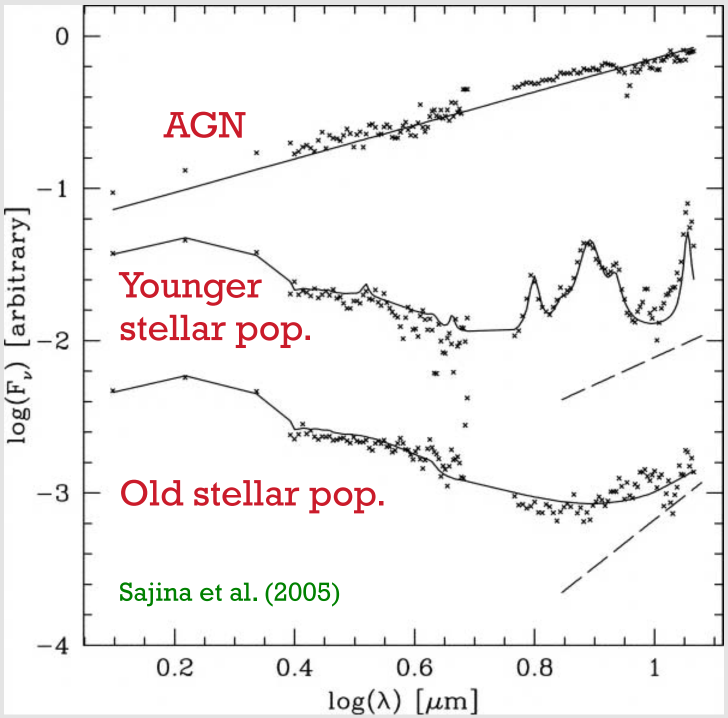

Mid-IR Excess

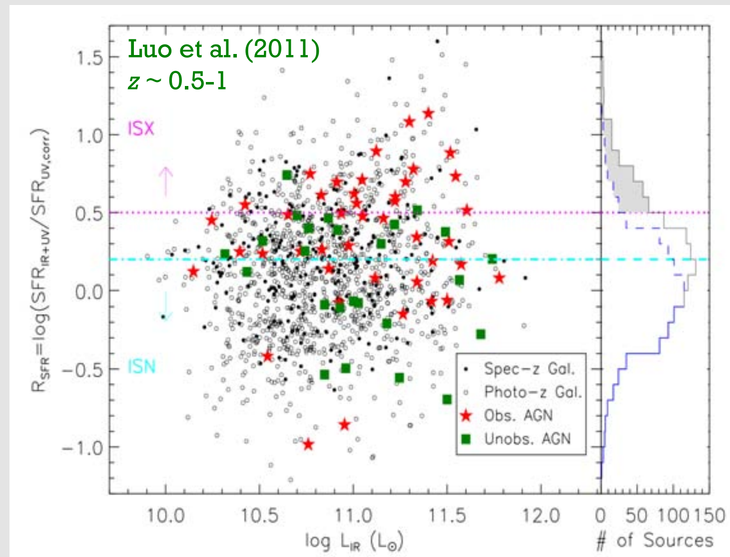

24 micron excess compared to expectation from star formation.

Some AGNs clearly confirmed by X-ray "stacking" studies and spectroscopy.

Not as "clean" as X-ray selection. AGN frequency and luminosities often unclear.

Need better source characterization via X-ray detection and infrared spectroscopy.

Also see, e.g., Stern et al. (2005, 2007); Polletta et al. (2006); Daddi et al. (2007); Donley et al. (2007, 2008); Hickox et al. (2007); Steffen et al. (2007); Alexander et al. (2008, 2011); Fiore et al. (2008, 2009); Treister et al. (2010); Georgantopoulos et al. (2011); Del Moro et al. (2013).

Demography

^

v

Physics

^

v

Ecology

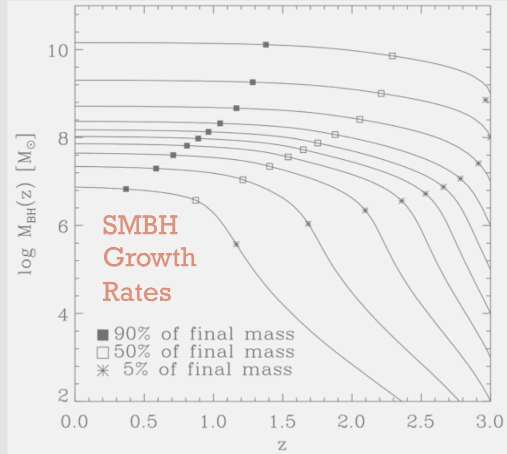

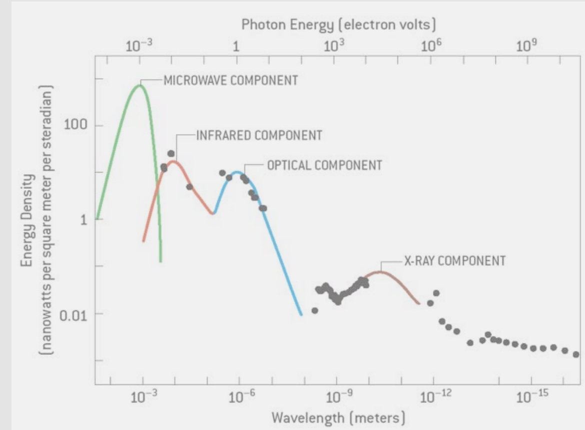

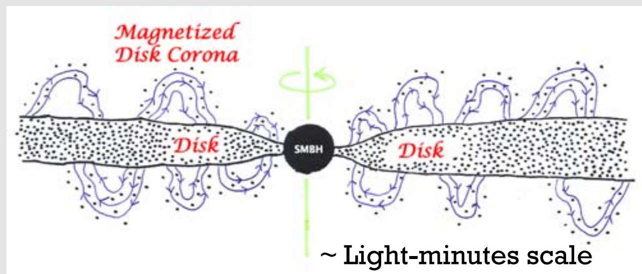

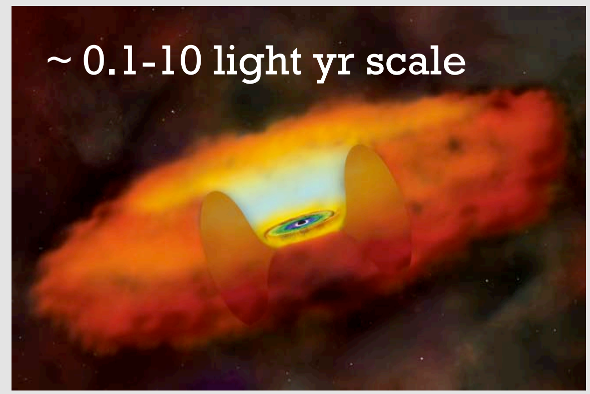

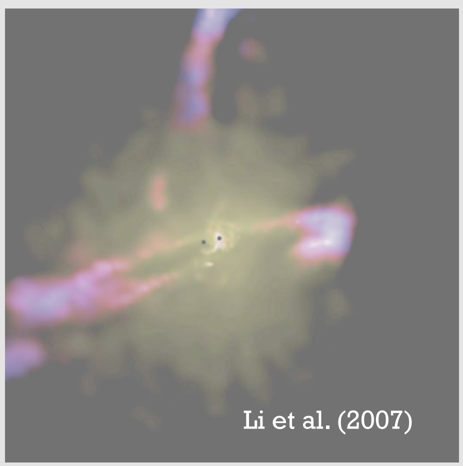

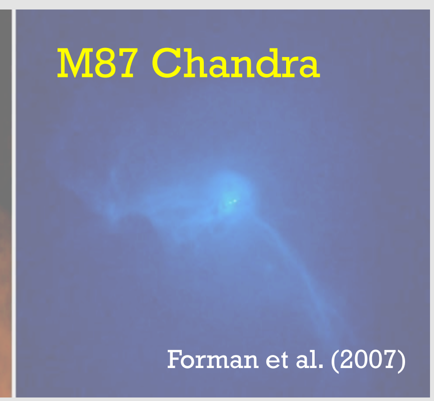

Are Distant AGNs Growing in Same Way?

α_{ox} as a Probe of Disk vs. Corona Power

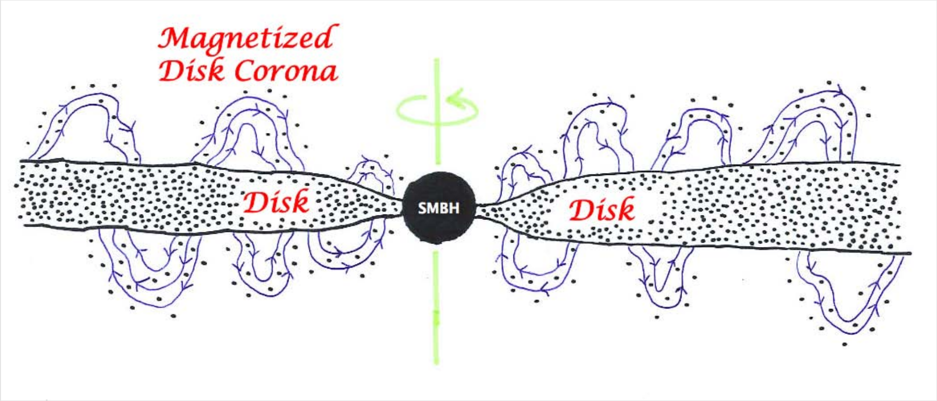

"o" - Optical/UV - 2500 Angstroms

"x" - X-ray - 2 keV

α_{ox} Versus Luminosity

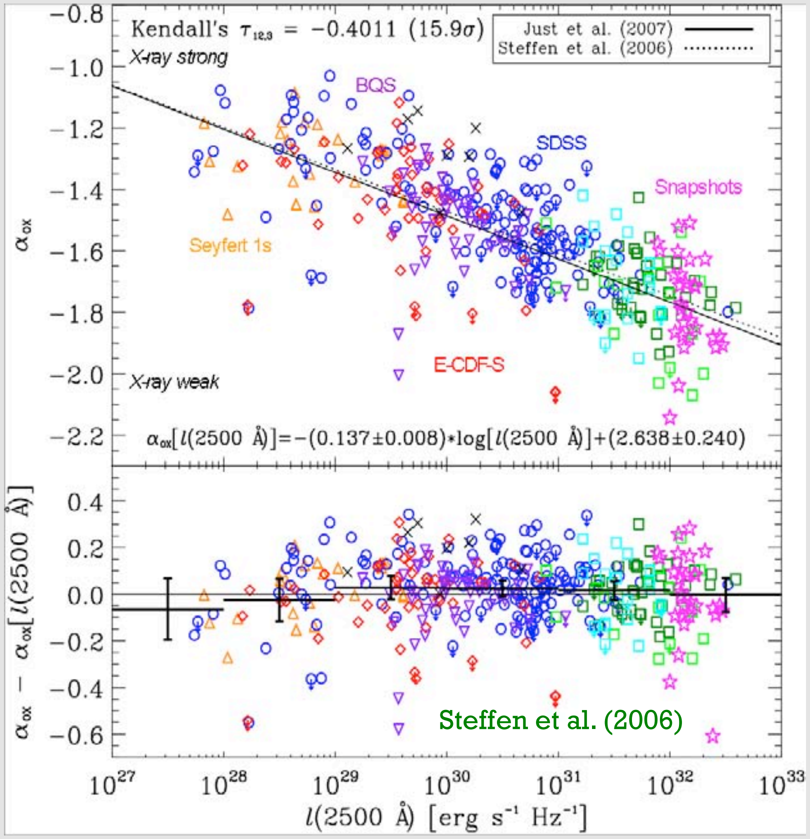

Accretion changes should cause SED changes. For example, α_{ox} probes disk vs. corona power.

Clear luminosity dependence - L_X / L_O declines with rising luminosity over range of ~ 100,000 in luminosity (probably non-linearly). Not well understood physically.

α_{ox} vs. Luminosity in X-ray Selected Samples

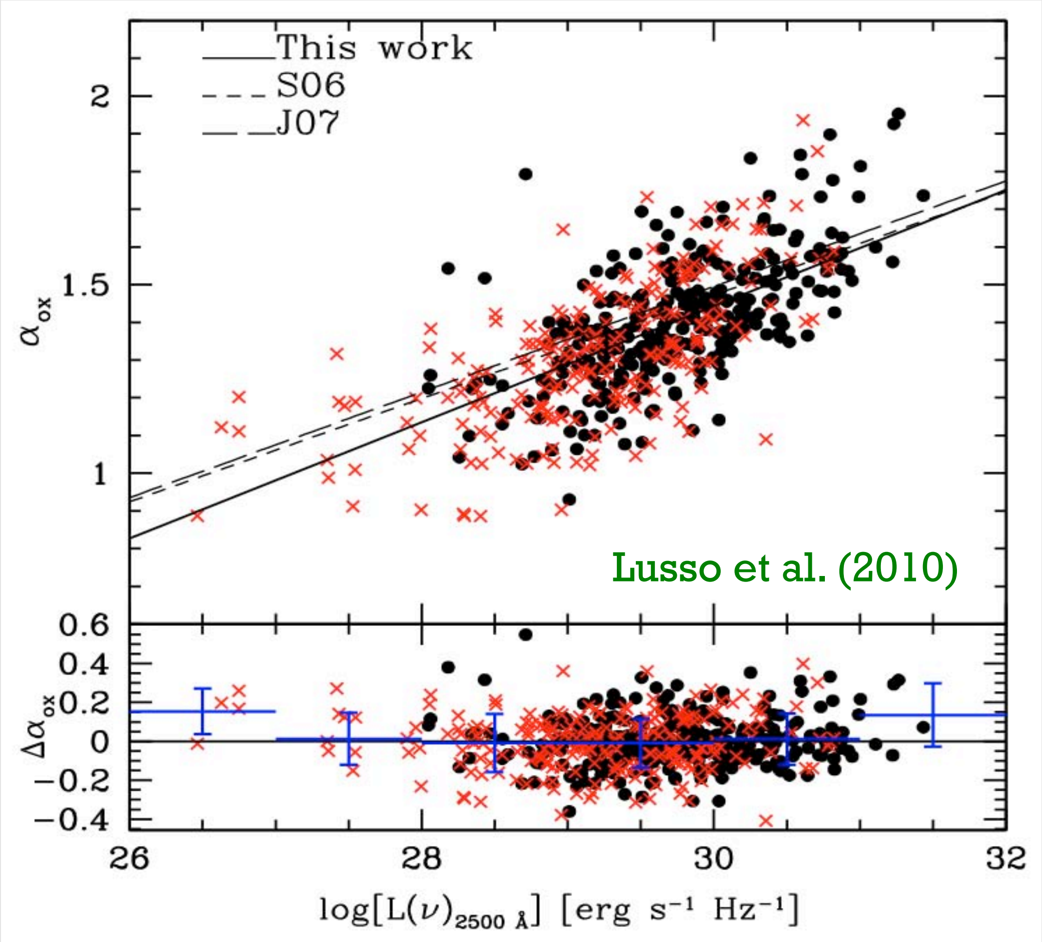

No Redshift Dependence of SED

Constraints on Redshift Evolution of α_{ox}

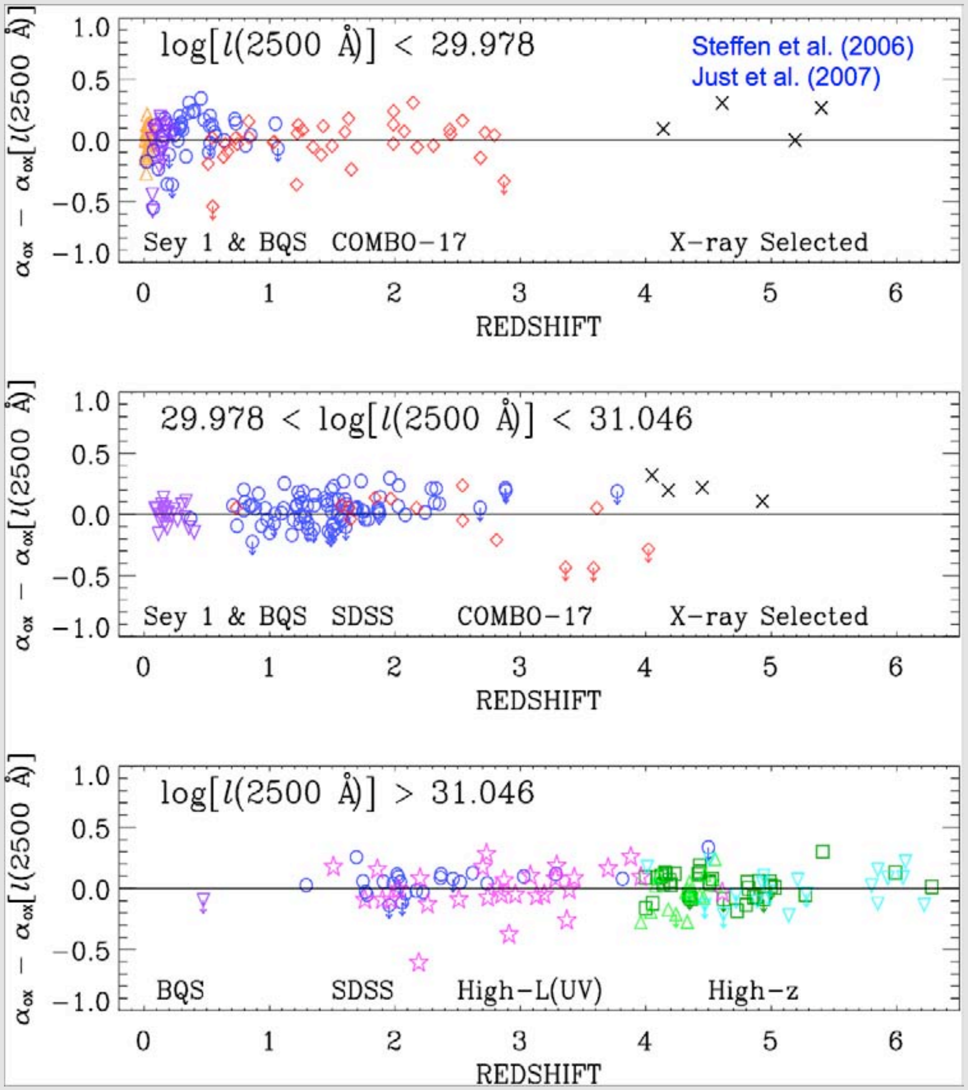

Generally no detectable redshift dependence (some counterclaims).

X-ray-to-optical ratios change by less than 30% from $z \sim 0$-5.

Basic emission processes of AGN appear remarkably stable, in spite of large number-density changes.

Obscuration Dependences

Obscured AGN Fraction Drops with Luminosity

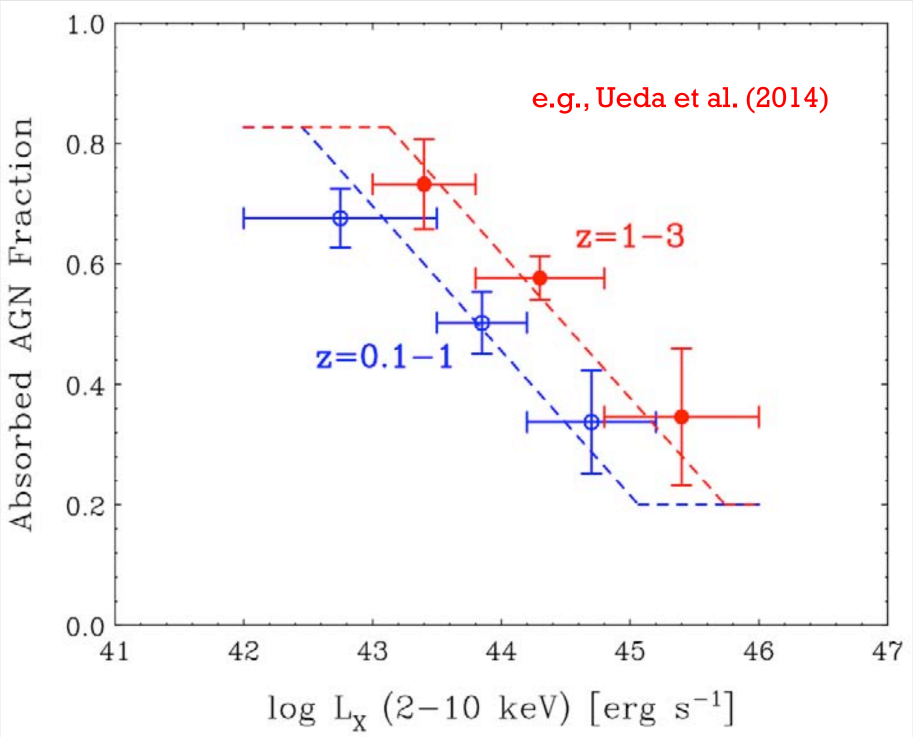

Obscured AGN Fraction Rises with Redshift

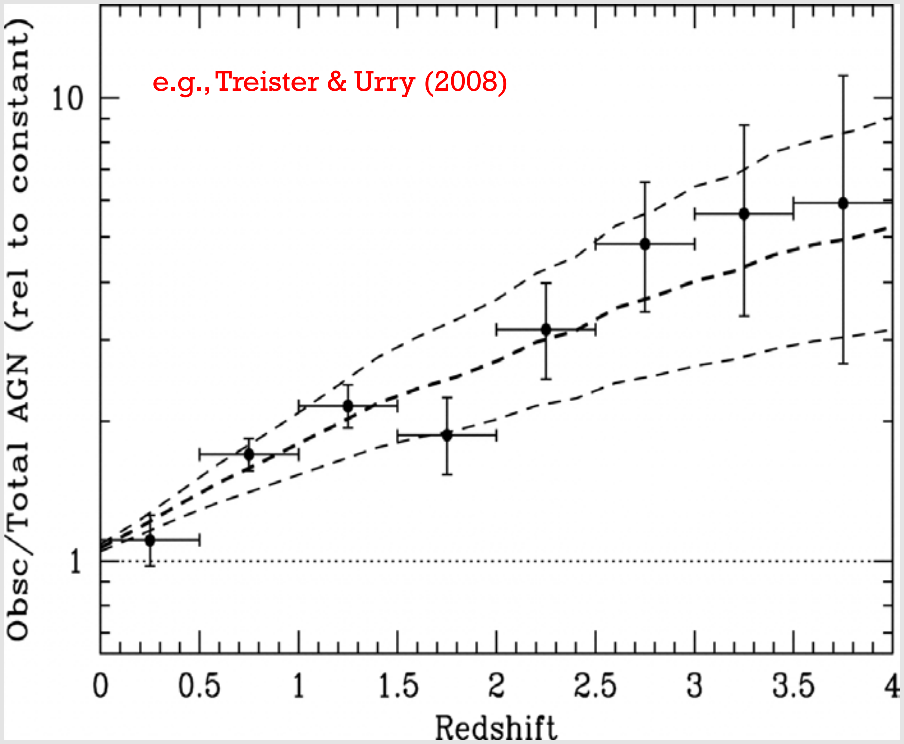

Useful, and long-expected, refinement of AGN unification models. More luminous AGNs can evacuate their environments better.

Obscured fraction scales as $(1+z)^{0.3\text{-}0.7}$, at least up to $z \sim 2$. Torus evolves but inner disk does not? More available gas and dust at early times?

Cosmic Balance of Power

Master Yoda

vs.

Emperor Palpatine
(a.k.a. Darth Sidious)

Cosmic Balance of Power

Supermassive Black Hole Accretion

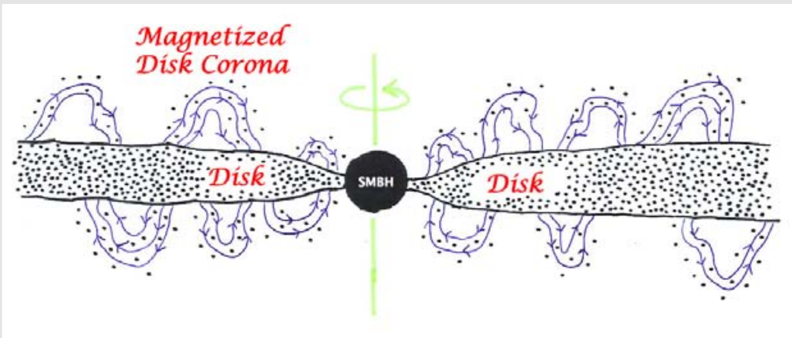

vs.

Stellar Fusion

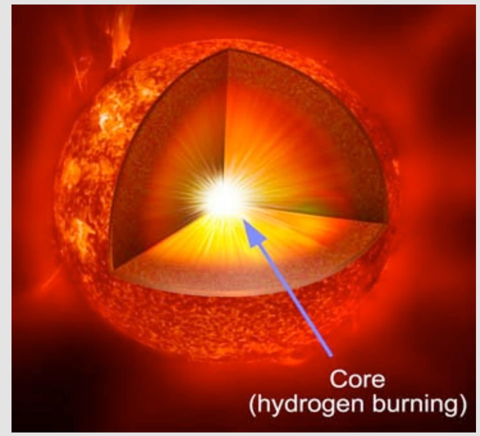

Predictions from around the Chandra and XMM-Newton launches…

Black Holes May Supply Up to Half the Universe's Energy Output

Contact:
Christopher Wanjek
wanjek@gsfc.nasa.gov
301-286-4453

September 10, 1999

Greenbelt, Md. -- Massive black holes, long-thought to produce only a mere fraction of the universe's total energy output, may actually be the force behind half of the universe's radiation produced after the Big Bang, chipping away the coveted power monopoly believed to be held by ordinary stars.

Details of this energy theory, based on measurements of background X-ray radiation and the gas-obscured growth of massive black holes, are presented today by the University of Cambridge Institute of Astronomy theorist Dr. Andrew Fabian at the X-ray Astronomy 1999 meeting in Bologna, Italy. The meeting is being chaired by Dr. Nicholas White, head of NASA Goddard Space Flight Center's (Greenbelt, Md.) X-ray Astrophysics Branch in the Laboratory for High Energy Astrophysics.

The Economical X-ray Universe

Supermassive Black Hole Accretion

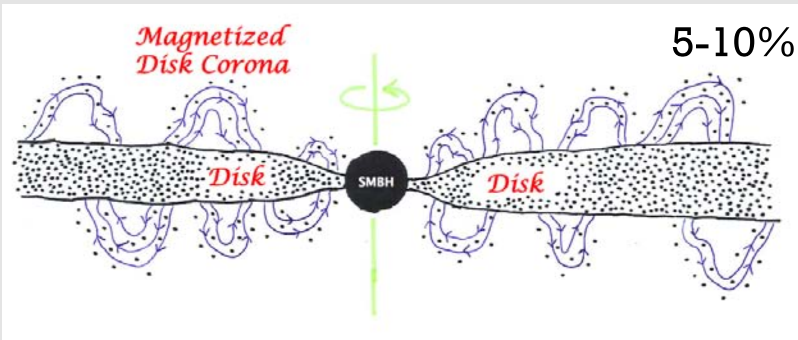

vs.

Stellar Fusion

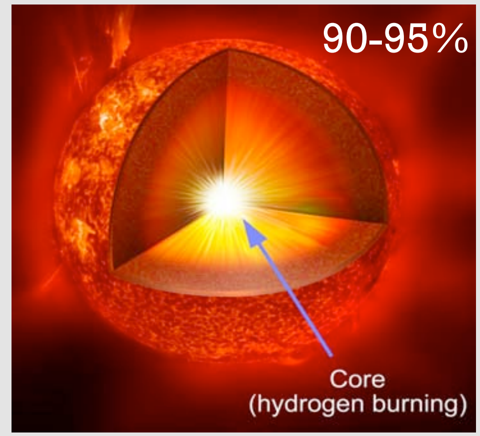

Chandra and XMM-Newton results show we live in a remarkably economical X-ray universe, more so than expected several years ago.

X-ray background not dominated by powerful obscured quasars at *z* ~ 2-4. Moderate-luminosity, obscured AGNs at *z* ~ 0.5-2 dominate.

SMBH accretion makes ~ 5-10% of cosmic power since galaxy formation.

Demography

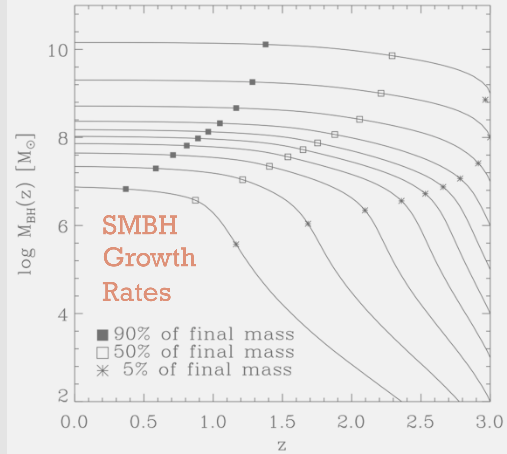

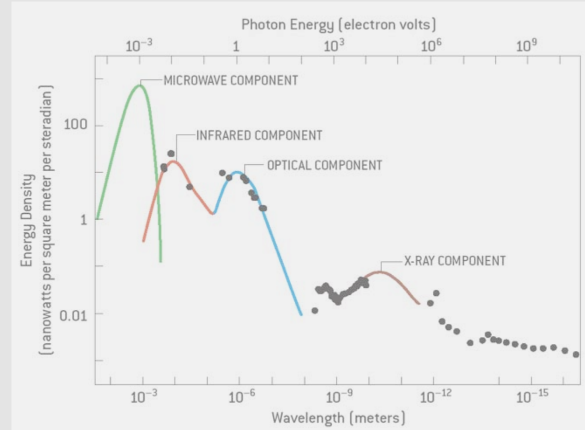

Physics

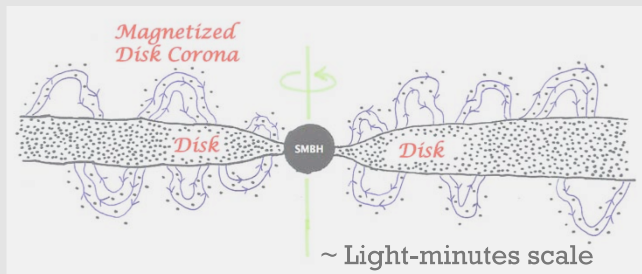

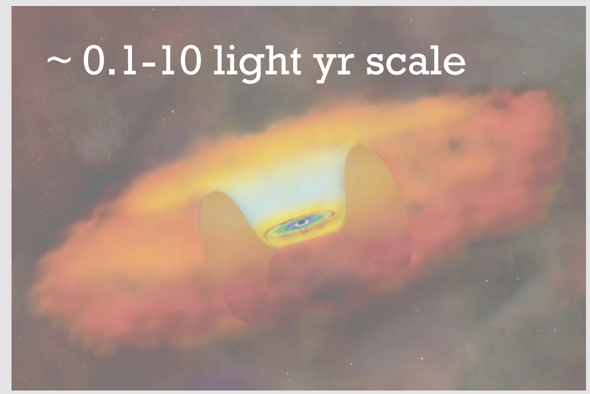

Ecology

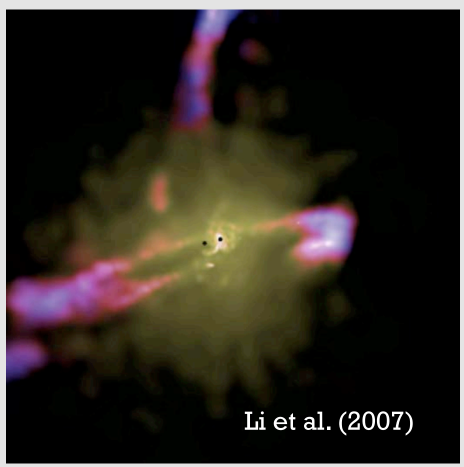

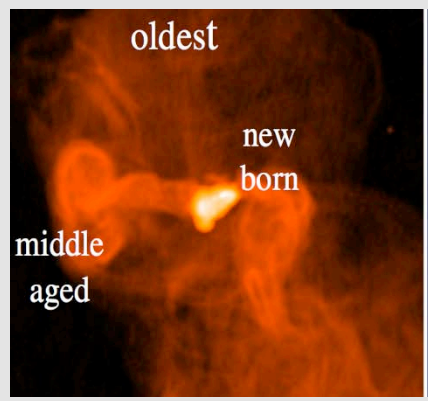

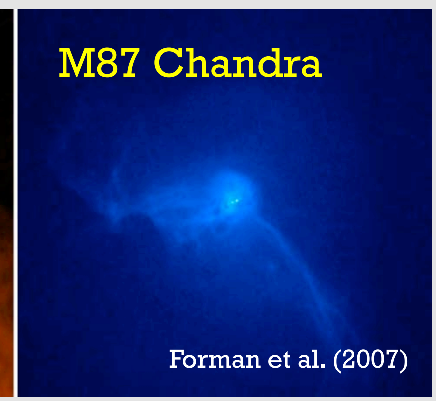

Relative Scales

SMBH Mass : Host Stellar Mass
is like
Small Mouse : Large Human

(Ratio of ~ 10^4)

SMBH Radius : Host Radius
is like
Rock : Earth

(Ratio of ~ 10^8)

Relative Energy

Relevant order-of-magnitude energies:

$E_{\text{SMBH}} \sim 30\text{-}100\ E_{\text{Galaxy Binding}}$

Even though the SMBH is small, it has the energetic potential to affect its host galaxy substantially.

If the SMBH energy can be liberated in a form that significantly affects host galaxy.

Evidence Suggesting SMBH and Galaxy Co-Evolution

SMBHs Common in Local Galaxies and Show Strong Bulge Relations

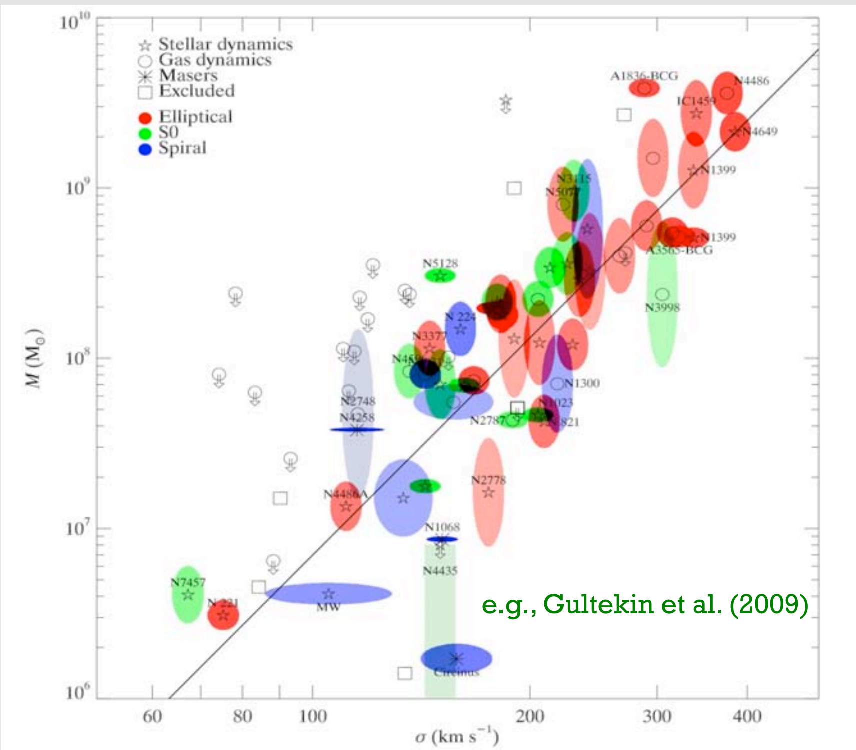

Broadly Similar AGN-SFR Evolution for Most of Cosmic Time (z < 2)

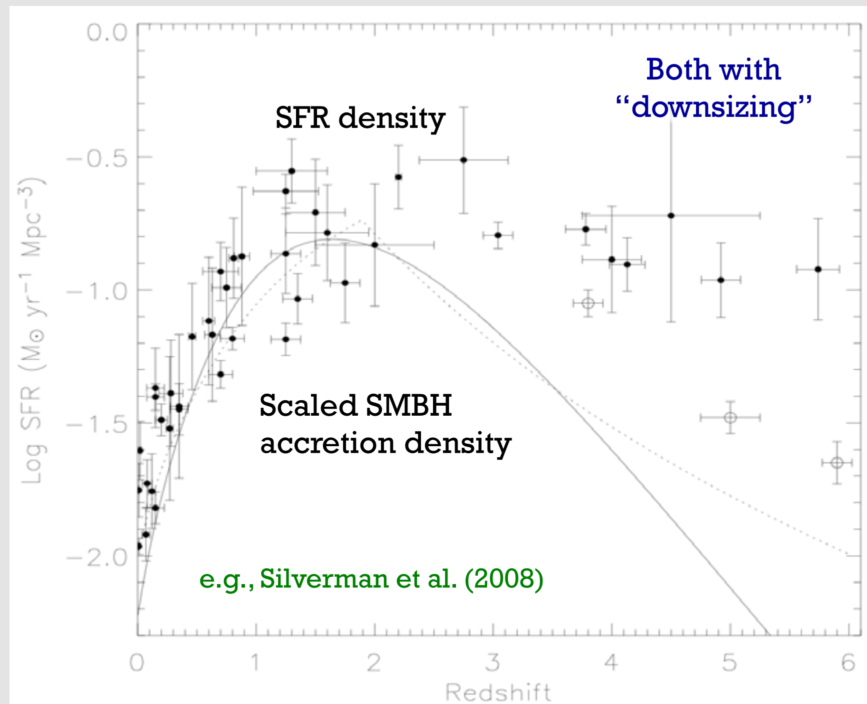

How could SMBH feedback occur? Hope for clues from AGN hosts.

Simulation of Wind Feedback

SMBH Wind Feedback Evacuating Gas and Quenching Star Formation

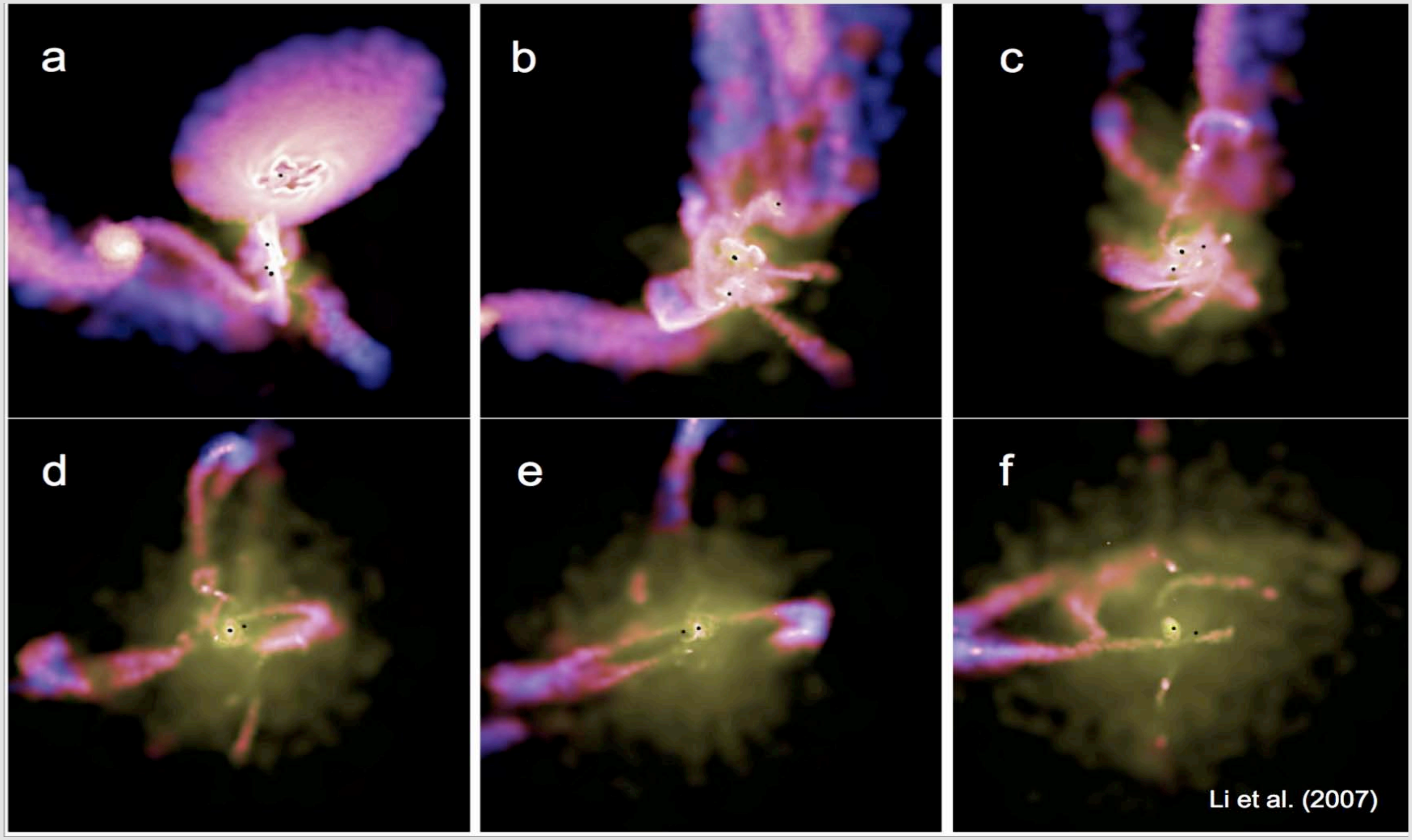

Intensity shows gas density - Color shows gas temperature – 600 Myr time span

Jet Feedback in Clusters

Jets can do substantial work against the hot gas in galaxy clusters

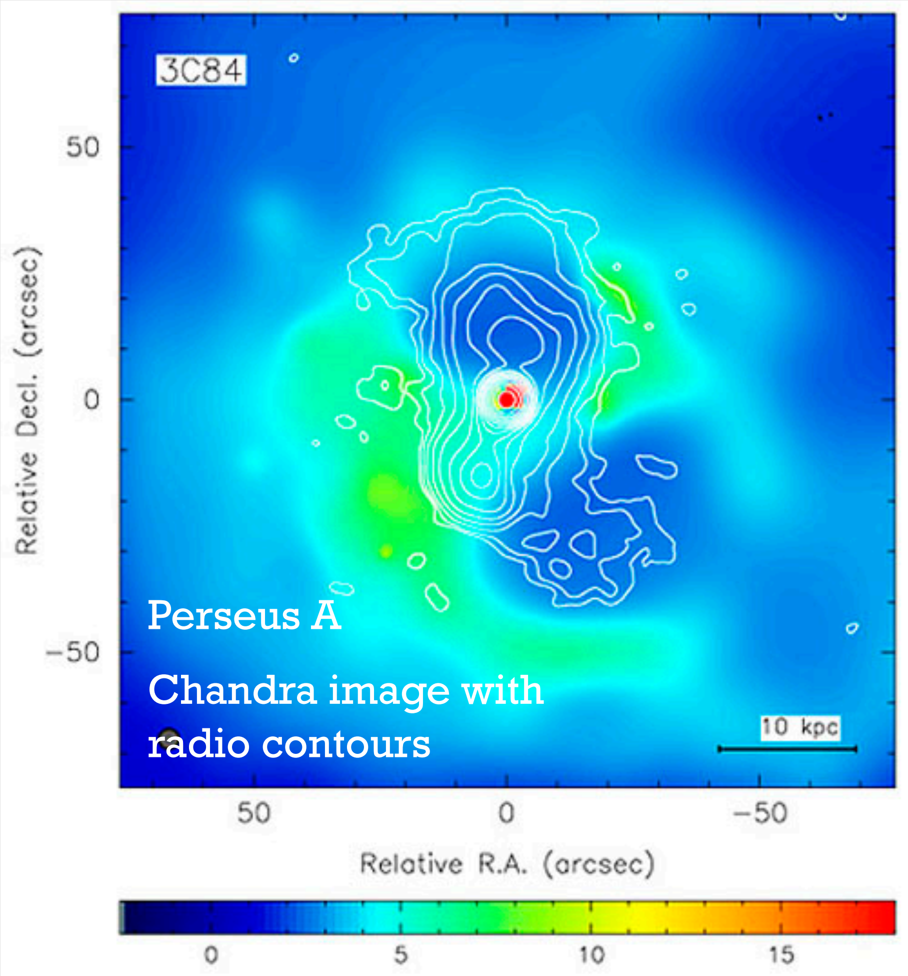

Fabian et al. (2003)

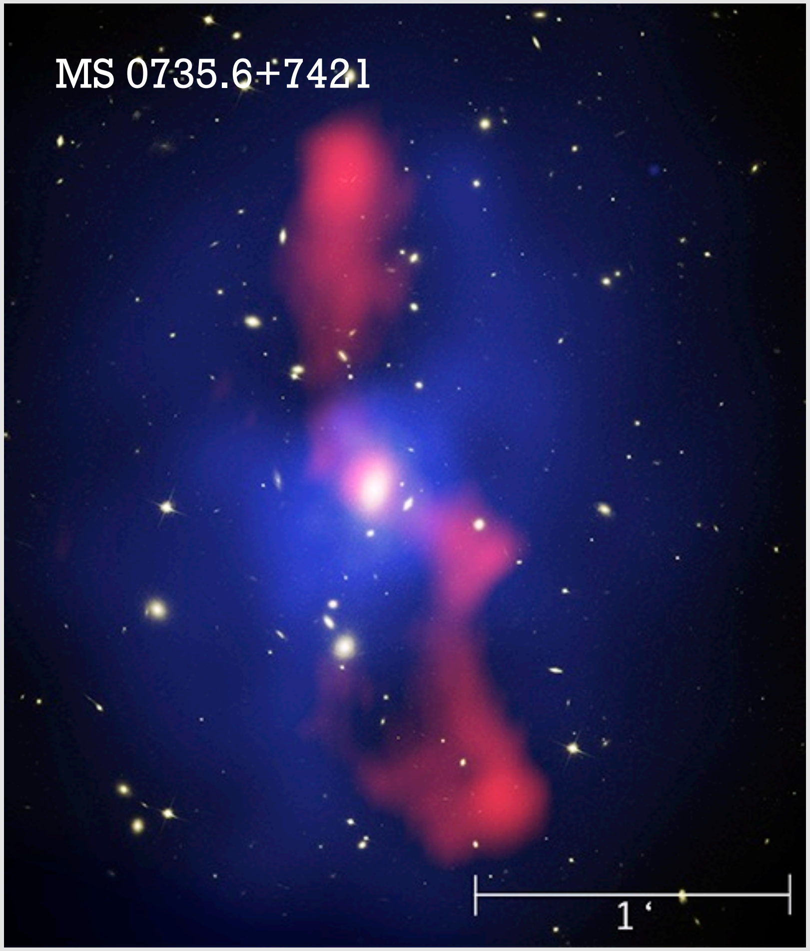

McNamara et al. (2005)

Relevant Observable Quantities

Black-Hole and Torus Regions

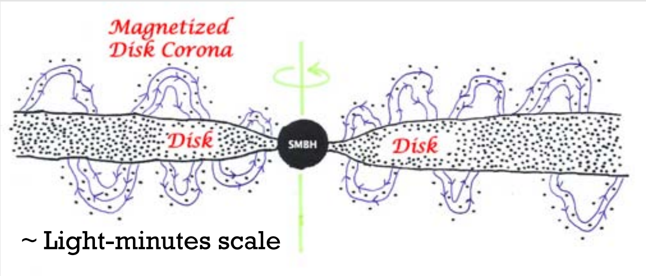

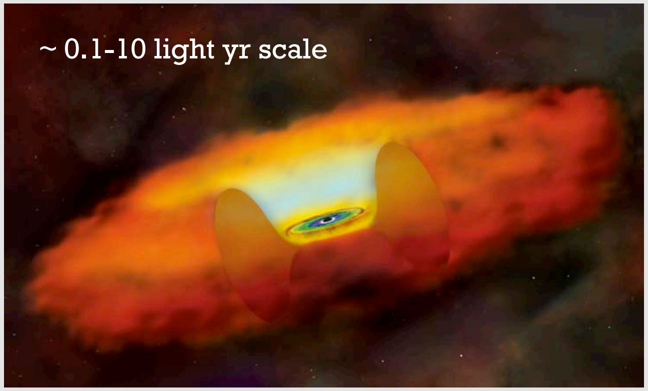

AGN Luminosity
SMBH Accretion Rate
Obscuration Properties
SMBH Mass

Fueling and Obscuration

◀

▶

Feedback

- Winds
- Jets
- Radiation

AGN Host Galaxies

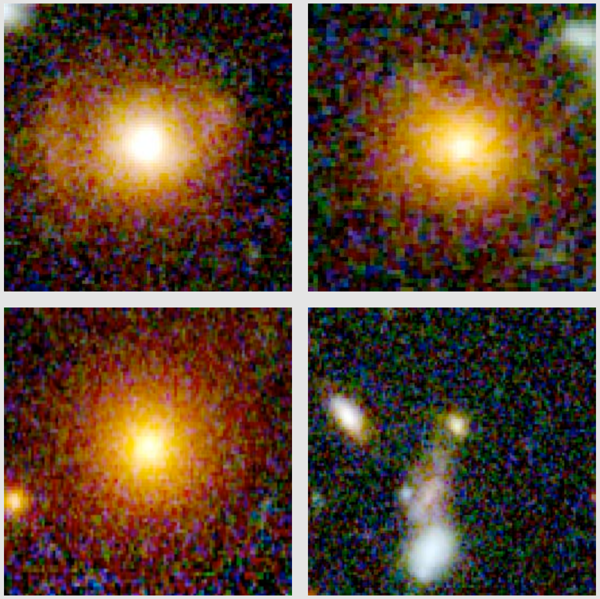

Stellar Luminosity
Colors
Stellar Mass
Star-Formation Rate
Morphology
Companions / Mergers
LSS Context

Practical Issues in Host-Galaxy Studies

Host-galaxy studies must overcome blending of host light and AGN light.

- Work at low AGN luminosities or on obscured AGNs.
- Work at wavelengths where host vs. AGN contrast is maximized.
- Use high angular resolution from HST or adaptive optics.

Practical Issues in Host-Galaxy Studies

HST Imaging of Low-Redshift Quasars

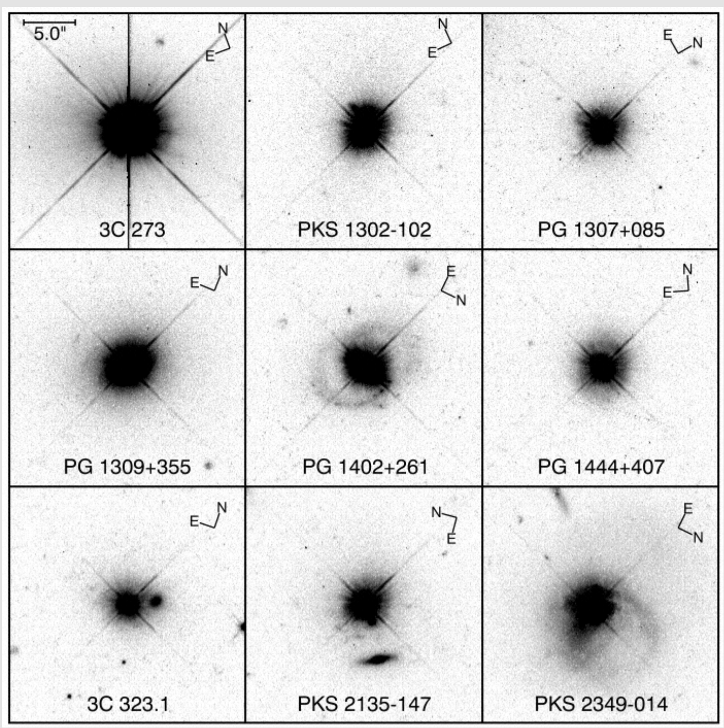

Bahcall et al. (1997)

HST Imaging of CDF-S X-ray AGNs

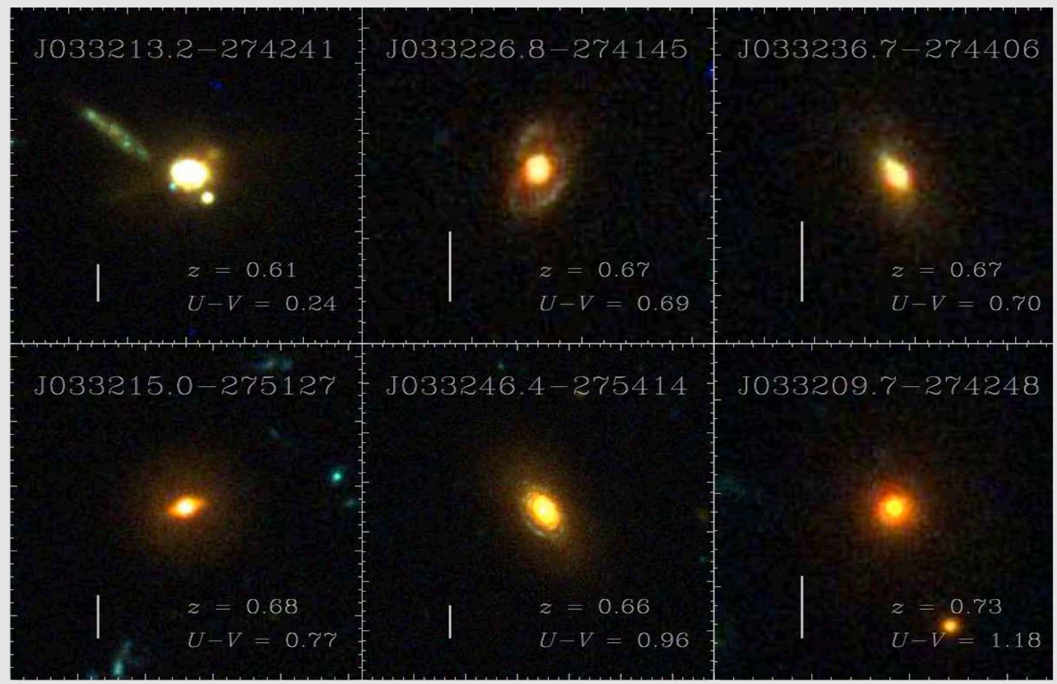

Silverman et al. (2008)

Feasibility of Host-Galaxy Measurements

Mean AGN SEDs in Chandra Deep Field-South (15-35 Bands)

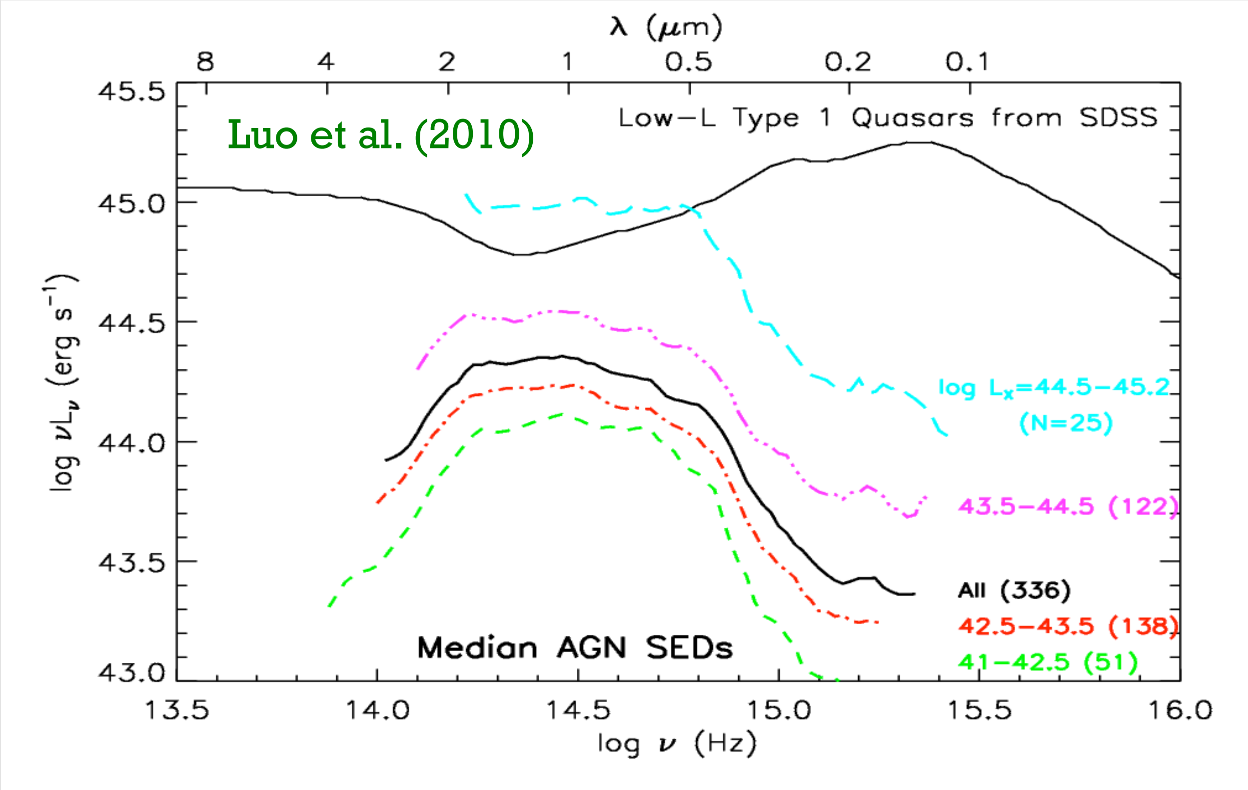

Many X-ray AGNs, especially those that are obscured, have rest-frame UV, optical, and infrared emission dominated by host starlight.

Still must be wary of problems due to AGN light – subtract when possible.

AGN Hosts Usually Massive

Stellar Mass vs. Redshift
for CDF-S AGNs

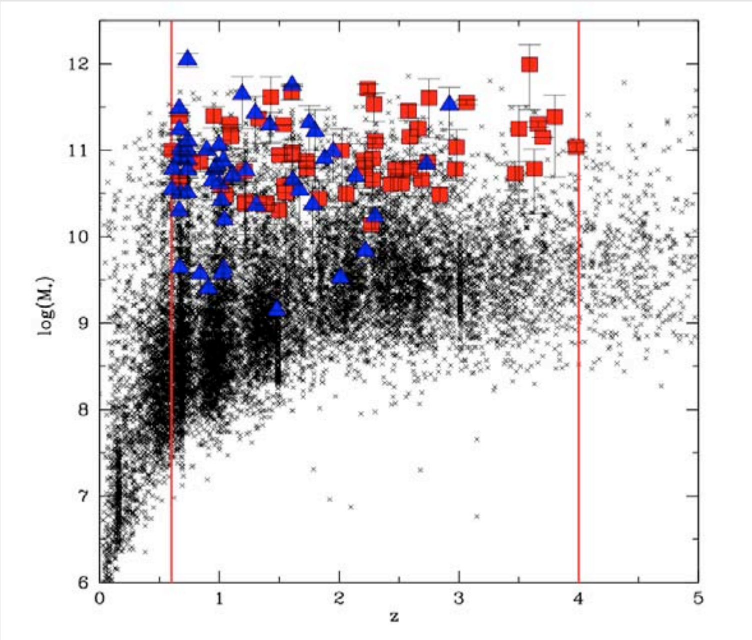

e.g., Brusa et al. (2009)

AGN Fraction Increases Toward
High Stellar Mass – AGNs Are Large Dots

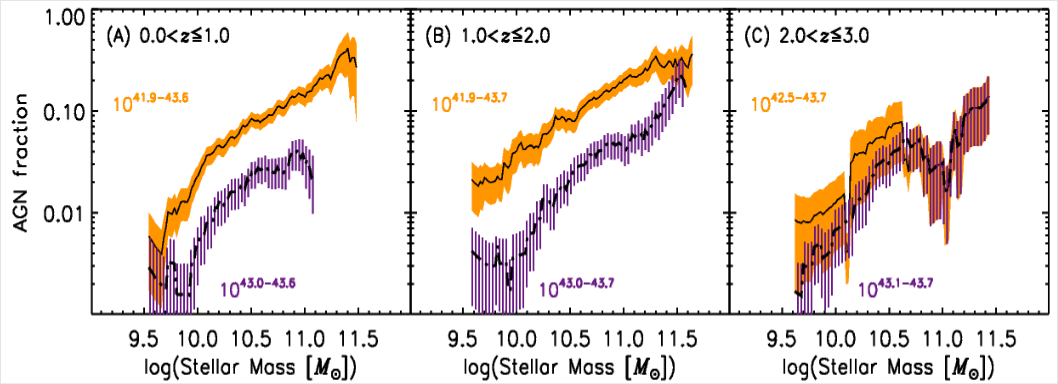

e.g., Xue et al. (2010)

Strongest result found at z = 0-3 – factor of ~ 40.

Must consider mass effects in studies of AGN host galaxies.

Wide Diversity of Morphological Types

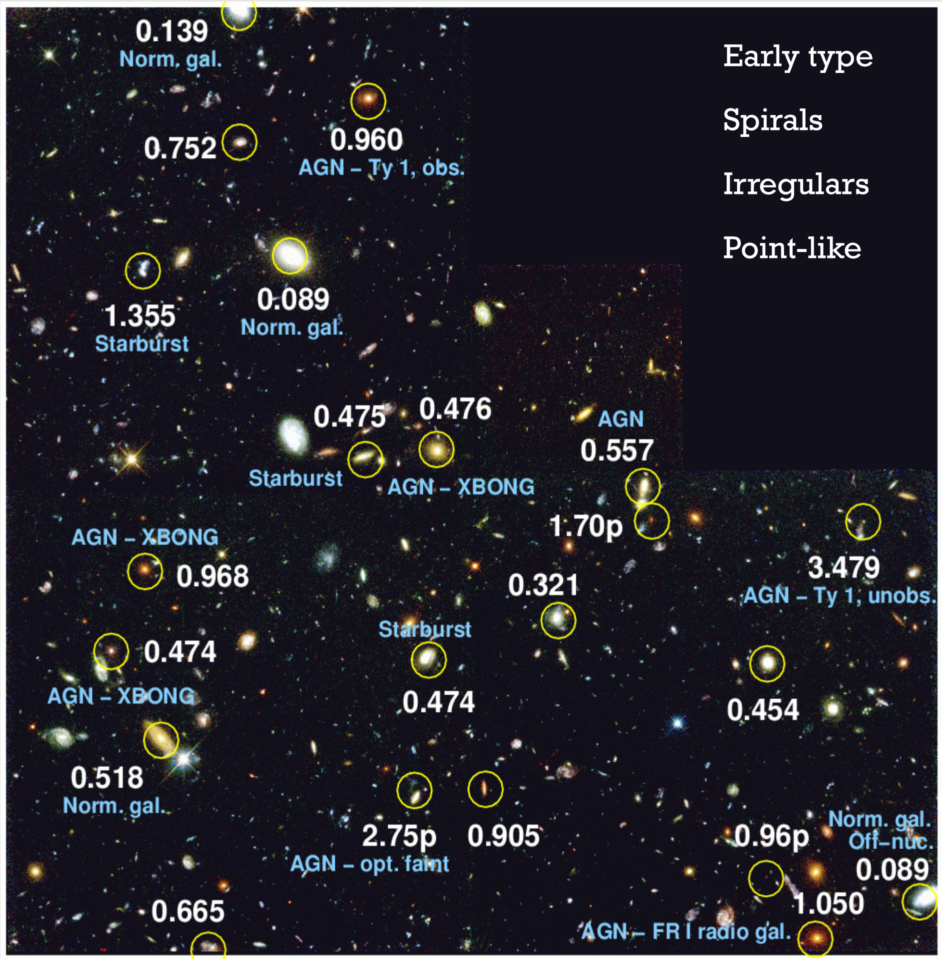

e.g., Brandt et al. (2001); Koekemoer et al. (2002)

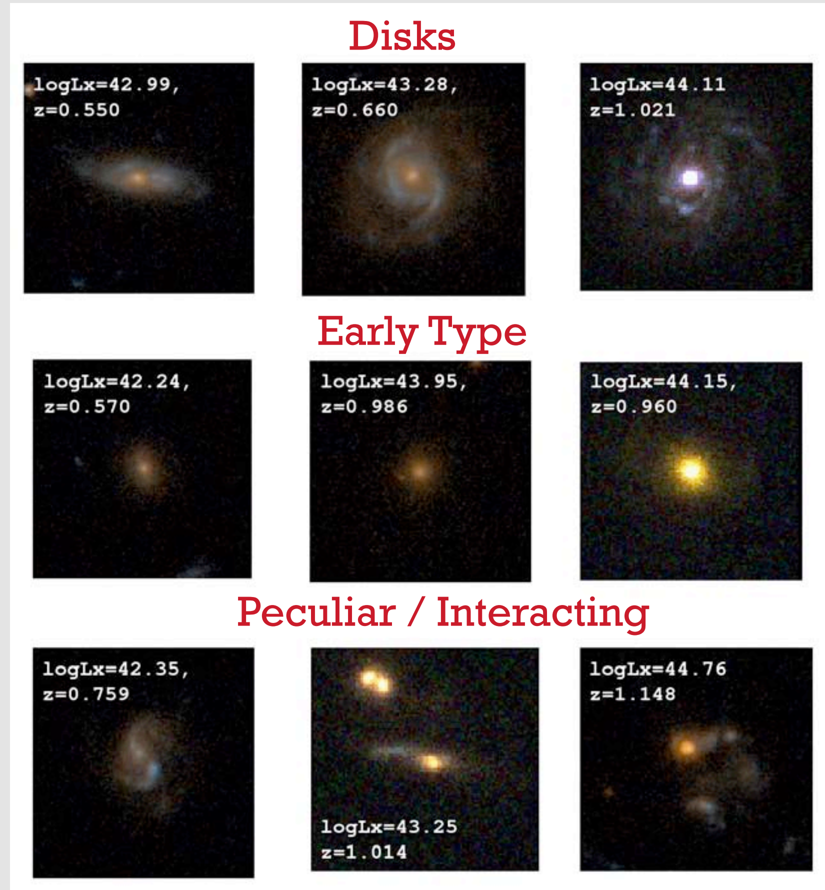

Georgakakis et al. (2009)

Broadly speaking, about 40-50% early types, 20-30% late types, rest irregular or point-like.

More bulge dominated than galaxy population overall, and no clear excess of mergers at moderate AGN luminosities.

AGN Hosts Show No Evidence for Excess Mergers/Interactions

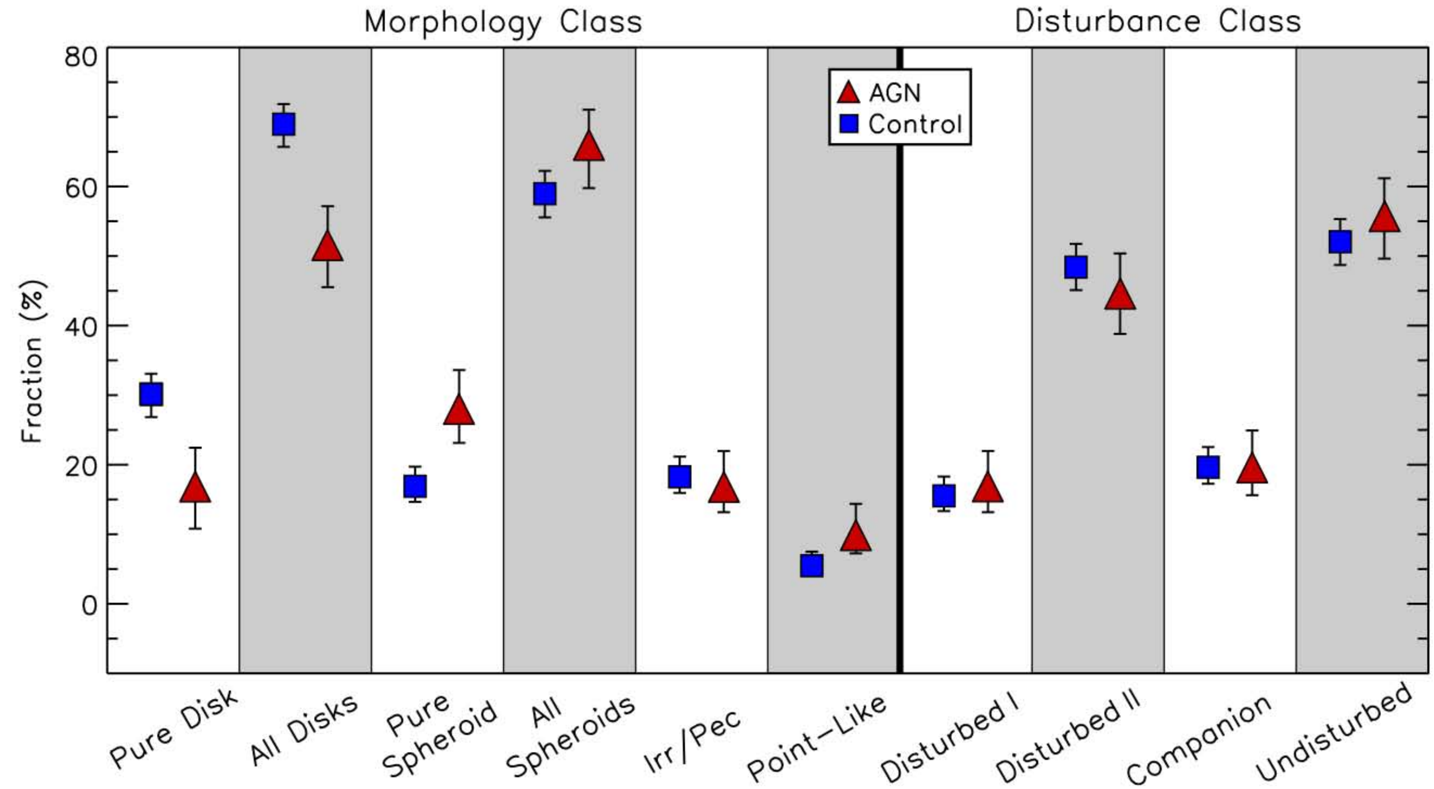

Figure 4. Fraction of AGN hosts (red triangles) and control galaxies (blue squares) at $1.5 < z < 2.5$ assigned to various morphological and disturbance classes. The *Pure Disk* class includes only disks without a central bulge. The *Pure Disk* class is a subsample of the *All Disks* class, which includes disks with and without a central bulge. Similarly, the *Pure Spheroid* class includes only spheroids with no discernible disk component. The *All Spheroids* class includes both *Pure Spheroids* and disk galaxies with a central bulge. The *Disturbed I* class is limited to heavily disturbed galaxies in a clear merger or interaction. The *Disturbed II* class includes galaxies in the *Disturbed I* class, as well as those showing even minor asymmetries in their morphologies. See the text for details.

e.g., Kocevski et al. (2012)

Moderate-Luminosity AGNs in the Color-Mass Diagram

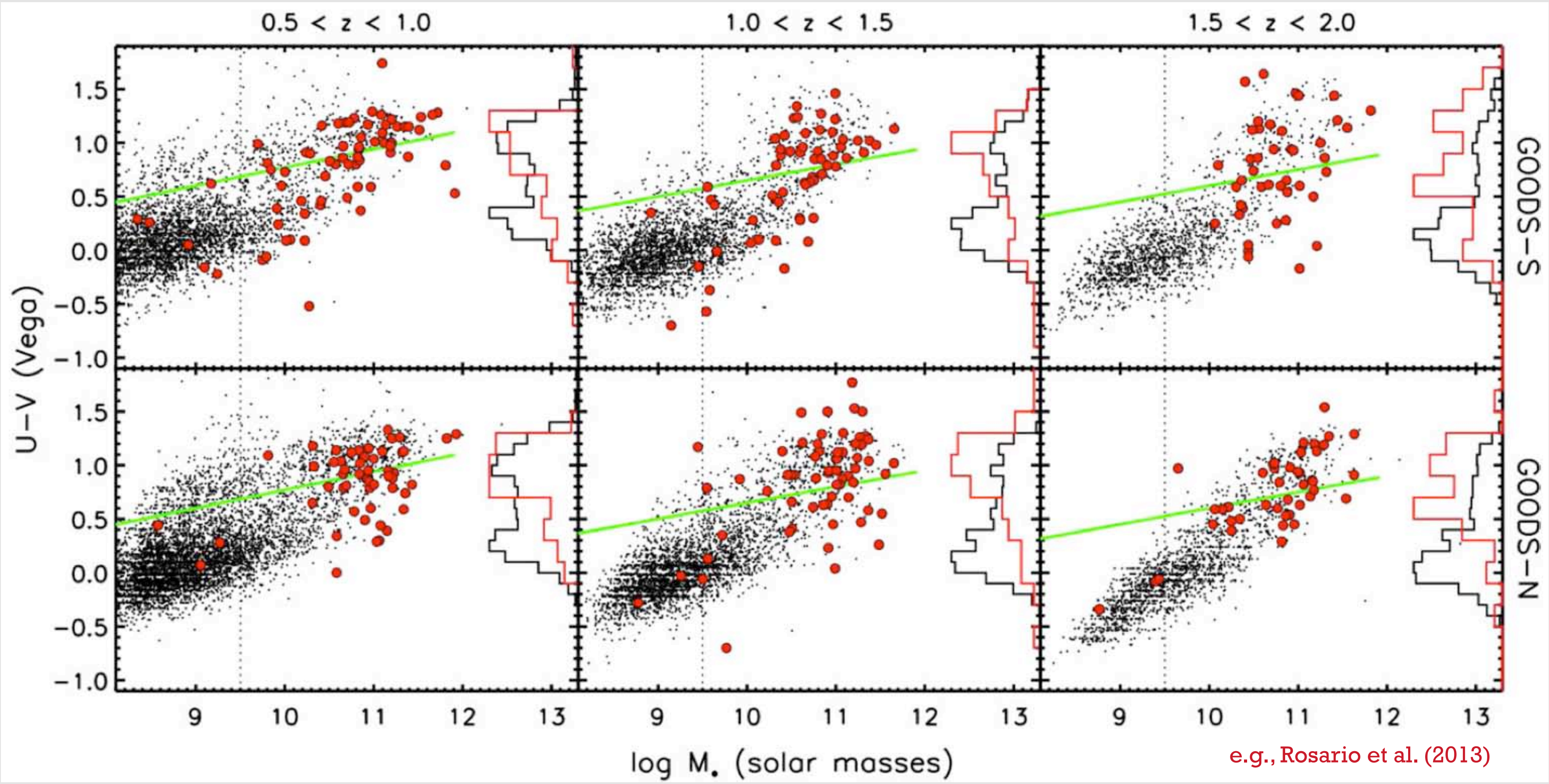

AGN hosts generally have colors consistent with mass-matched non-AGN hosts.

But note that colors are generally a poor tracer of star formation rate (e.g., dust).

FIR Measurements of SFR

SFR Per Unit Mass for AGNs and Non-AGNs as Measured by Herschel

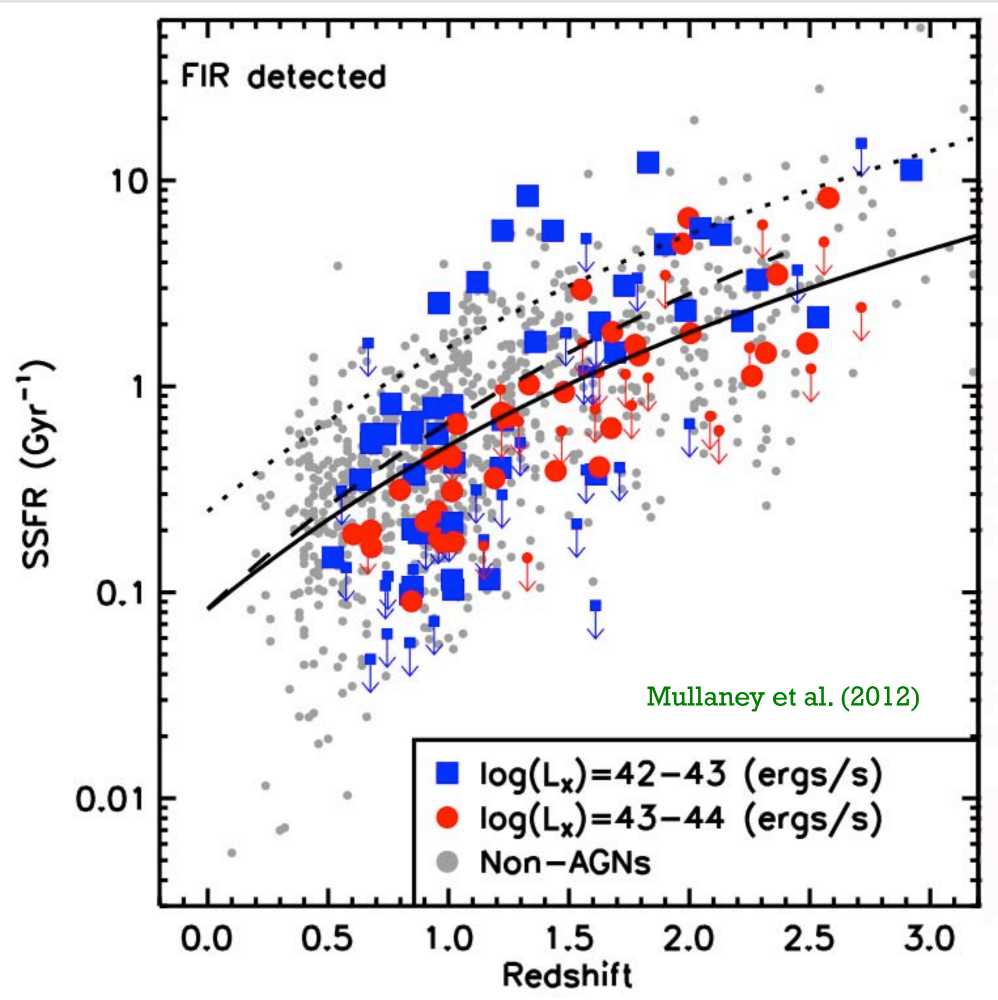

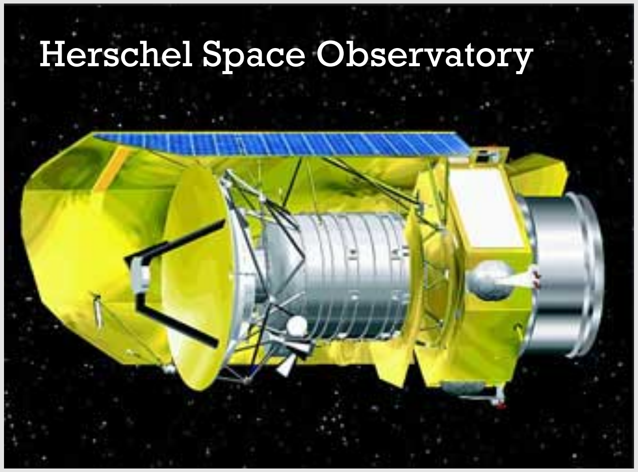

Herschel measurements at 100 and 160 μm allow better SFR measurements.

Appears any global SFR elevation in AGN hosts is mild at best.

Bootstrap Comparison of FIR SFRs for AGN Hosts vs. Non-AGNs

Galaxies are matched in mass and *z*

Considering only Herschel detected galaxies

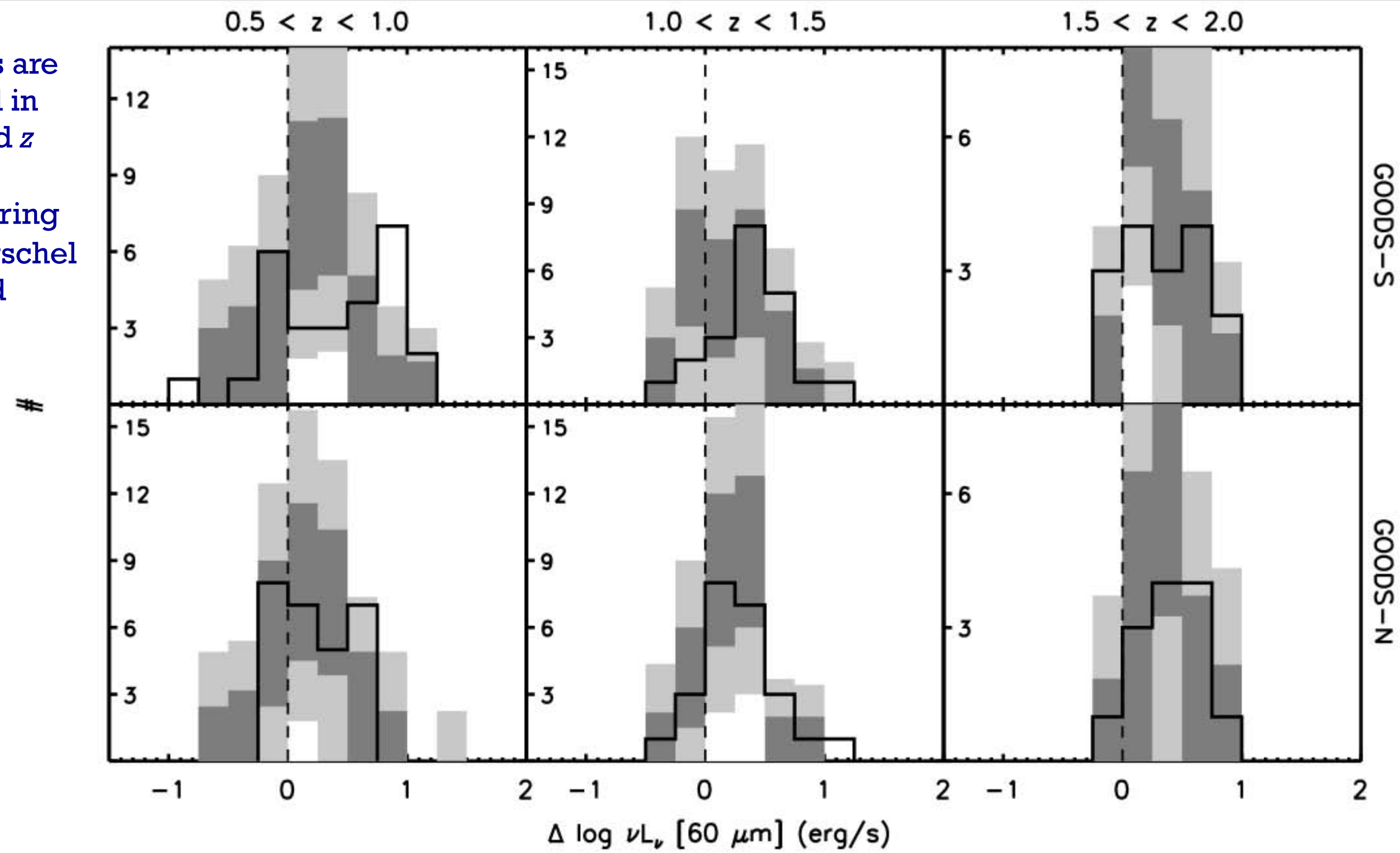

Figure 7. Comparison of the L_{60} offset (ΔL_{60}) of X-ray-selected AGNs and mass-matched inactive galaxies from the star formation mass sequence. The statistical uncertainty in the distributions of the inactive galaxies are shown by the shading in the histograms—dark gray sections show the 1σ uncertainty, due to the scatter in the population as well as small number statistics, while the light gray sections show 2σ. The dashed line at $\Delta L_{60} = 0$ corresponds to the center of the mass sequence. The AGNs show rather similar distributions to inactive galaxies.

Rosario et al. (2013)

But AGNs Do Preferentially Live in Star Forming Galaxies

Galaxies are matched in mass and *z*

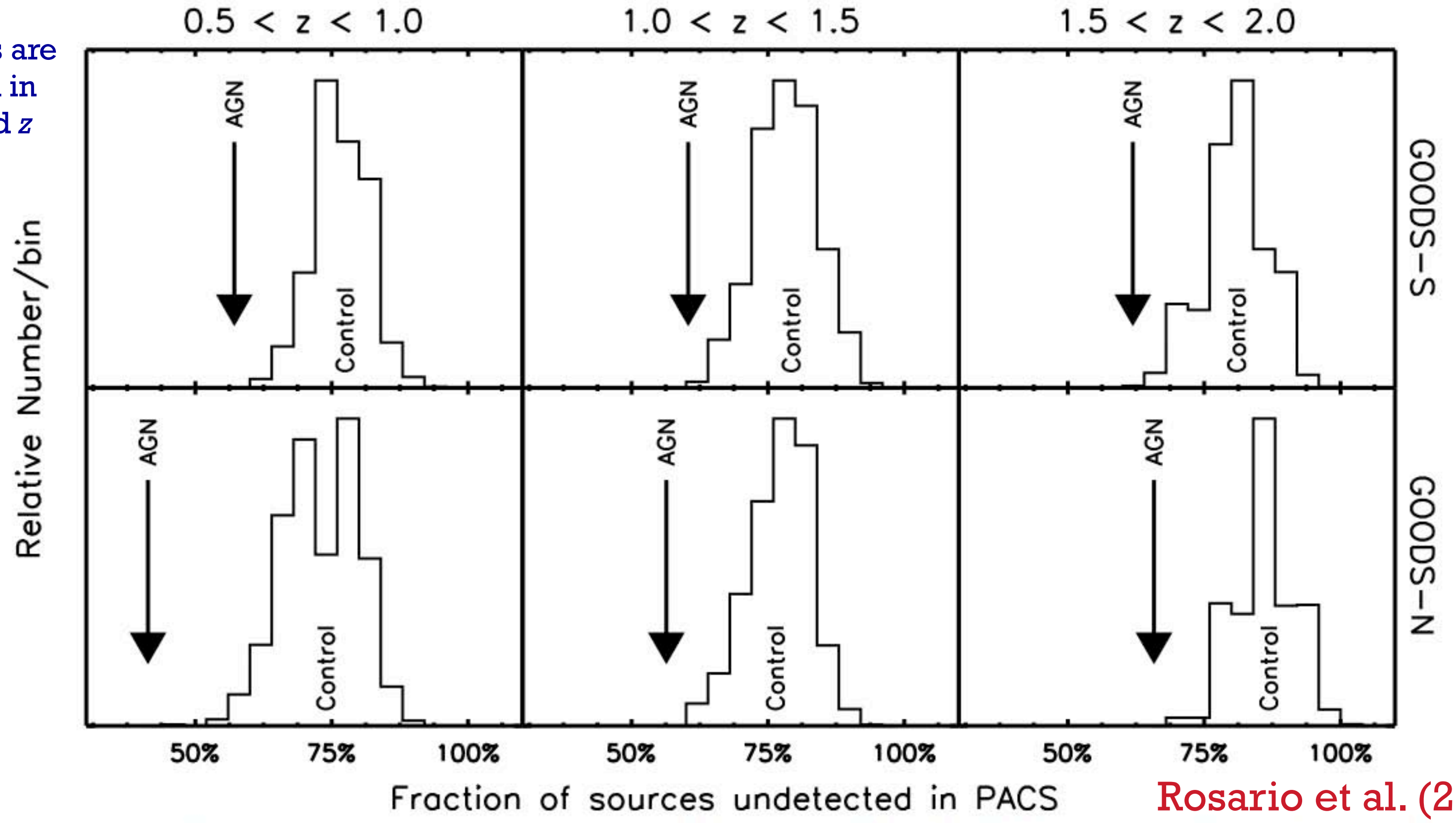

Rosario et al. (2013)

Figure 8. Histograms of the PACS non-detection fractions—the percentage of objects *not* detected in PEP+GH PACS maps—for 1000 realizations of the mass-matched comparison sample of inactive galaxies in the corresponding redshift bins. The median value of the histograms is shown by the location of the vertical label "Control." The non-detection fraction of X-ray AGNs in the same redshift bin is shown as a thick arrow for comparison. AGNs have a significantly higher chance of being detected in the deep *Herschel* data, which implies, given the depth of the PEP+GH maps, that they preferentially avoid weakly star-forming, quenching, or quiescent galaxies.

Distant Submillimeter Galaxies

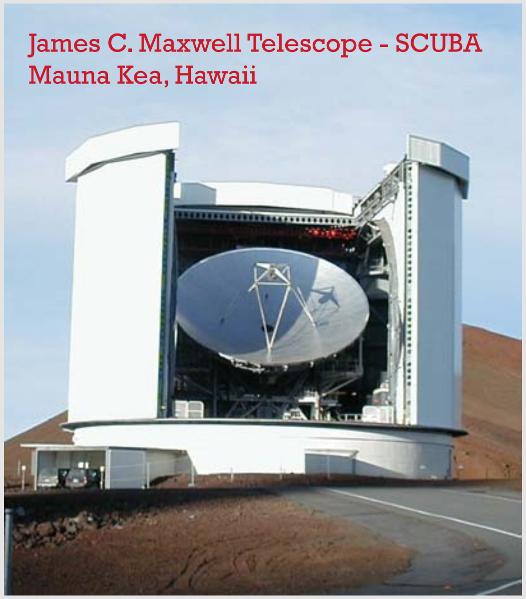

Dust-shrouded starbursts forming stars at ~ 1000 $M_\odot$ yr^{-1}.

Optically nondescript due to extinction by dust.

Bright in submm due to thermal emission from dust.

Typically z ~ 1.5-3 (~ 1000 times more common at z ~ 2).

Seeing epoch of bulge formation in massive galaxies.

Can we see accompanying supermassive black hole growth?

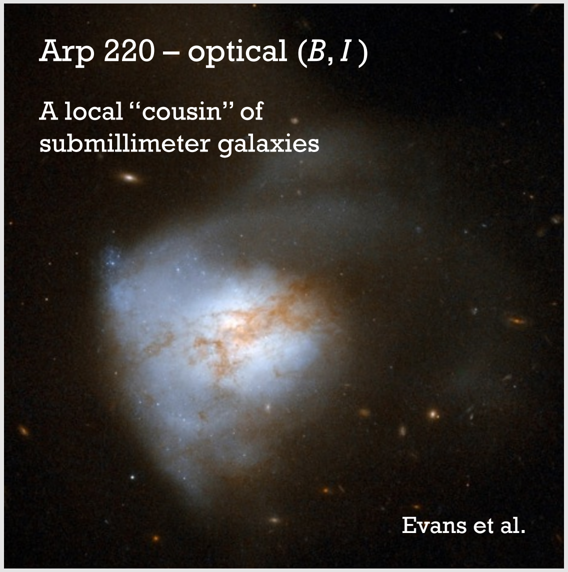

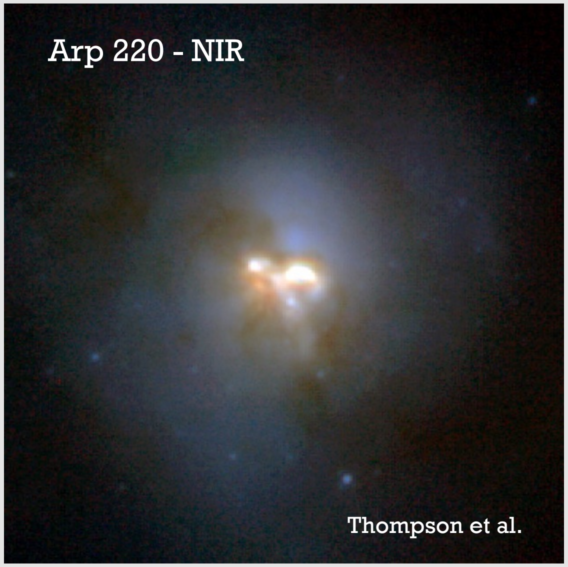

AGNs in Submillimeter Galaxies

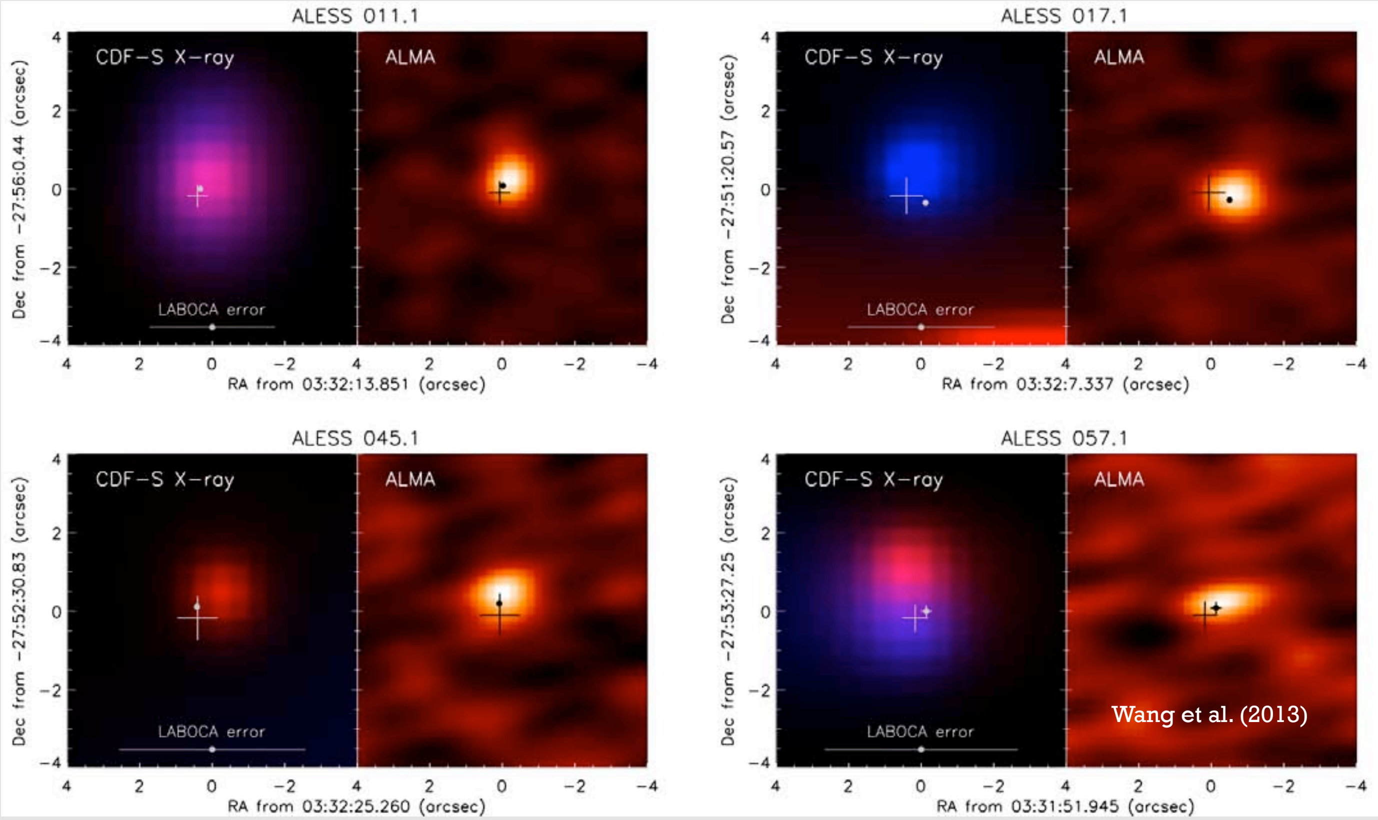

High fraction of submm galaxies at $z \sim$ 1-4 are X-ray detected in deepest X-ray surveys.

Often evidence for AGN activity. AGN fraction ~ 20-35%.

Suggests high duty cycle of black-hole growth in forming bulges.

Results at Higher Luminosities

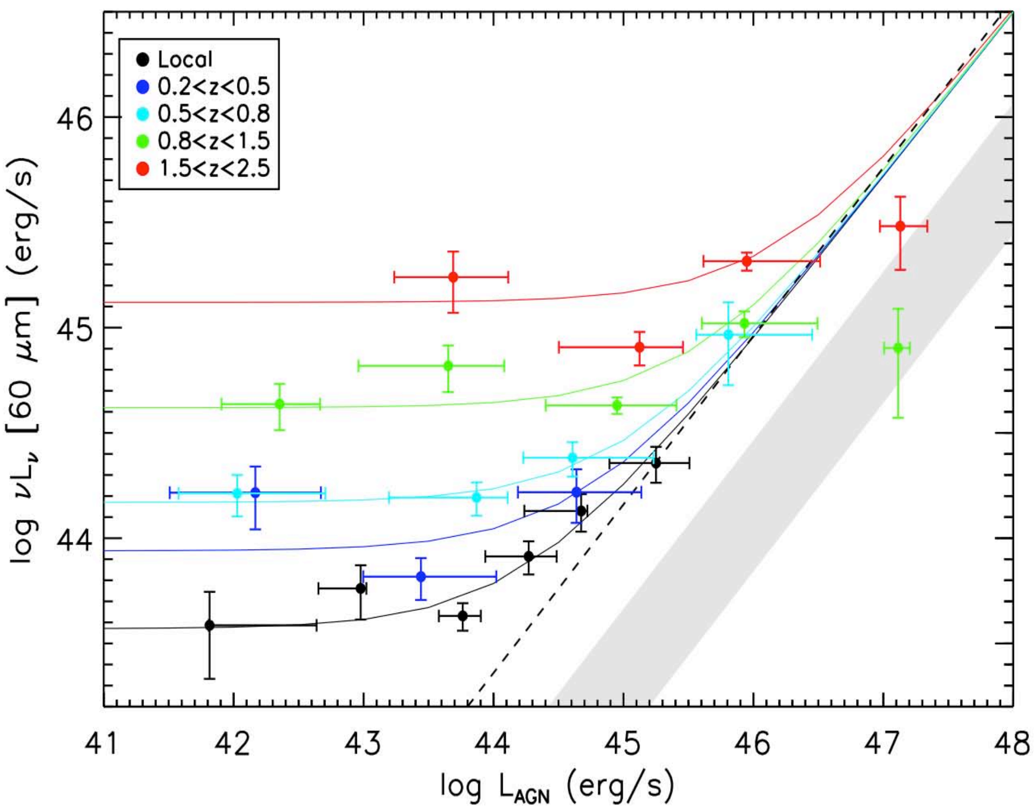

Fig. 4. Mean νL_ν(60 μm) (L_{60}) vs. L_{AGN} of X-ray selected AGNs in 5 different redshift bins from the local Universe to z = 2.5. The colored data points are combinations of mean measurements in 3 PEP fields: GOODS-N/S and COSMOS, while the black data points come from our analysis of the *SWIFT*-BAT sample. The solid colored lines are functional fits to the mean measurements, as described in Sect. 4.1.1. The dashed line is the correlation line shown by AGN-dominated systems in Netzer (2009). The shaded region corresponds to the approximate 1σ range exhibited by empirical pure-AGN SEDs. At low redshifts, a strong change in the mean trend exists as a function of L_{AGN}, which disappears at high redshifts. The mean L_{60} of low-luminosity X-ray AGNs increases monotonically with redshift, mirroring the increase in the mean SFR of massive galaxies across redshift.

At higher L_{AGN}, there does appear to be an L_{AGN}-SFR correlation.

Merger-driven co-evolution of SMBH and galaxies?

The redshift dependence of this correlation is debated at $z > 1$.

Perhaps secular processes become more important than mergers for AGN fueling at early epochs?

Rosario et al. (2012)

More to Come

The lectures by Luis Ho next week will address SMBH / host co-evolution in much further detail.

Some Future Prospects

Some Big Unresolved Questions

Missed highly obscured AGNs and their contribution to SMBH growth at $z \sim 1\text{-}4$.

SMBH growth and feedback at $z \sim 4\text{-}10$.

What sets the SMBH coronal X-ray luminosity?

Co-evolution of SMBH and galaxy stellar populations through the $z \sim 1\text{-}4$ formation era.

Effects of large-scale cosmic environment.

Chandra and XMM-Newton Are Healthy

State of Health for Major Chandra Subsystems

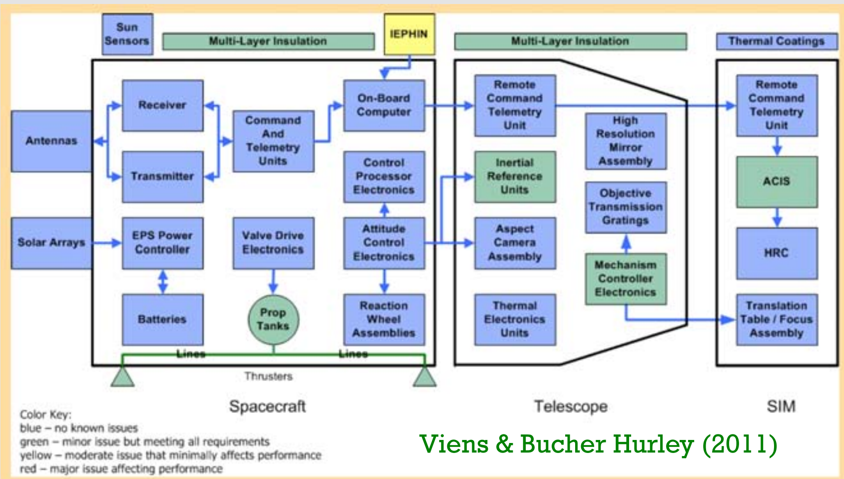

Viens & Bucher Hurley (2011)

A 20+ year Chandra mission appears entirely feasible.

Some XMM-Newton Mission Operations Parameters

Fuel	Remaining Use per year Estimated lifetime	71 kg <6 kg >2020
Solar array power	Maximum required Current margin Margin 2020	1350 W 550 W >400 W
Battery	Same capacity as launch	Reconditioning can be repeated
Gyros/(IMUs)	Usage	<20%
Reaction wheels	Usage	<38%
RCS FCV	Usage (A,B)	~50% A, B only ESAM
RF switches **Transponder switches**	Usage	Possibly stuck at one position Back up not used instead transponders are switched TX A /B switching <300 (Qualified to 25000)

Parmar et al. (2011)

XMM-Newton mission status is very good.

Consumable fuel good to 2020, and likely beyond with conservation.

Must maintain outstanding science output!

Let's Hope for Another Great Decade of Chandra and XMM-Newton Surveys!

Some Recent Contiguous Deep X-ray Surveys

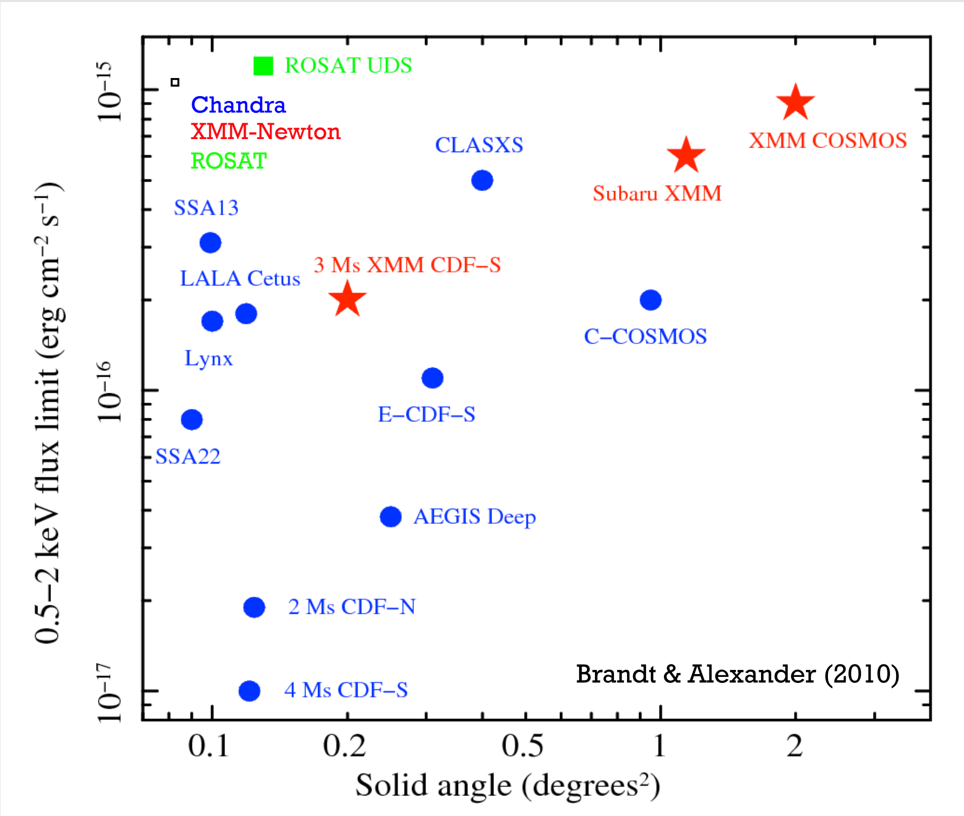

Can aim to push both deeper and wider.

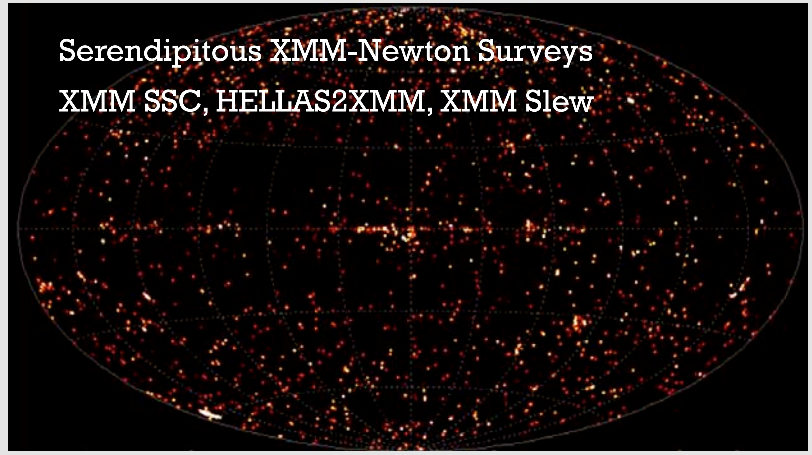

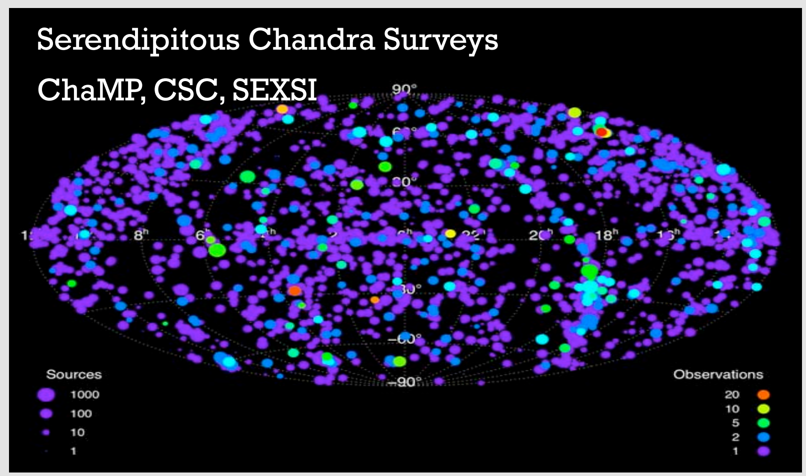

One Direction: Pushing Deeper with Chandra

Central Chandra Deep Field-South

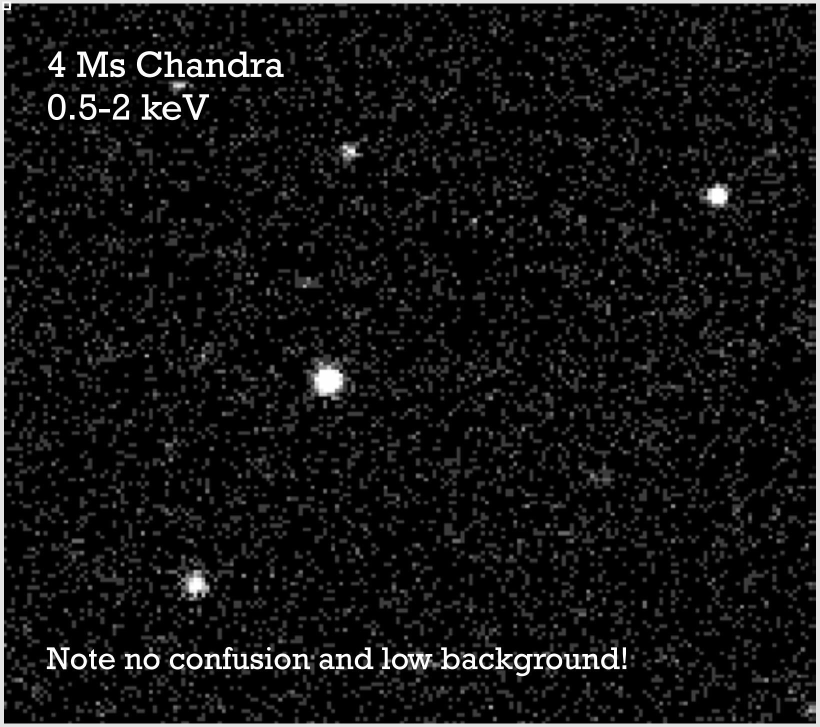

Missions – Depth vs. PSF Quality

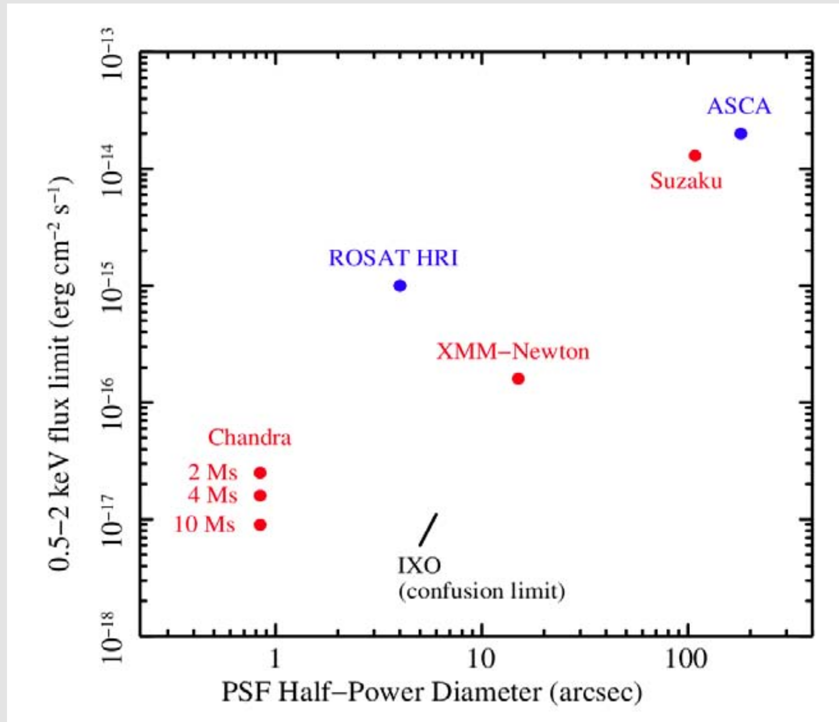

Chandra can still go deeper while remaining confusion free.

In 7-10 Ms can reach depths that were planned for IXO and go deeper than Athena.

A 20+ year legacy for Chandra.

Angular resolution and *positions* likely unmatched even by next generation missions.

Better photon statistics improve spectral and variability studies for hundreds of sources.

With Lots of New Complementary Multiwavelength Data Flooding In!

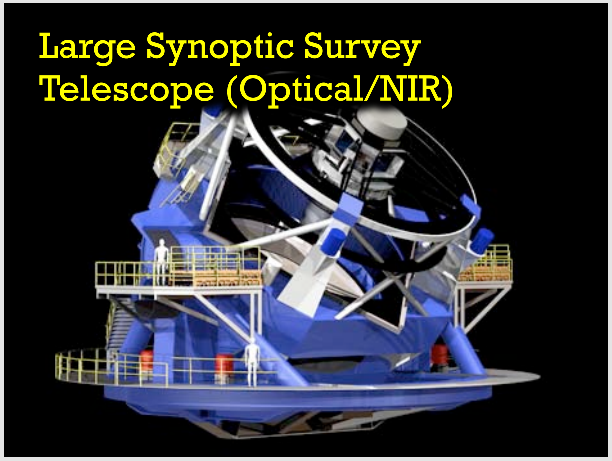

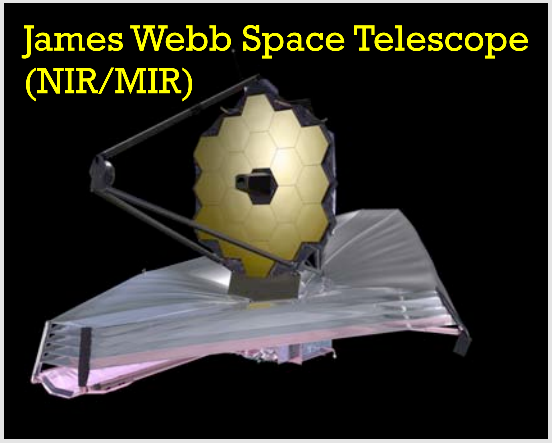

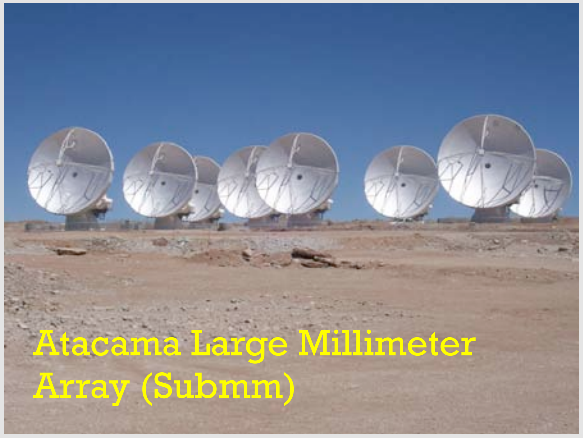

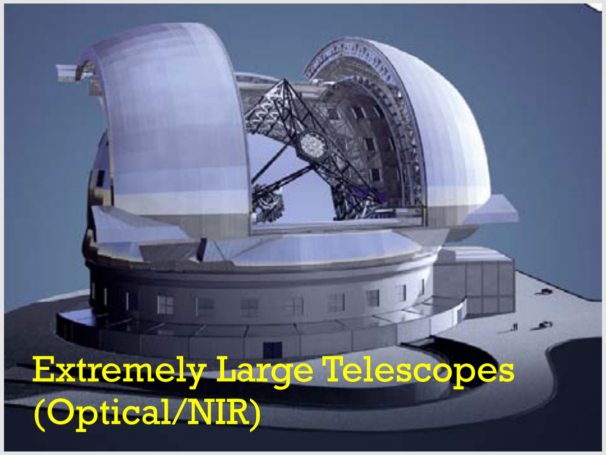

Near-Term and Long-Term New Surveyors of the X-ray Universe

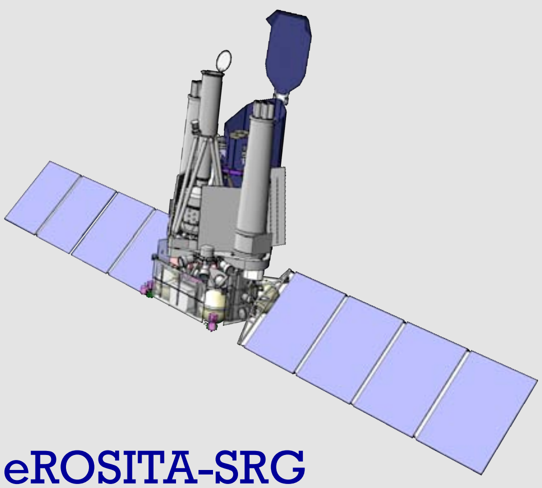

eROSITA-SRG
2015 launch

Very Long Term: Need New X-ray Mirrors Technology

Need X-ray mirrors that are much lighter but still with superb angular resolution.

One possibility is "active" mirrors adjusted (rarely) with thin-film piezo-electric actuators.

Under study for SMART-X, the Square Meter Arcsecond Resolution X-ray Telescope.

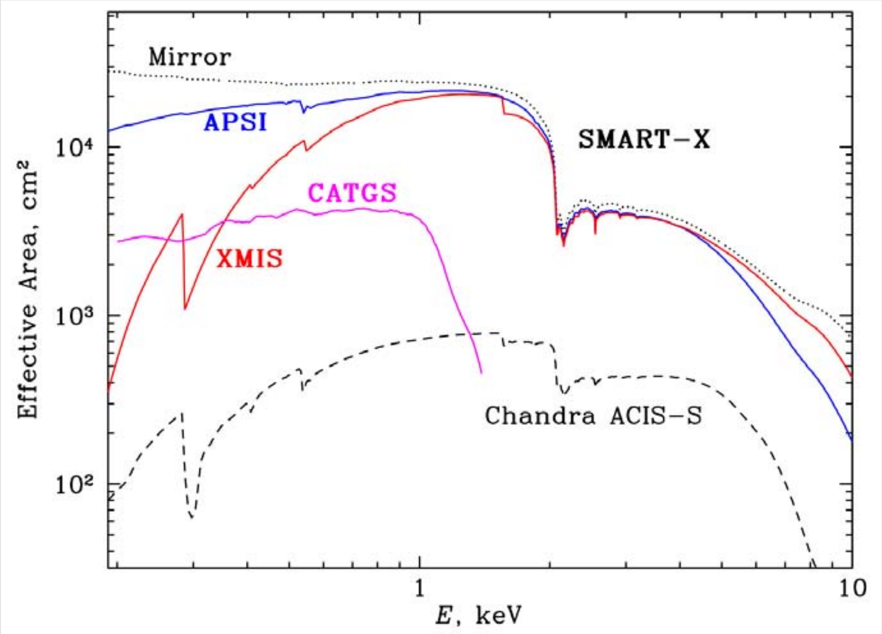

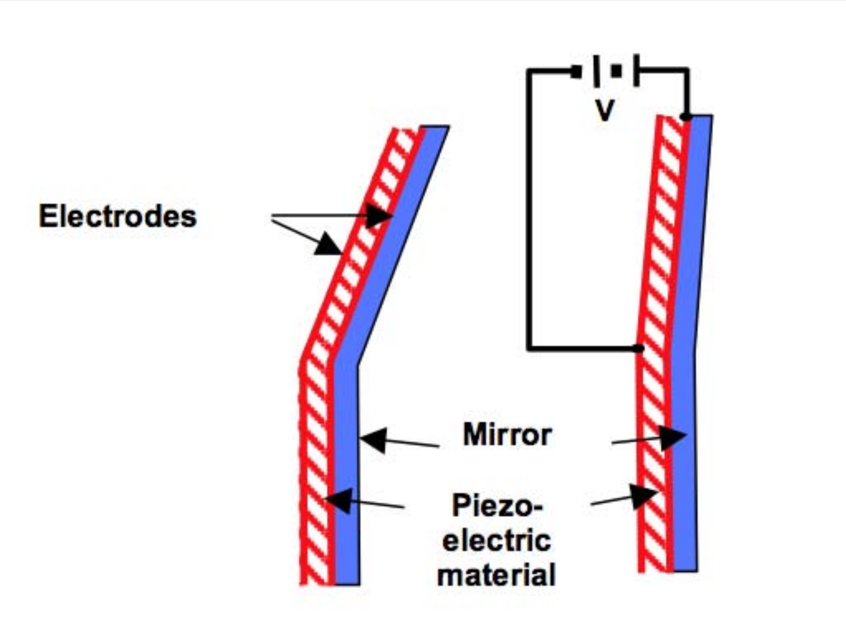

The End